The Development of Novel *N*-Heterocyclic Carbenes and Tools for Assessing Structural Variation Effects Upon Catalyst Reactivity

Alberto Muñoz

Submitted in partial fulfillment of the
requirements for the degree of
Doctor of Philosophy
in the Graduate School of Arts and Sciences

COLUMBIA UNIVERSITY

2018

ABSTRACT

The Development of Novel *N*-Heterocyclic Carbenes and

Tools for Assessing Structural Variation Effects Upon Catalyst Reactivity

Alberto Muñoz

N-Heterocyclic carbenes (NHCs) are an important class of compounds responsible for a wide variety of chemical transformations. NHCs may be used as organocatalysts that permit non-traditional carbon carbon bond formations due to their renowned ability to invert the electrophilic character of aldehyde carbonyl groups, a concept otherwise known as polarity reversal or *umpolung* reactivity. Despite their ubiquity with respect to accessing the umpolung of aldehydes, fundamental studies of these reactive species are still rather limited and narrow in scope. As a result, clarifying and solving problems relevant to umpolung-themed asymmetric catalysis becomes quite challenging. In this regard, our work has been focused on a three-pronged approach towards providing a more unified understanding of these complex catalytic systems. First, we describe the synthesis of unprecedented carboxylate-tethered triazolium NHCs and use them in the intramolecular Stetter reaction to understand their function. Second, we describe the acidities of a broad range of both chiral and achiral NHCs that have never had their acidities assessed before and use them to construct the first linear free-energy relationships of their kind. Finally, we develop a simple and noninvasive experimental protocol in which we can quickly benchmark the performance of a series of chiral catalysts by way of single competition experiments. We anticipate that these studies will have direct implications on the development of novel NHC-catalyzed reactions.

TABLE OF CONTENTS

LIST OF FIGURES

ACKNOWLEDGEMENTS

I would like to start off by first thanking my advisor, Professor Tomislav Rovis. Tom has mentioned in the past that he "mentors everyone differently". As a first-hand witness of his leadership for the past 4 years, not only can I verify this, I can confidently say that this is the mark of an advisor of the highest caliber. It takes someone who cares deeply about what they do in order to provide case-by-case mentorship on both professional and personal levels. Thank you, Tom, for your guidance, for all the times that you've challenged me to perform at a higher level, and for all your support throughout these years.

I would like to thank Professor Robert M. Williams as well. Despite not being in his research group, Bob never once hesitated to host me in his office to either have a chat or to offer advice that I still, to this day, hold close to my chest. Your strongly-worded bits of encouragement played a significant role in helping me self-sustain my perseverance. I am enormously grateful for all your help and continued support. We live and die by the pentatonic!

I would also like to thank my undergraduate advisor, Professor Ryan P. Murelli, for taking a (probably huge) chance on me when I asked to join his research group. Your continued faith in my potential as a scientist was integral to my success, especially during the times when imposter-syndrome would rear its ugly head. Thank you for your mentorship, friendship, and for your continued support.

To my cohort, both past and present, thank you for all your scientific input and support throughout the years. Thank you to Benjamin Ravetz, Scott Thullen, and Isra Hassan for your unique roles in helping me finish this thesis. I especially want to thank Dr. Fédor Romanov-Michailidis for being such an excellent role model, both professionally and personally. Your advice, incisive criticisms, support, frequent challenges, mentorship, and friendship represented a beacon throughout my time as a graduate student. I am incredibly grateful for everything you have done for me.

Akin to how it takes a village to raise a child, it takes a lot of help from a diverse set of people to raise a doctoral student. To all my friends that have supported and been patient with me while I traversed this path, thank you. A special shout out to Samantha "BingBong/Magic Toaster" Kang, Igor "Dostoevsky" Dukler, Ralph "The Mouth" Ranghelli, William "Will" Liu, Jack "The Mack" Goméz, Muhammad "Jet Eye" Suliman, Rodrigo "Rigo" Urbina, Bryce "Brailee" Rogers, Francisco "Narf" Sarabia, and Caressa "Nugent" Nguyen. Thank you all for always having my back and wishing the best for me.

Finally, I would like to thank my family. Without all the support I've received from my brother Aaron, my sister Cynthia, my mother Lucia, and my father Lorenzo, I would have never reached this level of achievement. You have all inspired me in more ways than I can possibly count. Para mis padres, quiero decirles que mis logros hasta ahora son tanto los suyos como son los míos. From the deepest wells of my heart, thank you.

Dedicado a mis héroes – mi madre y mi padre – y a las generaciones futuras.

Genitori, Genitoque
Laus et jubilatio,
Salus, honor, virtus quoque
Sit et benedictio:
Procedenti ab utroque
Compar sit laudatio.

Chapter 1: Introduction

1.1 An Evolution of Carbenes From Unstable Intermediates to Isolable Catalysts

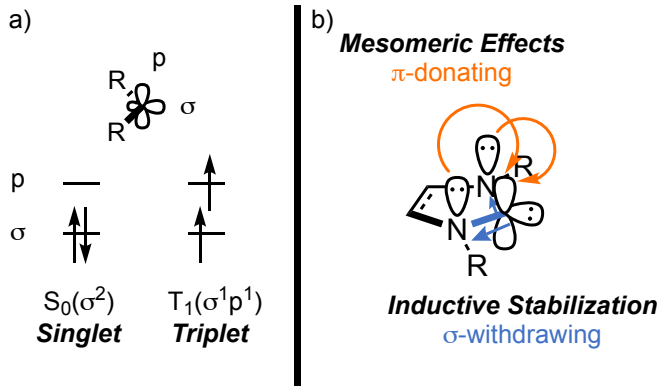

Figure 1.1.1. a) Single and triplet electron configurations of a carbene. b) Stabilizing effects from geminal heteroatom substitution.

A carbene is defined as a divalent carbon atom with six electrons in its outer shell.[1] Two of these electrons are nonbonding and exist most commonly in either anti-parallel or parallel spins (**Figure 1.1.1a**).[2] In the former case, according to the spin multiplicity 2s + 1 rule, the carbene exists as a singlet state and may act as a nucleophilic lone pair with the nonbonding electrons occupying a σ-orbital.[3] In the latter, the carbene exists as a triplet state and reacts as a diradical, with each of the nonbonding electrons singly occupying a σ- and p-orbital.[4] Furthermore, *N*-heterocyclic carbenes (NHCs), where the N may stand for either nitrogen or nucleophilic,[5,6] are carbenes that are covalently linked to one or more heteroatoms and are contained within a heterocycle.[7] These heteroatoms serve to stabilize the singlet state of the carbene through both mesomeric and inductive effects (**Figure 1.1.1b**). The first occurs by π-donation from the heteroatoms into the empty p-orbital of the carbene. This effect stabilizes the sp^2-hybridized state of the carbene and also serves to increase its nucleophilicity by imparting a more dipolar character

to the overall structure. Concurrently, the heteroatoms may help to lower the energy of the occupied σ-orbital through inductive effects, serving to increase the amount of s-character at the carbene. The cyclic nature of NHCs also serve to further stabilize the singlet-state of the carbene by geometrically constraining the carbene to an sp^2-hybridized state. As singlet-state carbenes, NHCs have been used as ligands for transition metal complexes,[9] as ligands for elements on the p-block of the periodic table,[10] as well as organocatalysts.[11,12] A complete overview on the history of NHCs in all of these applications extend well beyond the scope of this thesis. As such, we will instead focus on NHCs in their role as organocatalysts.

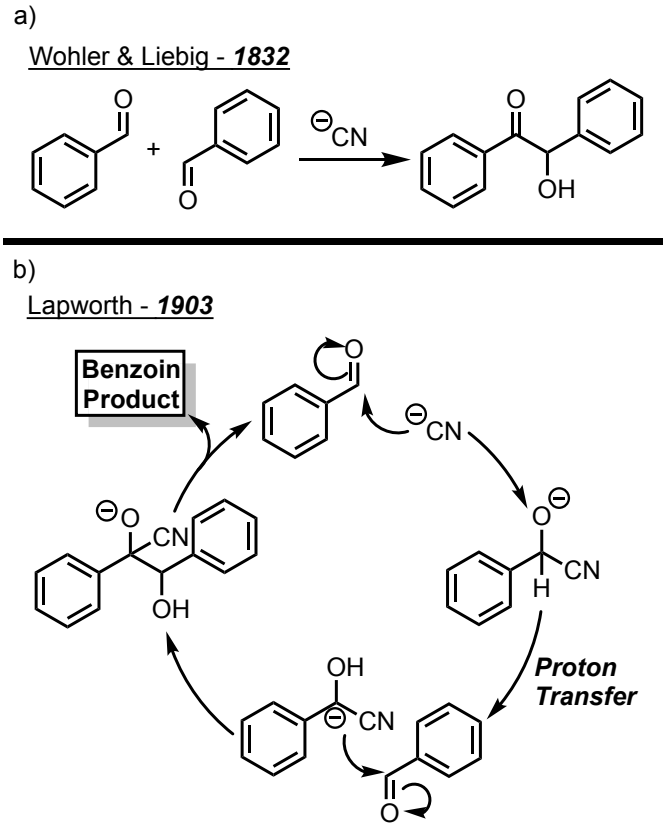

Figure 1.1.2. a) First reported benzoin reaction in 1832. b) First proposed mechanism for benzoin reaction in 1903.

NHCs have a rich and detailed history. When discussing these reactive intermediates as organocatalysts, it is worth going back to 1832 with the discovery of the first benzoin reaction.[13]

That year, Wohler and Liebig disclosed the cyanide catalyzed self-condensation of benzaldehyde to make α-hydroxyketone products (**Figure 1.1.2a**). This process represents one of the first instances where an electrophilic moiety is rendered nucleophilic, a mode of reactivity that is now known as *umpolung*, or polarity reversal. The currently accepted mechanism for this transformation was first proposed almost 70 years later, when the process was revisited in 1903 by Lapworth and coworkers (**Figure 1.1.2b**).[14] The connection of this mode of reactivity to NHCs was established in 1943, when Ukai and coworkers showed that the same type of reactivity can be achieved by thiazoliums.[15] Breslow proposed a mechanism for this transformation in 1958, which is reminiscent of the one proposed by Lapworth (**Figure 1.1.3**).[16] Here, thiamine **1** is deprotonated *in situ*, which can then nucleophilically add to an aldehyde carbonyl, forming tetrahedral intermediate **3**. This intermediate undergoes a formal 1,2-proton transfer, which forms enol **4**. This intermediate, which is called the Breslow intermediate in honor of its original proposer, is now nucleophilic at what used to be an electrophilic carbon atom. The Breslow intermediate adds to another equivalent of aldehyde to form the second tetrahedral intermediate **5**, which then undergoes a proton transfer to **6**. The alkoxide of **6** collapses to a carbonyl, which forms the benzoin product and subsequently restores the free carbene.

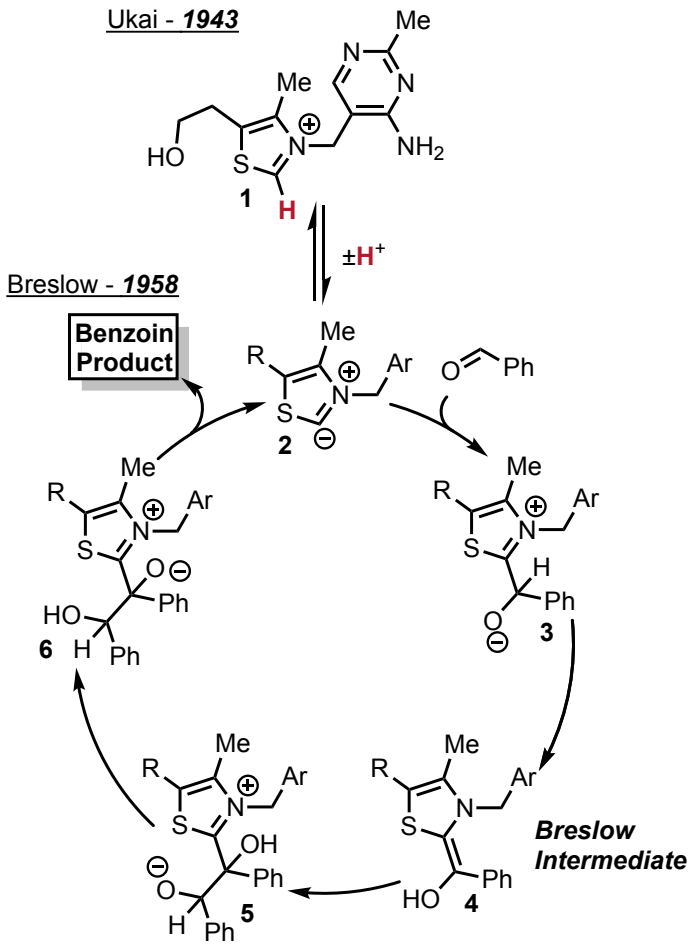

Figure 1.1.3. Breslow's proposal for the mechanism of the benzoin reaction.

In 1960, Wanzlick and coworkers proposed that the free carbene **8** may be generated from the parent compound **7** following thermal elimination of chloroform (**Figure 1.1.4**).[17] The dimer of the carbene was instead isolated at this time, the supposition being that an equilibrium exists between the free carbene and its dimeric form. The existence of this equilibrium would be the subject of much debate in the following years.[18] Nonetheless, the propensity of any two NHC units to form a dimer would later be commonly known and referred to as the Wanzlick equilibrium. In the meantime, Sheehan became the first to render the benzoin reaction enantioselective in 1966, albeit with rather low yields and enantioselectivities (**Figure 1.1.5a**).[19] Sheehan used the thiazolium-based catalyst **10**, wherein the use of this catalyst was most likely inspired by Ukai's

aforementioned discovery. In 1970, Wanzlick demonstrated that the free carbene of **11** can be formed by deprotonation with tBuOK.[20] Though the free carbene remained to be isolated, its intermediacy was evidenced via trapping with mercury salts and isothiocyanates (**Figure 1.1.5b**).

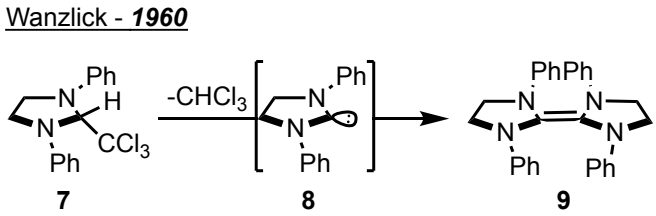

Figure 1.1.4. Wanzlick's equilibrium.

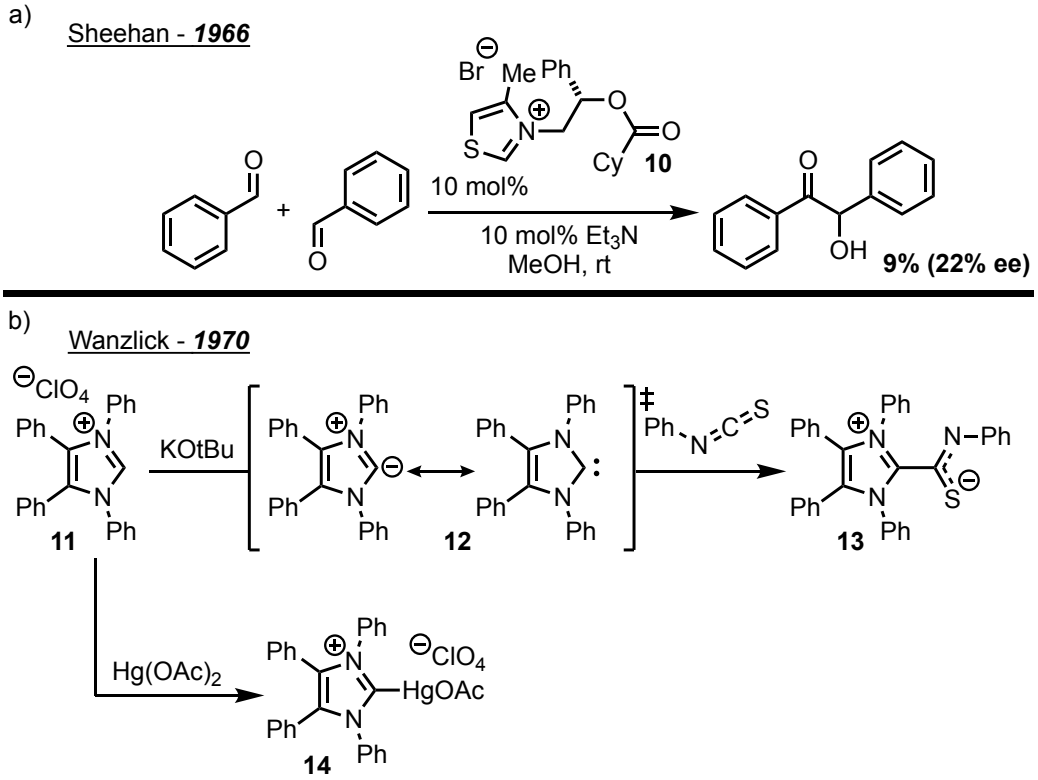

Figure 1.1.5. a) First enantioselective benzoin reaction in 1966. b) First insights into imidazolium based free carbene in 1970.

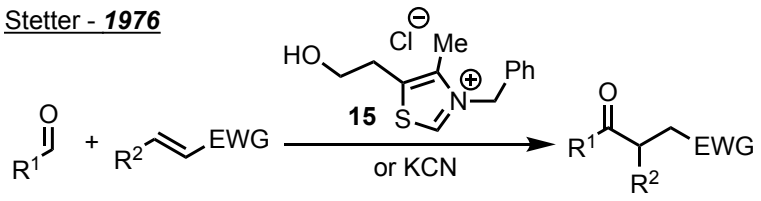

Figure 1.1.6. First intermolecular Stetter reaction in 1976.

In 1973, Stetter was able to take advantage of the umpolung of aldehydes by coupling them with α,β-unsaturated Michael acceptors. This mode of reactivity would later become known as the Stetter reaction.[21] Though Stetter's initial result was performed using cyanide as the catalyst, he demonstrated in 1976 that the same reactivity could be accomplished using thiazolium-based NHCs (**Figure 1.1.6**).[22] The mechanism for this transformation was adopted from Breslow's original proposal, with the exception that the acyl anion equivalent, or Breslow intermediate, adds into a Michael acceptor. During this time, efforts towards a more enantioselective variant of the benzoin reaction were also being attempted, though still with limited success (**Figure 1.1.7**).[23]

In 1988, Bertrand achieved a major breakthrough with the first reported isolable carbene, **18**, which is stabilized by the adjacent phosphorous and silicon atoms.[24] These NHCs would later become known as push-pull carbenes due to the difference in electronegativity of these neighboring heteroatoms.[25] The first isolated, stable, and "bottleable" NHC **19** was isolated in 1991 by Arduengo and coworkers.[26] This represents the first time that a carbene was characterized by X-ray crystallography, the data of which indicates very little double-bond character at the C–N bonds of the carbene, as is shown in **Figure 7**. Enders contributed toward this effort in 1995 with the isolation of triazolium based carbene **20**, the structure of which was also confirmed by X-ray crystallography.[27] The isolation of these carbenes ultimately represents the transition of carbenes from unstable and short-lived intermediates to stable and isolable species. As such, massive efforts

to expand the library of NHCs followed this publication were being undertaken. As a result, the reactivities and fundamental properties of these NHCs were gradually brought to light.

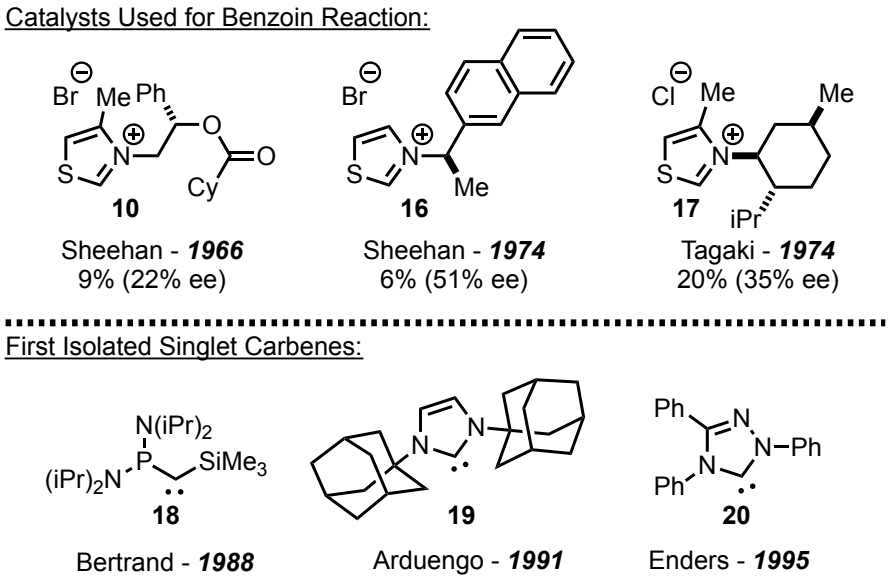

Figure 1.1.7. Progress of NHCs from 1966-1995.

The first intramolecular Stetter reaction was developed by Ciganek and coworkers in 1996, around 20 years after the initial discovery (**Figure 1.1.8**).[28] Around this time, Enders and Teles described a more enantioselective variant of the benzoin reaction using catalyst **21**, obtaining 66% yield and 75% ee.[29] Enders and Teles then applied this NHC to the intramolecular Stetter system as published by Ciganek as well, rendering it moderately enantioselective for the first time.[30] The discovery and use of this catalyst represented the first time that a triazolium-based NHC could achieve the same level of reactivity, albiet with higher enantioselectivities, as compared to their thiazolium counterparts. This indication was further demonstrated in 1998 when Leeper used the triazolium-based catalyst **22** for the purposes of the asymmetric benzoin reaction, surpassing the previous benchmark with an 80% ee, albeit with modest yields.[31] These results would represent

the beginning of a paradigm shift in NHCs used for the purposes of organocatalysts from thiazolium and imidazolium-based heterocycles to triazolium-based heterocycles.

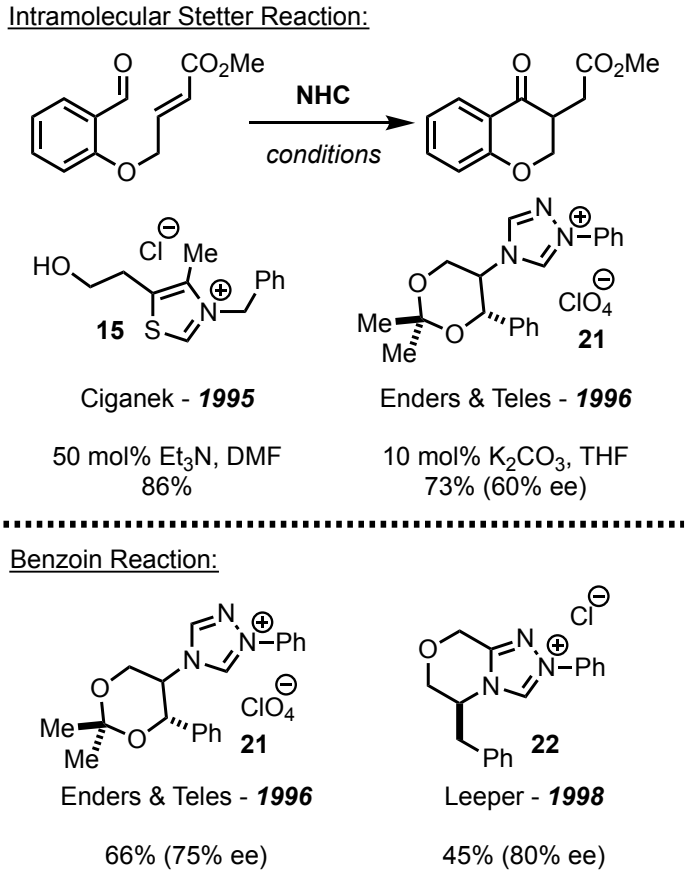

Figure 1.1.8. First uses of triazolium-based NHCs for purposes of organocatalysis.

In 2002, our group developed a series of novel triazolium-based NHCs that were used to render Ciganek's intramolecular Stetter system highly enantioselective, giving ee's upwards of 90% for several of the salicylaldehyde-derived substrates (**Figure 1.1.9a**).[32] This breakthrough represents one of the first instance in which, for any umpolung-themed reaction, such high enantioselectivities and reactivities were achieved by an NHC catalyst. The rationale for elevated levels of enantioselection for this series of catalysts are proposed to be two-fold: 1) the rigidity of the backbone, especially as compared to catalyst **21**, allows for a greater restriction of the

diastereomeric transition state leading to product; 2) the aryl group, which is missing in thiazolium-based NHCs as compared to catalyst **10**, also serves to block the opposing side of the carbene leading to further restriction in the enantiodetermining step.[33] Combined, in a mnemonic that was devised by our group, these factors combine to block three out of four quadrants that surround the reactive center (**Figure 1.1.9b**). Furthermore, the ease of which the counterion, steric, and electronic properties can be modified make these NHCs highly desirable for use in future umpolung-themed methodologies (**Figure 1.1.9c**).

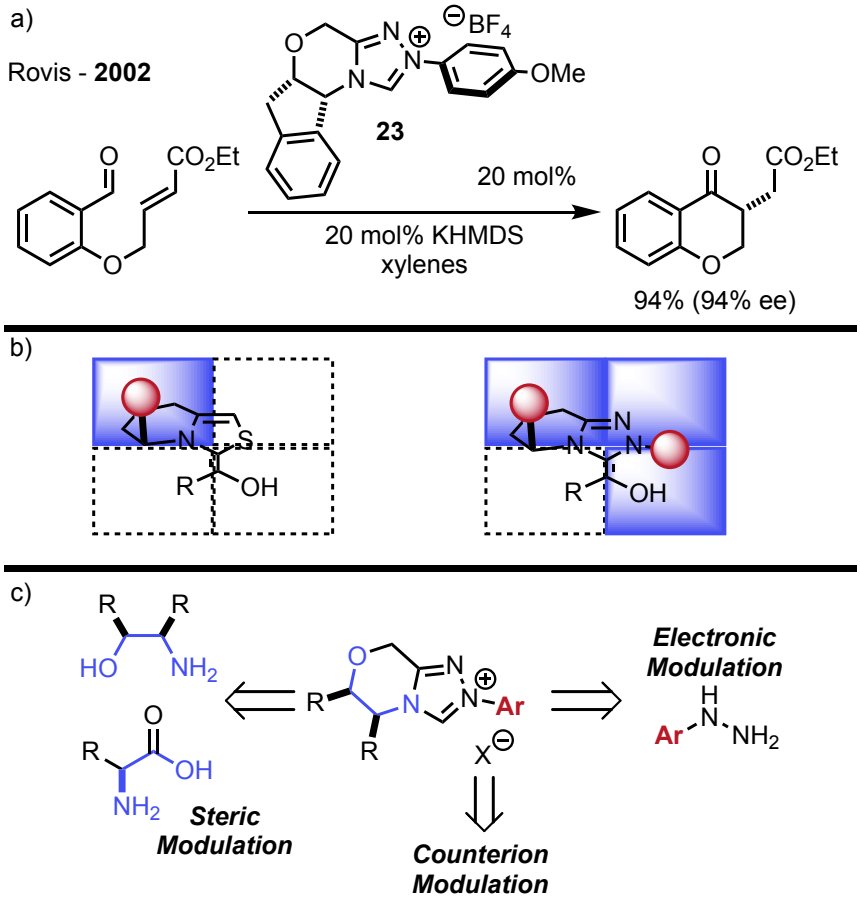

Figure 1.1.9. a) Highly asymmetric intramolecular Stetter in 2002. b) Steric space utilized by chiral thiazolium and chiral triazolium NHCs. c) Highly modular triazolium-based NHC system.

1.2 *N*-Heterocyclic Carbenes as Organocatalysts – Currently Available Reaction Classes

From this point on, though thiazolium and imidazolium-based scaffolds would both still find use for a number of applications,[34] the triazolium series of NHCs have proliferated tremendously and currently dominate the literature of umpolung-themed organocatalysis. The advent of triazolum-based NHC catalysts have created routes to many new and powerful chemical transformations, a number of which extend beyond umpolung at the carbonyl, or acyl anion, reactivity (**Figure 1.2.1**). The ease of which triazolium-based NHCs can be modified have allowed for the construction of many new NHCs to meet the demand of novel reactivity. Thus, an improvement in tools available for umpolung catalysis will be naturally followed by an improvement in the number of chemical transformations that may be achieved with these NHCs.

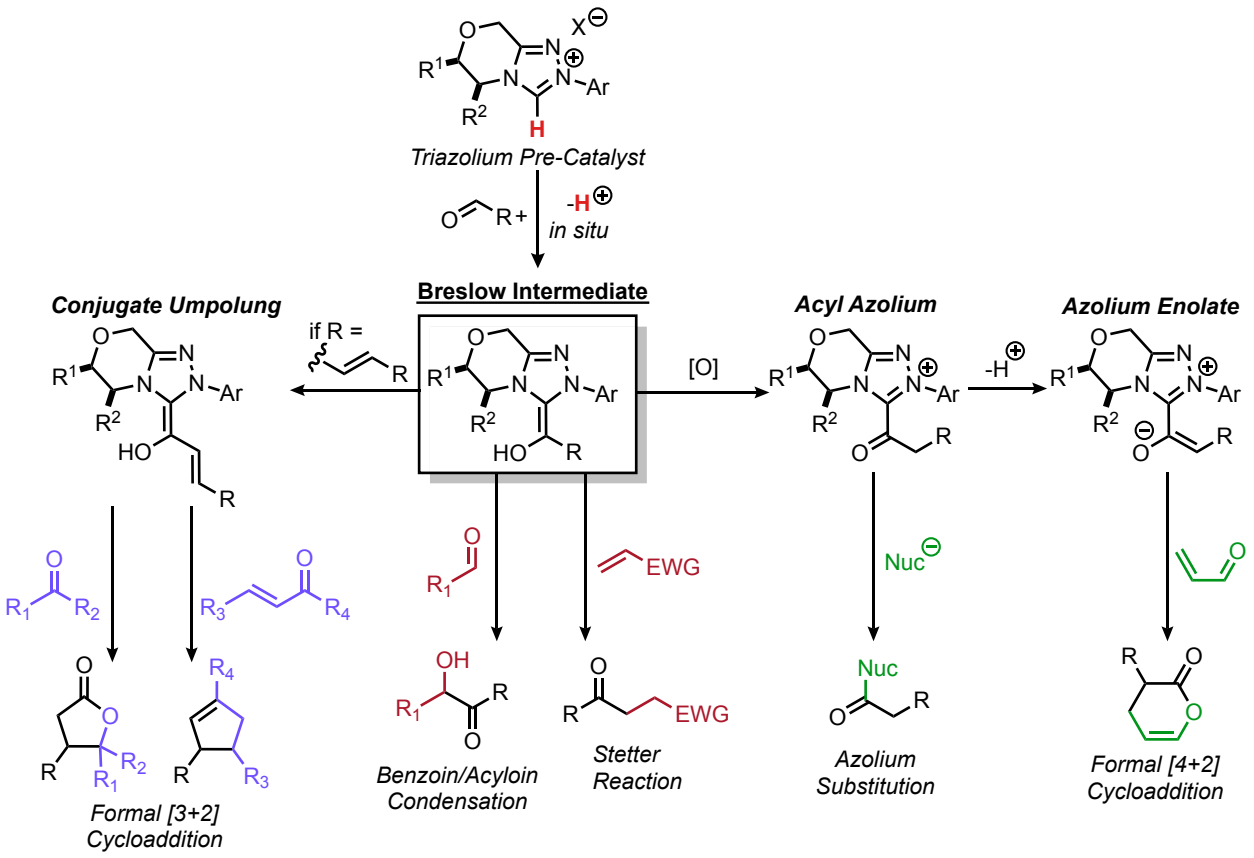

Figure 1.2.1. Different classes of reactions as catalyzed by NHCs proceeding through the Breslow intermediate.

If R in **Figure 1.2.1** is in conjugation with the Breslow intermediate, then nucleophilicity is no longer restricted to the previously aldehydic carbon: nucleophilic attack may now occur from the β-carbon.[35] This mode of reactivity opens access to enantioselective methodologies that form a functionally diverse set products such as oxygen and nitrogen heterocycles, as well as carbocycles and otherwise β-functionalized products. The first reactivity of this kind was demonstrated in 2006 by Nair and coworkers (**Figure 1.2.2**).[36] Here, upon formation of the Breslow intermediate, nucleophilic addition occurs from the β-carbon in a Michael-type fashion to the α,β-unsaturated enone. The resultant intermediary enol then performs an intramolecular aldol addition to the ketone moiety, which can then lactonize with the acyl azolium to furnish the β-lactone **30**. This lactone then thermally decarboxylates to furnish the cyclopentene product **31**.

This imidazolium-based NHC led to the development of a mesityl-substituted triazolium-based catalyst **32** in 2006 by Bode,[37] which was later used for the development of an enantioselective variant for the formation of the similar cyclopentene products.[38] Triazolium-based NHCs featuring mesityl substitution would later become recognized as one of the best catalysts for performing homoenolate-type additions (**Figure 1.2.3a**).[39] Though this *N*-aryl substituent is highly efficacious for activating homoenolate type additions, a catalyst can mimic this mode of reactivity by clever modulation of the backbone as opposed to the *N*-aryl substituent, as was demonstrated by our group in 2013 with the enantioselective homoenolate addition of enals to nitroalkenes with catalyst **33** (**Figure 1.2.3b**).[40]

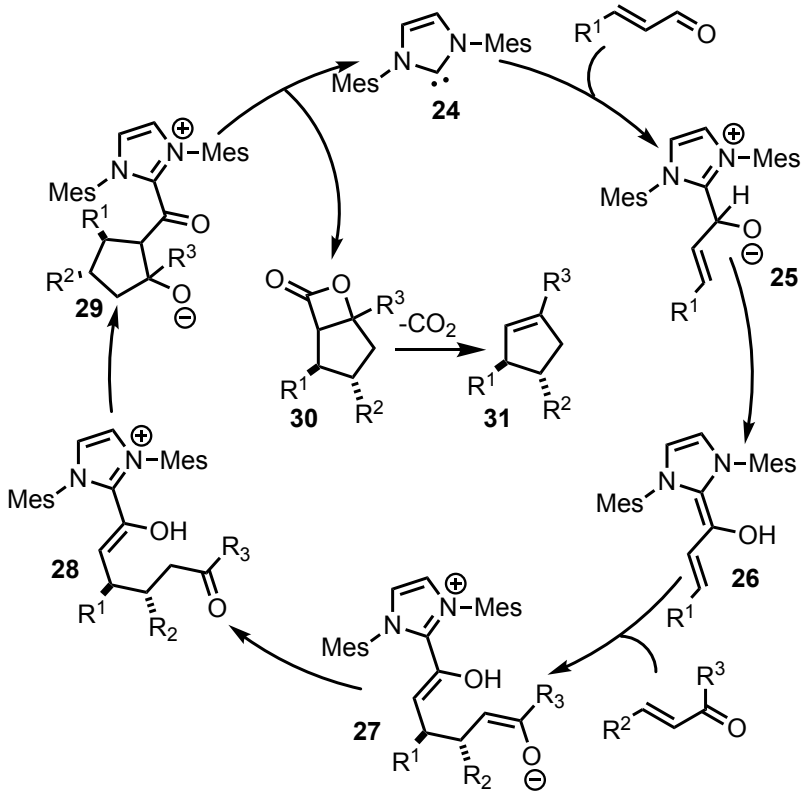

Figure 1.2.2. Nair's proposal for the homoenolate addition of enals to Michael acceptors *en route* to cyclopentenes.

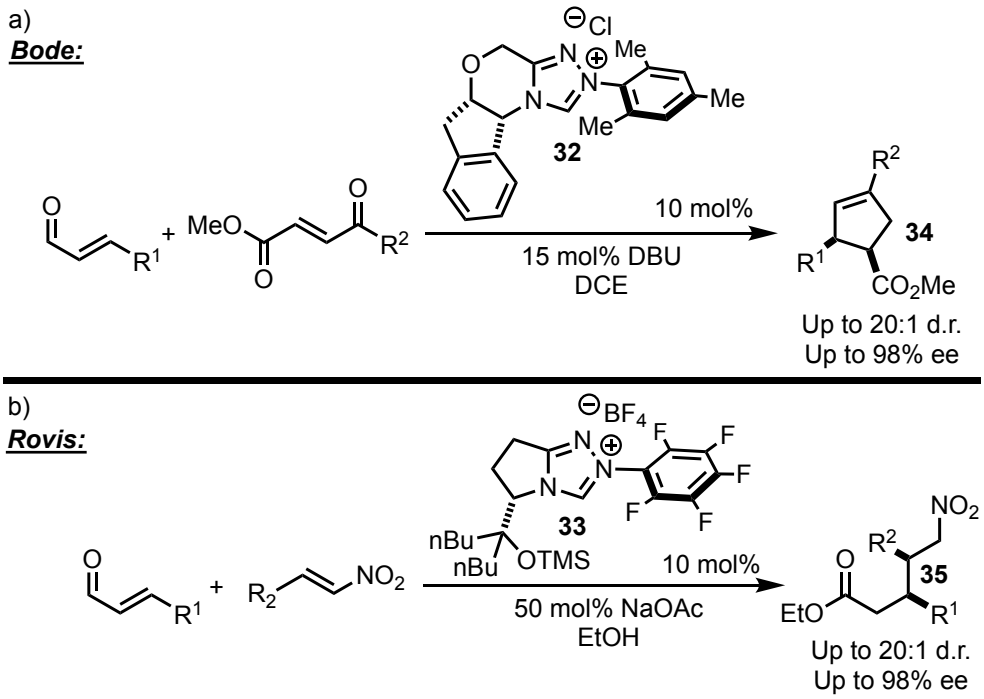

Figure 1.2.3. a) Bode's use of mesityl-substituted chiral NHC for the formation of cyclopentene products. b) Rovis' homoenolate addition of enals to nitroalkenes for the formation of β,γ-functionalized esters.

If the Breslow intermediate as shown in **Figure 1.2.1** undergoes a two-electron oxidation, reactivity stemming from acyl azolium intermediates is now made accessible.[41] The major difference with these structures and the Breslow intermediate is that their reactivity now lies outside the context polarity reversal. Here, the electrophilicity of the previously aldehydic carbon atom is now restored, but with different subsequent reactivity. These intermediates are susceptible to nucleophilic displacement of the NHC, an alternative mode of reactivity that has been used to development of a number of powerful new methodologies. For instance, Lupton showed in 2013 that α,β-unsaturated acyl fluorides may react with TMS-protected cyclopropenols to produce a broad range of β-lactone fused cyclopentanes using imidazolium-based NHC **24** (**Figure 1.2.4**).[42] The enolate **36** may nucleophilically add to the acyl azolium intermediate, which is then proposed to undergo an Ireland–Coates Claisen rearrangement to **38**. After an aldol cyclization, the newly

formed alkoxide displaces the NHC and forms the β-lactone fused product. These acyl azolium intermediates have also been utilized for dynamic kinetic resolutions (DKRs), as Chi and coworkers has shown in 2016 with the DKR of α,α-disubstituted and activated esters, achieving up to 99% yield and >98% ee with NHC **41** (**Figure 1.2.5**).[43]

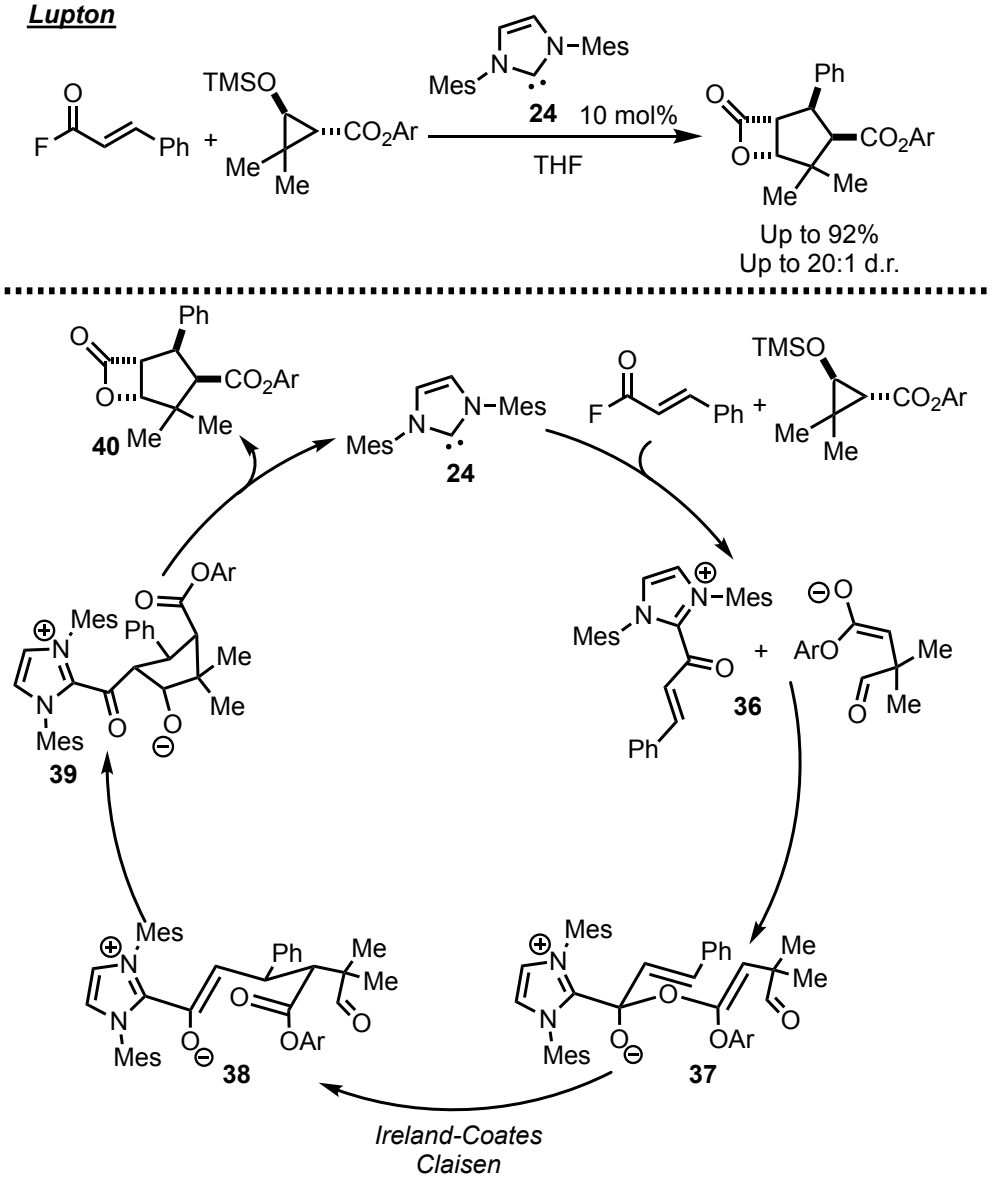

Figure 1.2.4. Lupton's synthesis of β-lactone fused cyclopentanes with the proposed mechanism.

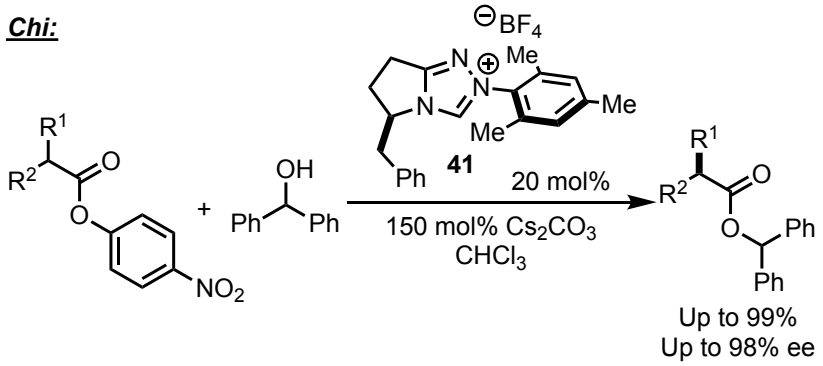

Figure 1.2.5. Chi's dynamic kinetic resolution of α,α-disubstituted and activated esters.

In the presence of a sufficiently strong base, acyl azolium intermediates may also be deprotonated at the α-position of the carbonyl to make azolium enolate intermediates. Alternatively, these intermediates may be formed directly from a variety of starting materials such as ketenes, α-reducible aldehydes, or enals.[44] Much like the aforementioned reactive pathways, these intermediates have been utilized for a number of powerful new synthetic methodologies. Some of these transformations include the formation of cycloaddition products, as well as asymmetric α-protonation and halogenation. In 2008, Ye and coworkers used NHC **42** to access this reactive pathway to catalyze the [4+2] cycloaddition of disubstituted ketenes with enones to produce γ-lactone products that bear α-quaternary and β-tertiary stereocenters (**Figure 1.2.6a**).[45] Our group has also developed a number of methods that proceed through these intermediates, such as in 2010 with our report of an asymmetric hydration of α,α-dichloro aldehydes and α-haloenals as catalyzed by NHC **43** (**Figure 1.2.6b**).[46] This process yields a diverse set of enantioenriched α-halocarboxylic acids with up to 95% yield and 96% ee.

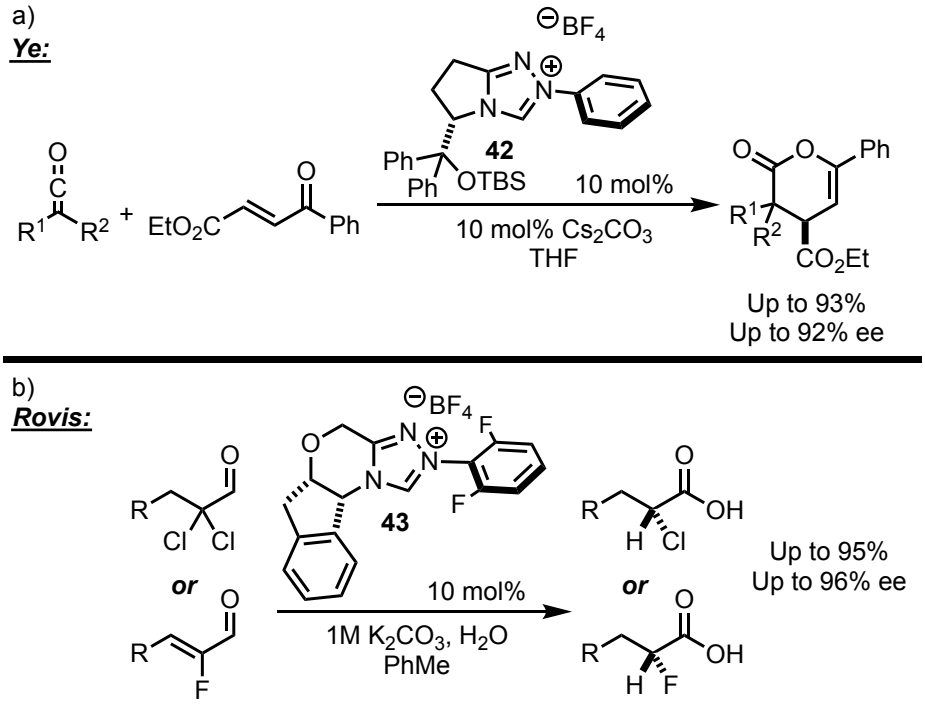

Figure 1.2.6. a) Ye's [4+2] cycloaddition of ketenes and α,β-unsaturated ketones. b) Rovis' asymmetric α-hydration of α-reducible aldehydes.

The aforementioned classes of reactions represent advances beyond what was thought to be conceivable during the time when the Stetter and benzoin reactions were still in their infancy. Looking forward, we can expect more reaction classes to emerge as we continue to increase our understanding of these complex catalytic systems. For instance, one very promising class of reactivity, yet still largely underexplored, merges single electron transfers (SET) with NHC catalysis.[47] Studer was the first to demonstrate the viability of this reaction pathway in 2008, showing that the Breslow intermediate may be oxidized to the radical cation by TEMPO before oxidizing twice to furnish an acyl azolium intermediate.[48] Significant effort geared towards trapping the radical cation before the second oxidation event immediately ensued, with some initial successes by the Chi and Ye groups.[49] The first asymmetric variant of this reactive pathway was disclosed concurrently by Chi's group, as well as our own, in 2014.[50] In our report, alkyl and aryl

α,β-unsaturated aldehydes undergo β-hydroxylation through an oxygen atom transfer from nitrobenzenes. Chi produces the same products, but with slightly different reaction conditions (**Figure 1.2.7**). Here, nitrobenzene first oxidizes the Breslow intermediate of the enal to the radical cation, which can then do a radical recombination at the β-position with an oxygen atom of the reduced nitrobenzene. We later found that the radical cation of the Breslow intermediate may recombine with another extended Breslow intermediate, both at the β-positions, to form cyclopentanone products.[51] Despite these successes, the challenge of controlling the single-electron oxidation of Breslow intermediates is still largely unmet and is sure to be the focus of a number of research groups in the near future.

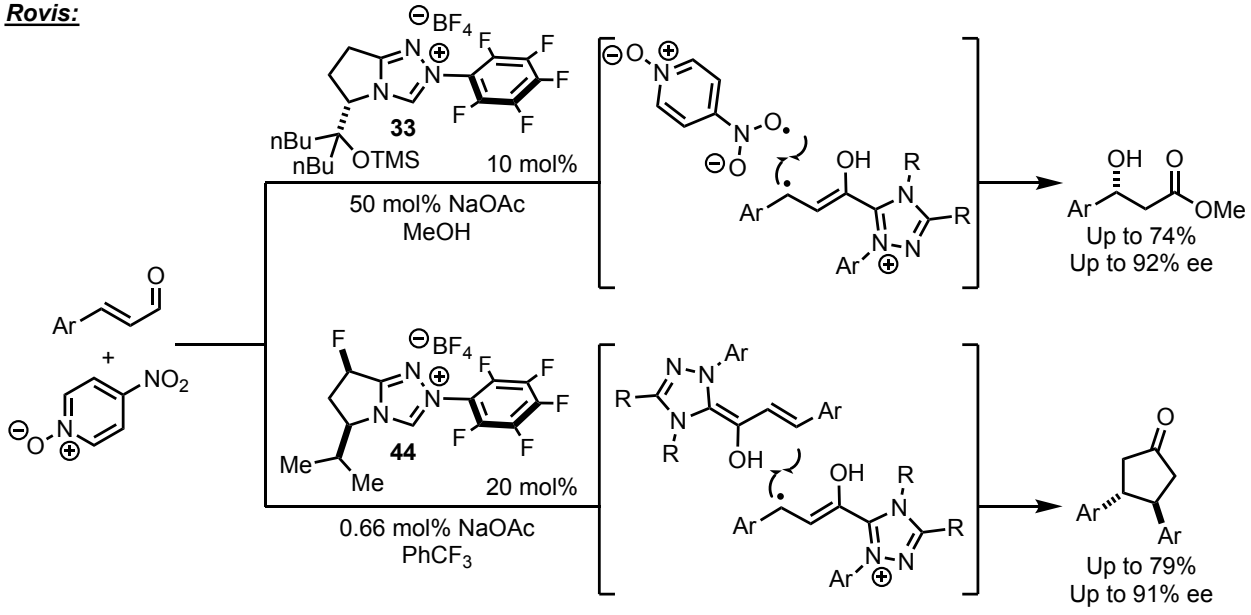

Figure 1.2.7. First known asymmetric NHC-catalyzed SET transformations for the synthesis of β-hydroxylated esters and cyclopentanones.

1.3 Outlook: Where Further Work Is Needed

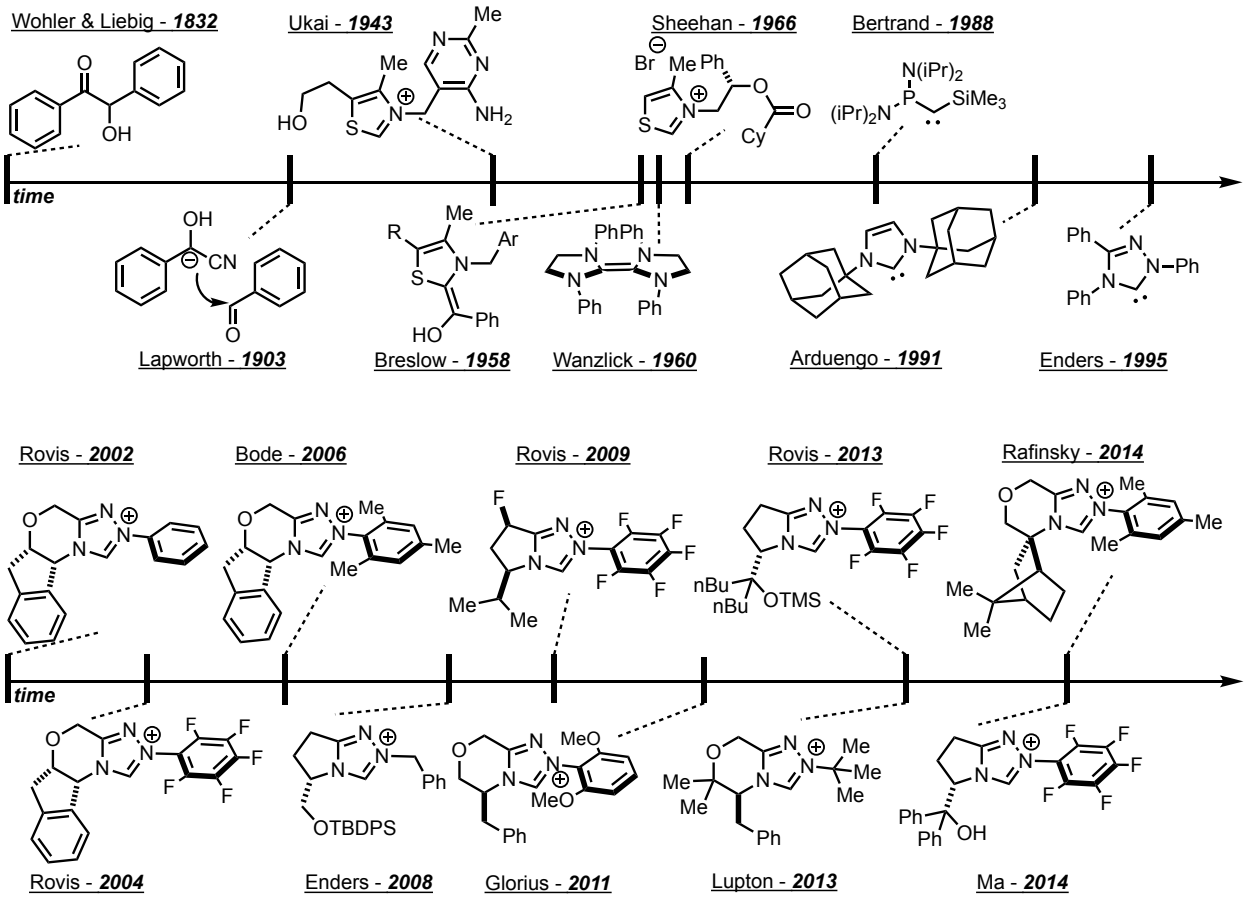

Figure 1.3.1. Timeline of NHCs.

Despite the tremendous advances in this field, it would be imprudent to say that it is anywhere near complete. For instance, a closer look at the second timeline in **Figure 1.3.1** reveals a different *N*-aryl substituent for different classes of reactivity. At the onset of our studies, the impact that the *N*-aryl group has upon reactivity was not well understood, as is made evident by the relative lack of research articles addressing this point.[52] Furthermore, it is unclear what role the backbone of the NHC has upon reactivity. There are currently over 50 unique triazolium-based NHC structures that are known.[12] Despite this structural wealth and diversity, there seems to be limited apparent benefits outside of the context of providing access to NHCs that originate from

different sources of chirality.[53] In this regard, we were unable to find any literature that explicitly addresses this point and provides a way to compare and contrast catalysts with different backbones for a given reaction. Also, out of all these known triazolium-based structures, there does not seem to be any one backbone structure that is either universally reactive or significantly outcompetes the rest of the series. We thus began to wonder what this hypothetical universal catalyst would look like, and what structural features would be needed to give this NHC a significant advantage over all others.

Herein we describe our three-pronged approach towards addressing these issues. The first describes our efforts toward the synthesis of a carboxylated triazolium-based NHCs, the synthesis of which was unknown at the start of our studies. In light of some recently attained experimental evidence, we believe that incorporation of a carboxylate onto the backbone of the catalyst would serve to decrease the energetic barrier for the turn-over limiting steps of acyl anion reactivity.[54] We hypothesized that this catalyst could represent the next evolutionary sequence in NHC catalysis. The second describes our efforts to parametrize the electronic effects that are imparted by the *N*-aryl substituent. We hypothesized that a data set that accurately describes and measures these perturbation effects could in turn be used to parameterize facets of reactivity, such as stereoselectivity or reactivity, regardless of reaction class. Such a data set could then be used to decrease the degree of serendipity that occurs when choosing an NHC for a given situation and would increase our fundamental understanding of these NHCs. The third is focused on parameterizing the steric and electronic effects that are imparted by the backbone of the NHC. Despite the numerous triazolium-based NHCs found in literature, such an approach, as far as we know, has never been attempted. Thus, disclosing a method that can quickly assess these effects may not only serve to increase our understanding of the interplay between the backbone of an NHC

and its reactivity, it may also shed insights into previously hidden or otherwise unaccounted-for effects that may be capitalized upon for future purposes. We will describe our results in this regard throughout the following chapters.

1.4 References

1) Arduengo, A. J.; Bertrand, G. *Chem. Rev.* **2009**, *109*, 3209–3210.
2) Hirai, K.; Itoh, T.; Tomioka, H. *Chem. Rev.* **2009**, *109*, 3275–3332.
3) Bourissou, D.; Guerret, O.; Gabbaï, F. P.; Bertrand G. *Chem. Rev.* **2000**, *100*, 39–92.
4) Hirai, K.; Itoh, T.; Tomioka, H. *Chem. Rev.* **2009**, *109*, 3275–3332.
5) Del Bene, J. E.; Alkorta, I.; Elguero, J. *J. Phys. Chem. A* **2017**, *121*, 8136–8146.
6) Krishnan, J.; Jose, A.; Sasidhar, B. S.; Suresh, E.; Menon, R. S.; Nair, V. *Org. Chem. Front.* **2018**, *5*, 1202–1208.
7) Hopkinson, M. N.; Richter, C; Schedler, M.; Glorius, F. *Nature* **2014**, *510*, 485–496.
8) Vora, H. U.; Rovis, T. *Aldrichimica Acta* **2011**, *44*, 3–11.
9) Díez-González, S.; Marion, N.; Nolan, S. P. *Chem. Rev.* **2009**, *109*, 3612–3676.
10) Soleilhavoup, M.; Bertrand G. *Acc. Chem. Res.* **2015**, *48*, 256–266.
11) Enders, D.; Niemeier, O.; Henseler, A. *Chem. Rev.* **2007**, *107*, 5606−5655.
12) Flanigan, D. M.; Romanov-Michailidis, F.; White, N. A.; Rovis, T. *Chem. Rev.* **2015**, *115*, 9307−9387.
13) Wohler, F.; Liebig, J. *Annalen der Pharmacie* **1832**, *3*, 249−282.
14) Lapworth, A. *J. Chem. Soc. Trans.* **1903**, *83*, 995−1005.
15) Ukai, T.; Tanaka, R.; Dokawa, T. *J. Pharm. Soc. Jpn.* **1943**, *63*, 296−300.
16) Breslow, R. *J. Am. Chem. Soc.* **1958**, *80*, 3719−3726.
17) Wanzlick, H. W.; Schikora, E. *Angew. Chem.* **1960**, *72*, 494.
18) (a) Lemal, D. M.; Lovald, R. A.; Kawano, K. I. *J. Am. Chem. Soc.* **1964**, *86*, 2518−2519. (b) Winberg, H. E.; Carnahan, J. E.; Coffman, D. D.; Brown, M. *J. Am. Chem. Soc.* **1965**,

87, 2055–2056. (c) Wiberg, N. *Angew. Chem., Int. Ed. Engl.* **1968**, *7*, 766. (d) Denk, M. K.; Hatano, K.; Ma, M. *Tetrahedron Lett.* **1999**, *40*, 2057−2060.

19) Sheehan, J. C.; Hunneman, D. H. *J. Am. Chem. Soc.* **1966**, *88*, 3666−3667.

20) Schönherr, H. J.; Wanzlick, H. W. *Liebigs Ann. Chem.* **1970**, *731*, 176−179.

21) Stetter, H.; Schrekenberg, M. *Angew. Chem. Int. Ed. Engl.* **1973**, *12*, 81.

22) Stetter, H.; Kuhlmann, H. *Chem. Ber.* **1976**, *109*, 2890−2896.

23) (a) Sheehan, J. C.; Hunneman, D. H. *J. Am. Chem. Soc.* **1966**, *88*, 3666−3667. (b) Sheehan, J. C.; Hara, T. *J. Org. Chem.* **1974**, *39*, 1196−1199. (c) Tagaki, W.; Tamura, Y.; Yano, Y. *Bull. Chem. Soc. Jpn.* **1980**, *53*, 478−480.

24) Igau, A.; Grutzmacher, H.; Baceiredo, A.; Bertrand, G. *J. Am. Chem. Soc.* **1988**, *110*, 6463−6466.

25) Pauling, L. J. *Chem. Soc., Chem. Commun.* **1980**, *0*, 688−689.

26) Arduengo, A. J.; Harlow, R. L.; Kline, M. *J. Am. Chem. Soc.* **1991**, *113*, 361−363.

27) Enders, D.; Breuer. K.; Raabe, G.; Runsink. J.; Teles, J. H.; Melder, J. P.; Ebel, K.; Brode, S. *Angew. Chem. Int. Ed. Engl.* **1995**, *34*, 1021−1023.

28) Ciganek, E. *Synthesis* **1995**, 1311−1314.

29) Enders, D.; Breuer, K.; Teles, J. H. *Helv. Chim Acta* **1996**, *79*, 1217−1221.

30) Enders, D.; Breuer, K.; Runsink, J.; Teles, J. H. *Helv. Chim Acta* **1996**, *79*, 1899−1902.

31) Knight, R. L.; Leeper, F. J. *J. Chem. Soc., Perkin Trans. 1*, **1998**, 1891−1893.

32) Kerr, M.; Read de Alaniz, J.; Rovis, T. *J. Am. Chem. Soc.* **2002**, *124*, 10298−10299.

33) Rovis, T. *Chem. Lett.* **2008**, *37*, 2−7.

34) (a) Jang, K. P.; Hutson, G. E.; Johnston, R. C.; McCusker, E. O.; Cheong, P. H. Y.; Scheidt, K. A. *J. Am. Chem. Soc.* **2014**, *136*, 76−79. (b) Chen, X.-Y.; Sun, L.-H.; Ye, S. *Chem. Eur. J.* **2013**, *19*, 4441−4445.

35) Nair, V.; Vellalath, S.; Poonoth, M.; Suresh, E. *J. Am. Chem. Soc.* **2006**, *128*, 8736 – 8737.

36) Menon, R. S.; Biju, A. T.; Nair, V. *Chem. Soc. Rev.* **2015**, *44*, 5040−5052.

37) He, M.; Struble, J. R.; Bode, J. W. *J. Am. Chem. Soc.* **2006**, *128*, 8418–8420.

38) Chiang, P. C.; Kaeobamrung, J.; Bode, J. W. *J. Am. Chem. Soc.* **2007**, *129*, 3520–3521.

39) Mahatthananchai, J.; Bode, J. W. *Chem. Sci.* **2012**, *3*, 192−197.

40) White, N. A.; DiRocco, D. A.; Rovis, T. *J. Am. Chem. Soc.* **2013**, *135*, 8504–8507.

41) Zhang, C.; Hooper, J. F.; Lupton, D. W. *ACS Catal.* **2017**, *7*, 2583–2596.

42) Candish, L.; Lupton, D. W. *J. Am. Chem. Soc.* **2013**, *135*, 58–61.

43) Chen, X.; Fong, J. Z. M.; Xu, J.; Mou, C.; Lu, Y.; Yang, S.; Song, B. A.; Robin Chi, Y. *J. Am. Chem. Soc.* **2016**, *138*, 7212–7215.

44) Douglas, J.; Churchill, G.; Smith, A. D. *Synthesis* **2012**, *44*, 2295−2309.

45) Zhang, Y. R.; Lv, H.; Zhou, D.; Ye, S. *Chem. Eur. J.* **2008**, *14*, 8473−8476.

46) Vora, H. U.; Rovis, T. *J. Am. Chem. Soc.* **2010**, *132*, 2860–2861.

47) Zhao, K.; Enders, D. *Angew. Chem. Int. Ed.* **2017**, *56*, 3754−3756.

48) Guin, J.; Sarkar, S. D.; Grimme, S.; Studer, A. *Angew. Chem. Int. Ed.* **2008**, *47*, 8727−8730.

49) (a) Du, Y.; Wang, W.; Li, X.; Shao, Y.; Li, G.; Webster, R. D.; Robin Chi, Y. *Org. Lett.* **2014**, *16*, 5678–5681. (b) Yang, W.; Hu, W.; Dong, X.; Li, X.; Sun, J. *Angew. Chem. Int.*

Ed. **2016**, *55*, 15783−15786. (c) Wang, Y.; Du, Y.; Huang, X.; Wu, X.; Zhang, Y.; Yang, S.; Robin Chi, Y. *Org. Lett.* **2017**, *19*, 632–635.

50) (a) White, N. A.; Rovis, T. *J. Am. Chem. Soc.* **2014**, *136*, 14674–14677. (b) Zhang, Y.; Du, Y.; Huang, Z.; Xu, J.; Wu, X.; Wang, Y.; Wang, M.; Yang, S.; Webster, R. D.; Robin Chi, Y. *J. Am. Chem. Soc.* **2015**, *137*, 2416–2419.

51) White, N. A.; Rovis, T. *J. Am. Chem. Soc.* **2015**, *137*, 10112–10115.

52) (a) Rovis, T. *Chem. Lett.* **2008**, *37*, 2−7. (b) Mahatthananchai, J.; Bode, J. W. *Chem. Sci.* **2012**, *3*, 192−197. (c) Collett, C. J.; Massey, R. S.; Maguire, O. R.; Batsanov, A. S.; O'Donoghue, A.C.; Smith, A. D. *Chem. Sci.* **2013**, *4*, 1514−1522. (d) Massey, R. S.; Collett, C. J.; Lindsay, A. G.; Smith, A. D.; O'Donoghue, A. C. *J. Am. Chem. Soc.* **2012**, *134*, 20421−20432.

53) (a) Brand, J. P.; Siles, J. I. O.; Waser, J. *Synlett* **2010**, *6*, 881−884. (b) Rong, Z. Q.; Li, Y.; Yang, G. Q.; You, S.L. *Synlett* **2011**, *7*, 1033−1037. (c) Rafiński, Z.; Kozakiewicz, A.; Rafińska, K. *ACS Catal.* **2014**, *4*, 1404−1408. (d) Ozboya, K. E.; Rovis, T. *Synlett* **2014**, *25*, 2665−2668.

54) DiRocco, D. A.; Rovis, T. *J. Am. Chem. Soc.* **2011**, *133*, 10402–10405.

Chapter 2. The Development of Novel Carboxylate-Containing NHCs.

2.1 Introduction

As was seen in the previous chapter, a structural evolution of the carbenes used as organocatalysts was necessary to achieve more robust and stereoselective transformations. As a consequence of this evolution, new classes of reactivity that extend beyond the umpolung of aldehydes were made accessible.[1] This trend continues to exist today, as access to newer and more improved NHCs results in both improvements in reactivity as well as granting access to nascent and promising classes of reactivity. Thus, an improvement in the tools available for catalysis will naturally lead to an improvement in the transformations catalyzed by these species. As for NHCs and their role as organocatalysts, there are still many areas across different reaction classes that leave much to be desired. In the Stetter reaction there is a rather strict electronic requirement for the participating Michael acceptor. Here, the Michael acceptor must be sufficiently electron deficient to accept a Breslow nucleophile. Participating Michael acceptors for the intermolecular Stetter reaction are shown in **Figure 2.1.1**, where the least electronically activated substrate was published by Glorius and coworkers in 2012.[2] In comparing the catalyst used for this transformation to the previous ones in this figure, the *N*-aryl substituent features a strongly electron-donating 2,6-dimethoxyphenyl group. Although this substrate indeed represents the least activated coupling partner for the intermolecular Stetter reaction, it employs one of the most nucleophilic triazolium-based NHCs. Furthermore, with respect to general NHC limitations, typical catalyst loadings for these reactions tend to range anywhere from 5 – 25 mol%, which is much higher relative to commonplace transition-metal complexes used for catalysis.

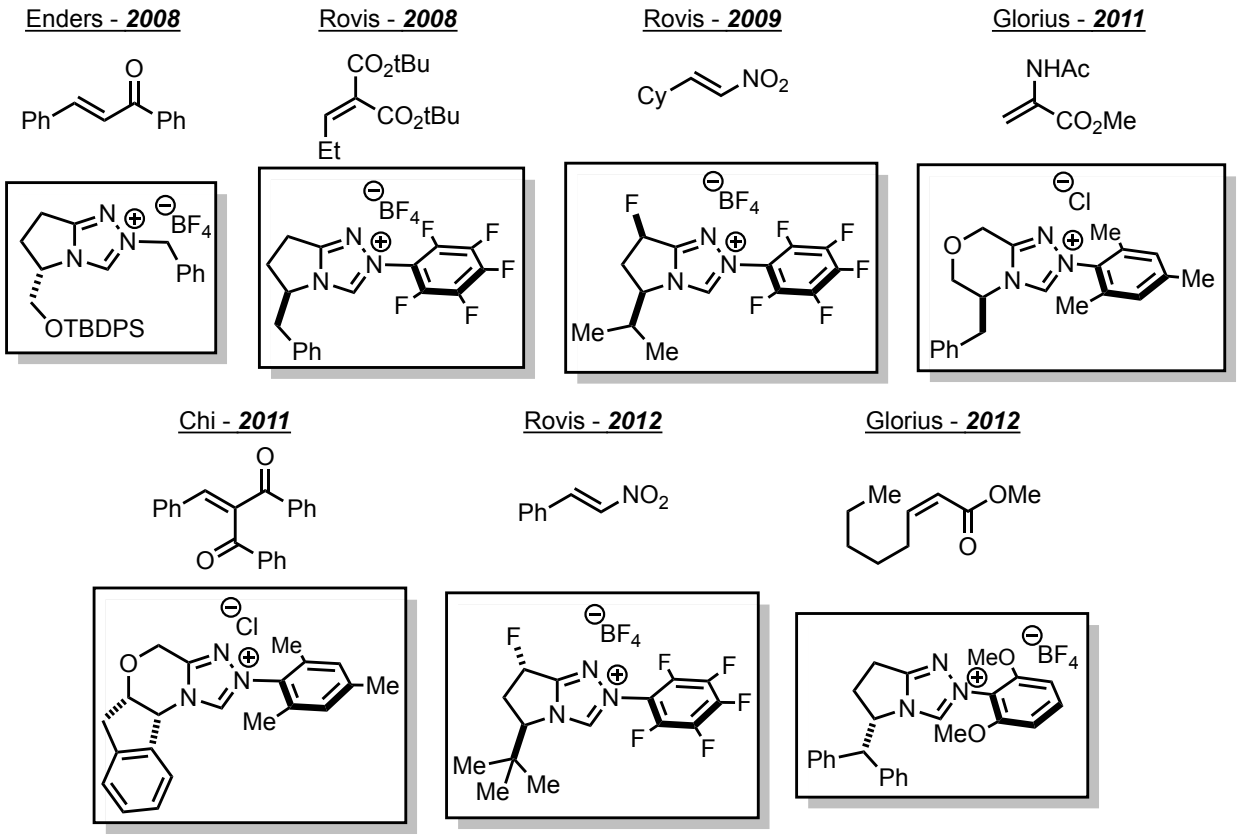

Figure 2.1.1. Michael acceptors previously employed for the intermolecular Stetter reaction.

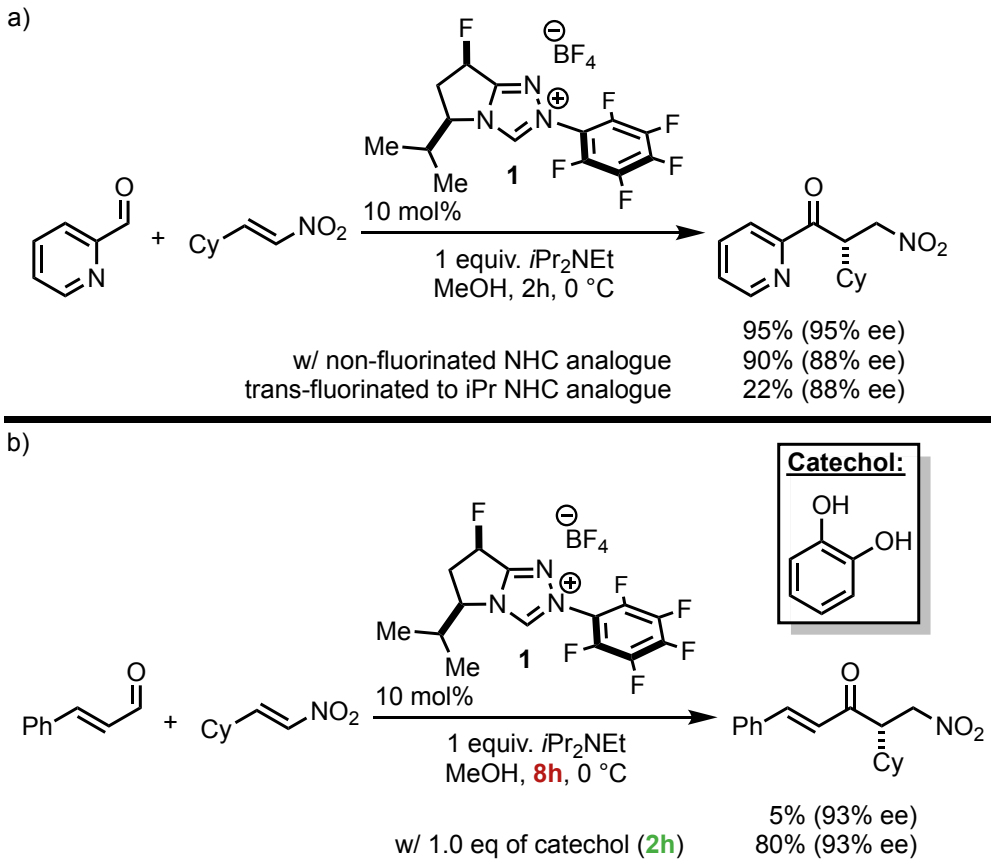

Figure 2.1.2. a) Intermolecular Stetter reaction between heteroaryl aldehydes and aliphatic nitroalkenes. b) Catechol-assisted intermolecular Stetter reaction between α,β-unsaturated aldehydes and aliphatic nitroalkenes.

In light of these points, we began to think of ways to address these apparent limitations. Since it was ultimately a deeper understanding of the fundamental properties of carbenes that led way to the advent of triazolium-based NHCs, we turned to the literature for examples of highly efficient NHC-catalyzed systems to help guide us. In 2009, our group discovered that adding a fluorine atom to the backbone of the pyrrolidine-based NHC **1** improves the selectivity of the asymmetric intermolecular Stetter reaction between heterocyclic aryl aldehydes and nitroalkenes (**Figure 2.1.2a**).[3] The presence of fluorine is thought to help stabilize the developing charges on the incoming electrophile through a series of net-attractive interactions.[4] An apparent limitation to this transformation is its requirement of a heteroatom in close proximity to the carbonyl group of

the aldehyde. There are two reasons proposed for this requirement: 1) the heteroatom reduces $A^{1,3}$-strain in the formation of the Breslow intermediate, and 2) a lone-pair on the heteroatom plays a role in assisting with the proton-transfer step, thought to be the rate-limiting step for Stetter-type transformations. In consideration of these points, it was reasoned that α,β-unsaturated aldehydes may be good coupling partners for the same reaction. This notion led to the discovery of the intermolecular Stetter reaction between enals and nitroalkenes (**Figure 2.1.2b**).[5] The initial yield was below 10%, but the enantiomeric excess (ee) was promising. Comparing this reaction to the previous one, the steric component was satisfied because this Breslow intermediate does not possess much in the way of $A^{1,3}$-strain, but assistance in the 1,2-proton transfer event was non-existent. Exogenous protic additives were thus introduced to attempt to satisfy this criterion. It was found that the introduction of 1.0 equivalent of catechol resulted in both dramatically increased yields and decreased reaction times. Without catechol, the reaction proceeded to 5% yield and 93% ee in 8 hours – in the presence of catechol, the reaction proceeded to 80% yield and 93% ee in only 2 hours. Here, the active species of this protic additive was proposed to be a catecholate monoanion. It is believed that in this monodeprotonated state, catechol is able to act as a proton shuttle through an eight-membered transition state. By shuttling a proton back and forth from the catecholate to the tetrahedral intermediate, the energetic requirement for this step is thought to be greatly reduced, allowing for a much more reactive system (**Figure 2.1.3a**). For further evidence in this regard, a ^2H kinetic isotope effect study was performed using cinnamaldehyde and its deuterated isotopologue. The reactions were performed in either methanol or methanol-d_4. The k_H/k_D value was found to be 4.2 when run in methanol-d_4 and 2.7 when run in non-deuterated methanol (**Figure 2.1.3b**). These data suggest that the initial proton transfer to form the acyl anion intermediate is turnover-limiting in this mechanism.

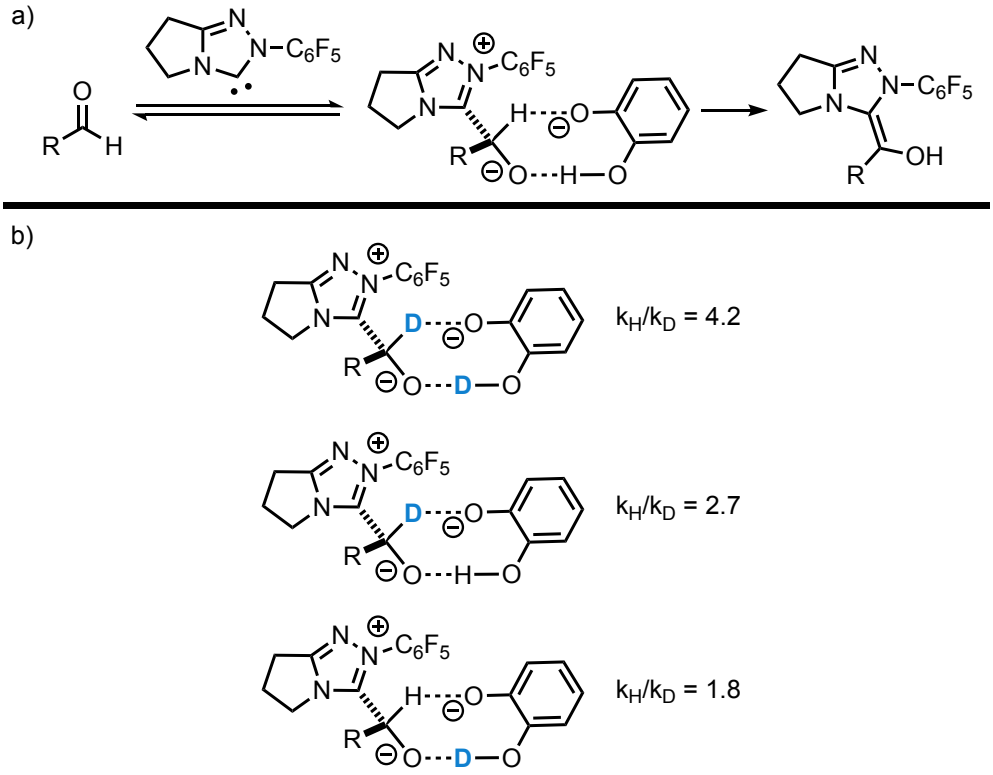

Figure 2.1.3. a) Proposed eight-membered transition state for assistance in the 1,2-proton transfer. b) ^{2}H-Kinetic isotope effect studies suggesting the role of catechol in in the rate-limiting step.

The facilitation of the rate-limiting proton transfer event may also be used to render other Stetter systems more reactive (**Figure 2.1.4**). For instance, in the intramolecular Stetter reaction of salicylaldehyde-derived substrate **3** with 0.1 mol% of NHC **2**, the presence of 0.2 mol% of catechol allows the reaction to proceed to completion in eight hours, where this low catalyst loading without the presence of catechol only goes to 34% in the same time frame. These results indicate that lowering the energy required for the 1,2-proton shift towards the formation of the Breslow intermediate may have a broad range of implications towards umpolung-themed catalysis. This prospect excited us and led us to study these Stetter systems more closely.

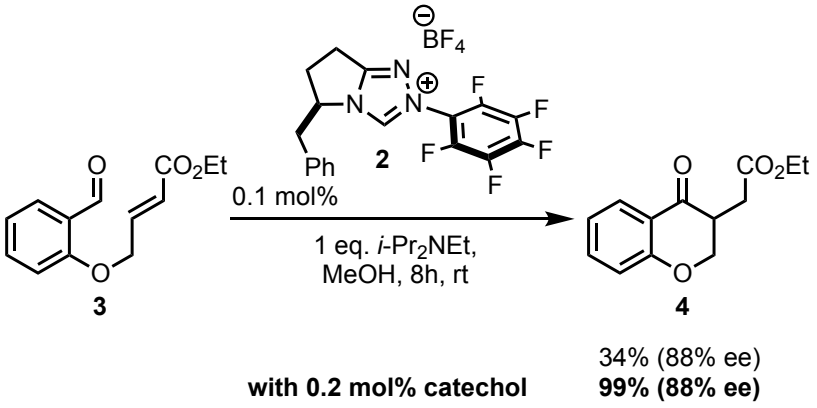

Figure 2.1.4. Effect of catechol on intramolecular Stetter system.

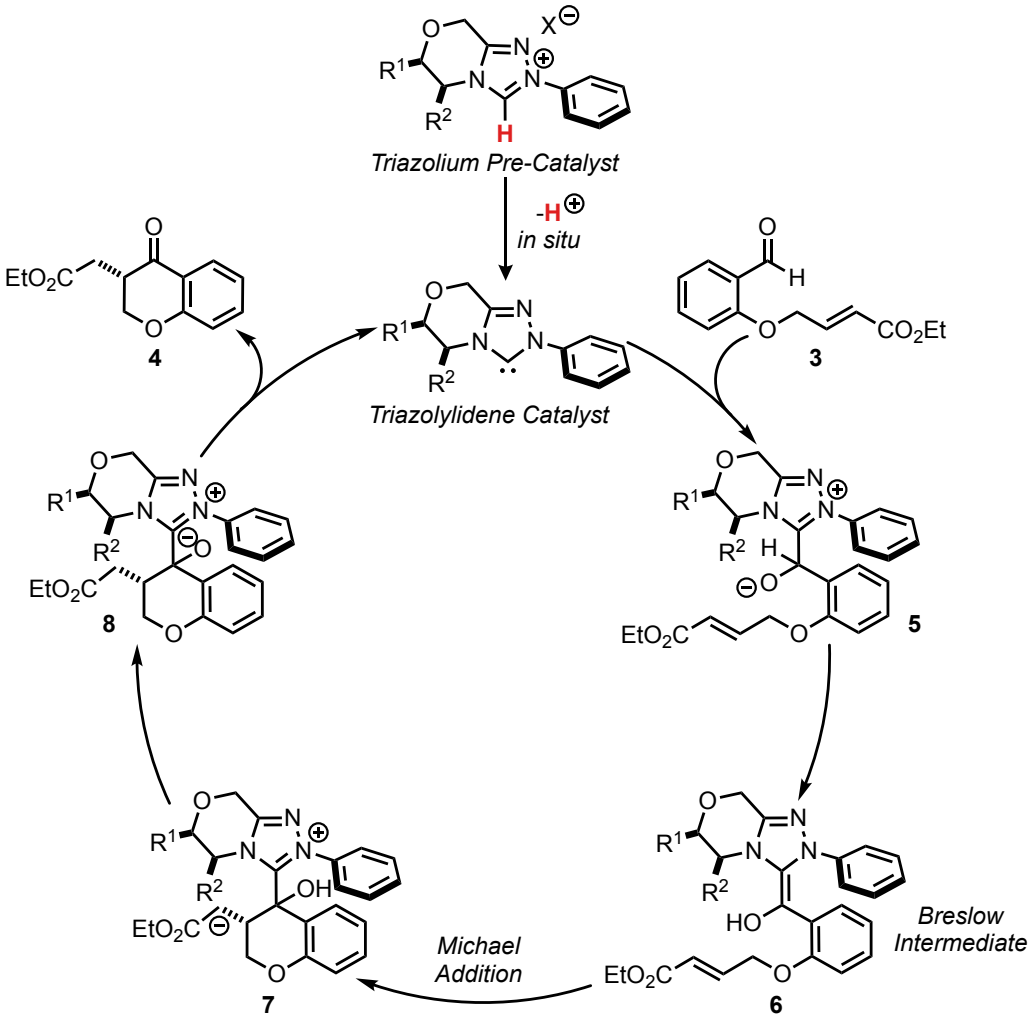

Figure 2.1.5. Mechanism for the intramolecular Stetter reaction.

In the same year, our group performed a series of mechanistic investigations on the intramolecular Stetter system.[6] As a brief recap of the corresponding mechanism, first the triazolium precatalyst is deprotonated *in-situ* to liberate the carbene, which then adds to substrate **3** to form the tetrahedral intermediate **5** (**Figure 2.1.5**). Intermediate **5** then undergoes a formal 1,2-proton transfer to form the Breslow intermediate **6**, which is now nucleophilic at the aldehydic carbonyl. This can conjugately add to the tethered Michael acceptor to form the secondary tetrahedral intermediate **8**. The electron density on the newly formed alkoxide then collapses to form both product **4** and regenerate the active form of the catalyst. In this manuscript, a series of competition experiments were described that implicate the 1,2-proton transfer to be the first energetically significant step in the reaction. In the competition experiment between substrate **3** and **9**, where **9** has a σ-withdrawing chlorine at the *meta*-position relative to the carbonyl, substrate **3** reacts 0.099 times as fast as substrate **9** (**Figure 2.1.6a**). This result is to be expected because the chlorine renders the aldehyde more electrophilic and thus more susceptible to nucleophilic attack from the carbene. In the competition experiment between substrate **3** and substrate **10**, where **10** has a strongly π-donating methoxy group at the *para*-position relative to the carbonyl, **3** is shown to react 7.7 times faster than **10** (**Figure 2.1.6b**). This result also makes sense because the methoxy group serves to render the carbonyl less electrophilic and thus less reactive. By the logic of the two former cases, we note that the phenolic oxygen in substrate **3** is in an ortho position relative to the aldehyde. In this position, this oxygen may serve to decrease the electrophilicity of the carbonyl in substrate **3**. Thus, we can conclude that in the competition between substrate **3** and **11**, that of which has no π-donor at the *ortho*-position, substrate **11** should in theory be faster. This hypothesis turns out to not be the case, where substrate **3** is faster than **11** by about 10.4 times (**Figure 2.1.6c**). What is thought here is that the phenolic oxygen is non-innocent in the rate limiting 1,2-proton

transfer, where this oxygen may be Lewis basic enough to assist in the deprotonation of the tetrahedral intermediate *en route* to the Breslow intermediate (**Figure 2.1.7**). In light of these results, and of the apparent benefits of adding catechol in the aforementioned intermolecular Stetter system, we postulated that the incorporation of a reactive moiety onto the backbone of the catalyst that mimicked the action of catechol could similarly benefit these Stetter-type systems. As opposed to having an exogeneous equivalent of catechol in the reaction system, a catalyst that could perform a similar proton-shuttling intramolecularly may increase the catalyst reactivity even more by way of reducing a bimolecular event to a unimolecular one. Such a catalyst could potentially represent the next evolutionary sequence in NHCs used for organocatalysis.

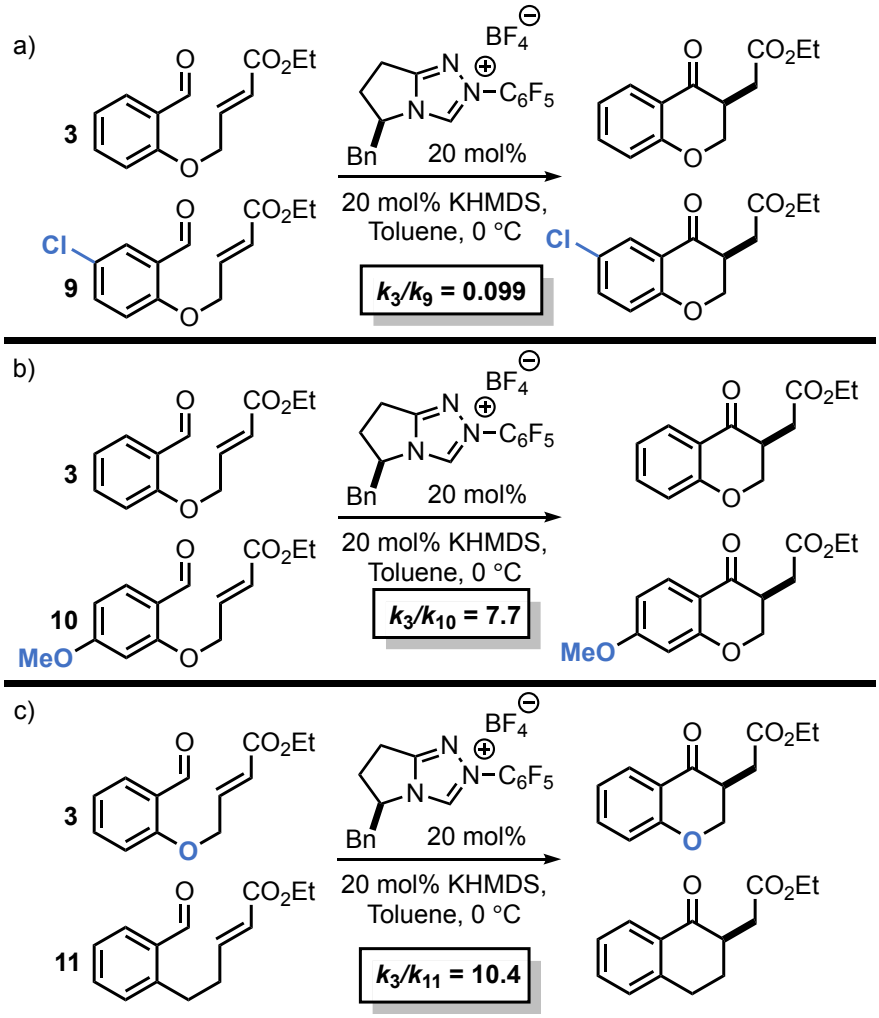

Figure 2.1.6. Competition experiments implicating the involvement of the phenolic oxygen in substrate **3** in the rate-determining step for the intramolecular Stetter reaction.

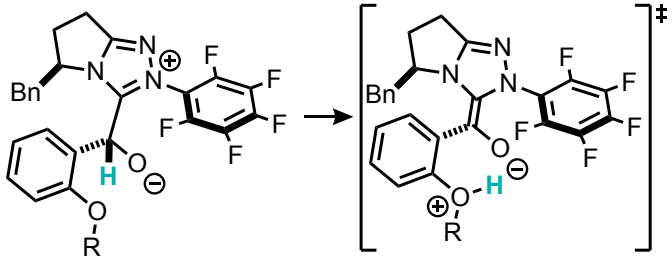

Figure 2.1.7. Potential role of the phenolic oxygen in substrate **3** in assisting the 1,2-proton transfer.

Our group has previously made several attempts to synthesize a catalyst with this goal in mind. We initially hypothesized that simply installing a catechol moiety onto the carbene

framework should deliver a more reactive catalyst. Thus, several triazolium pre-catalysts that feature either catechol or pyridyl groups were synthesized by a number of former group members (**Figure 2.1.8a**). These NHCs were not restricted to cyclic triazoliums, as thiazolium based and acyclic triazolium catalysts, both of which are quicker to synthesize, were also synthesized. Pyridyl-tethered NHCs **14** and **15** were also synthesized in the hopes of mimicking the heteroatom effect described earlier. Unfortunately, the carbenes with pyridyl motifs offered little to no advantage relative to typical triazolium-based NHCs in the reaction. The installation of a catechol moiety, as in catalyst **16**, resulted in decomposition of the precatalyst to a hydroxyl-tethered NHC and an *ortho*-quinone methide (**Figure 2.1.8b**). This hydroxylated catalyst unfortunately delivers no apparent additional benefit to Stetter-type systems.

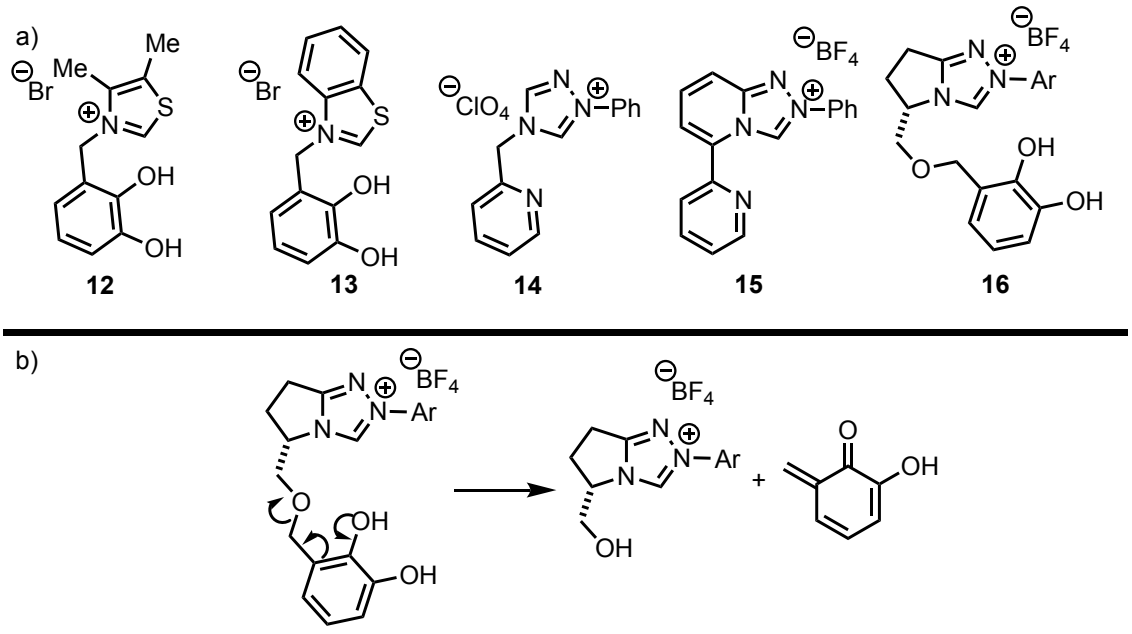

Figure 2.1.8. a) Previously synthesized NHCs for the purposes of intramolecular rate-acceleration. b) Decomposition pathway of catechol-containing NHC **16**.

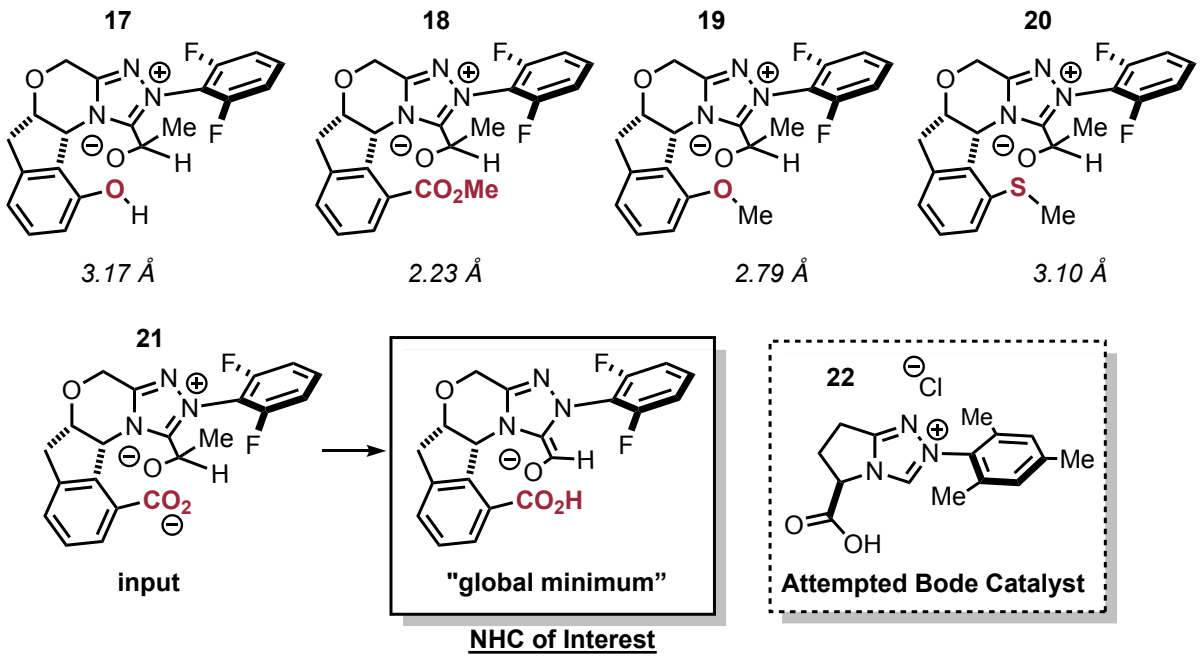

Figure 2.1.9. Calculated NHCs featuring proposed non-innocent features and Bode's attempted NHC **22**.

To better rationalize which catalysts were worth the time and effort to synthesize, we computationally evaluated various several NHC-structures to identify scaffolds that can mimic the effect of catetchol (**Figure 2.1.9**). In these calculations, a tetrahedral intermediate was input as the initial structure. Ground state optimizations using the B3LYP functionality and 6-311G basis set would then shed insight into the influence that a reactive side handle could exert upon the tetrahedral intermediate. For instance, a closer distance of the non-innocent structural feature to the reactive center could imply an interaction between them. As a result of these computations, it was determined that a well-placed carboxylate, such as the one in NHC **21**, could also facilitate the proton transfer. With this structure, the tetrahedral intermediate input converges directly to the Breslow intermediate, regardless of the input structure. This result suggests that strategic placement of a carboxylic acid on the backbone of an NHC may destabilize the tetrahedral intermediate to the point where the Breslow intermediate is the closest energetic minimum. Furthermore, this result implied to us that the carboxylate may be assisting in the 1,2-proton

transfer much to the point that the energetic barrier for the formation of the Breslow intermediate becomes negligible. If we could synthesize a carboxylated catalyst that significantly lowers the energetic requirement for the rate-limiting step of the Stetter reaction, we could potentially provide access a catalyst with superior reactivity, and perhaps selectivity, as compared to other more commonly used NHCs. It is worth noting at this point that, despite the existence of many unique triazolium-based NHCs, no structures are known that possess a tethered carboxylic acid moiety. Bode and coworkers have previously made attempts to synthesize the proline-derived carboxylated NHC **22**, but failed due to unavoidable epimerization at the stereogenic center of the NHC.[7] Herein we propose the first successful synthesis of these structurally novel NHCs and describe their reactivities with respect to the Stetter reaction.

2.2 Aminoindanol and Aryl Carboxylated NHCs – Attempted Synthesis

We have proposed and attempted several synthetic routes to catalysts with strategically placed carboxylates, as suggested by our calculations. The earliest implemented strategy toward the synthesis of catalyst **29** is listed in **Figure 2.2.1**. The goal here was to use a directed ortho-lithiation strategy using racemic 1-indanol **23** as the starting material. Dehydration was achieved during the work-up step, producing the desired indene product **24** in 14% yield. Esterification in methanol and thionyl chloride produced the methyl ester **25**, which can then be easily epoxidized by *m*-chloroperoxybenzoic acid (mCPBA). Esterification was deemed necessary for ease of future handling. Treatment of epoxide **26** with triflic acid in acetonitrile initiated a Ritter reaction pathway to afford the esterified aminoindanol **27**.[8] The next step involved treatment with ethyl chloroacetate and sodium hydride in THF, resulting in the formation of morpholinone **28**.[9] From here, following known steps in the synthesis of triazolium salt pre-catalysts should result in the

methyl ester version of the catalyst. Subsequent treatment with lithium hydroxide will have then result in the deprotected anionic carboxylate. Quenching this saponification step with fluoroboric acid may then yield racemic carboxylated catalyst **29**.

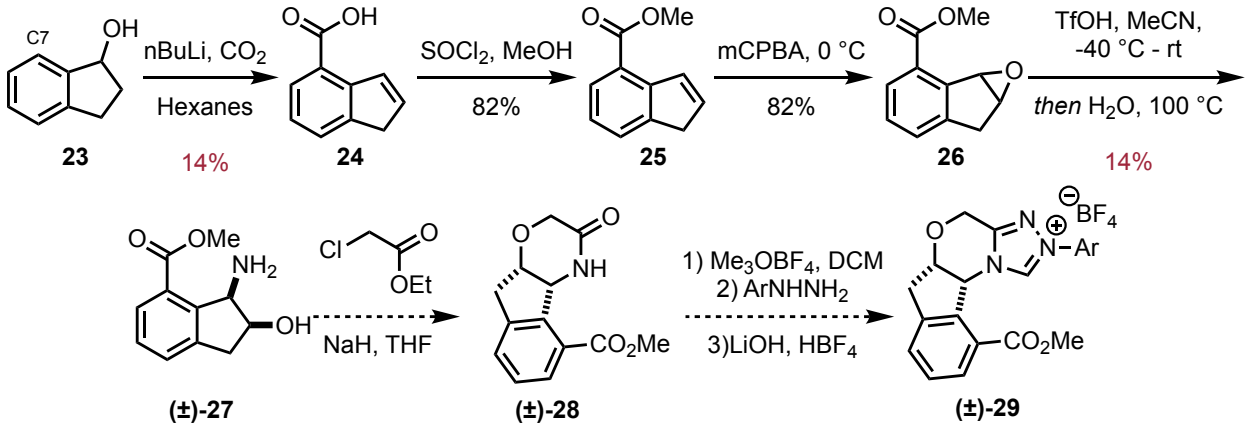

Figure 2.2.1. First synthetic route for the synthesis of proposed NHC **29**.

There were several problems with this approach. To start, the highest recovered yield obtained with the directed lithiation step was 14%, the average actually being somewhere around 8-10%. There is likely several potential reasons for this. An ^{1}H-NMR spectrum of the unpurified reaction mixture with an internal standard indicated a maximum yield of 25-30%. The directed ortho-lithiation step is most likely challenging due to the position of the hydroxyl moiety on the indane ring. The alkoxy-coordinated lithium base likely lies outside of the plane of the C7 proton, reducing the amount of effective molecular orbital overlap that drives directed-ortho lithiations forward. Aside from this, the acidic nature of the work up produces a mixture of olefinic isomers which are may be separated by column chromatography. Unfortunately, all attempts at reducing the degree of olefin isomerization were met with no success. The next most problematic step was the Ritter sequence. The presence of the carboxylic ester presented a couple of problems. In the second part of the Ritter sequence, hydrolysis of the complex in **Figure 2.2.2** requires strong

heating and acidic aqueous conditions. These conditions led primarily to the free acid first, upon which hydrolysis of **26-int** to the aminoindanol would ensue. All attempts at a second esterification protocol led to significant product decomposition. Any variation of the methyl ester to different esters were also met with little to no improvement at this step. Oddly enough, several attempts at isolating the product failed. The deprotected ester was later isolated as the triflate salt, but the yield of this reaction was quite abysmal at 14%. At this point, in consideration of the relative cost of 1-indanol, this route was abandoned.

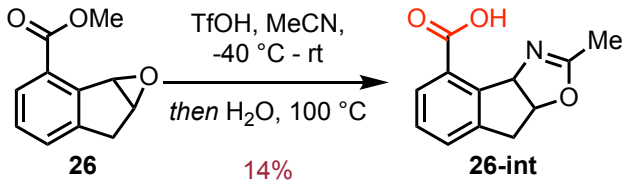

Figure 2.2.2. Ritter sequence toward the synthesis of NHC **29**.

Another route, along with its enantioselective variant, for the synthesis of catalyst **29** was devised (**Figure 2.2.3**). Here we chose to start with cheap and commercially available 2-bromobenzoic acid. Treatment of compound **30** with thionyl chloride affords the acid halide, which is then treated with ethylene gas in aluminum trichloride to initiate an intramolecular Friedel-Crafts alkylation to form the indenone intermediate **31**. Reduction with $NaBH_4$ and subsequent treatment with pyridinium *p*-toluenesulfonate (PPTS) would then afford brominated indene **32**, which would then go through an epoxidation, Ritter,[10] and cyclization sequence to compound **34**. After this, a lithium-halogen exchange and electrophilic trapping of CO_2 strategy would be employed to obtain the carboxylated morpholinone **28**. It was thought that the presence of a bromine atom instead of a carboxylic acid or ester would address the problems encountered with the aforementioned route. A key feature of this route is the PPTS dehydration step, which was purported to inhibit double

bond isomerization of indenes. Unfortunately, upon executing this synthetic route, this supposition turned out to be incorrect. Indeed, a model study with indanol **23** displayed no improvement to the degree of double bond isomerization relative to all previous attempts. Due to the problems associated with the synthesis of carboxylated morpholinone **29**, the target catalyst was changed to **42**.

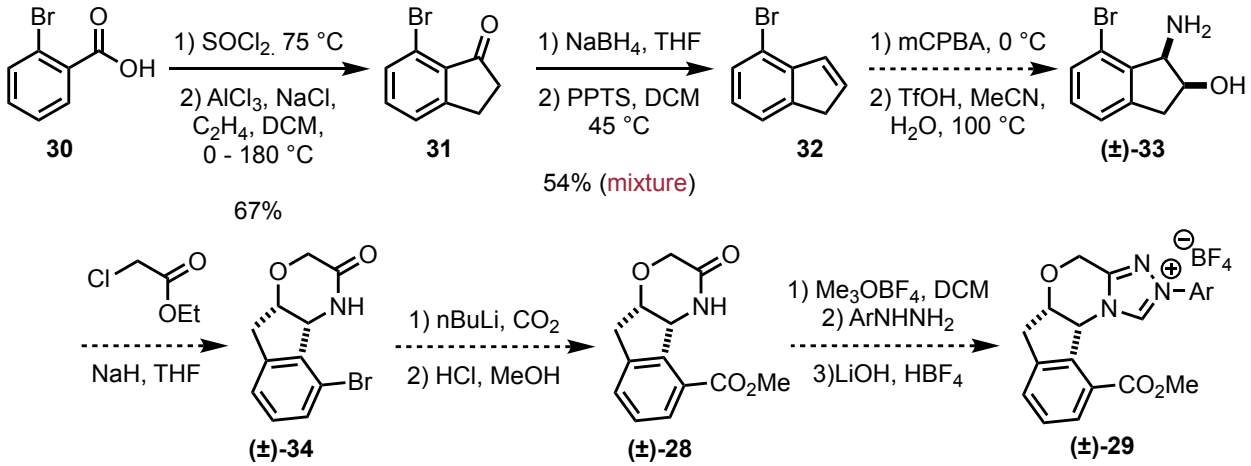

Figure 2.2.3. Second synthetic route for the synthesis of proposed NHC **29.**

With catalyst **42**, we started our synthesis with cheap and commercially available L-phenylglycine (**Figure 2.2.4**). Reduction of the carboxylic acid with $NaBH_4$ in I_2 produces aminoalcohol **36**, upon which amidation with picolinic acid would produce amide **37**. The purpose of this step was to install a directing group for a C–H activation protocol which would permit the installation of a bromine at one of the *ortho*-positions of the arene, a strategy inspired by Chen and coworkers.[11] After this step, deprotection of the amide and a late-stage cyclization/lithium-halogen exchange sequence, as described above, would be targeted. Unfortunately, there were immediately several issues with this route. The step that presented the most difficulty was the Pd-catalyzed C–H activation step. No reactivity was seen with substrate **37**, most likely due to catalyst inhibition

by way of tridentate ligand coordination of substrate **37** to Pd. This problem was fixed by acyl protecting the alcohol moiety, but a new problem presented itself. Regioselectivity at the *ortho*-position was easy to achieve, but unfortunately bromination at both *ortho*-positions to product **45** was something that, despite several modifications to the substrate, could not be fixed. A closer look at Chen's reaction protocol clarified this result. The majority of his substrates were ortho-substituted (**Figure 2.2.5**), leaving only one *ortho* site to be brominated. Furthermore, another issue with this route was the inability to cyclize either mono or dibrominated **38** to morpholinone **39**, a problem that will be revisited later (*vide infra*). In light of these issues, a new route to synthesize catalyst **42** was devised.

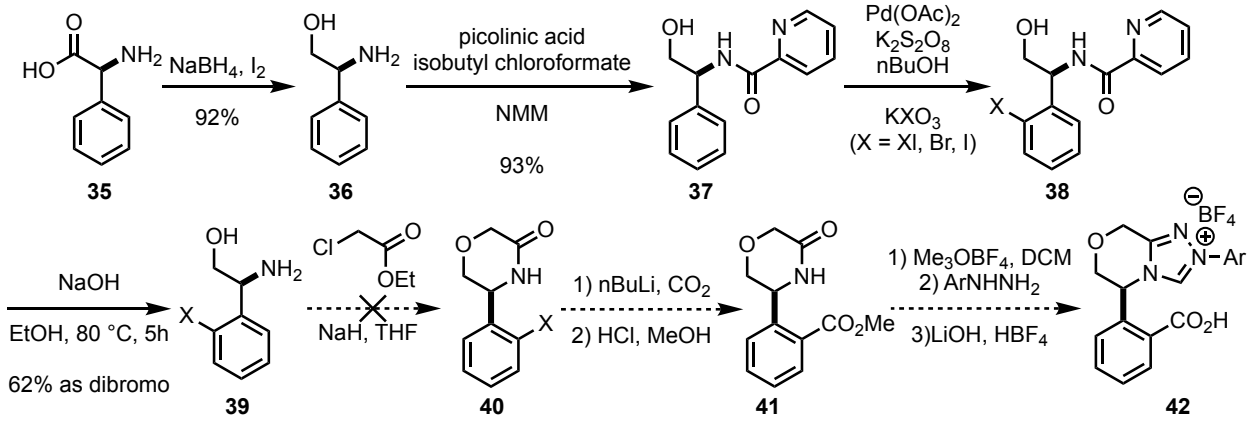

Figure 2.2.4. Synthetic route for the synthesis of proposed NHC **42**.

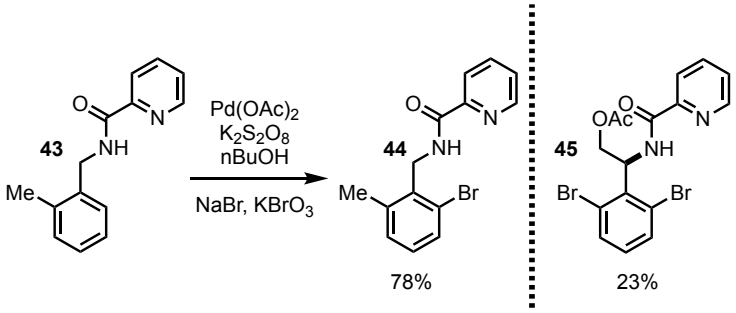

Figure 2.2.5. Sample from Chen's C-H activation strategy.

Inspired by Chen's strategy, we wondered if we could activate the C7 position of morpholinone **46** without needing to install an exogenous directing group. Thus, we hypothesized that perhaps the activated amide **47**, which is synthesized via *O*-methylation with trimethyloxonium tetrafluoroborate, could act as a directing group for the functionalization of this position via a directed *ortho*-lithiation strategy (**Figure 2.2.6**). A brief MM2 analysis on the structure of the activated amide **47** implied that there is a close enough proximity, planarity requirement notwithstanding, to the desired C7 position for the molecule to engage in a directed deprotonation. In implementing this strategy with several organolithium bases and electrophiles, the most encouraging result was obtained when CO_2 was used as the electrophile with *t*BuLi as the base. LCMS and NMR analysis suggested < 10% formation of the desired product. Unfortunately, in consideration of the unreliable nature of this transformation coupled with the instability of the imino ether moiety of substrate **47**, this plan was abandoned.

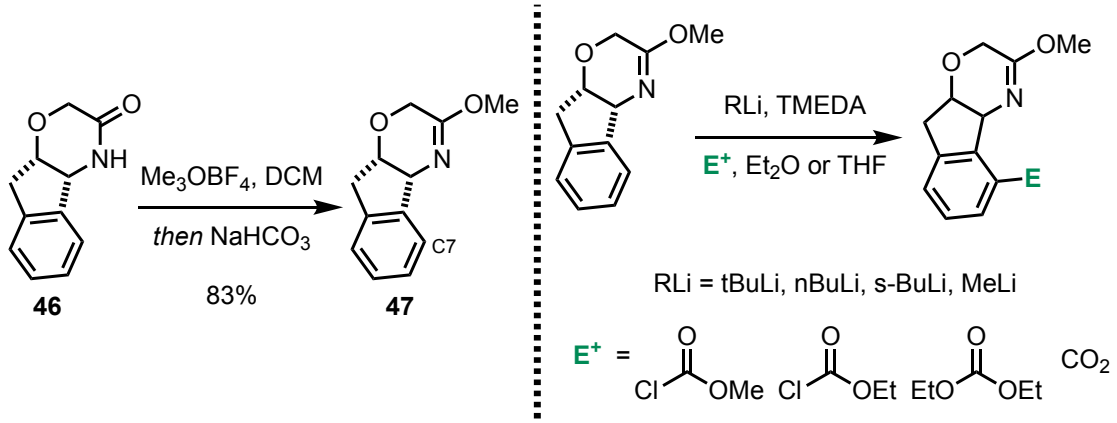

Figure 2.2.6. Attempts at activating C-H bond of C7 carbon on morpholinone **46**.

New routes for the synthesis catalyst **42** were devised (**Figure 2.2.7**). This second strategy begins with commercially available 2-bromobenzaldehyde. A Wittig olefination sequence was performed to form 2-bromostyrene **48**, followed by epoxidation to form styryl oxide **49**. Treatment

with sodium azide and a subsequent Staudinger reduction produces aminoalcohol **51**. The synthesis of morpholinone **52** was achieved by isolating the S_N2 product first, followed by isolation and purification, and then intramolecularly cyclizing the amine to the ester with the pure material, solving our previous problems with this step. Following this step, synthesis of the brominated catalyst **53** was relatively straight-forward. The reduction of the triazolium core to a triazoline is quite reliable and proceeds in good yields.[12] Unfortunately, all attempts to trap CO_2 using a lithium-halogen exchange strategy to synthesize triazoline **54** was met with failure. This ultimately led to the abandonment to any and all routes that started with 2-bromobenzaldehyde.

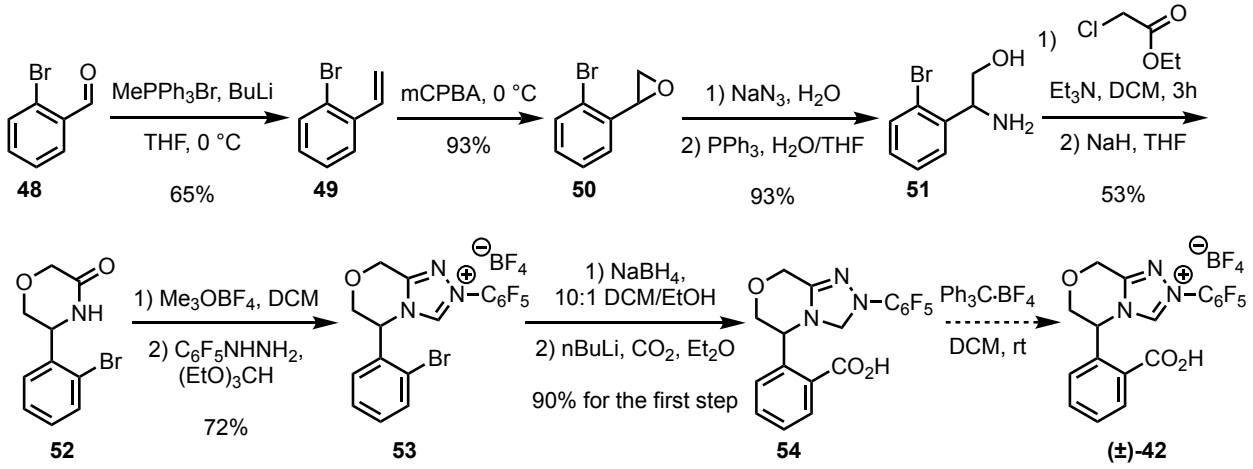

Figure 2.2.7. Proposed synthetic route for the synthesis of racemic NHC **42**.

2.3 Glutamic Acid Derived Carboxylated NHCs – Synthesis and Characterization

In searching for a more synthetically accessible carboxylated NHC-precursor that has a similar distance between the carboxylate and the carbene as the one in the calculated structure **21**, we chose to synthesize NHC **61**. Here, **61** would come from L-glutamic acid, which is ideal for obtaining an enantioenriched catalyst with minimal effort as well. Our first proposed route started from commercially available L-Glu(OtBu)OH **55** (**Figure 2.3.1**). Fmoc protection would afford

56, which would then be reduced to alcohol **57** after making the mixed anhydride with isobutyl chloroformate. Fmoc deprotection to the aminoalcohol **58** would follow. From here, cyclization to morpholinone **59** would follow using a new set of conditions. From here, cyclization to set the triazolium core using known conditions would follow. The *t*-butyl group was proposed to be cleaved at the last cyclization step, where an excess of fluoroboric acid could be used to deprotect the ester and catalyze the trimethyl orthoformate cyclization in a single pot.

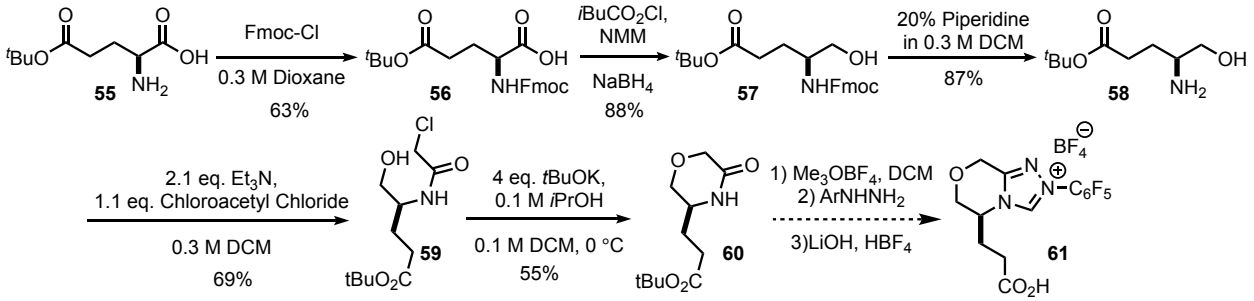

Figure 2.3.1. Proposed synthetic route for the synthesis of carboxylated NHC **61.**

Initially, all attempts to synthesize morpholinone **60** from ethyl chloroformate showed significant amounts of product decomposition. According to UPLC-MS traces, the side products constituted largely of oligomers. To fix this problem, the reaction conditions were changed again, where aminoalcohol **58** was first treated with chloroacetyl chloride to make the amide, and then subsequent intramolecular S_N2 cyclization would furnish the desired morpholinone **60**. A second and perhaps more significant issue arose at this point, where the *t*-butyl ester decomposed to a variety of products under the trimethyloxonium tetreafluoroborate conditions (**Figure 2.3.2**). The desired imino ether functionality was formed in some products, but each methylation sequence forms one equivalent of fluoroboric acid. This acid is strong enough to deprotect the *t*-butyl ester, where the resultant carboxylic acid can then stay as the acid and undergo another formation of the

imino ether, or it can methylate at the recently liberated ester to form a methyl ester. Assuming there is enough unreacted trimethyloxonium tetrafluoroborate in the reaction, the methyl ester can then undergo amide activation to the imino ether. Signature ^{1}H-NMR peaks for all of these side products were detected and their existence was further confirmed via UPLC-MS. All attempts to convert the starting material to the desired methyl ester imino ether in one pot were met with varying degrees of failure.

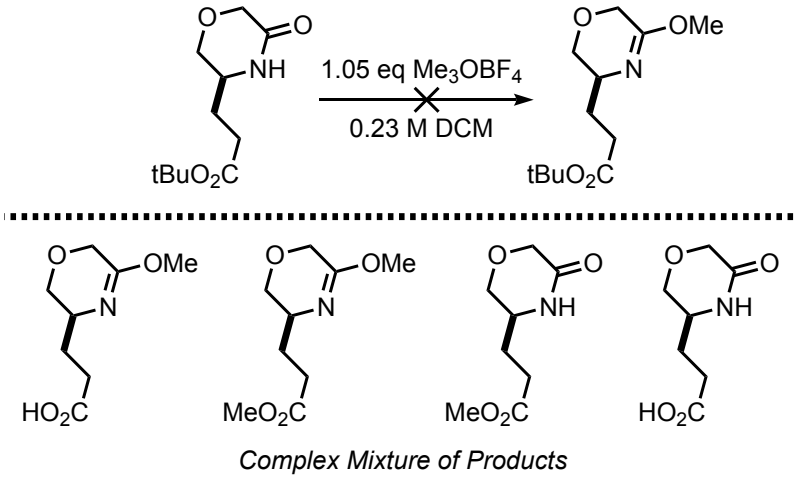

Figure 2.3.2. Decomposition pathways for the first step towards setting the triazolium core of **61.**

To solve this, we chose to change our starting material to commercially available Boc-L-Glu(OBn)OH **62** (**Figure 2.3.3**). Here, the reduction procedure is the same as in above. The Boc-group was deprotected using 0.3 M of 1:1 TFA/DCM to produce aminoalcohol **64**. The same two-step cyclization to set the morpholinone core as described above was successfully utilized here. From here, standard conditions to set the triazolium core of NHC **61** would follow. Ideally, the benzyl ester would be deprotected to the acid using H_2/Pd conditions. We would again run into some minor issues with our route, where the benzyl ester protected amide **65** would decompose under the subsequent reaction conditions (**Figure 2.3.4**). The lability of the benzyl ester was

surprising, but nonetheless was ultimately responsible for substrate decomposition and unproductive product formation. All optimization attempts to render this path viable were largely met with failure.

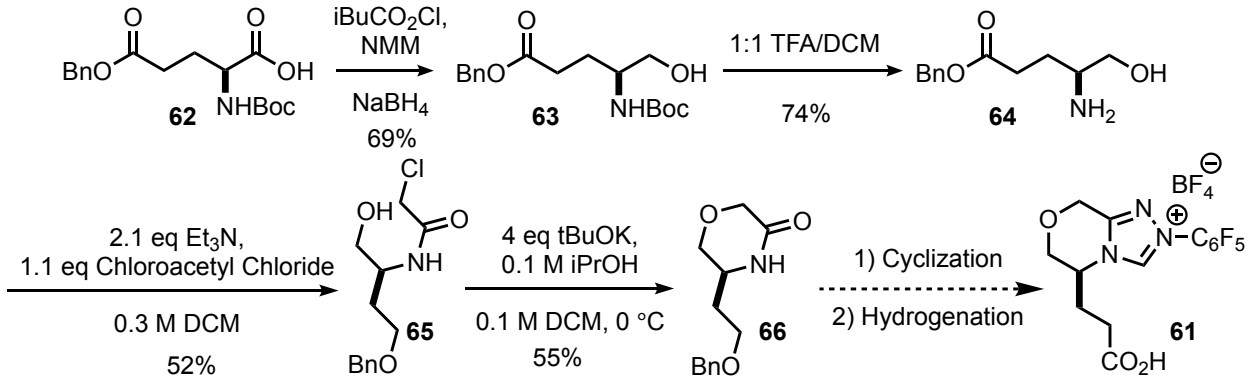

Figure 2.3.3. Second proposed synthetic route for the synthesis of carboxylated NHC **61**.

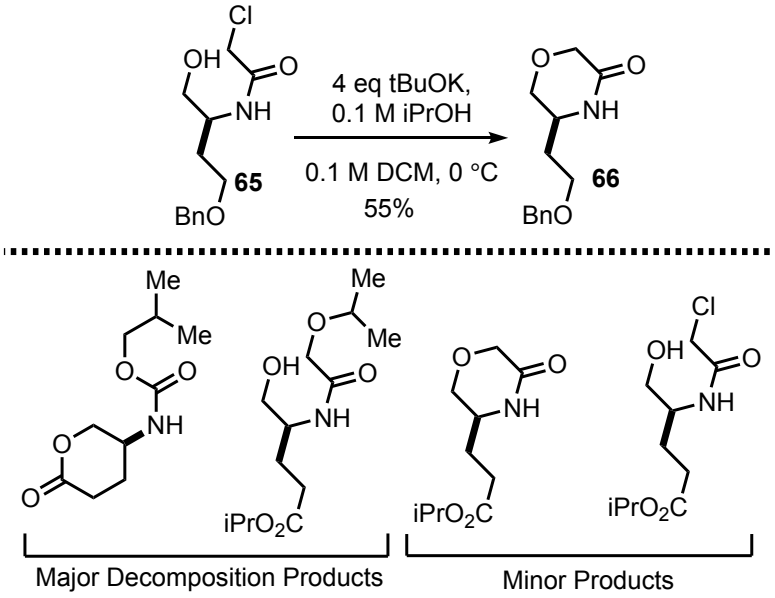

Figure 2.3.4. Decomposition products for the cyclization of **65** to **66**.

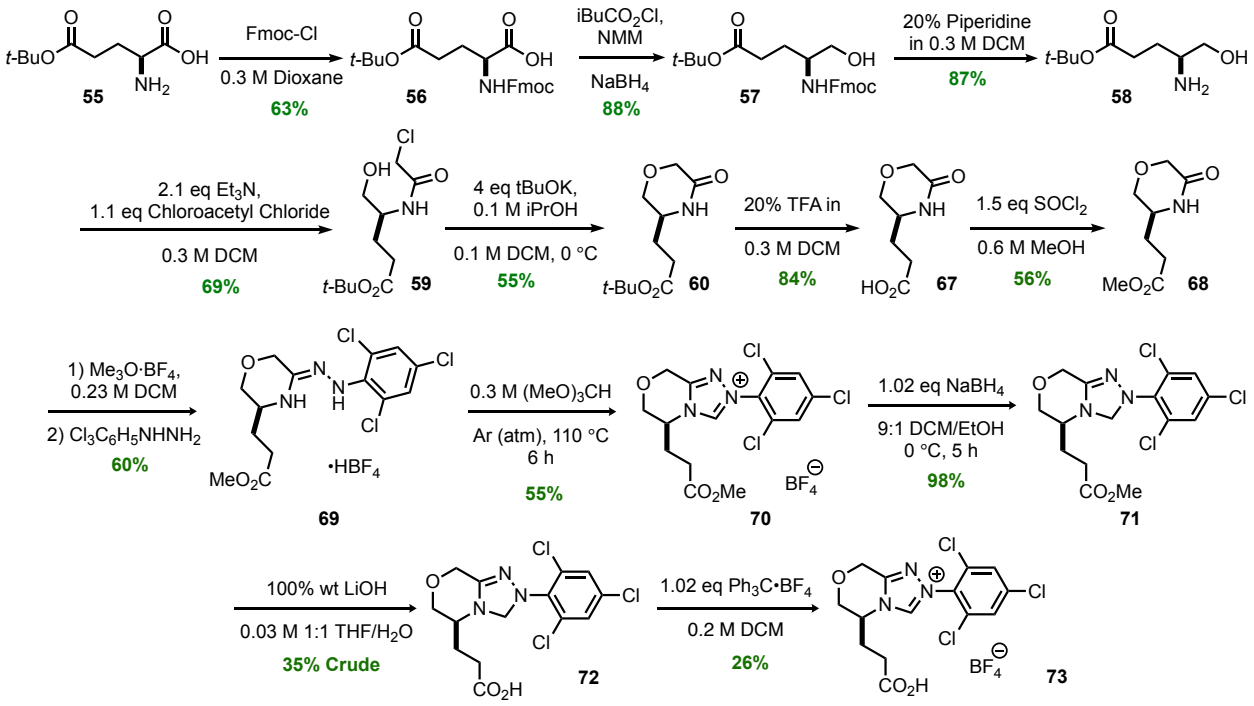

Figure 2.3.5. Third proposed synthetic route for the synthesis of carboxylated NHC **73**.

As such, we turned our attention back to L-Glu(OtBu)OH **55**. Here, we would follow much of the same procedure as was originally described in **Figure 2.3.1** towards morpholinone **60**. In this updated synthesis, the *t*-butyl ester was deprotected in 20% TFA in DCM and then re-protected to the methyl ester **68** (**Figure 2.3.5**). At this point we opted to proceed forward with trichlorophenyl hydrazine for the *N*-aryl substituent, since these NHCs tend to be more crystalline and easier to handle. An important yet subtle point in this synthesis is the use of trimethyl orthoformate for the final triazolium-setting cyclization step. We noticed that using triethyl orthoformate provided a mixture of both methyl and ethyl ester products, which then proved difficult to purify. As such, we were able to synthesize the methyl ester protected NHC **70** easily. From here, we chose to employ a reduction-manipulation-oxidation strategy as was disclosed by a former group member.[12] Reduction of the triazolium core to a triazoline proceeded in 98% yield. The next step, after significant optimization, was elected to be a LiOH-mediated saponification.

This step produced the crude carboxylic acid **72**, which was then oxidized using triphenylcarbenium tetrafluoroborate to produce, for the first time, our desired carboxylated NHC **73**. Shortly afterward, we were able to synthesize two other carboxylated NHC variants, pentafluorophenyl-substituted NHC **61** in 30% overall yield at the final step, and mesityl-substituted NHC **74** in 16% yield at the final step (**Figure 2.3.6**).

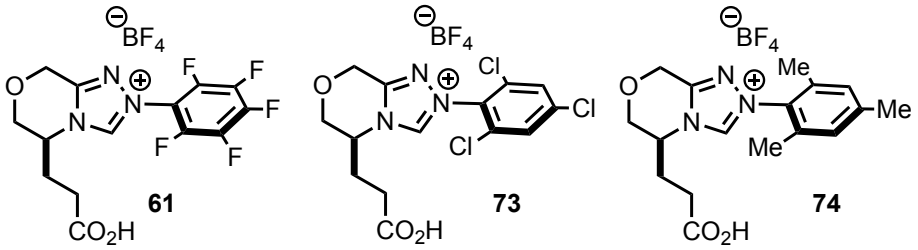

Figure 2.3.6. Carboxylated NHCs made available using synthetic route outlined in Figure 2.3.5.

An NMR spectrum for pentafluorophenyl-substituted NHC is shown in **Figure 2.3.7**. In deuterated acetonitrile referenced to δ 1.94 ppm, the proton of the triazolium core shows up at δ 9.89 ppm and the proton of carboxylic acid shows up at δ 9.21 ppm. The methylene protons lying between the azolium core and the oxygen of the secondary ring lie at 5.12 ppm and exist as a doublet of doublets. The methyne proton on the secondary ring exists as a multiplet at 4.74 ppm. The second pair of methylene protons are found at 4.15 ppm, also existing as a doublet of doublet of doublets. The protons on the alkyl chain are found as a triplet and a multiplet at 2.54 ppm and 2.30 ppm, respectively. The structure for this NHC was unambiguously assigned by X-ray crystallography (**Figure 2.3.8**). It is worth noting that the proton of the carboxylic acid was easy to detect in the crystal structure. This finding would shed some insight into its reactivity during the course of some later experiments, where the kinetic acidity of this proton would later be discovered to be abnormally high.

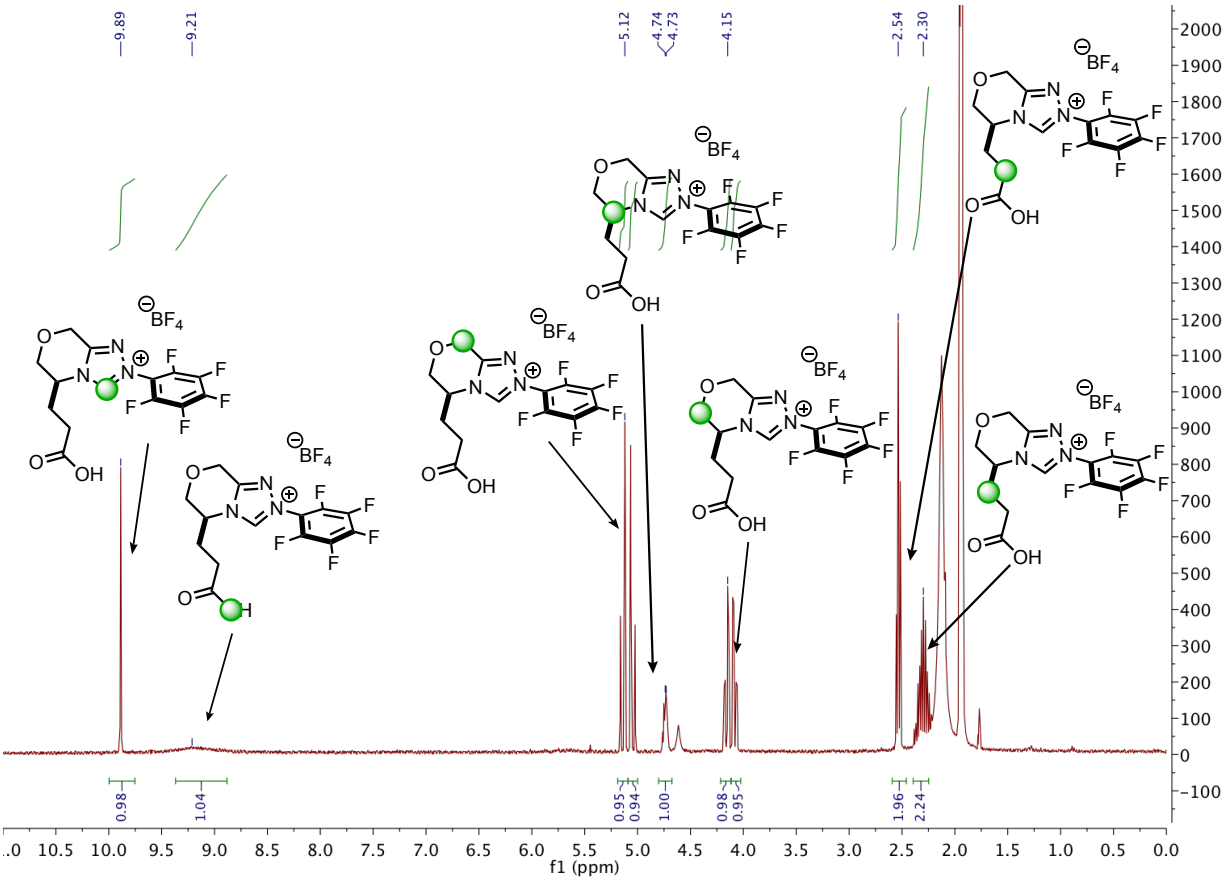

Figure 2.3.7. ^{1}H-NMR Spectrum in MeCN-D_3 for carboxylated NHC **61.**

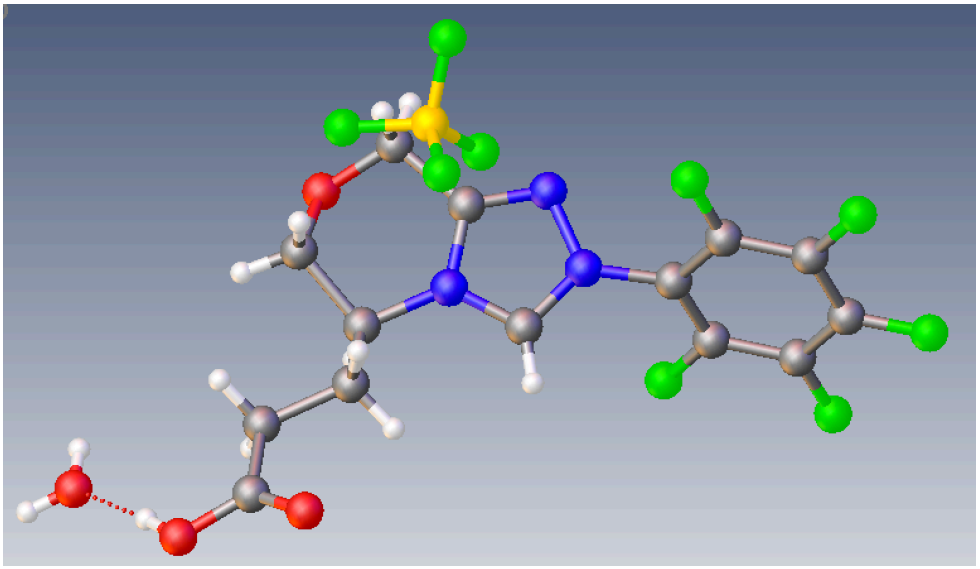

Figure 2.3.8. Crystal structure of NHC **61.**

At this point, we wished to analyze the deprotonated forms of NHC **61**. What separates this NHC from others is the existence of two acidic sites, namely the proton of the carboxylic acid and the proton of the triazolium core. First principles dictate that the proton of the carboxylic acid should be more acidic, but the identity upon first deprotonation may vary even if this is the case. For instance, deprotonating the carboxylic acid leads to a carboxylate. Sodium acetate has been shown to be sufficiently basic enough to deprotonate electronically analogous NHCs.[13] Thus, it would stand to reason that this carboxylate may serve to interact with the acidic proton of the azolium core. Furthermore, we wondered how full deprotonation would affect the proton signals on the NHC. The first experiment we performed in this regard was to treat the carboxylated NHC **61** with 1.0 equivalent of Proton Sponge. Here, we thought that the proton sponge base would be sufficiently basic enough to deprotonate the carboxylic acid selectively. Model studies with other pentafluorophenyl-substituted NHCs in the presence of proton sponge agree with this assessment, where the proton signal for the triazolium proton is left largely intact. In our case, we see a complete disappearance of both the triazolium peak and the carboxylic acid peak in the ^{1}H-NMR spectrum (**Figure 2.3.9**). VT-NMR studies were performed at this point, and what is found is that the proton signal for the azolium peak coalesces to δ 11.3 ppm at about -40 °C. This result suggests that the proximal carboxylate interacts significantly with the proton of the azolium core and that in the monodeprotonated form, the NHC exists as a zwitterion with the carboxylate tightly H-bonded to the proton of the azolium core. Unfortunately, all attempts at monitoring the fully deprotonated form of the NHC led to significant catalyst decomposition. We have yet to detect the fully deprotonated NHC species.

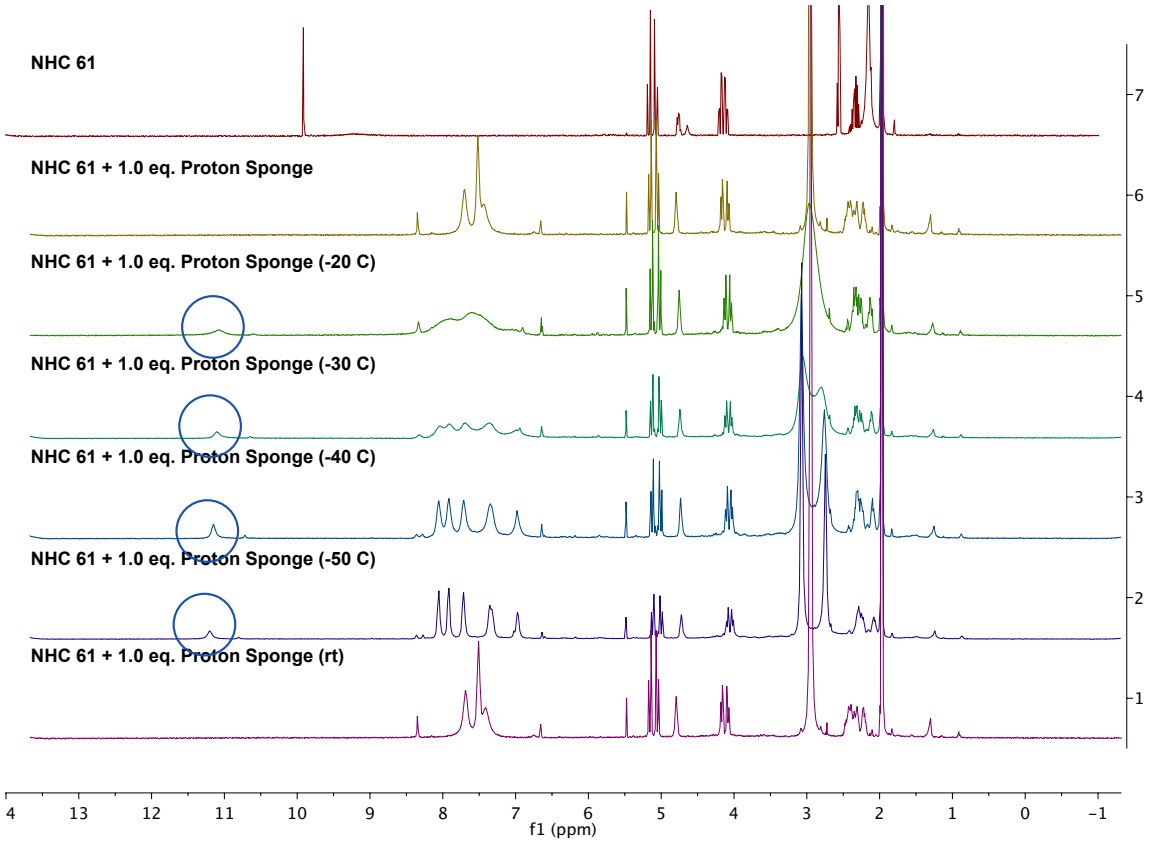

Figure 2.3.9. VT-NMR Spectra in MeCN-D_3 for carboxylated NHC **61** showing coalescence of proton at -50 °C.

2.4 Examining Carboxylated NHC Reactivity with The Intramolecular Stetter Reaction

After having synthesized the carboxylated NHC, we wished to assess their performance as compared to other NHCs in the intramolecular Stetter reaction (**Figure 2.4.1**). For these experiments, we chose the pentafluorophenyl-substituted NHC **61** and substrate **11**. For the NHC component, it has been previously demonstrated that the best performing catalysts for this transformation are those which bear pentafluorophenyl substitution.[14] For these experiments, we synthesized NHC **75** from commercially available L-norvaline. This NHC is as structurally similar to the carboxylated series as possible, but with a methyl group in place of a carboxylic acid. For the substrate component, we chose **11** in light of the experiments described in **Figure 2.1.6**. A

more general substrate for this transformation is salicylaldehyde-derived substrate **3**, but the phenolic oxygen of this substrate has been implicated to be involved in assisting the 1,2-proton transfer to the Breslow intermediate. Substrate **11** would allow us to unambiguously assess the reactivity of NHC **61** as compared to NHC **75** and the more standard NHC **76**.

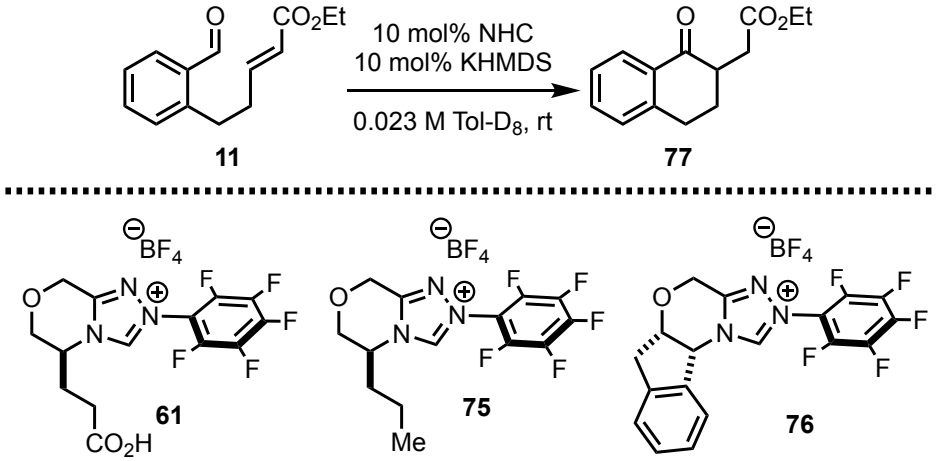

Figure 2.4.1. Substrate and NHCs chosen to assess reactivity of carboxylated NHC **61**.

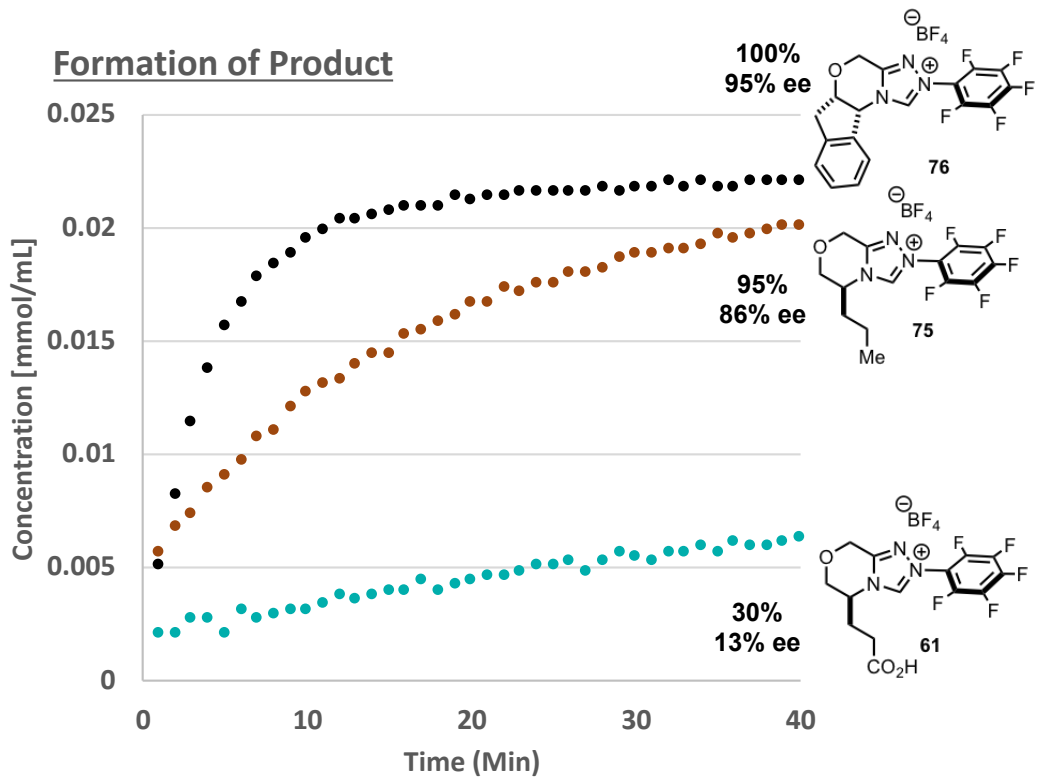

Figure 2.4.2. Formation of product as monitored via NMR for substrate **11**, comparing NHCs **61**, **75**, and **76**.

The results for this experiment are shown in **Figure 2.4.2**. The best performing catalyst in this experiment is catalyst **76**, the reaction proceeding to completion in 40 minutes and producing 95% ee. The second-best catalyst in this experiment is catalyst **75**, going up to 95% yield and 86% ee in the same time. The drop in ee makes sense, seeing as how catalyst **76** is both larger and more structurally rigid than catalyst **75**. Unfortunately, our recently synthesized carboxylated NHC **61** is the poorest performing in this series, yielding 30% in the same reaction time and producing a meager 13% ee. At this point, we wished to troubleshoot this catalyst in the hopes of gaining more insight as to what is causing this precipitous drop in reactivity. As such, we chose to move back to substrate **3**.

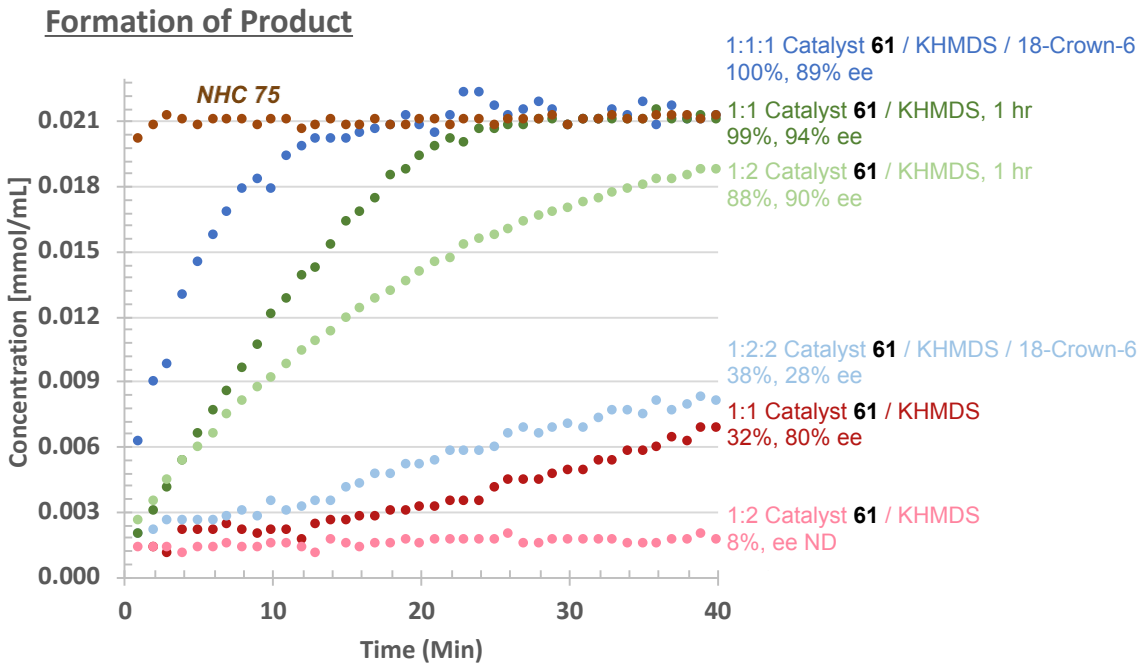

Figure 2.4.3. Formation of product **4** from salicylaldehyde-derived substrate **3** as monitored via NMR, comparing NHCs **61** and **75**.

In the first two runs, we performed the reaction in a 1:1 and a 1:2 ratio of NHC to KHMDS (**Figure 2.4.3**). In the first trial of these experiments, the 1:1 case produces a yield of 32% and an 80% ee. In the 1:2 case, only an 8% yield is produced and the ee was undetermined. In the 1:1 trendline, we noticed that there is a sudden increase in reactivity starting at the 12-minute mark. This result implied to us that the active form of the catalyst was not fully produced up until a certain point. We hypothesized at first that this observation was due to the existence of potassium chelated NHC intermediates that were insoluble in the reaction conditions. In order to address this, we ran another two reactions that have a 1:1:1 and a 1:2:2 ratio of NHC to KHMDS to 18-crown-6. Immediately, we see a huge improvement in the 1:1:1 case, where we see a 100% yield and 89% ee in a 40-minute time period. Again, the 1:2:2 case is a much less reactive system, producing only 38% yield and 28% ee. At this point, it became clear to us that the role of 18-crown-6 was not to

solubilize potassium-chelated NHC species, but rather to increase the basicity of KHMDS. This tells us that there is a relatively large energetic barrier for the first deprotonation relative to the triazolium protons of more common NHCs. In addressing this problem, we simply removed the 18-crown-6 and allowed the carboxylated NHC to react with the KHMDS base for a longer period of time. When pre-stirred for one hour in both a 1:1 and a 1:2 ratio of NHC to KHMDS, we still see that the 1:1 case is more reactive than the 1:2 case, where for the former we obtain 99% yield and 94% ee and in the latter we see 88% yield and 90% ee. Though the reactivity of these NHCs seemed to be promising, we still needed to compare it to a more standard catalyst. In this regard, we re-ran the reaction with NHC **75** and see that product formation goes to completion in less than 3 minutes, with 92% ee.

2.5 Troubleshooting

We have two working theories as to why these carboxylated NHCs display such attenuated reactivities. The first theory was hypothesized in light of the fully deprotonated NHC always performing poorly. The implication here is that there is a significant amount of decomposition with the fully deprotonated state. We also observed this NHC instability in our attempts to monitor the fully deprotonated state via ^{1}H-NMR, where all attempts to do so were met with failure. To better quantify this, we measured the amount of decomposition after 40 minutes in the above reaction with substrate **3** for the carboxylated NHC **61**, as well as for a series of NHCs (**Figure 2.5.1**). The percent decompositions were all measured in reference to an internal standard by UPLC-MS. For NHC **75**, we see a decomposition of 8% in 40 minutes and for NHC **76** we see a decomposition of 30%. For these purposes, a standard amount of catalyst decomposition will lie anywhere from 8% to 30%, as is suggested by the percent decompositions of NHCs **78**, **79**, and **80**. For the

carboxylated NHC **61**, in the 1:1 NHC to base experiment, we see an acceptable 20% decomposition. For the 1:2 case, we see that 51% of the NHC decomposes over the reaction period.

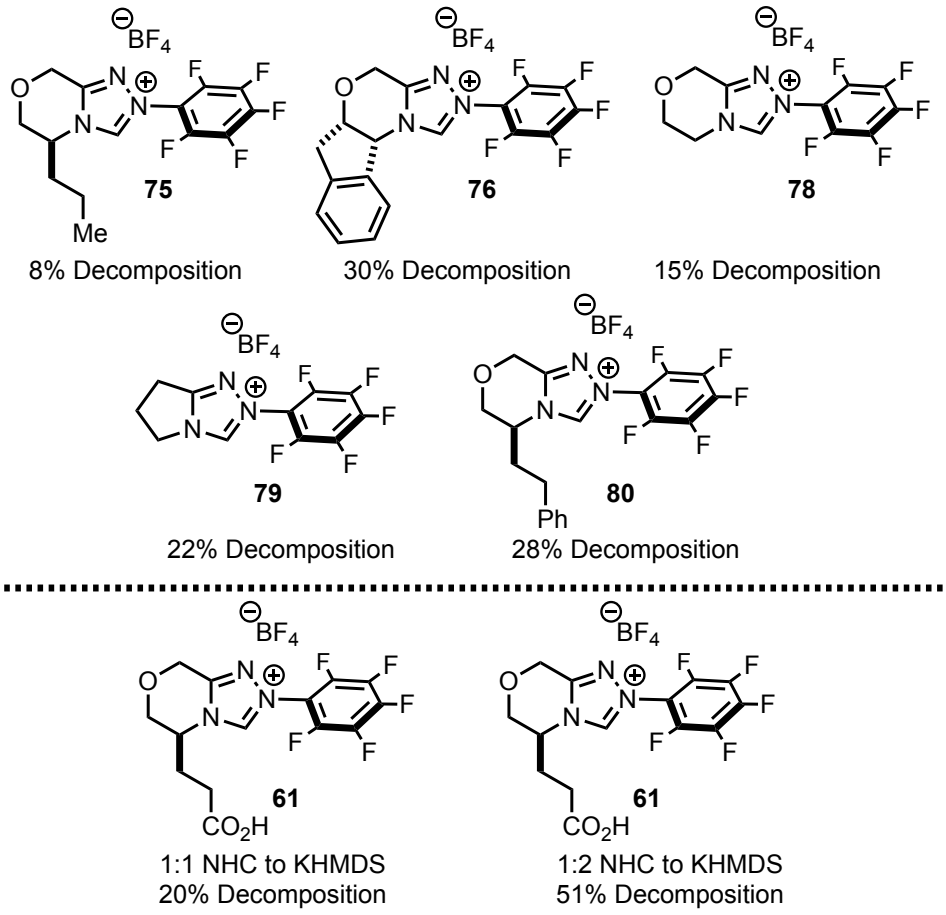

Figure 2.5.1. Percent decompositions for a variety of NHCs in the intramolecular Stetter reaction with substrate **3**.

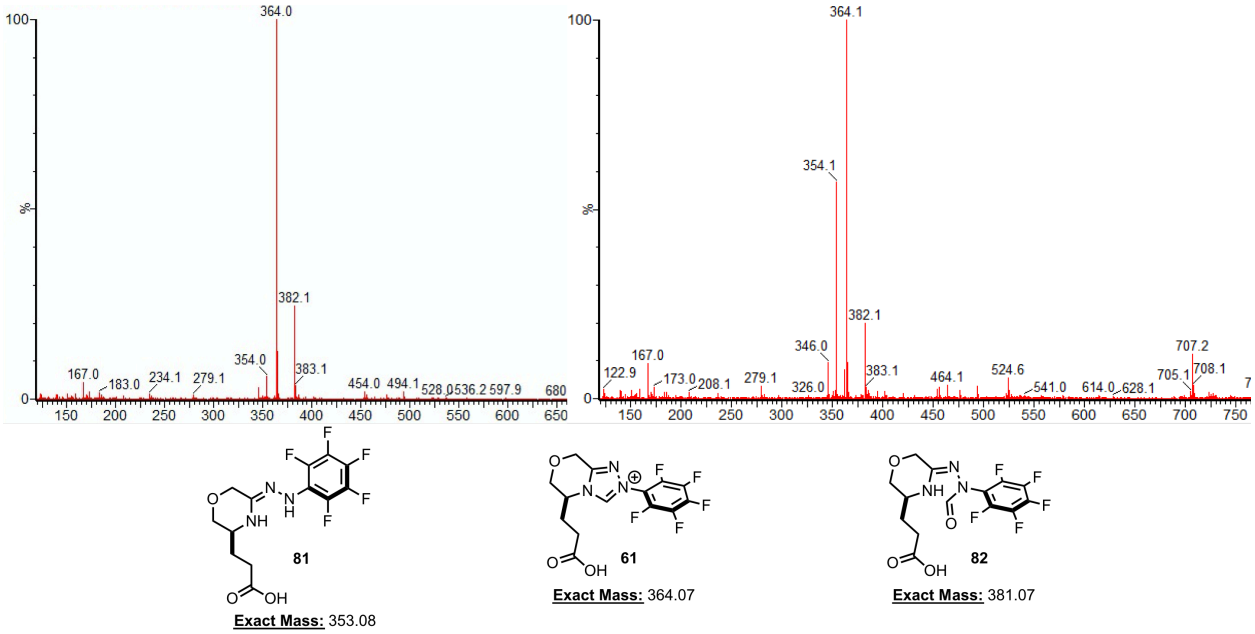

Figure 2.5.2. Decomposition products for NHC **61** in the intramolecular Stetter reaction with substrate **3**.

There are two main decomposition products in the UPLC-MS mass spectrum. One has a mass of 354.0 and the other 382.1 (**Figure 2.5.2**). These peaks account for decomposition products **81** and **82**, respectively. The proposed mechanism of decomposition is shown in Figure **2.5.3**, where a formal addition of water may occur during the doubly deprotonated state, or from the mono-deprotonated state. Proton transfer to one of the free amine groups forms decomposition product **82**, which can further react with water to liberate one equivalent of formic acid as well as decomposition product **81**. We hypothesize that the net-anionic fully-deprotonated form is more hydrophilic than a standard net-neutral free carbene NHC, thus rendering it significantly more prone to decomposition.

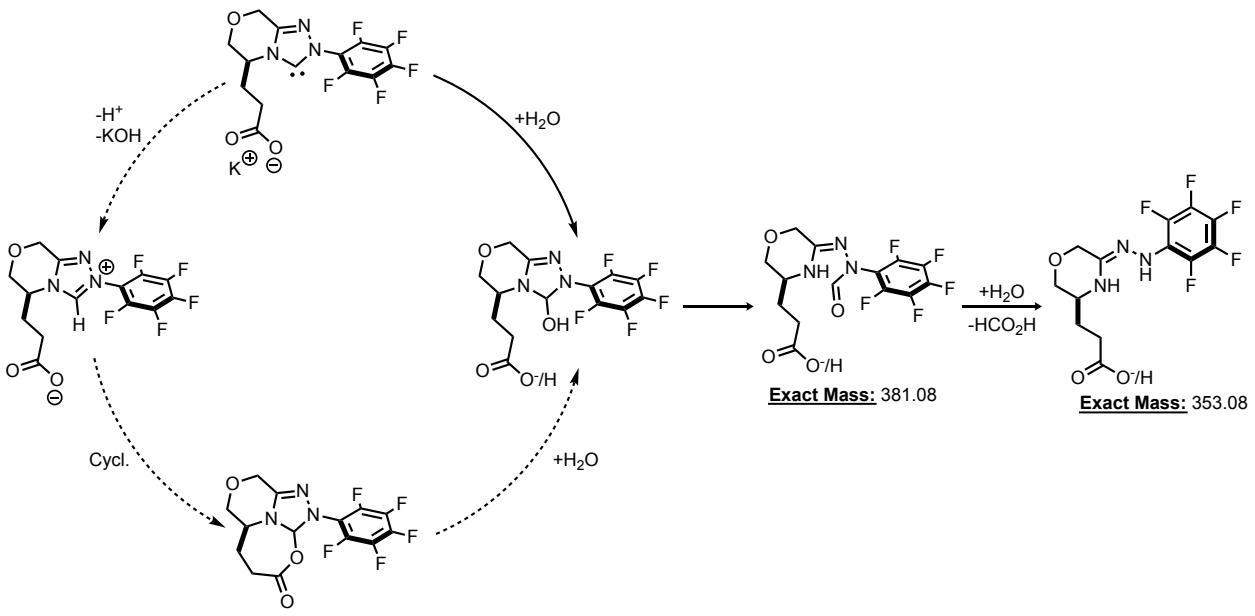

Figure 2.5.3. Proposed mechanism for the decomposition of NHC **61** to decomposition products **81** and **82**.

The second theory is that the presence of a negative charge in close proximity to the reactive center serves to increase the energetic requirement for the formation of intermediates that proceed through a negative charge. For instance, addition of the NHC into an aldehyde first forms the tetrahedral intermediate, which develops a negative charge at the oxygen atom. In a standard NHC, this species is net-neutral. In our carboxylated NHC, the carboxylate may discourage the formation of this intermediate through Coulombic repulsion. To probe this further, we developed another NHC that would have the tethered carboxylate in a closer proximity relative to NHC **61**. We thus synthesized NHC **83** using a similar strategy to the one listed above, but starting from methyl ester protected L-pyroglutamic acid (**Figure 2.5.4**). We examined this catalyst with salicaldehyde-derived substrate **3**. As per the inverse square law,[15] we should see a precipitous drop-off in reactivity for this NHC relative to NHC **61**. Our results agree with our hypothesis, suggesting that the presence of a negative charge in the proximity of the reactive center may serve to inhibit one or more steps along the catalytic cycle of the Stetter reaction.

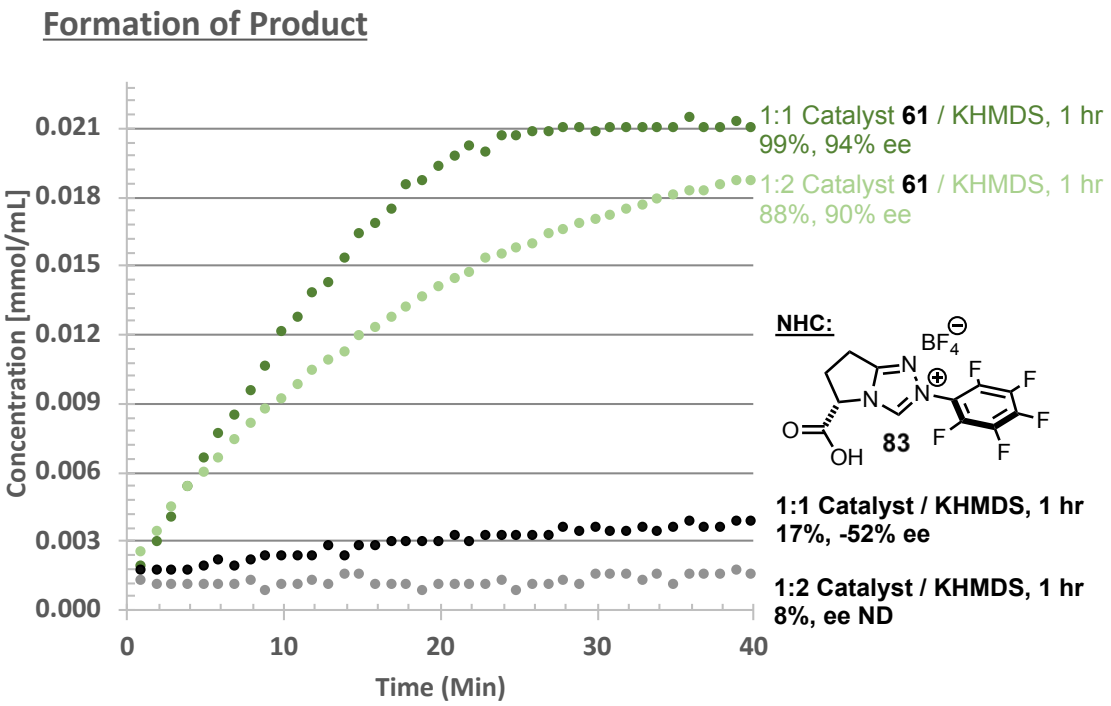

Figure 2.5.4. Formation of product **4** from salicylaldehyde-derived substrate **3** as monitored via NMR for carboxylated catalyst **83**.

2.6 Conclusion

Herein, we report the first successful synthetic route for access to carboxylated triazolium-based NHCs. We unambiguously assigned the product via x-ray crystallography, which indicates an unusually strong electron density at the proton of the carboxylic acid handle. We found that these catalysts work best when in the monodeprotonated form. In the fully deprotonated form, the catalyst decomposition pathway is faster than in any NHC tested in the experiments listed above. In the monodeprotonated form, we report that the presence of a carboxylate in close proximity to the triazolium proton can perform an intramolecular deprotonation. This represents the first class of NHCs that have a tethered internal base. More on this is currently being pursued.

2.7 References

1) (a) Enders, D.; Niemeier, O.; Henseler, A. *Chem. Rev.* **2007**, *107*, 5606−5655. (b) Flanigan, D. M.; Romanov-Michailidis, F.; White, N. A.; Rovis, T. *Chem. Rev.* **2015**, *115*, 9307–9387.
2) (a) Enders, D.; Han, J.; Henseler, A. *Chem. Commun.* **2008**, *34*, 3989–3991. (b) Liu, Q.; Perreault, S.; Rovis, T. *J. Am. Chem. Soc.* **2008**, *130*, 14066–14067. (c) DiRocco, D. A.; Oberg, K. M.; Dalton, D. M.; Rovis, T. *J. Am. Chem. Soc.* **2009**, *131*, 10872–10874. (d) Jousseaume, T.; Wurz, N. E.; Glorius, F. *Angew. Chem. Int. Ed.* **2011**, *50*, 1410–1416. (e) Wurz, N. E.; Daniliuc, C. G.; Glorius, F. *Chem. Eur. J.* **2012**, *18*, 16297–16301. (f) Liu, F.; Bugaut, X.; Schedler, M.; Fröhlich, R.; Glorius, F. *Angew. Chem. Int. Ed.* **2011**, *50*, 12626–12630. (g) Fang, X.; Chen, X.; Lv, H.; Chi, Y. R. *Angew. Chem. Int. Ed.* **2011**, *50*, 11782–11785.
3) DiRocco, D. A.; Oberg, K. M.; Dalton, D. M.; Rovis, T. *J. Am. Chem. Soc.* **2009**, *131*, 10872–10874.
4) DiRocco, D. A.; Noey, E. L.; Houk, K. N.; Rovis, T. *Angew. Chem., Int. Ed.* **2012**, *51*, 2391–2394.
5) DiRocco, D. A.; Rovis, T. *J. Am. Chem. Soc.* **2011**, *133*, 10402–10405.
6) Moore, J. L; Silvestri, A. P.; de Alaniz, J. R.; DiRocco, D. A.; Rovis, T. *Org. Lett.* **2011**, *13*, 1742–1745.
7) Zheng, P.; Gondo, C. A.; Bode, J. W. *Chem. Asian J.* **2011**, *6*, 614–620.
8) Tanaka, K.; Kobayashi, T.; Mori, H.; Katsumura, S. *J. Org. Chem.* **2004**, *69*, 5906–5925.
9) Vora, H. U.; Lathrop, S. P.; Reynolds, N. T.; Kerr, M. S.; Read de Alaniz, J.; Rovis, T. *Org. Synth.* **2010**, *87*, 350.

10) Larrow, J. F.; Roberts, E.; Verhoeven, T. R.; Ryan, K. M.; Senanayake, C. H.; Reider, P. J.; Jacobsen, E. N. *Org. Synth.* **1999**, *76*, 46.

11) Lu, C.; Zhang, S.Y..; He, G.; Nack, W. A.; Chen, G. *Tetrahedron*, **2014**, *70*, 4197–4203.

12) Ozboya, K. E.; Rovis, T. *Synlett*, **2014**, *25*, 2665–2668.

13) (a) Flanigan, D. M.; Rovis, T. *Chem. Sci.* **2017**, *8*, 6566–6569. (b) Chen, D. F. *Synthesis*, **2016**, *49*, 293–298. (c) White, N. A.; Rovis, T. *J. Am. Chem. Soc.* **2014**, *136*, 14674–14677. (d) White, N. A.; Rovis, T. *J. Am. Chem. Soc.* **2015**, *137*, 10112–10115.

14) Mahatthananchai, J.; Bode, J. W. *Chem. Sci.* **2012**, *3*, 192–197.

15) Williams, E. R.; Faller, J. E.; Hill, H. A. *Phys. Rev. Lett.* **1971**, *26*, 721–724.

Chapter 3. Electronic Effects: *N*-Aryl Substituent Effects Upon Reactivity

3.1 Introduction

After having revealed the zwitterionic character of thiazolium salts through a series of deuterium exchange experiments,[1] Breslow became the first to propose the mechanism of thiamine diphosphate as a coenzyme for a series of biochemically relevant reactions. This proposal initiated a revolution in terms of our fundamental understanding of carbenes and their subsequent reactivity.[2] Prior to this point, carbenes were generally considered to be too reactive and transient of a species to serve for any useful and general purpose. This notion has since changed, due largely to the enormous efforts and discoveries based around Breslow's pioneering work.[3] From a more modern perspective, a greater understanding of the fundamental properties that underlie these reactive intermediates has created new opportunities for their application in a broad range of novel settings.[4] As such, NHCs have been used as ligands for both transition metal complexes and for elements on the p-block of the periodic table, as well as for the purposes of organocatalysis. Regardless of the setting, it has become common knowledge that a variance in the steric and electronic properties surrounding the reactive center of the carbene will in turn modulate the reactivity of the NHC or NHC-bearing complex. Thus, a deeper understanding of how the fundamental properties of a carbene changes in tandem with alterations to the structure of the NHC becomes critical when choosing an NHC for a specific application.

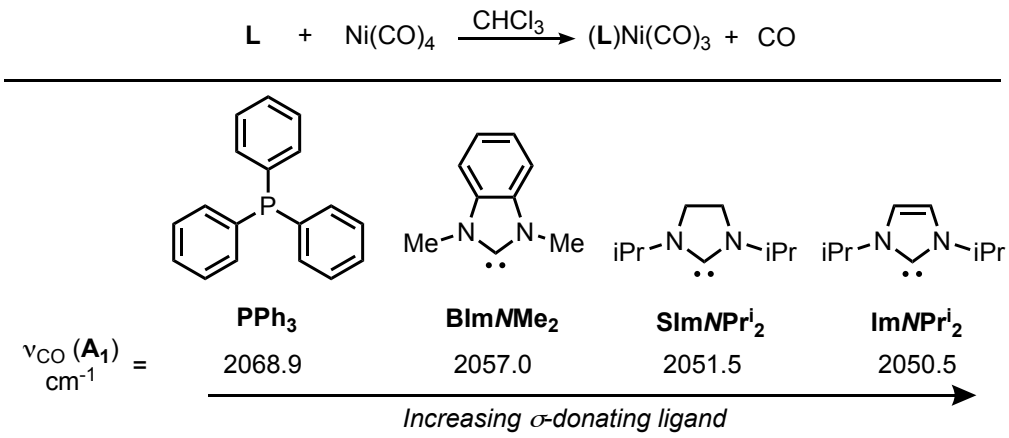

Figure 3.1.1. Order of increasing σ-donating ligands as indicated by CO stretching frequency of (L)Ni(CO)$_3$ complex.

The concept of choosing an NHC that is specifically tailored to achieve a certain degree of desired reactivity can perhaps be best illustrated with NHCs that are used as ligands for transition metal complexes. When used in this fashion, NHCs are often considered to be mimics of their phosphorous-based ligand counterparts, much in the way that they are both strong σ-donors and weak π-acceptors.[5] Despite this similarity, there are some important differences between these two ligand classes. One such difference is highlighted in the more electron-donating ability of NHC-ligands over their phosphorous counterparts, leading to TM-complexes that have higher bond dissociation energies and thus shorter ligand to metal bonds.[6] Furthermore, in terms of σ-donating ability, the benzimidazole ligand BIm*N*Me$_2$ is more electron donating than triphenylphosphine, and for NHCs the general order of the least to most electron donating is as follows: benzimidazole, imidazoline, imidazole (**Figure 3.1.1**).[7,8,9] Another important difference between these two compound classes is the ease of which the electronic character of the NHC can be modulated. This may be achieved simply by changing the *N*-aryl substituent, generally done with a simple change in the NHC precursor. This character change is best reflected in the reduced carbonyl IR-stretching frequencies of (NHC)Ni(CO)$_3$ complexes of **Ipr**, **Imes**, and **Icy**, an indication that the

metal has become more electron rich as a result of a more strongly σ-donating NHC ligand (**Figure 3.1.2**).[10] With all of this in mind, it becomes apparent that careful choice of an NHC can produce tremendously robust TM-complexes for a given application, as is made evident with the Grubbs-II catalyst for olefin-metathesis reactions.

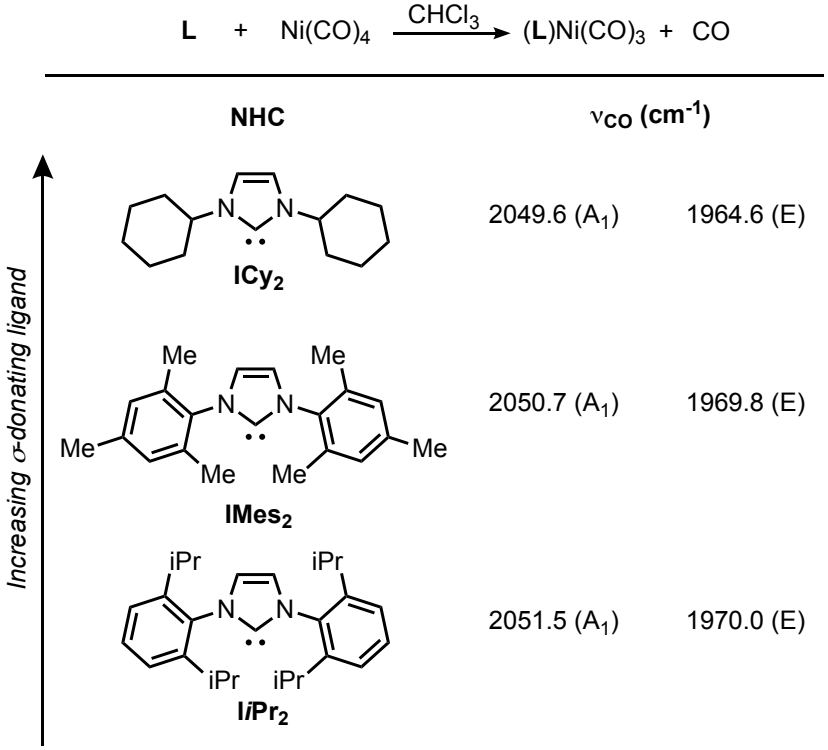

Figure 3.1.2. Controlling the σ-donating character of NHC ligands via *N*-aryl substituent modulation as indicated by CO-stretching frequency of (L)Ni(CO)$_3$ complex.

For instances where NHCs are employed as organocatalysts, modulation of the *N*-aryl substituent is perhaps the best and easiest way to tailor the reactivity of the free carbene to a suited purpose. There are many examples where some function of reactivity is shown to have a dependence upon electronics.[11] One such instance is shown with the intramolecular Stetter reaction of as shown in **Figure 3.1.3**, where for catalysts **I**, **II**, and **III** there is a gradual increase in the amount of product formed as the electron donating ability of the *N*-aryl substituent is tapered.[12]

This dependence was later explored by Bode and coworkers, wherein they reported a higher preference for Stetter-type pathways with more electron-deficient NHCs.[13] The existence of this preference was further supported by a series of kinetic experiments as performed by O'Donoghue, Smith and coworkers, where it is made evident that a more electron-deficient NHC creates a more acidic proton in the tetrahedral intermediate prior to the formation of the famed Breslow intermediate, which is believed to be the rate limiting step for the intramolecular Stetter reaction (**Figure 3.1.4**).[14] This dependence is beautifully illustrated further with a series of achiral NHCs that bear different *N*-aryl substituents. These NHCs are tested for a similar intramolecular Stetter reaction as in **Figure 3.1.3**, where it is shown that the more reactive NHCs will be those that feature more electron-deficient substitution patterns (**Figure 3.1.5**).

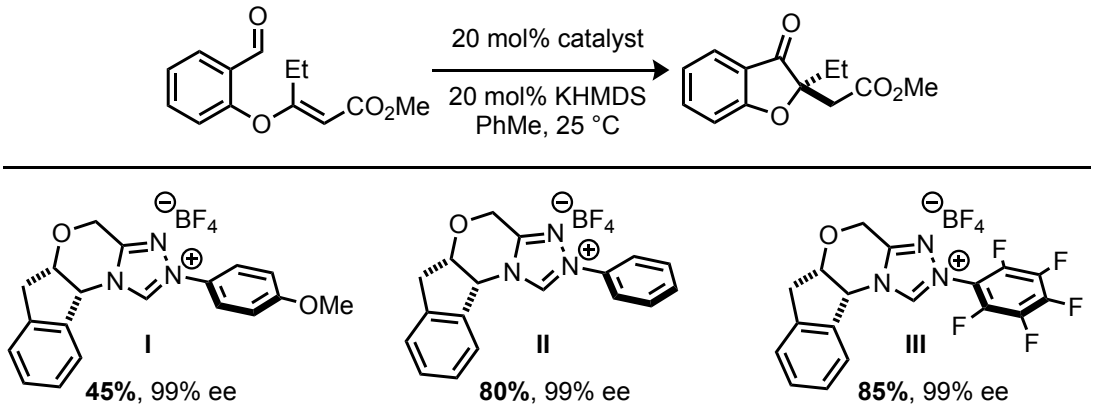

Figure 3.1.3. Quaternary-center forming asymmetric intramolecular Stetter shows higher yields with more electron-withdrawing *N*-aryl substitution.

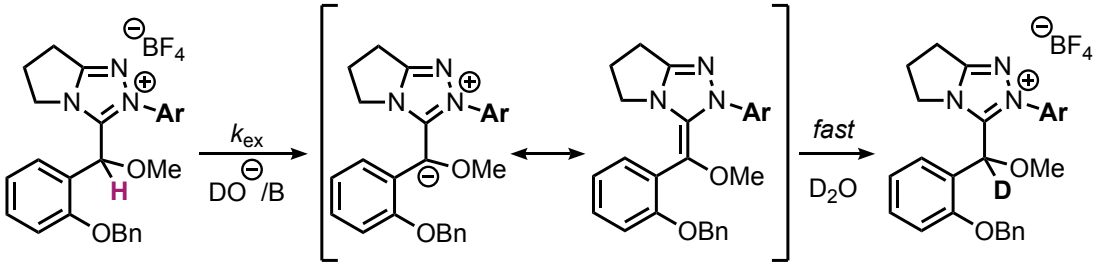

Ar	p*D*	k_{ex} (s^{-1})
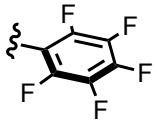	**10.9**	**2.03×10^{-3}**
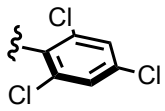	**10.9**	**7.30×10^{-4}**
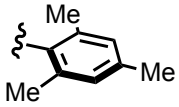	**10.9**	**2.61×10^{-5}**
	**10.9**	**9.60×10^{-5}**
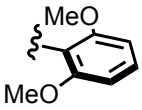	**10.9**	**2.32×10^{-6}**

Figure 3.1.4. Deuterium exchange studies for *N*-aryl differentiated 3-(methoxybenzyl)azolium salts, wherein fastest exchange occurs for NHCs with most electron deficient aryl substitution.

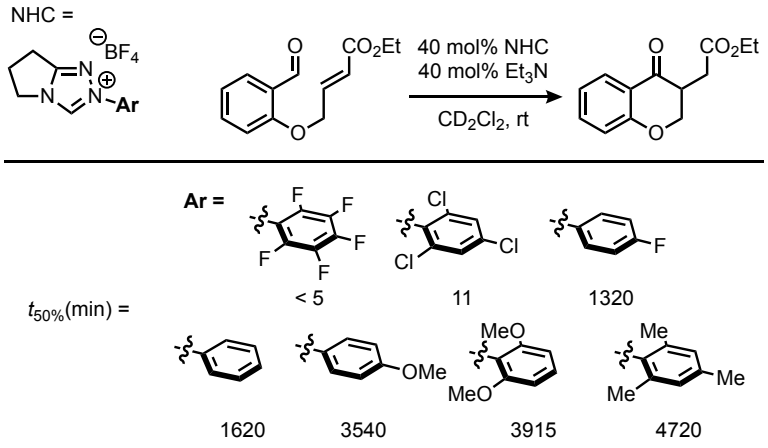

Figure 3.1.5. Time at which 50% of product is observed for the intramolecular Stetter reaction, according to a variance in *N*-aryl substituent.

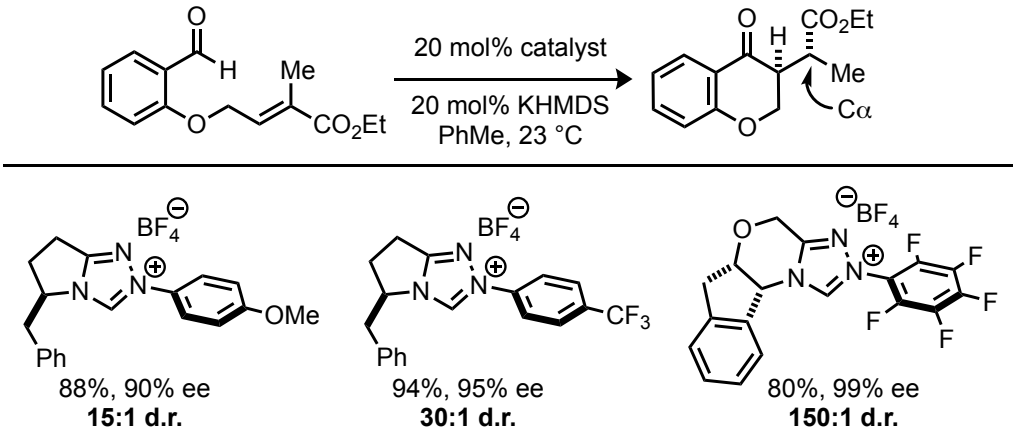

Figure 3.1.6. Effect of the *N*-aryl substituent on diastereoselectivity for the intramolecular Stetter reaction.

The *N*-aryl substituent has also been shown to affect diastereoselectivity, where for the dual-stereocenter setting intramolecular Stetter there is an increase in diastereoselectivity when using an electron poor *N*-aryl group.[15] The origin of this effect was found to be related to epimerization of the C-α stereocenter. An NHC with an electron-deficient *N*-aryl substituent will correspond to a relatively less Lewis-basic free carbene, thus mitigating the degree of epimerization that occurs at this carbon center during the course of the reaction (**Figure 3.1.6**). A more electron-rich *N*-aryl substituent may also serve to dramatically increase reactivity, as was shown by Glorius and coworkers' elegant efforts towards the discovery of an intermolecular asymmetric hydroacylation between aldehydes and cyclopropenes (**Figure 3.1.7**).[16] Here, the electron-rich 2,6-dimethoxy-substituent serves to increase the overall nucleophilicity of the Breslow intermediate, thus creating a more reactive NHC relative to the previously most electron rich NHC.[17]

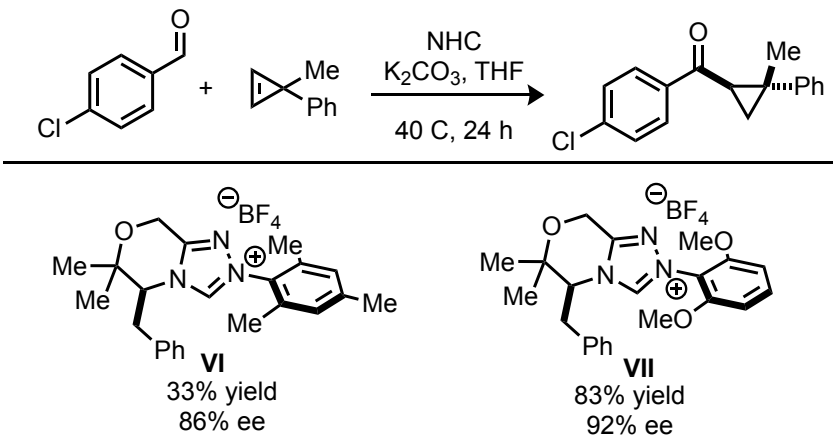

Figure 3.1.7. 2,6-Dimethoxyphenyl substituted NHC **VII** creates a more nucleophilic Breslow intermediate as compared to NHC **VI**.

Nonetheless, in consideration of the aforementioned examples, it becomes important to parameterize these effects to better understand and correlate some function of reactivity. The main idea here is that a parameterizing data set may be used to decrease the degree of serendipity that is utilized when selecting an NHC for novel use, such as can often be the case during the course of methods development. Such a data set may also provide a more logical vista of the effects that the *N*-aryl substituent has upon carbene reactivity, which may then grant a more logical vista towards catalyst development as well. A parameterizing data set of this kind may also be used to establish linear free-energy relationships (LFER) with some function of reactivity, those of which, prior to these research efforts, have never been achieved before. Herein are described our efforts towards achieving these goals.

3.2 Assessing Acidities – Intrinsic & Extrinsic Properties of NHCs

At the onset of our studies, we proposed that a direct way of parametrizing the electronic effects as imparted by the *N*-aryl substituent is by assessing the acidity of the C2-proton of these triazolium salts. Due to the enormous past efforts of a number of research groups with the goal of

disclosing the pKa's of various NHCs,[18,19] some generalizations can now be made: 1) imidazolium and saturated imidazolium-based NHCs are the least acidic of the organocatalyst series, ranging from 20.7 to 25.4 pKa units; 2) thiazolium-based NHCs follow the imidazolium species with an increasing acidity, ranging from 16.9 to 18.9 pKa units; 3) triazoliums are the most acidic of the two aforementioned classes of NHCs, slightly topping the thiazoliums with a range of 16.5 to 18.5 pKa units (**Figure 3.2.1a**). Smith, O'Donoghue and coworkers put forth the most recent of these efforts, disclosing a number of aqueous-phase pKa's for triazolium-based NHC organocatalysts as recently as 2012.[20] In this manuscript, the authors illustrated the significant dependence that the nature of the *N*-aryl substituent has upon acidity. The most acidic of the measured NHCs has pentafluorophenyl substitution, with a pKa of 16.5. From here, first principles will dictate that an appropriate attenuation of the electron-withdrawing nature of this substituent will in turn increase the pKa, and it accordingly does (**Figure 3.2.1b**). Overall, the contributions listed above have collectively allowed for a greater understanding of the fundamental properties of NHCs and how they can impact reactivity. These studies play a significant role in predicting how structural perturbation's may affect their function, and are thus powerful in their own right.

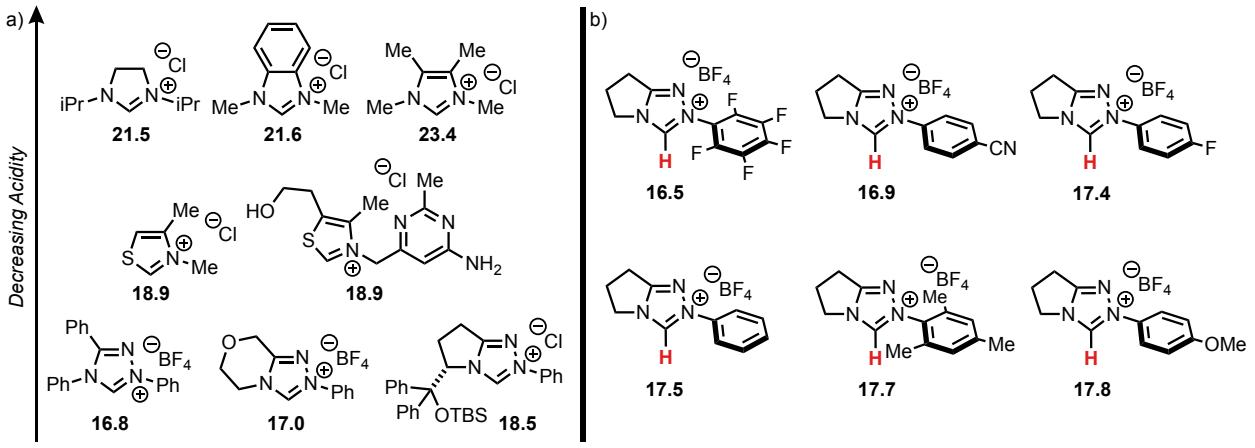

Figure 3.2.1. a) Some pKa examples for a class of imidazolium, thiazolium, and triazolium NHCs. b) pKa's as disclosed by the Smith and O'Donoghue groups for the achiral triazolium NHCs.

Unfortunately, up until the point of the aforementioned manuscripts, studies that correlate some function of reactivity to the pKa of these triazolium salts have yet to be achieved. The most likely reasons for this are two-pronged: 1) the pKa values for triazoliums of interest to synthesis are not only scarce, the differences between them are rather small; 2) any discussion involving pKa's are limited to the solvent in which those values are measured – in other words, pKa's are an extrinsic property. The range of pKa's for the achiral NHCs shown in **Figure 3.2.1b** range from 16.5 to 17.8, corresponding to a difference of 1.3 pKa units or, according to the Gibbs free energy relationship $\Delta G^{o}_{298} = 1.4pK_{eq}$, 1.8 kcal/mol. This energy difference, especially when attempted to be used in the context of establishing an LFER, is small. This point becomes increasingly troublesome as we consider the extrinsic nature of pKa values, wherein the solvent effects upon pKa become quite pronounced when moving from water to more organic solvents – the latter of which are much more amenable for NHCs when used as organocatalysts. Due to this, a study on the toluene-solvated intramolecular Stetter system shown in **Figure 3.1.3** as compared to the aqueous-phase pKa values may have produced undependable or otherwise erroneous trends.

Unfortunately, these combined factors preclude a researcher's ability to study a given function of reactivity as compared to acidity.

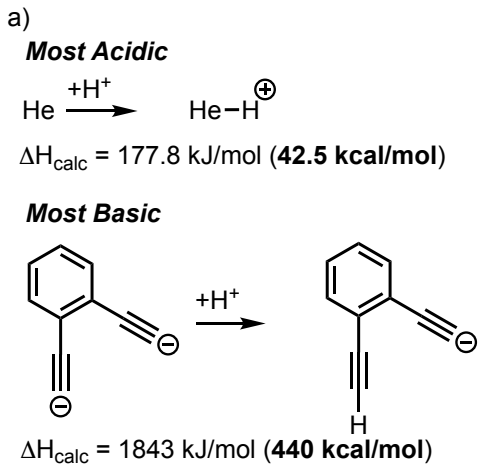

b)

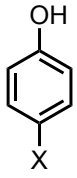

X	PA_{calc} (kcal/mol)
NO_2	323.6
CN	329.4
CF_3	334.6
Cl	341.3
F	345.2
H	347.8
CH_3	349.0
OH	350.1
OCH_3	350.2
NH_2	352.3

Figure 3.2.2. a) The most acidic and basic known species, according to proton affinities b) Calculated proton affinities for a series of differentially *para*-substituted phenols.

In consideration of an alternative approach to this problem, a successful collaboration with Jeehuin Katherine Lee and coworkers was established with the intent to assess the proton affinities (PAs) of triazolium-based NHCs. Proton affinities are generally defined as the negative enthalpy of the gas phase reaction between a conjugate base and a proton.[21] These values can be expressed as kcal/mol and have a current limit of 42.5 kcal/mol for the most acidic known species to 440 kcal/mol for the most basic (**Figure 3.2.2a**).[22,23] More specifically, for a species of phenols that feature varying substitution with both electron-withdrawing and electron-donating groups at the *para*-position, the range of proton affinities lie between 323.6 kcal/mol for the most acidic phenol to 352.3 kcal/mol for the least acidic (**Figure 3.2.2b**).[24] The energetic range here accounts for 28.7 kcal/mol, which is much broader as compared to the 1.8 kcal/mol energetic difference for the pKa values. Due to the parameters that define proton affinities, we can see that these values exist outside of the context of solvation – thus, they reflect the *intrinsic* properties of an acid. With this in mind,

and in consideration of the potentially wider energetic range of proton affinities for triazolium-based NHCs as exemplified by our comparison with phenols, we sought to first assess these values for a series of triazolium-based NHCs.

3.3 Calculated Proton Affinities

Through our collaboration, one in which all acidity assessments were done by Lee and coworkers and all synthetic work and subsequent attempts at correlations were performed by us, we obtained a number of calculated proton affinities initially for a series of achiral triazolium salts.[25] The reason for starting with the achiral series was to first assess the electronic impact that comes with varying the *N*-aryl substituent. Also, as mentioned before, several pKa values for these achiral azoliums already exist and would serve well as a point of comparison. These proton affinities were calculated using DFT methodology with a B3LYP functionality. The basis set of choice is 6-31+G(d), which adds diffuse functions and is available for all atoms from hydrogen to krypton. As per the results of our calculations, the most acidic NHC is **1c** with a PA of 242.7 kcal/mol and the least acidic is **1k** with a PA of 267.5 kcal/mol (**Figure 3.3.1**). Overall, the calculations make sense and were subsequently compared to the pKa values of those NHCs which are known. As anticipated, the PA values show an excellent correlation with the pKa values (**Figure 3.3.2**).

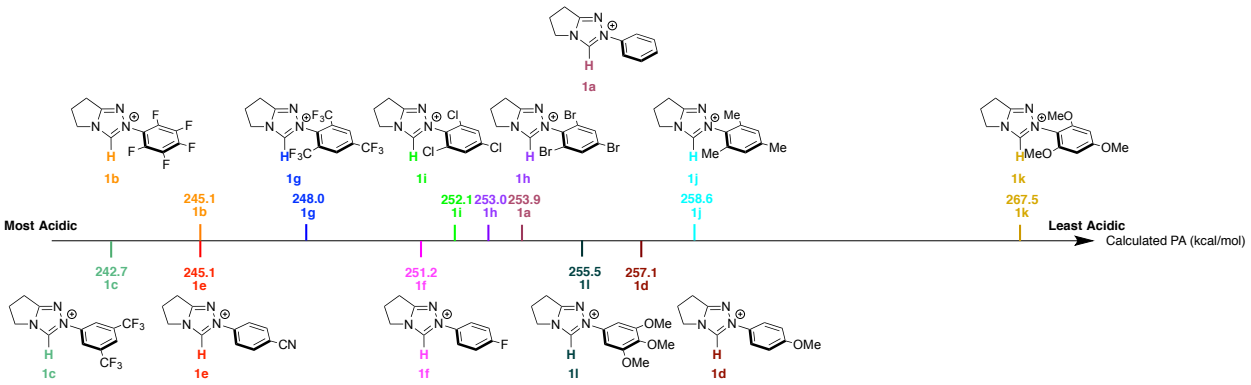

Figure 3.3.1. Calculated proton affinities for the achiral series of triazolium NHCs, as ordered from most acidic to least acidic.

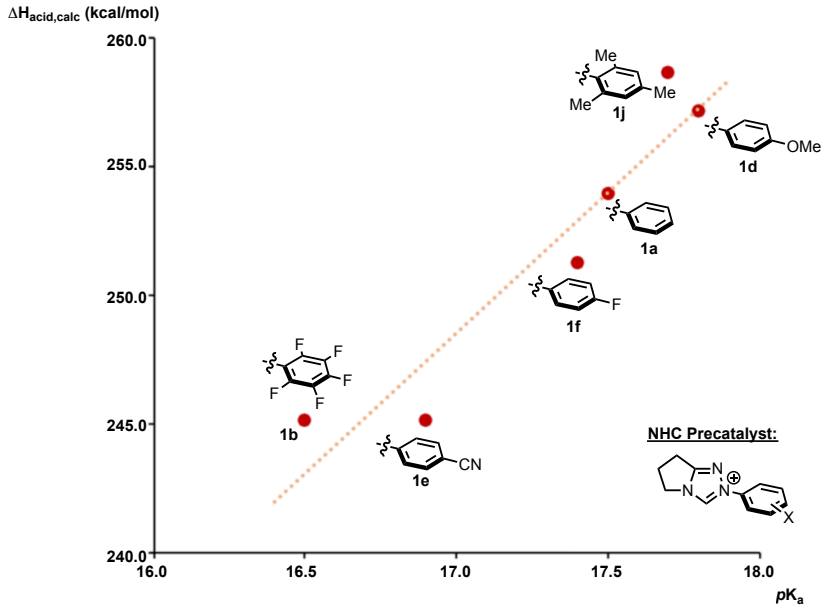

Figure 3.3.2. Calculated proton affinities vs. pKa for the achiral series of triazolium NHCs.

The range of proton affinities for the achiral NHCs account for an energy differential of 24.8 kcal/mol. This range is somewhat smaller than those of the phenols from **Figure 3.2.2b**, which accounts for 28.7 kcal/mol. This point becomes more significant when considering that the perturbations done to the NHC series are more pronounced and drastic than those of the selected phenols. On a similar note, a closer analysis of the calculated PAs reveals some minor

discrepancies, such as the one between NHCs **1c** and **1g**. Here, **1c** features only two -CF_3 groups while **1g** has three. Despite this additional trifluoromethyl group, **1c** is calculated to be more acidic than **1g**. The proposed reason for this is that the dihedral angle between the plane of the triazolium core to the plane of the aryl ring is dramatically increased for **1g** relative to **1c** (**Figure 3.3.3**). In order to calculate these angles for both NHCs, the same DFT method and basis set as described above was used. These calculations yielded a dihedral angle of 34.7° for **1c** and an angle of 90.4° for **1g**. This result implies that the effective molecular orbital overlap of **1g** is much lower than that of **1c**, thus reducing the overall π-withdrawing ability of the **1g** and making it more of a σ-withdrawing group, thus measurably mitigating the contribution of the third CF_3 group. The issue of planarity is non-existent with the phenol series as described above, thus the range of PAs for these species should be expected to be somewhat larger than those of the NHCs. All of these factors indicate that the calculated PAs for our achiral series is accurate thus far.

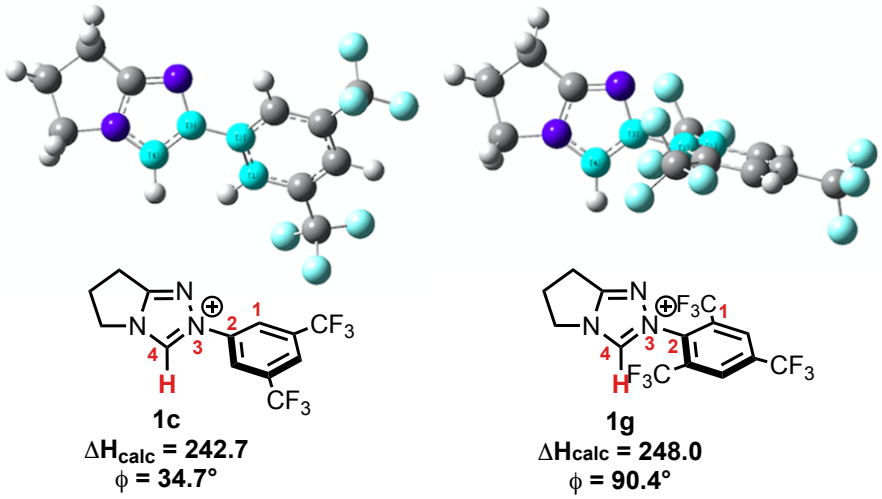

Figure 3.3.3. Calculated dihedral angles for achiral NHCs **1c** and **1g**.

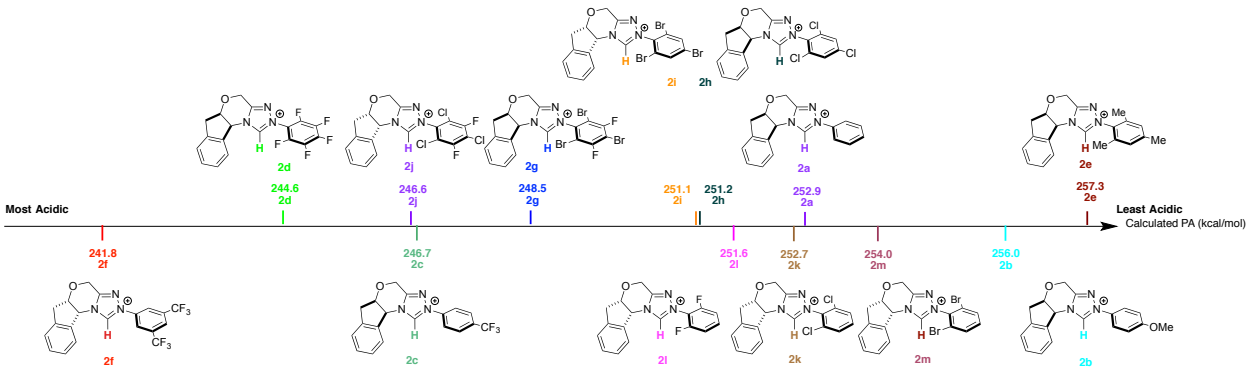

Figure 3.3.4. Calculated proton affinities for the chiral series of triazolium NHCs, as ordered from most to least acidic.

With the same basis set, we also calculated the proton affinities for a small library of chiral aminoindanol-based NHCs (**Figure 3.3.4**). Here, the most acidic chiral NHC, **2f** with a PA of 241.8 kcal/mol, is again 3,5-trifluoromethylphenyl substituted. The least acidic is mesityl substituted NHC **2e** at 257.3 kcal/mol. The energetic range for the chiral series is 15.5 kcal/mol, which is less than for the achiral species. This ultimately makes sense since there is no chiral NHC that bears the same *N*-aryl substitution as that of the least acidic achiral NHC **1k**. The energetic difference for the achiral series, omitting NHC **1k**, is 15.9 kcal/mol. These values are thus in excellent agreement. As for any apparent discrepancies, phenyl substituted chiral NHC **2a** is more acidic than 2,6-dibromophenyl substituted NHC **2m**. This would at first seem counter-intuitive, but the dihedral angle argument that already posed for the achiral NHCs **1c** and **1g** is still operative here. For **2a** the dihedral angle is 36.6° and for **2m** is 95.0° (**Figure 3.3.5**). These angles explain well the attenuated acidity for **2m** over **2a**.

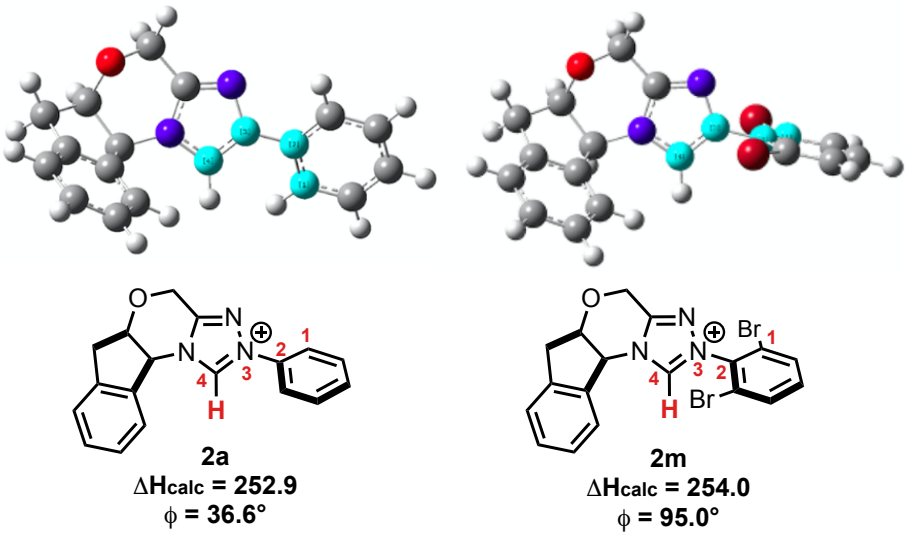

Figure 3.3.5. Calculated dihedral angles for NHCs **2a** and **2m**.

3.4 Experimental Proton Affinities

Encouraged by these results, we then sought to obtain the PAs of the aforementioned NHCs experimentally. These values would ideally correlate to the calculated values and further demonstrate the reliability of our selected *ab initio* approach. The earliest and most popular way of obtaining PAs experimentally is by utilizing bracketing techniques.[21] Here, a proton transfer reaction is carried out in the presence of a reference base that has its PA already well established in literature. First, ESI-ionization of a protonated carbene is measured. Then, the absence or presence of this signal in the presence of a suitable reference base will indicate if a proton transfer to the base has occurred. Unfortunately, this method is limited by the overall amount of reference bases that have known PAs. Because of this limitation, we can expect to see rather large error margins for the experimentally obtained PA data.

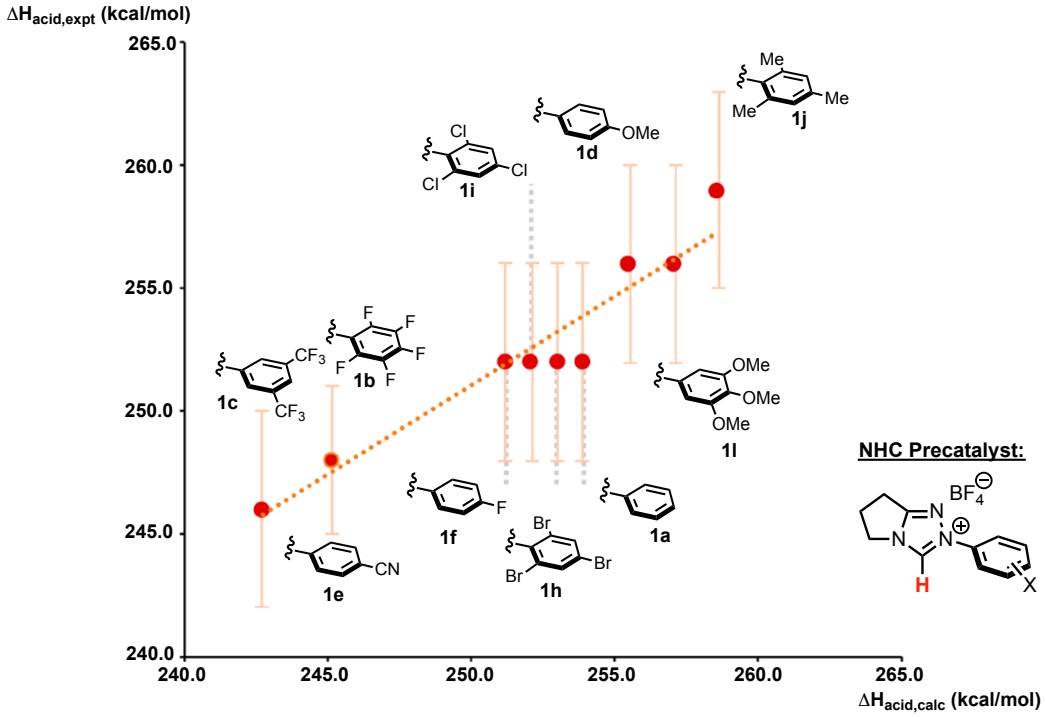

Figure 3.4.1. Calculated proton affinities vs. experimental proton affinities for the achiral series of triazolium NHCs.

For the achiral species, the experimental PAs as compared to the calculated values are shown in **Figure 3.4.1**. Despite the aforementioned limitation inherent to the bracketing methodology, we still see an excellent correlation between the calculated and the experimentally obtained values. For the chiral species, this correlation is also readily apparent (**Figure 3.4.2**). Geared with both of these data sets, and in consideration of a broader energetic range than has been previously made available, we sought to discover some correlations between a given function of reactivity as compared to the newly obtained proton affinities. In this regard, and in consideration of the error margin naturally associated with the experimental data set, any attempted correlation will be compared to the calculated PA values.

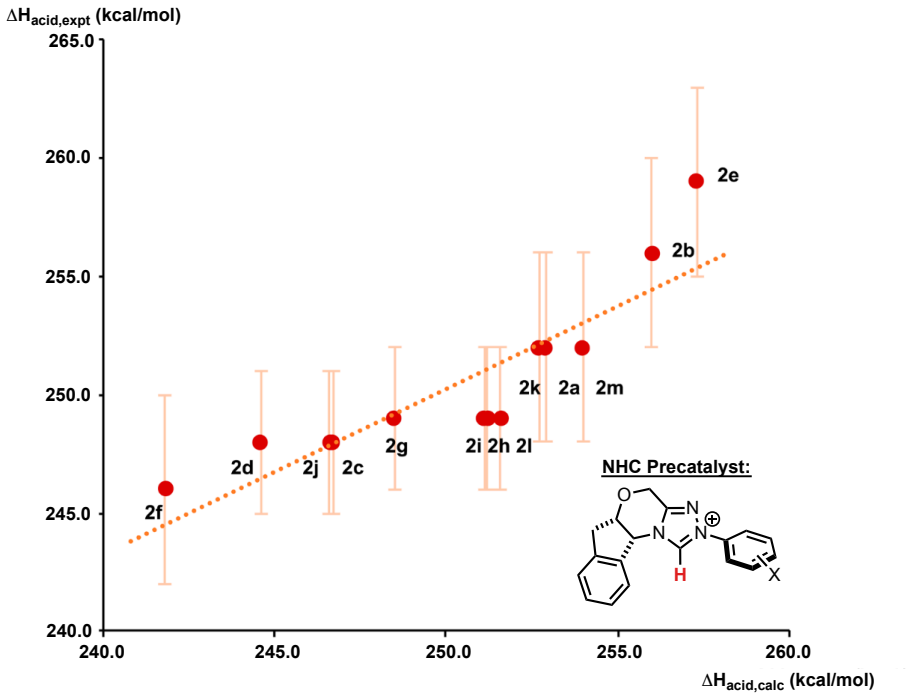

Figure 3.4.2. Calculated proton affinities vs. experimental proton affinities for the chiral series of triazolium NHCs.

3.5 Correlations with Achiral Species/Trends with Diastereoselectivity

Since variances in reactivity have already been both well-explored and documented for the Stetter-type pathways, we first chose to begin our studies with an intermolecular homoenolate addition as was previously disclosed by the Nair and Liu groups, as well as by our own (**Figure 3.5.1**).[26,27,28] This reaction has also already shown a difference in diastereoselectivity, where Liu's 2,6-diethylphenyl substituted NHC produces a high preference for the anti-product and our own pentafluorophenyl substituted NHC gives a large preference for the syn-product. This curious switch in diastereoselectivity was studied by Yao Fu and coworkers, wherein they disclosed a lower energetic barrier for the formation of the syn-product relative to the anti-product via *ab initio* calculations with the pentafluorophenyl-substituted NHC that was used in our prior publication.[29] Despite this finding, the precise origin on this effect has thus far eluded detection.

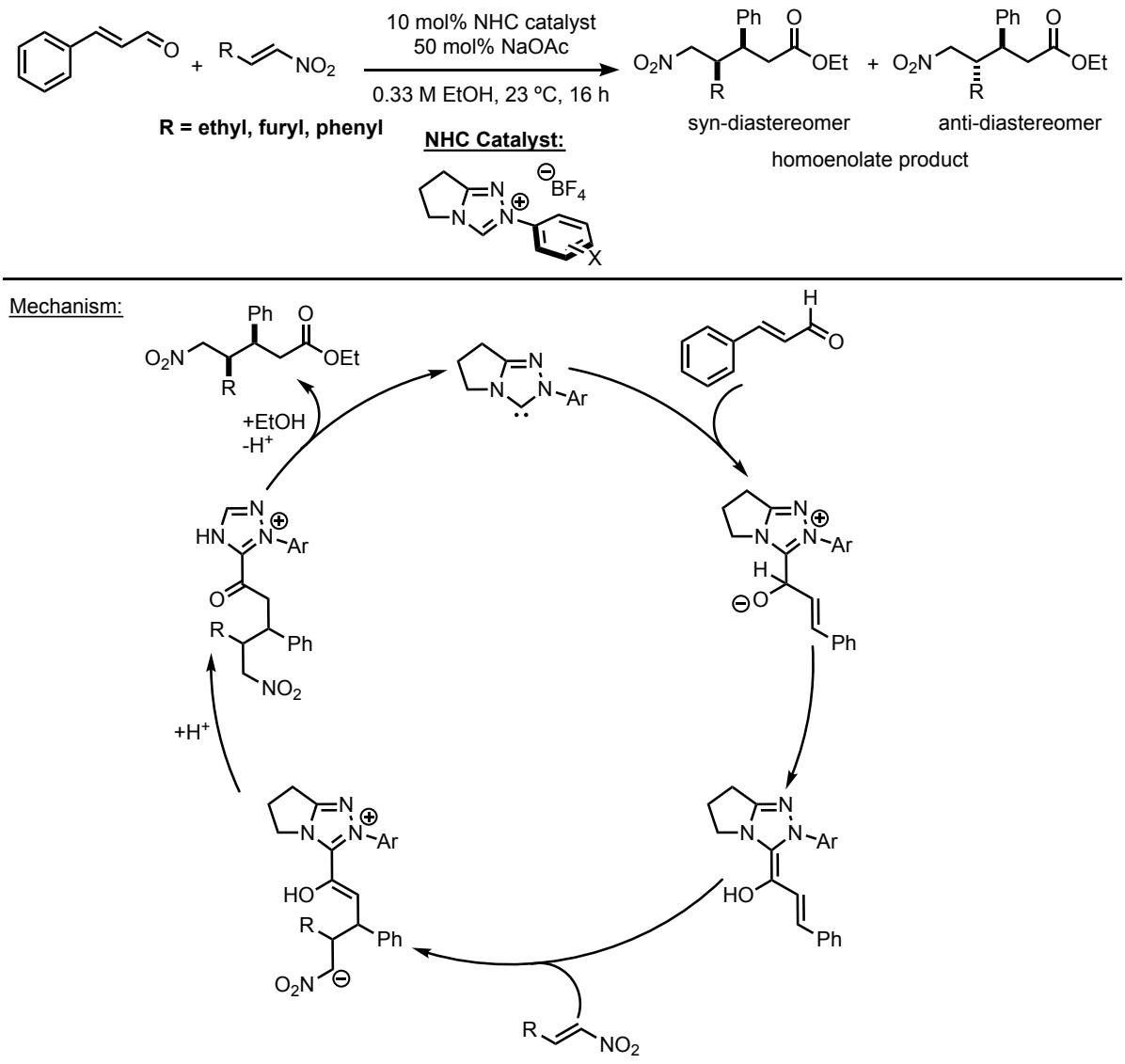

Figure 3.5.1. NHC-catalyzed intermolecular homoenolate addition of cinnamaldehyde to nitroalkenes, as well as the currently accepted mechanism.

Upon performing these reactions with our achiral series of catalysts, we were very pleased to find that, for the selected model reaction with (*E*)-1-nitrobut-1-ene, a trend that links acidity to diastereoselectivity does indeed exist (**Figure 3.5.2**). We wanted to see if this correlation was general, so we also repeated the analysis with the (*E*)-2-(2-nitrovinyl)furan and (*E*)-(2-nitrovinyl)benzene and were gratified to find that linear correlations exists with these substrates as well (**Figures 3.5.3 and 3.5.4**). For (*E*)-1-nitrobut-1-ene, a trend is revealed such that a more acidic

NHC corresponds to more syn-product. As the acidity of the NHC is attenuated, or the PA increases, the amount of anti-product start to increase as well. For achiral NHC **1c**, the preference is 3.5:1 for the syn-product, and for achiral NHC **1j** the preference is 3.5:1 for the anti-product. These results reflect the preferences as seen by both Liu's group, as well as that of our own.

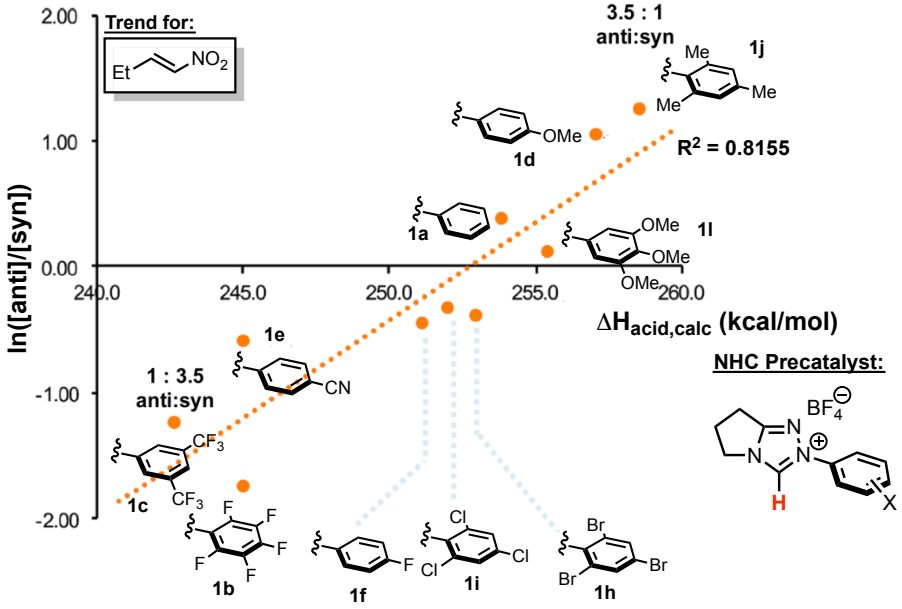

Figure 3.5.2. Natural log plot of the anti/syn ratios vs. calculated PAs for the achiral series of NHCs for the model homoenolate reaction with (*E*)-1-nitrobut-1-ene.

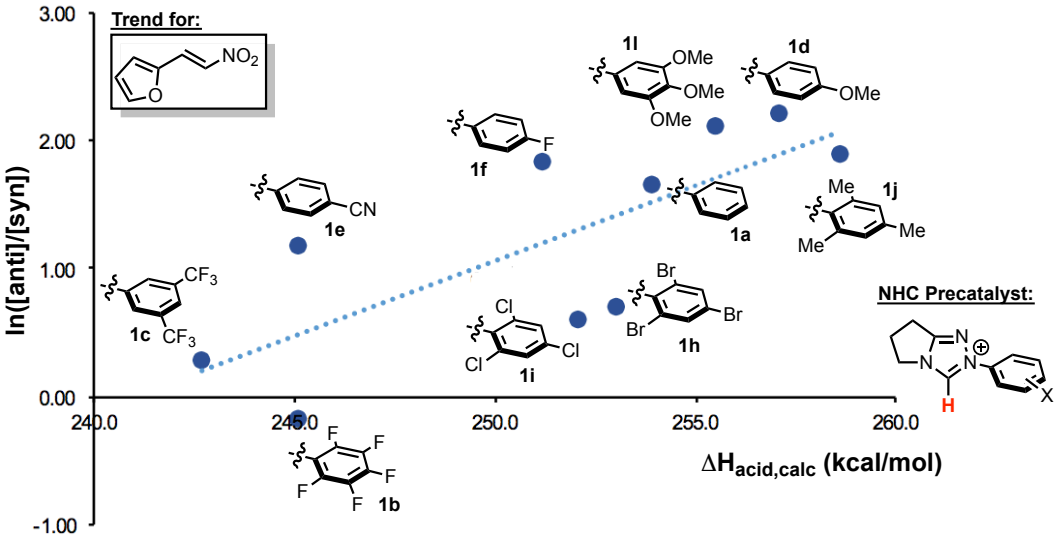

Figure 3.5.3. Natural log plot of the anti/syn ratios vs. calculated PAs for the achiral series of NHCs for the model homoenolate reaction with (*E*)-2-(2-nitrovinyl)furan.

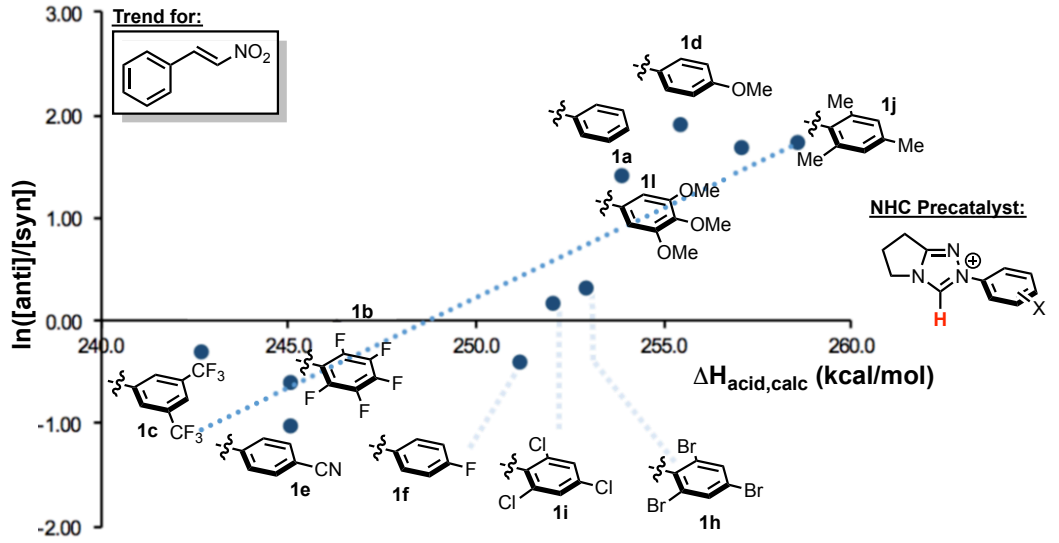

Figure 3.5.4. Natural log plot of the anti/syn ratios vs. calculated PAs for the achiral series of NHCs for the model homoenolate reaction with (*E*)-(2-nitrovinyl)benzene.

We noted some minor discrepancies in our correlations during a preliminary analysis of the newly discovered trends, such as the ones existing between NHCs **1b** and **1e**. In this case, both NHCs feature the same 245.1 kcal/mol proton affinity. Despite this similarity, there is an apparent

difference in diastereoselectivity, where pentafluorophenyl substituted **1b** gives a higher preference for the formation of syn-product as compared to the 4-cyanophenyl substituted NHC. As was previously mentioned, the calculated PA of a given NHC is affected by the amount of significant molecular orbital-overlap that occurs between the planes of the triazolium core and the *N*-aryl substituent. The amount of effective overlap is reduced by substitution at the ortho positions of the *N*-aryl substituent. In light of this effect, we felt that a more accurate description of this trend would be one that separates those NHCs that feature diortho substitution from those that do not (**Figures 3.5.5 and 3.5.6**). Both of these plots show the same trend, where a more acidic NHC gives a higher preference for the syn-product, with the exception that the correlations are more accurate.

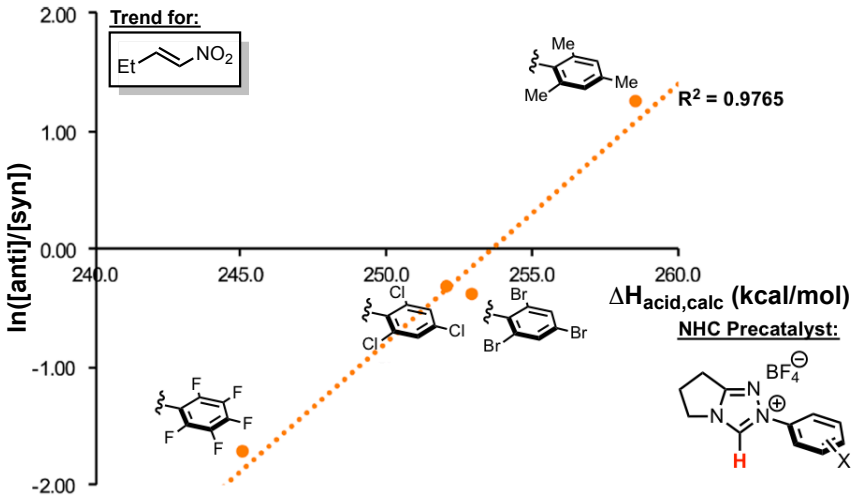

Figure 3.5.5. Natural log plot of the anti/syn ratios vs. calculated PAs for the diorthosubstituted achiral series of NHCs for the model homoenolate reaction with (*E*)-(2-nitrovinyl)benzene.

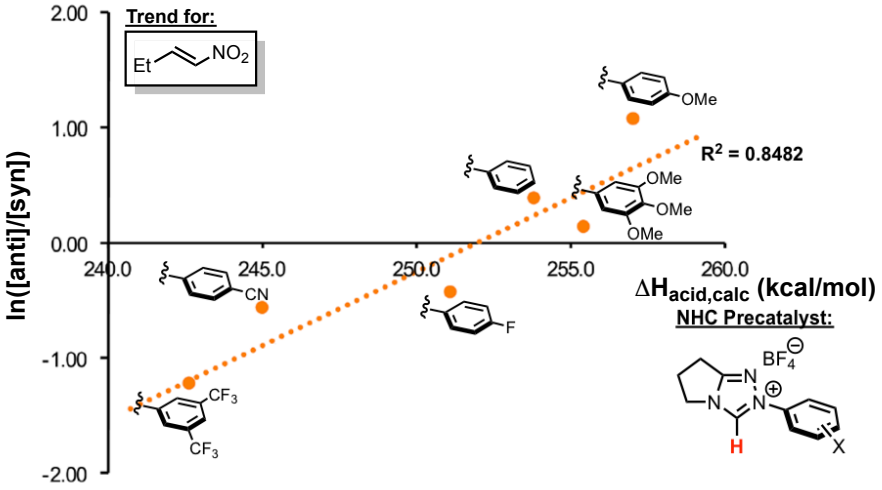

Figure 3.5.6. Natural log plot of the anti/syn ratios vs. calculated PAs for the non-diorthosubstituted achiral series of NHCs for the model homoenolate reaction with (*E*)-(2-nitrovinyl)benzene.

We began to investigate the origin of this effect at the point of discovering this trend. The transition states leading towards the syn- and the anti-product are shown in **Figure 3.5.7**, as has been shown previously. The main difference between these two states is the geometry of the Breslow intermediate enol. For Liu's case, the anti-diastereomer is formed via the E-enol. For our case, the syn-diastereomer is formed through the Z-enol. Given the linear nature of the trend, we hypothesized that the acidity is perhaps reflective of an electron density change at the triazolium core. More specifically, we thought that a more electron-withdrawing *N*-aryl substituent will decrease the electron density at the tethering nitrogen atom (N1). This would in turn serve to give a larger preference for the formation of the Z-enol by way of electrostatic attraction of the oxygen of the Breslow. The opposite would be true for a more electron-donating *N*-aryl substituent – this would increase the electron density at N1 and thus serve to repulse the Breslow oxygen, creating a lower energetic barrier for the formation of the E-enol.

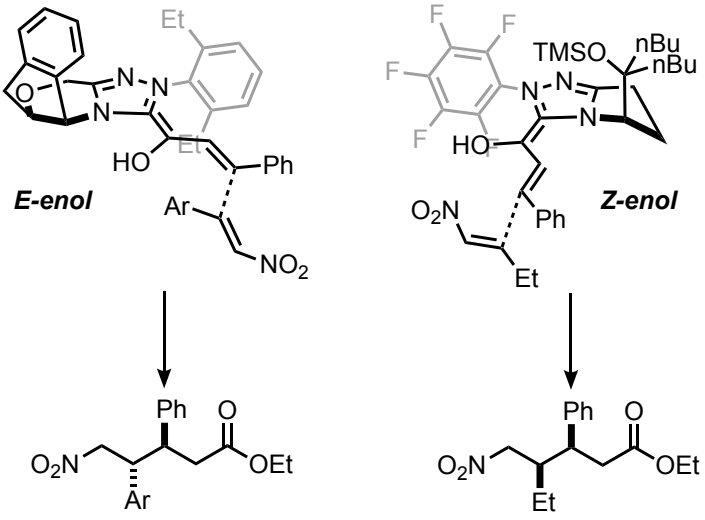

Figure 3.5.7. Proposed transition states for the formation of both anti- and syn-product for Liu's electron rich and Rovis' electron poor catalysts, respectively.

To support this hypothesis, we calculated the transition state energies for the formation of both Z- and E-enols by way of acetate deprotonation (**Figure 3.5.8**). For the highly acidic NHC **1c**, the transition state TSb to form the Z-enol is lower than the transition state to for the E-enol by 3.3 kcal/mol. Alternatively, for the less acidic NHC **1d** the transition state TSa to form the E-enol is lower by 1.5 kcal/mol relative to the transition state TSb to form the Z-enol. To further support this hypothesis, the point-to-plane distances of the oxygen of the Breslow intermediate to the plane of the *N*-aryl substituent were also calculated for catalysts **1c** and **1d** (**Figure 3.5.9**). These calculations reveal a closer proximity of the Breslow oxygen to the plane of the aryl group for the more electron deficient NHC **1c**. The distance for **1c** is 2.23 Å and 2.39 Å for the more electron rich NHC **1d**. These calculated distances support the hypothesis that a net-electrostatic effect may contribute significantly to the formation of either E- or Z-enols – the calculated PAs do an excellent job of providing a tangible data set for the creation of such a LFER. Thus, this data set has been shown to be enabling and could potentially be used as a tool for a more guided approach in improving reaction selectivities or some other function of NHC reactivity.

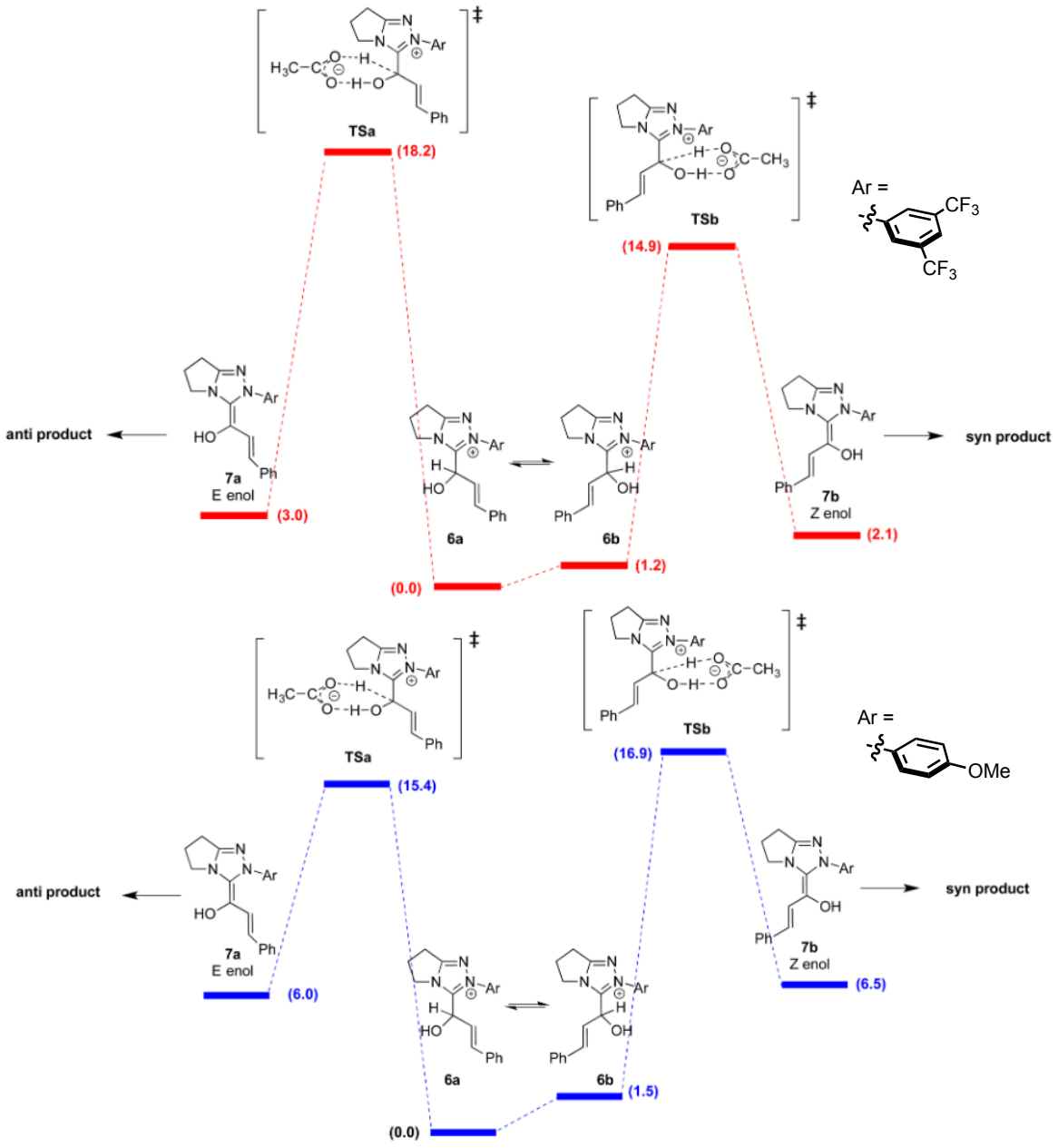

Figure 3.5.8. Acetate catalyzed free energy profiles for the transition states leading towards the E- and Z-enol for an electron poor and an electron rich *N*-aryl substituent.

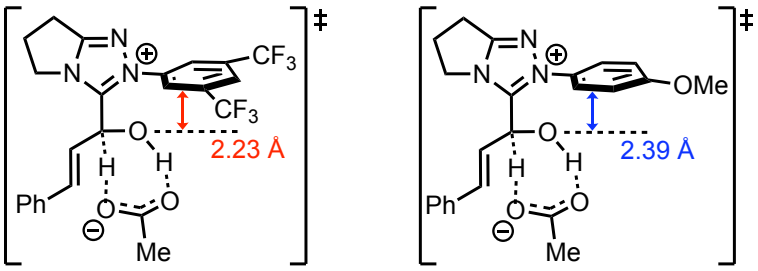

Figure 3.5.9. Calculated distances from **TSb** from **Figure 3.5.8** for both electron poor and electron rich *N*-aryl substitutents.

3.6 Correlations with Chiral Species/Trends with Enantioselectivity

Encouraged by our findings with the achiral species, we wished to perform a similar analysis for the chiral NHCs used in this study. For this, we elected to examine an intramolecular desymmetrizing intramolecular Stetter as was previously reported by our group (**Figure 3.6.1**).[30] An initial series of experiments with R^1, R^2 = *t*Bu revealed no correlation as compared to enantioselectivity. We noted that this particular substrate has a reported >99% ee for NHC ent-**2b**. We thus considered that perhaps the two *t*Bu-groups on the *diortho*-positions of the substrate may serve to override any bias that may occur as a function of acidity due to their size. In order to amend this issue, we chose to move to the less sterically-biased substrate R^1 = H, R^2 = 4-BrC_6H_5. Upon changing substrates, we were very pleased to find an excellent correlation between enantioselectivity and acidity (**Figure 3.6.2**). In this case, a more acidic precatalyst results in greatly reduced enantioselectivities, while a less acidic catalyst will produce higher enantioselection.

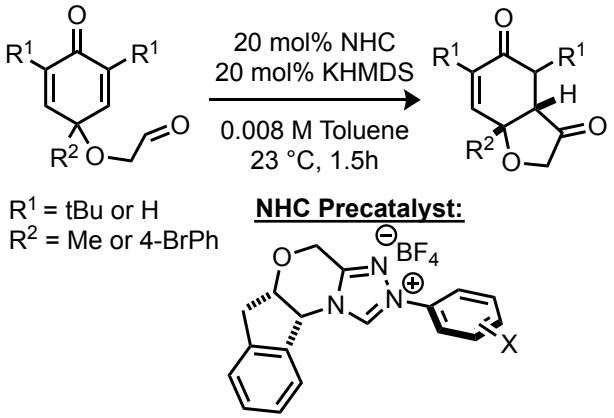

Figure 3.6.1. NHC-catalyzed desymmetrizing intramolecular Stetter model reaction for chiral NHCs.

We propose that the correlation between NHC proton affinity and enantioselectivity may be the result of a bimolecular interaction during the enantiodetermining step. In a previous study by our group, we found that an increasing amount of additive isopropanol decreased the enantioselectivity of the model reaction.[31] It was proposed that the alcohol perturbs the transitition state by hydrogen bonding to some hydrogen-bond acceptor on the Breslow intermediate, such as the dienone carbonyl or the oxygen of the Breslow. Paralleling these results to our study, in the absence of IPA additive, another NHC species could be responsible for this deleterious effect. In our case, we propose that a more acidic NHC results in a more acidic Breslow enol. A more acidic Breslow enol will thus increase the propensity for unfavorable hydrogen-bond interactions to occur during the course of the reaction (**Figure 3.6.3**). We see this reflected well in our trend, where a less acidic NHC reduces this hydrogen-bond interaction, thus allowing the enantiodetermining step to occur unimpeded.

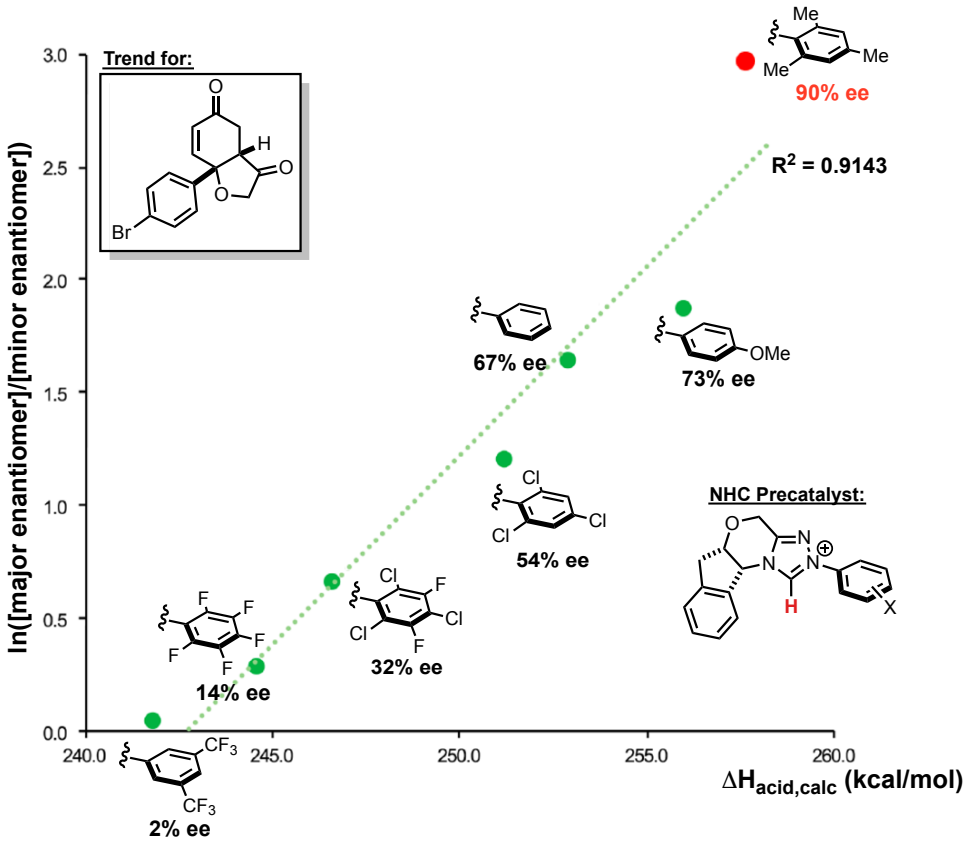

Figure 3.6.2. Natural log plot of the major enantiomer/minor enantiomer ratios vs calculated PAs for the enantioselective model reaction.

It is also worth noting that our previous benchmark for this substrate was 73% ee for NHC ent-**2b**. Through our analysis, hypothesized that a less acidic catalyst should give an increase in enantioselectivity. As a result, we improved the enantioselectivity of the reaction to 90%, exceeding our previous benchmark by 17%. This jump accounts for an energy of about 0.6 kcal/mol at room temperature. This improvement showcases the power of the calculated and experimental proton affinity data sets – these numbers allow for assessment of enantioselection as a function of acidity, thus this approach can ultimately aid in a more rational catalyst choice during the course of methods development.

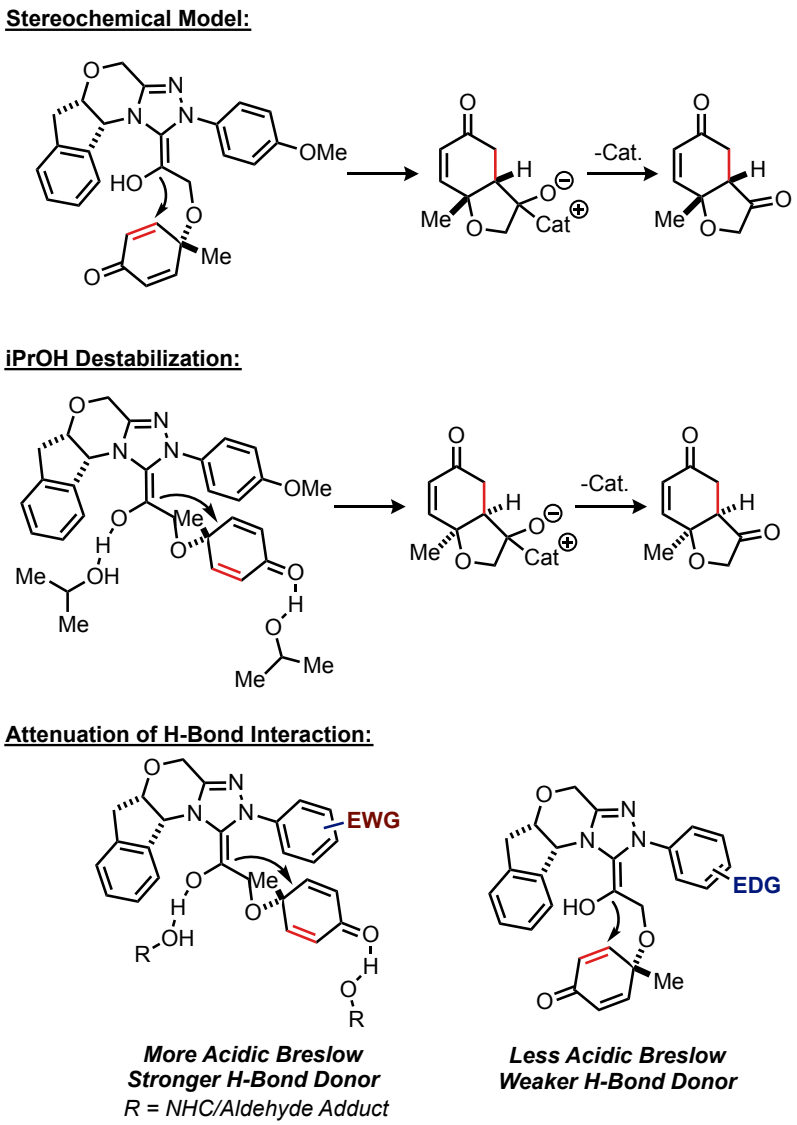

Figure 3.6.3. Stereochemical explanation for correlation between calculated proton affinities and enantioselectivity.

3.7 Conclusion

Through our collaboration, we have disclosed both calculated and experimental gas phase acidities, or proton affinities, for a series of achiral and chiral triazolium-based NHCs that are frequently used as organocatalysts. Not only is the approach of acidity assessment for NHCs novel, the acidities of a number of triazolium precatalysts that have never had their acidities assessed before were studied here for the first time. This point is made especially apparent with the

aminoindanol-based chiral NHCs, where only one scaffold with one *N*-aryl substitution has ever had its acidity assessed (**2a** has a pKa of 17.4 and a PA of 252.9 kcal/mol) prior to this point. The wider energetic range for the proton affinities, as compared to the energetic range of the pKa values, allows for a much easier construction of linear free-energy relationships. As such, we were able to establish the first correlations of their kind for both achiral and chiral NHCs. For the achiral family of NHCs used in this study, we disclosed a correlation between acidity and diastereoselectivity. For the chiral family of NHCs used herein, we were able to correlate enantioselectivity to acidity. Both of these trends prove the original hypothesis to be true – a data set with a sufficiently large enough energetic range can indeed be used as a synthetically enabling tool. Moving forward, we anticipate that researchers will be inspired to use these gas phase acidities as a predictive tool for a less randomized approach towards tackling problems in umpolung-themed reactions.

3.8 References

1) Breslow, R. J. *J. Am. Chem. Soc.* **1957**, *79*, 1762–1763.
2) Breslow, R. *J. Am. Chem. Soc.* **1958**, *80*, 3719–3726.
3) Creary, X. *J. Am. Chem. Soc.* **2003**, *125*, 1439–1439
4) a) Bourissou, D.; Guerret, O.; Gabbaï, F. P.; Bertrand, G. *Chem. Rev.* **2000**, *100*, 39−91. b) Hahn, F. E.; Jahnke, M. C. *Angew. Chem. Int. Ed.* **2008**, *47*, 3122−3172. c) Hopkinson, M. N.; Richter, C; Schedler, M.; Glorius, F. *Nature* **2014**, *510*, 485–496.
5) Crabtree, R. H. *J. Organomet. Chem.* **2005**, *690*, 5451–5457.
6) Crudden, C. M.; Allen, D. P. *Coord. Chem. Rev.* **2004**, *248*, 2247–2273.
7) Tolman, C. A. *J. Am. Chem. Soc.* **1970**, *92*, 2953–2956.
8) Gusev, D. G. *Organometallics* **2009**, *28*, 6458–6461.
9) Dorta, R.; Stevens, E. D.; Scott, N. M.; Costabile, C.; Cavallo, L.; Hoff, C. D.; Nolan. S. P. *J. Am. Chem. Soc.* **2005**, *127*, 2485–2495.
10) Díez-González, S.; Nolan, S. P. *Coord. Chem. Rev.* **2007**, *251*, 874−883.
11) Rovis, T. *Chem. Lett.* **2008**, *37*, 2−7.
12) Kerr, M.S.; Rovis, T. *J. Am. Chem. Soc.* **2004**, *126*, 8876−8877.
13) Mahatthananchai, J.; Bode, J. W. *Chem. Sci.* **2012**, *3*, 192−197.
14) Collett, C.J.; Massey, R.S.; Maguire, O. R.; Batsanov, A. S.; O'Donoghue, A.C.; Smith, A.D. *Chem. Sci.* **2013**, *4*, 1514−1522.
15) de Alaniz, J. R.; Rovis, T. *J. Am. Chem. Soc.* **2005**, *127*, 6284−6289.
16) Liu, F.; Bugaut, X.; Schedler, M.; Fröhlich, R.; Glorius, F. *Angew. Chem. Int. Ed.* **2011**, *50*, 12626−12630.

17) Schedler, M.; Fröhlich, R.; Daniliuc, C. G.; Glorius, F. *Eur. J. Org. Chem.* **2012**, *22*, 4164−4171.

18) Dröge, T.; Glorius, F. *Angew. Chem., Int. Ed.* **2010**, *49*, 6940−6952.

19) Flanigan, D. M.; Romanov-Michailidis, F.; White, N. A.; Rovis, T. *Chem. Rev.* **2015**, *115*, 9307−9387.

20) Massey, R. S.; Collett, C. J.; Lindsay, A. G.; Smith, A. D.; O'Donoghue, A. C. *J. Am. Chem. Soc.* **2012**, *134*, 20421−204232.

21) Maksić, Z. B.; Borislav Kovačević, B.; Vianello R. *Chem. Rev.* **2012**, *112*, 5240–5270.

22) Lias, S. G.; Liebman, J. F.; Levin, R. D. *J. Phys. Chem. Ref. Data.* **1984**, *13*, 695−808.

23) Poad, B. L. J.; Reed, N. D.; Hansen, C. S.; Trevitt, A. J.; Blanksby, S. J.; Mackay, E. G.; Sherburn, M. S.; Chan, B.; Radom, L. *Chem. Sci.* **2016**, *7*, 6245−6250.

24) Chandra, A. K.; Uchimaru, T. *Int. J. Mol. Sci.* **2002**, *3*, 407−422.

25) Niu, Y.; Wang, N.; Muñoz, A.; Xu, J.; Zeng, H.; Rovis, T.; Lee, J. K. *J. Am. Chem. Soc.* **2017**, *139*, 14917−14930.

26) Nair, V.; Sinu, C. R.; Babu, B. P.; Varghese, V.; Jose, A.; Suresh, E. *Org. Lett.* **2009**, *11*, 5570−5573.

27) Maji, B.; Ji, L.; Wang, S.; Vedachalam, S.; Ganguly, R.; Liu, X.-W. *Angew. Chem., Int. Ed.* **2012**, *51*, 8276−8280.

28) White, N. A.; DiRocco, D. A.; Rovis, T. *J. Am. Chem. Soc.* **2013**, *135*, 8504−8507.

29) Zhang, Q.; Yu, H.-Z.; Fu, Y. *Org. Chem. Front.* **2014**, *1*, 614−624.

30) Liu, Q.; Rovis, T. *J. Am. Chem. Soc.* **2006**, *128*, 2552−2553.

31) Liu, Q.; Rovis, T. *Org. Process Res. Dev.* **2007**, *11*, 598−604.

Chapter 4. Gaining Insights into Asymmetric Catalysis on the Basis of Benchmarking

4.1 Introduction

Modern kinetic analyses of chemical reactions provide both the infrastructure and practical means for the elucidation of reaction mechanisms.[1] Understanding a mechanism is generally considered to be critical towards achieving an overall successful transformation – this is made evident whether in an academic setting when attempting to optimize a novel catalytic methodology,[2] or in an industrial setting wherever efforts are made toward either catalyst discovery or process development.[3] This is especially true for asymmetric catalytic transformations, where the extra considerations that pertain to rendering a reaction both enantioselective and robust present additional hurdles with respect to obtaining an economically viable chemical transformation. In consideration of this importance and given the complexity often associated with chemical kinetics in tandem with asymmetric catalysis, a significant effort has been made to render available methods more accessible, precise, and powerful.[4]

As a result of these efforts, experimental methodologies offering increasingly accurate insights into chemical reactivity on the basis of kinetic analysis continue to be established. One such modern technique, pioneered by Blackmond and coworkers, utilizes reaction calorimetry, wherein it is possible to monitor the progress of a reaction by monitoring its instantaneous heat flow, directly relating to its enthalpy change and reaction rate.[5] In-situ IR spectroscopy can also be utilized for these purposes, relying on the presence of distinctive absorbance peaks in the IR region of a monitored substrate or product.[6] NMR spectroscopy is often the most ideal method of choice for the purposes of obtaining information from a given reaction over a period of time. To improve the accuracy and precision of these results, there have been significant advances in the

development of rapid-injection NMR apparatuses (RI-NMR).[7] All of these methods have proven to be robust and quite powerful in their mechanism-elucidating capabilities. Unfortunately, with respect to interrogating catalytic asymmetric transformations, there are a lack of non-invasive methods that effectively utilize enantiomeric excess (ee) to extract important information of a given reaction on the basis of the chiral catalyst.

In this regard, Blackmond and coworkers have very recently published a powerful method to monitor the ee of kinetic resolutions using vibrational circular dichroism in combination with FT-IR spectroscopy.[8] Prior to this, studies dedicated to this have been limited largely to either calculation-dense or invasive methodologies.[9] Furthermore, a common drawback with more traditional methods is the indeterminate error that may occur when analyzing physically and temporally separated reaction runs. For example, early data-points may be lost in between the variable amount of time it takes to administer a reaction-activating reagent and then obtain the first spectroscopic datum. As a result of this fluxional inaccuracy, reliable data often requires multiple and averaged runs to increase accuracy as well as precision. RI-NMR has made impressive headway to resolve these issues, but much like the aforementioned modern methodologies, this technique suffers somewhat from both instrumental and method unavailability.

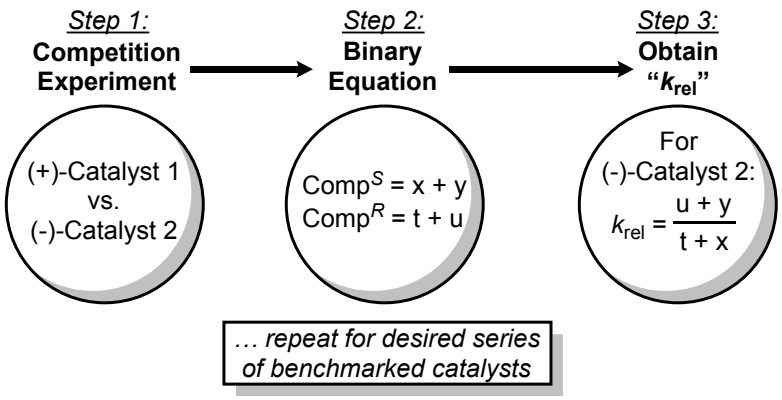

Figure 4.1.1. Proposed Experimental Protocol: Step 1: Run competition between benchmarking cat. 1 and to-be benchmarked cat. 2. Step 2: Plug ee from step 1 to binary equation. Step 3: Obtain k_{rel} from calculated variables in Step 2.

We thus considered a way to overcome these limitations. Devising an analytical tool with interrogating capabilities would require both simplicity for the sake of user-friendliness and the overall accuracy of the aforementioned techniques, while allowing for greater accessibility. Keeping in mind the challenges associated with asymmetric catalysis, we postulated that we can obtain a significant amount of information from a given enantioselective reaction by comparing the relative rate (k_{rel}) of one chiral catalyst to one that is structurally dissimilar. As was previously disclosed by our group, one way to determine the k_{rel} between two chiral catalysts is to measure it first with an achiral catalyst – the two $k_{rel's}$ can then be used to calculate the k_{rel} between the two aforementioned chiral catalysts.[10] We wished to take further advantage of this experimental set-up, simplifying the protocol to obviate the need for an achiral component to instead derive our desired k_{rel} directly from a simple competition experiment between the two chiral components (**Figure 4.1.1**). Streamlining this protocol offers a facile and overall noninvasive method of assessing and comparing the reactivity of a series of chiral catalysts on the basis of a single competition experiment. When comparing these catalysts against a standardized chiral catalyst, we can benchmark their reactivities for the pathway towards a single enantioenriched product

against the standard, revealing the effects upon reactivity associated with structural perturbations. We anticipate that the benefits offered by this approach will be complementary to those offered by the more well-established aforementioned methodologies. Described herein are our efforts towards achieving this goal.

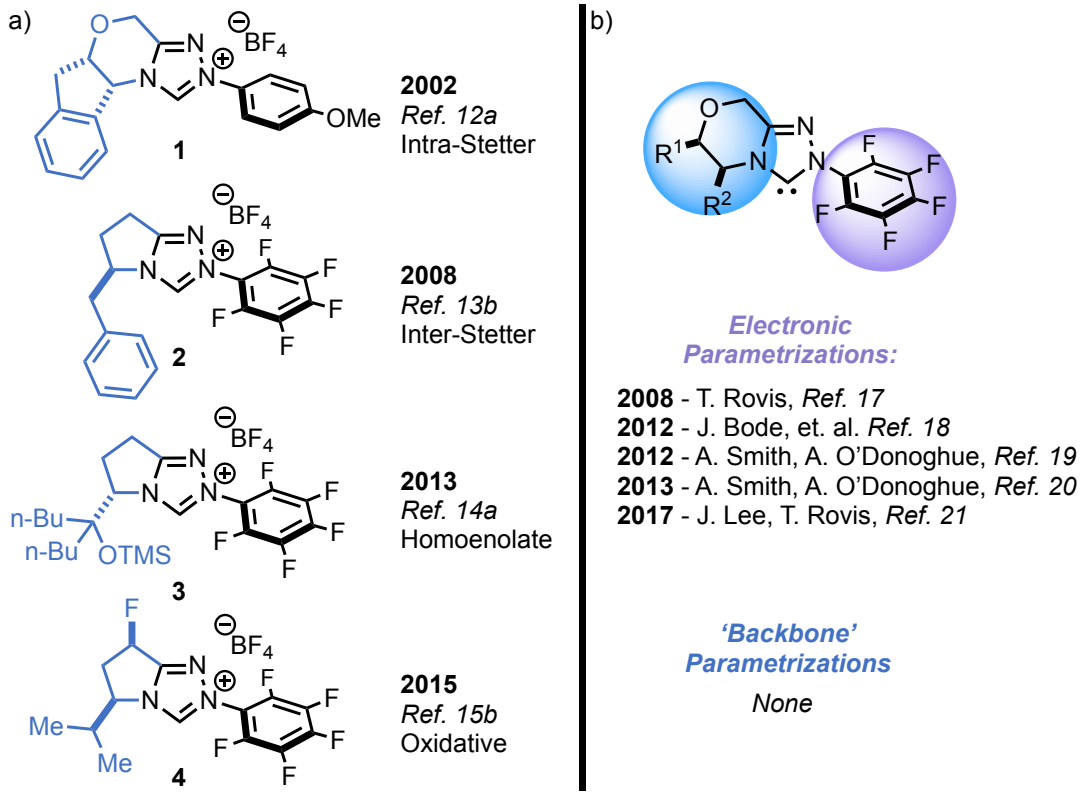

Figure 4.2.1. a) Optimized catalyst architectures associated with intra- and intermolecular Stetter, homoenolate, and oxidative reactions. b) Studies associated with effects on reactivity associated with changes to the catalyst structure – several studies performed on the *N*-Aryl substituent, none on the backbone of the catalyst.

4.2 Validating Approach with Asymmetric Organocatalysis – *N*-Heterocyclic Carbenes

We first wished to demonstrate the validity of this experimental protocol with its application towards the use of *N*-heterocyclic carbenes (NHCs) as chiral organocatalysts. Our research group has a rich history in this field and has thus made a number of contributions.[11] If we quickly analyze the NHCs used in this field, starting with a highly asymmetric intramolecular

variant of the Stetter reaction,[12] continuing with asymmetric intermolecular variants of the Stetter,[13] and further opening NHC reactivity towards homoenolate[14] and oxidative pathways,[15] we can quite clearly see that is an optimization sequence and evolution of the architectures best suited for these transformations (**Figure 4.2.1a**). In this vein, a tremendous effort has been made by the synthetic community towards synthesizing novel NHC architectures. These structures often possess enormous variances in their backbones relative to the more well-known aminoindanol and pyrrolidine based triazolium salts.[11,16] Of these triazolium-based NHCs, the most well studied, but still limited, impacts upon reactivity associated with structural modifications are those related to changes to the *N*-aryl substituent (**Figure 4.2.1b**).[17] One such of these studies was performed by Bode and coworkers, wherein they found that NHCs possessing aryl-groups that feature substitution at the *ortho* and *ortho'* positions tend to favor annulation, oxidation, and redox-type pathways. This is due to fast and irreversible formation of Breslow intermediates from α,β-unsaturated aldehydes, the origin of which arises largely from steric effects.[18] Conversely, Bode concluded that the less hindered and more electron deficient pentafluorophenyl-substituted NHC tends to favor Stetter and benzoin-type reactions. Smith, O'Donoghue and coworkers further studied this, providing experimental and kinetic evidence supporting Bode's hypothesis, showing that increased acidity of the aldehydic proton in the tetrahedral intermediate prior to formation of the Breslow intermediate plays a large role in dictating this selectivity.[19] The same groups also provided a number of solution-phase pKa's for a series of synthetically relevant azolium salts, showcasing their dependence on the *N*-aryl substituent.[20] A complementary study assessing the proton affinities of a series of synthetically relevant triazolium precatalysts was done by our group in collaboration with Lee and coworkers,[21] where in the same publication correlations were found linking acidity with several functions of reactivity with both chiral and achiral NHCs. Given these

studies, there should be no doubt that the *N*-aryl substituent plays a critical role in determining catalyst reactivity and selectivity.

Despite the large and diverse set of unique architectures that exist dedicated for the purposes of asymmetric umpolung reactivity, papers commenting on the origin of effects as dictated by the *other* half of the catalyst are non-existent at the onset of our studies. Perhaps one of the reasons for this is that this half of the catalyst is generally considered to be at its most useful when utilized for the purposes of inducing asymmetry in enantioselective transformations. Regardless, stereoelectronic effects that are critical to both reactivity and stereoselectivity can arise from the backbone of the catalyst structure and indeed have been already been demonstrated.[22] Thus, an application of the proposed benchmarking tool towards NHC catalysis offers a unique way to search for and assess these often "hidden", "difficult-to-account for", or otherwise "unpredictable" catalyst backbone-effects in what amounts to a very simple experimental protocol.

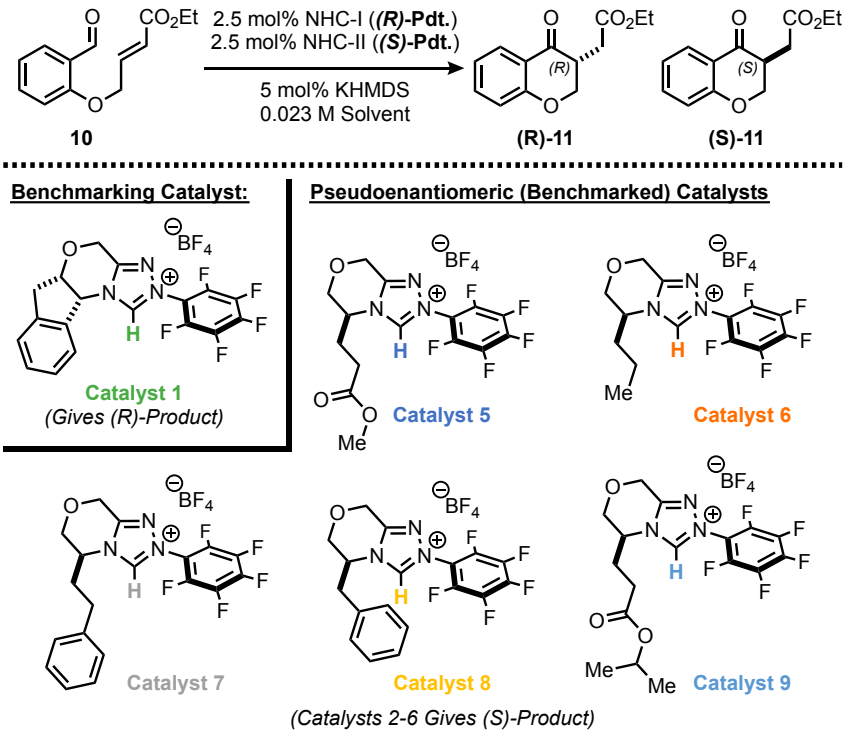

Figure 4.2.2. Proof-of-concept model reaction, wherein **Catalyst 1** is the benchmarking catalyst with respect to a class of structurally perturbed, yet electronically analogous, series of catalysts that are pseudoenantiomeric in product formation.

We chose to start with a variant of the intramolecular Stetter reaction as was previously published by our group (**Figure 4.2.2**).[13a] When comparing two catalysts in a single reaction for the formation of an enantioenriched product, we must first meet several important criteria. The first condition is that the reaction must be first order with respect to the catalyst. This substrate is excellent for the purposes of testing catalyst performance for newly developed NHCs, and is especially suitable for our purposes since it satisfies this important criterion. Indeed, it has already been shown that the catalyst for this transformation is first order with respect to the intramolecular Stetter reaction.[23] Another important criterion that must be met at this point is the absence of subsequent reactivity for the enantioenriched product. Again, our chosen reaction manifold succeeds in this respect since it has been previously shown that the Stetter reaction is an irreversible transformation.[24] Although catalyst-induced epimerization has been previously demonstrated to

be an issue for this transformation for the more Lewis basic NHCs,[17] under the right set of reaction conditions,[25] as well as considering that the NHCs used in this study are all *N*-pentafluorophenyl substituted and thus relatively weakly basic, the deleterious contribution of this effect is substantially mitigated.[26] The last condition that must be met is the product cannot contain multiple stereocenters.[27] Again, our chosen proof-of-concept reaction manifold succeeds in this regard since only one stereogenic center is formed.

4.3 Obtaining k_{rel} values for Benchmarking Experiments

Our reaction set-up is as follows: For the first step we obtain the ee's of each chiral catalyst selected for our protocol. We then re-run the same reaction in the presence of equimolar amounts of the designated chiral catalysts under a total mole percent equal to the original runs.[28] For best results, one chiral catalyst should ideally give one enantiomer of product and the other should be stereoselective for the antipode. For the second step, we use **Equation 1** to solve for the amount of *(S)*- and *(R)*-product that is given in the competition experiment (**Figure 4.3.1a**). Here, $Comp^S$ and $Comp^R$ refer to the ratio of *(S)*- to *(R)*-product, respectively, as measured by the competition experiment in the previous step. The variables x^S and t^R denote the amount of *(S)*- and *(R)*-product, respectively, that is formed by the standalone benchmarking catalyst – y^S and u^R are the expressions for the catalyst that is being benchmarked. The purpose of this binary equation is to obtain the amount of *(S)*- and *(R)*-product that was given in the course of the competition experiment, and then plug those values into our ratio as shown in **Equation 2**. Solving this equation with our values from **Equation 1** gives the relative rate of one chiral catalyst versus the other. As an example, in the competition between **catalyst 5** (**C-5**) and **catalyst 1** (**C-1**) for the reaction with substrate **10**, the ee given by **C-1** is 93% ee^R, or a ratio of 27.57 : 1 *(R)*- to *(S)*-product. For **C-5**,

we see 96% ee^S, or a ratio of 49:1 *(S)*- to *(R)*-product. At this point, we choose to express variable t in terms of x, and variable u in terms of y, thus reducing a binary equation system with four variables to a much simpler two-variabled system. For **C-1**, since the ratio is 27.57^R : 1^S, and x equals the amount of *(S)*-product by **C-1** and t equals the amount of *(R)*-product by the same catalyst, we can thus say that t = 27.57x. Likewise, in doing the same with the reciprocal of **C-5**, we obtain u = 0.02041y. After having appropriately expressed **Equation 1** with the proper substitutions, we can easily solve for both y and x. In the third and final step, we again express t and u in terms of x and y for **Equation 2**, plug in our obtained values and thus arrive at our desired k_{rel}, which for this instance is 0.370 (**Figure 4.3.1b**).[29] This protocol was repeated three-fold and an average k_{rel} of 0.375 ± 0.016 was measured for the competition experiments in toluene for **C-5** and **C-6** in the formation of product **11**.

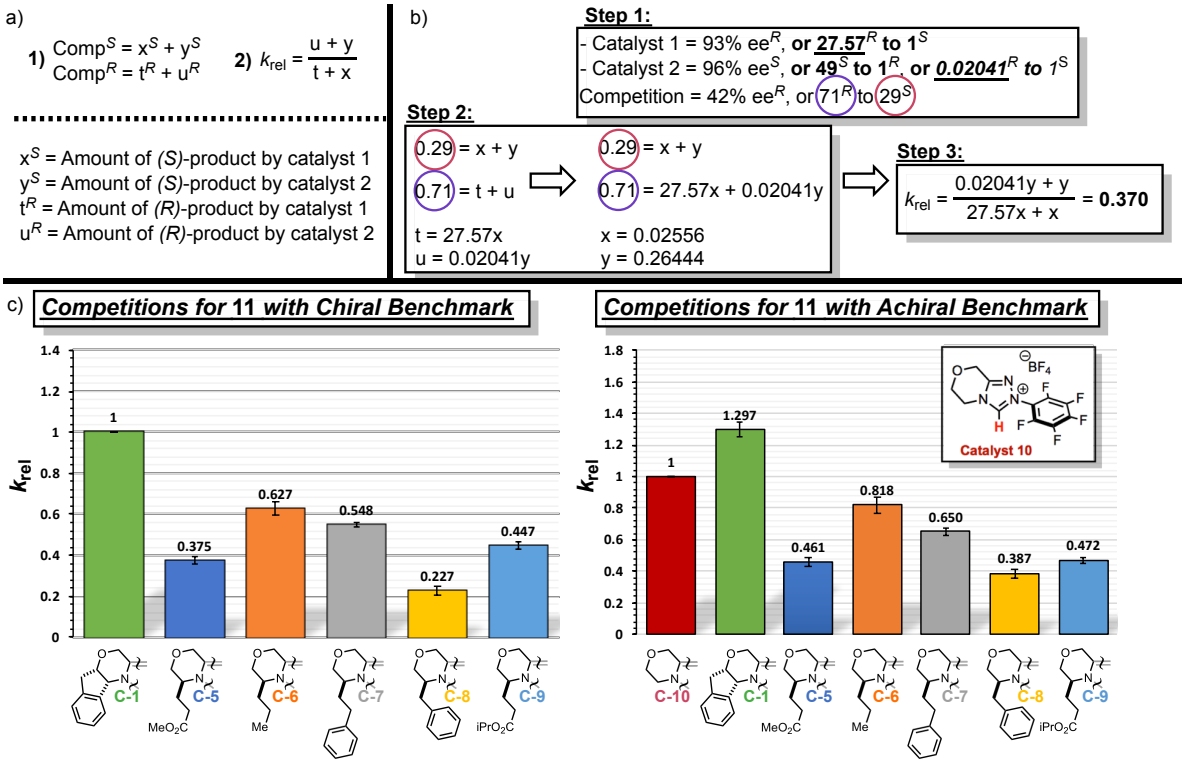

Figure 4.3.1. a) Binary equation and k_{rel} expression, where the solutions for variables from equation 1 will be used to solve equation 2. b) Sample solution for k_{rel} expressions. c) k_{rel} values for formation of **11** as benchmarked against **Catalyst 1** and achiral **Catalyst 10**.

We continue this analysis with **C-6**, **C-7**, **C-8**, and **C-9**, giving us k_{rel} values of 0.627 ± 0.033, 0.548 ± 0.012, 0.227 ± 0.022, and 0.447 ± 0.019, respectively. In each case, we can quite clearly see that the benchmarking catalyst is faster than each catalyst in our designated pseudoenantiomeric series (**Figure 4.3.1c**). To demonstrate the modularity and reproducibility of these results, achiral benchmarking NHC **C-10** was chosen and the experimental protocol was repeated for toluene.[25] The trends in reactivity for these experiments reflect those for when **C-1** was chosen as the benchmarking catalyst. Furthermore, to showcase the ease of this experimental methodology, k_{rel} values were easily obtained over a range of different solvents (**Figure 4.3.2**). In every single case, the much more widely known **C-1** was shown to be more reactive for the selected intramolecular Stetter reaction. Some basic trends do exist strictly for the pseudoenantiomeric series, wherein **C-6** is shown to be generally more reactive and **C-9** is often the worst performing. The exception here is when the reaction is conducted in acetonitrile, where the overall reactivity for the pseudoenantiomeric series seems to equalize. A number of factors may be operative here, ranging anywhere from steric influence for the initial addition of the NHC to the carbonyl of the aldehyde to differential rates of catalyst decomposition. Though further studies in this regard are currently underway, the premise of the tool is appropriately demonstrated wherein we can quickly and quantitatively assess the differences in reactivity as dictated by the backbone of the NHC.

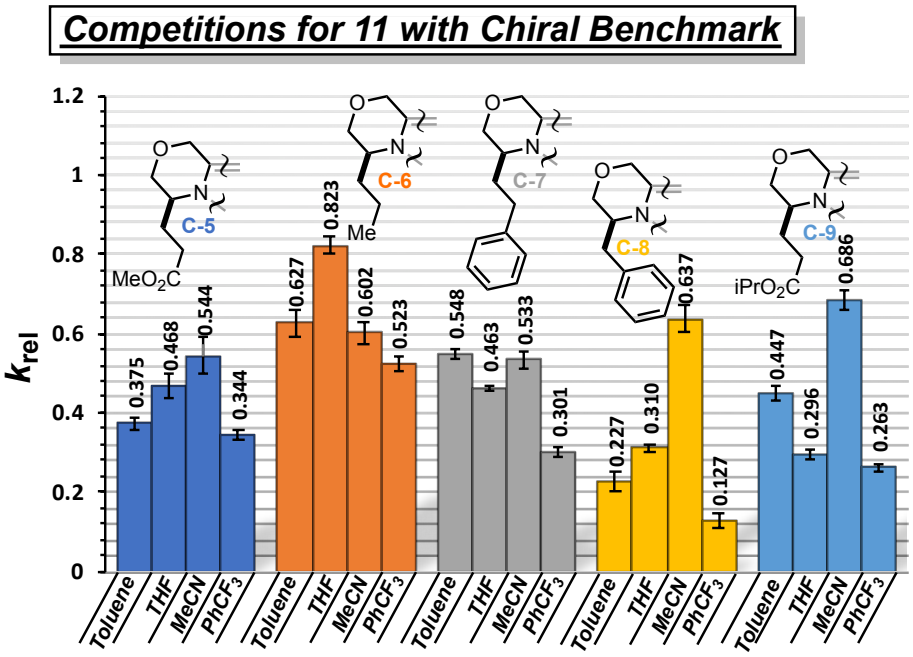

Figure 4.3.2. k_{rel} values for formation of **11** as benchmarked against catalyst **1** in several solvents.

4.4 Comparing Benchmarking Protocol to NMR-Spectroscopy

As previously mentioned, the same data can be potentially extracted by following conversion using NMR spectroscopy and comparing initial rate kinetics. In this regard, we moved to substrate **12** and re-ran the proposed analysis (**Figure 4.4.1**). This substrate is of special interest to us since it lacks the phenolic oxygen of the previous substrate, which has been implicated in assisting with the turn-over limiting step of the Stetter reaction.[23] We thus believed that the differences in catalyst reactivity could be further demonstrated by the proposed benchmarking methodology using a substantially less reactive substrate. Under our optimal conditions, with our most precise initial points, we still see the same issues as we have previously described. Because of the limit in precision with these early timepoints, any kinetic analysis with respect to a change in chiral catalysts using NMR is prone to a large degree of error. Likewise, the same error is

propagated to the end points and it thus becomes difficult to make any conclusions with respect to differential catalyst reactivity. This further validates the notion that utilizing this experimental protocol can provide uniquely robust and precise data, since both catalysts are run in the same reaction conditions at the same time, thus greatly reducing the risk of error propagation between separate runs. In this case, we see that **C-6** is 2.051 ± 0.048 times faster than **C-1**, demonstrably enhancing the trends that we saw in the previous experiments. This trend is also reflected in a select choice of different solvents as was the case above.[25] Overall, this approach shows that we can use this approach not only as a high-throughput assessment of differences in catalyst reactivity for a given reaction, which can be used to more clearly define an appropriate catalyst for a given use, but it can also be used to increase the serendipity with which one finds these potentially hidden catalyst backbone effects.

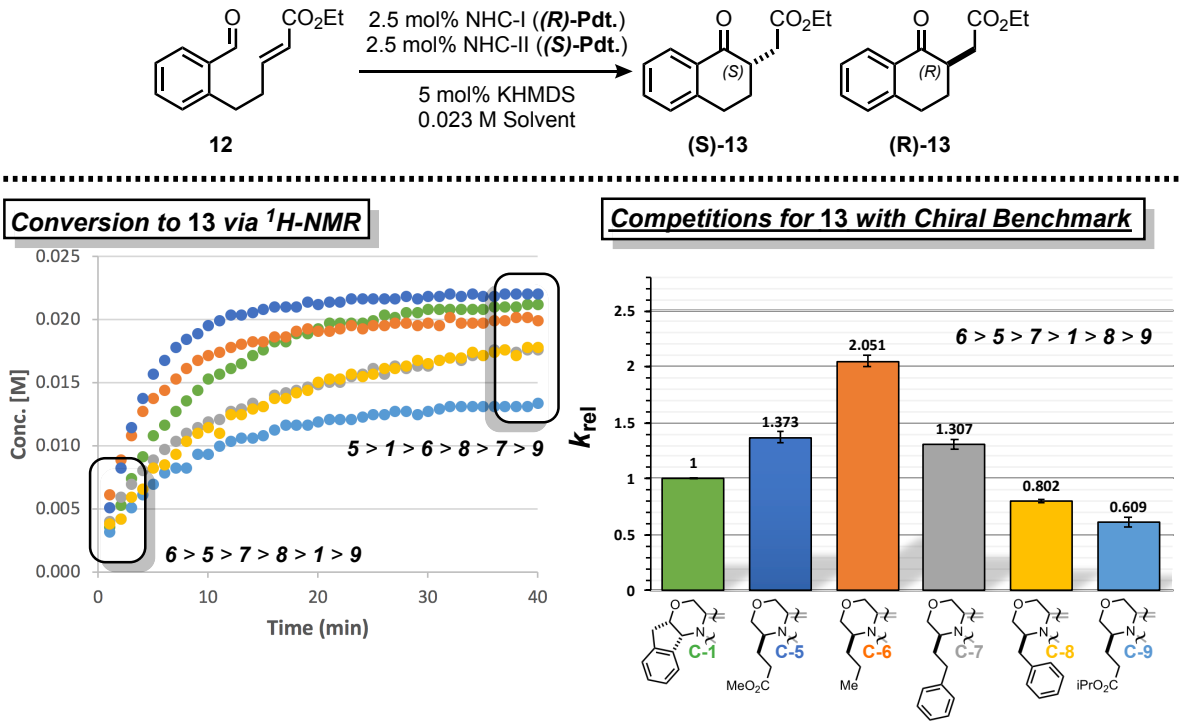

Figure 4.4.1. Catalyst reactivity assessment as performed ^{1}H-NMR, as well as with proposed "benchmarking" approach.

4.5 Validating Approach with Asymmetric TM Catalysis – Rh(I)-Catalysis

Upon demonstrating that the protocol is operative for asymmetric organocatalytic transformations, we wished to establish its applicability to a broad range of asymmetric catalytic transformations. We chose to demonstrate this with an asymmetric Rh(I)-catalyzed [2+2+2] cycloaddition of alkenyl isocyanates and aromatic alkynes, as was previously discovered by our group (**Figure 4.5.1**).[30] There are two productive pathways for this approach, one that forms vinylogous amides following an oxidative cyclization, CO migration, migratory alkene insertion, and subsequent reductive elimination sequence, while the other produces cyclic lactams, both of which have been rendered highly enantioselective (**Figure 4.5.2**).[31] This divergence in reactivity offers a unique opportunity to showcase the proposed methods ability to assess catalyst reactivity for a single productive pathway in the presence of others. The measured k_{rel} for one pathway may indicate the preference of one pathway to another strictly based on catalyst structure. This body of work bears its inception in 2006 with the initial discovery of the achiral transformation.[32] Following an approximately seven year effort, our group disclosed a number of trends and generalizations in terms of which ligands worked best for a given substrate, where electron-deficient ligands give a higher preference for the vinylogous amide product, bulkier substitution at the amine gives a higher preference for the lactam product, and binol/bisphenol ligands tend to favor vinylogous amide products with aliphatic alkynes.[33]

Using this benchmarking approach, we wondered if we could encapsulate these enormous efforts within a single experimental protocol. On a related note, we have already demonstrated above with the pseudoenantiomeric series of NHCs that complex situations can arise in which it becomes exceedingly difficult to generalize some function of a stereoelectronic nature with respect to reactivity, especially one that is universal across a broad range of substrates for a specific

transformation. This paradigm is also reflective in asymmetric catalysis for TM-metal catalyzed reactions. Thus, an application of our experimental protocol under this scenario can potentially enable a quick assessment of which chiral ligand is best for a given substrate at any time, a concept that is of high interest to industry.[34] We thus employed the approach described herein for the cycloaddition between aliphatic isocyanate **14** and aryl alkyne **15**. We chose **ligand 1** (**L-1**) as the benchmark since it has been recognized to be the most chemoselective ligand for the pathway invoking a CO-migration.[35] The results are shown below, wherein the benchmarking ligand is substantially faster than **L-2**, **L-3**, **L-5**, and **L-6** (**Figure 4.5.3**). Since a surprising rate acceleration was noted for *m*-xylyl substituted **L-4**, we synthesized **L-8** to see if a ligand that is isoelectronic to **L-1,** yet isosteric to **L-4**, would be benchmarked somewhere between them. The results are as expected, where **L-8** is benchmarked at 1.275 ± 0.028, thus showcasing the potential for application of this approach for a more logic-based approach in catalyst development.

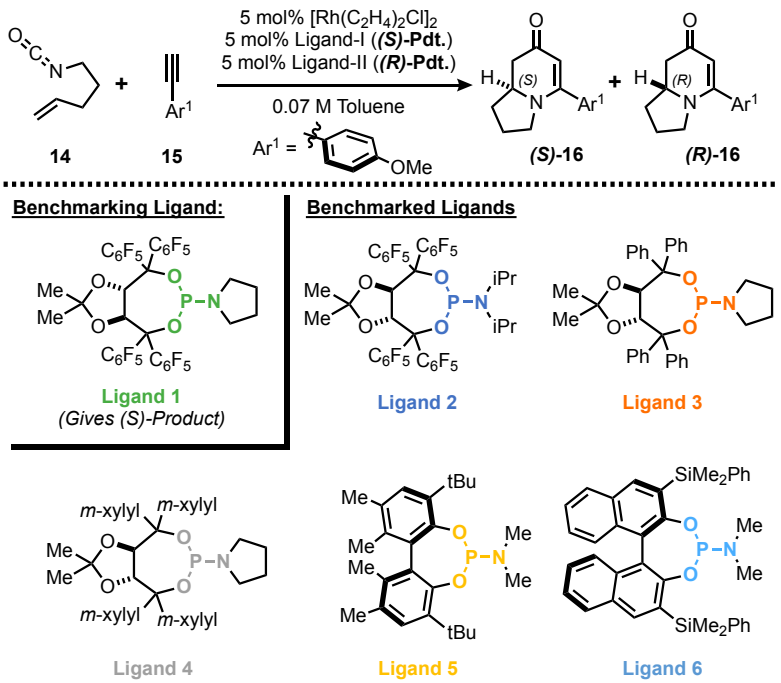

Figure 4.5.1. Rh(I)-cycloaddition of isocyanate **14** with aryl alkyne **15**. Ligand **1** is the benchmarking phosphoramidite ligand as compared to a wide range of different phosphoramidite ligands.

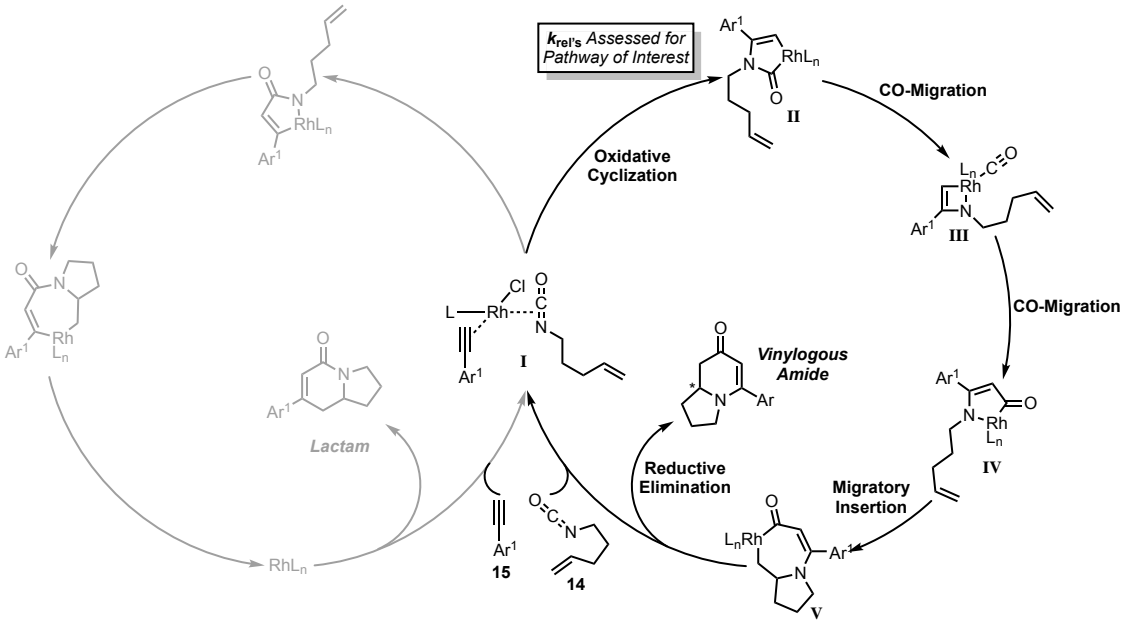

Figure 4.5.2. Mechanism for the synthesis of vinylogous amides and lactams through the studied Rh(I)-catalyzed [2+2+2] cycloaddition.

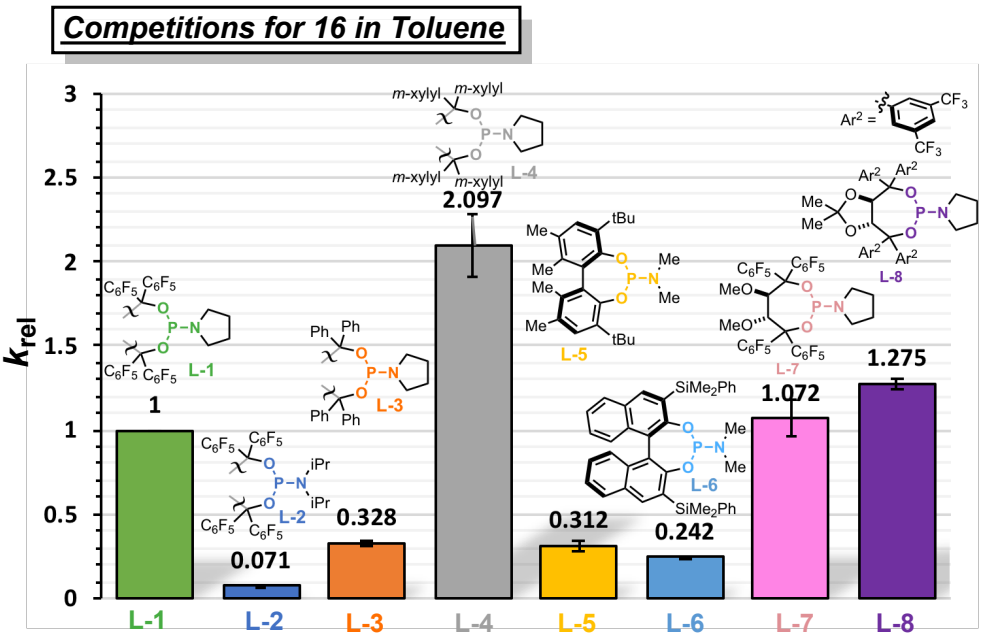

Figure 4.5.3. Ligand-Benchmarking results for phosphoramidite series summarizing a 7-year effort.

Nonetheless, as was predicted, we were able to summarize three key conclusions from our previous efforts: 1) An increase in the steric bulk on the amine of the phosphoramidite ligand negatively affects the amount of vinylogous amide that is formed, thus resulting in a less reactive **L-2**. 2) A more electron-deficient ligand tends to favor more vinylogous amide product, and thus **L-1** and **L-8** are more reactive than **L-2**, **L-3**, **L-5** and **L-6** 3) Structural changes to the acetonide of the TADDOL-based phosphoramidites results in little to no change in reactivity (**L-7**). Furthermore, in terms of biphenyl **L-5** and bisphenol **L-6**, it has been previously demonstrated that **L-6** is generally better than **L-5** for the formation of vinylogous amide product.[36] This conclusion is also reflected in the benchmarking data, where **L-5** is benchmarked at 0.312 ± 0.036 and **L-6** at 0.242 ± 0.013. Thus, for future cases, in an appropriate asymmetric transformation that is not well understood, a researcher may be interested in using this tool for a more rapid discovery of these stereoelectronic effects, the data of which can provide a broad platform for further scientific discovery and catalyst development.

4.6 Conclusions

In summary, the proposed benchmarking approach has been shown to be a facile and demonstrably accurate way of assessing differences in reactivity between various chiral components in a given asymmetric reaction, on the basis of their enantioselectivities. The consistency and reproducibility of this data was demonstrated for runs where both chiral and achiral NHCs act as the benchmark. Furthermore, this method of assessment has been shown to be amenable to two distinct fields within asymmetric catalysis – organocatalysis, as well as transition metal catalysis. Though shown to be robust in the reaction paradigms as shown above, as goes with any tool, judicious choice of this approach must be made where inconsistent data may be indicative of anything from variable rates of catalyst decomposition between runs, erosion of substrate ee by fault of reaction conditions, catalyst-induced epimerization, to even perhaps nonlinearity. Nonetheless, the approach is highlighted by its use as a high-throughput manner of assessing catalyst activity for a given enantioselective transformation. This raises the potential to not only highlight hidden and previously unaccounted for stereoelectronic effects of these chiral components, but also to be used as a more logical approach towards catalyst choice in the course of methods development.

4.7 References

1) Skinner, G. B. Introduction to Chemical Kinetics; Elsevier Inc. 1974; 1-3.

2) For select instances where kinetics played a significant role in mechanism elucidation, see: (a) Shekhar, S.; Ryberg, P.; Hartwig, J. F.; Mathew, J. S.; Blackmond, D. G.; Strieter, E. R.; Buchwald, S. L. *J. Am. Chem. Soc.* **2006**, *128*, 3584–3591. (b) Zuend, S. J.; Jacobeson, E. N. *J. Am. Chem. Soc.* **2009**, *131*, 15358–15374. (c) Hein, J. E.; Armstrong, A.; Blackmond, D. G. *Org. Lett.* **2011**, *13*, 4300–4303.

3) For select reviews on the role of kinetics in industry, see: (a) Bos, A. N. R.; Lefferts, L.; Marin, G. B.; Steijns, M. H. G. M. *Applied Catalysis A: General 160* **1997**, 185-190. (b) Berger, R. J.; Stitt, E. H.; Marin, G. B.; Kapteijn, F.; Moulijn, J. A. *CATTECH* **2001**, *5*, 36-60.

4) Blackmond, D. G. *J. Am. Chem. Soc.* **2015**, *137*, 10852 – 10866.

5) Blackmond, D. G.; Rosner, T.; Pfaltz, A. *Org. Proc. Res. Dev.* **1999**, *3*, 275–280.

6) Rein, A. J.; Donahue, S. M.; Pavlosky, M. A. *Curr. Opin. Drug Discovery Dev.* **2000**, *3*, 734–742.

7) Denmark, S. E.; Williams, B. J.; Eklov, B. M.; Pham, S. M.; Beutner, G. L. *J. Org. Chem.* **2010**, *75*, 5558–5572.

8) Mower, M. P.; Blackmond, D. G. *ACS Catal.* **2018**, *8*, 5977–5982.

9) a) Guo, C.; Shah, R. D.; Dukor, R. K.; Cao, X.; Freedman, T. B.; Nafie, L. A. *Anal. Chem.* **2004**, *76*, 6956 – 6966. b) Dey, S.; Karukurichi, K. R.; Shen, W.; Berkowitz, D. B. *J. Am. Chem. Soc.* **2005**, *127*, 8610–8611. c) Fink, M. J.; Rial, D. V.; Kapitanova, P.; Lengar, A.; Rehdorf, J.; Cheng, Q.; Rudroff, F.; Mihovilovic, M. D. *Adv. Synth. Catal.* **2012**, *354*, 3491 – 3500. d) Rintjema, J.; Kliej, A. W. *ChemSusChem* **2017**, *10*, 1274 –1282. e) Companyó, X.; Burés, J. *J. Am. Chem. Soc.* **2017**, *139*, 8432–8435.

10) DiRocco, D. A.; Noey, E. L.; Houk, K. N.; Rovis, T. *Angew. Chem. Int. Ed.* **2012**, *51*, 2391–2394.

11) Flanigan, D. M.; Romanov-Michailidis, F.; White, N. A.; Rovis, T. *Chem. Rev.* **2015**, *115*, 9307-9387.

12) a) Kerr, M. S.; Read de Alaniz, J.; Rovis, T. *J. Am. Chem. Soc.* **2002**, *124*, 10298–10299. b) Kerr, M. S.; Rovis, T. *J. Am. Chem. Soc.* **2004**, *126*, 8876–8877.

13) a) Enders, D.; Niemeier, O.; Henseler, A. *Chem. Rev.* **2007**, *107*, 5606−5655. b) Liu, Q.; Perreault, S.; Rovis, T. *J. Am. Chem. Soc.* **2008**, *130*, 14066–14067. c) Liu, Q. Rovis, T. *Org. Lett.* **2009**, *11*, 2856–2859. For a review of early work on Stetter-type pathways, see: d) Read de Alaniz, J.; Rovis, T. *Synlett* **2009**, *8*, 189-1207.

14) a) White, N. A.; DiRocco, D.; Rovis, T. *J. Am. Chem. Soc.* **2013**, *135*, 8504–8507. b) Lakshmi K. C. S.; Paul, R. R.; Suresh E.; Nair V. *Synlett* **2014**, *25*, 853-857. For a review of early work on homoenolate-type pathways, see: c) Menon, R. S.; Biju, A. T.; Nair, V. *Chem. Soc. Rev.* **2015**, *44*, 5040-5052.

15) a) White, N. A.; Rovis, T. *J. Am. Chem. Soc.* **2014**, *136*, 14674–14677. b) White, N. A.; Rovis, T. *J. Am. Chem. Soc.* **2015**, *137*, 10112–10115. For a general review on oxidative pathways, see: c) De Sarkar, S.; Biswas, A.; Samanta, R.C.; Studer, A. *Chem. Eur. J.* **2013**, *19*, 4664-4678.

16) In this regard, over 50 unique structures are known for triazolium precatalysts (see citation 1). For select papers dedicated to the synthesis of unique structures, see: a) Brand, J. P.; Siles, J. I. O.; Waser, J. *Synlett* **2010**, *6*, 881−884. b) Rong, Z. Q.; Li, Y.; Yang, G. Q.; You, S.L. *Synlett* **2011**, *7*, 1033−1037. c) Rafíński, Z.; Kozakiewicz, A.; Rafińska, K. *ACS Catal.* **2014**, *4*, 1404−1408. d) Ozboya, K. E.; Rovis, T. *Synlett* **2014**, *25*, 2665-2668.

17) Rovis, T. *Chem. Lett.* **2008**, *37*, 2-7.

18) Mahatthananchai, J.; Bode, J. W. *Chem. Sci.* **2012**, *3*, 192-197.

19) Collett, C. J.; Massey, R. S.; Maguire, O. R.; Batsanov, A. S.; O'Donoghue, A.C.; Smith, A. D. *Chem. Sci.* **2013**, *4*, 1514-1522.

20) Massey, R. S.; Collett, C. J.; Lindsay, A. G.; Smith, A. D.; O'Donoghue, A. C. *J. Am. Chem. Soc.* **2012**, *134*, 20421-204232.

21) Niu, Y.; Wang, N.; Muñoz, A.; Xu, J.; Zeng, H.; Rovis, T.; Lee, J.K. *J. Am. Chem. Soc.* **2017**, *139*, 14917-14930.

22) a) DiRocco, D. A.; Oberg, K. M.; Dalton, D. M.; Rovis, T. *J. Am. Chem. Soc.* **2009**, *131*, 10872-10874. b) Um, J. M.; DiRocco, D. A.; Noey, E. L.; Rovis, T.; Houk, K. N. *J. Am. Chem. Soc.* **2011**, *133*, 11249-11254. c) DiRocco, D. A.; Noey, E. L.; Houk, K. N.; Rovis, T. *Angew. Chem. Int. Ed.* **2012**, *51*, 2391-2394. d) Langdon, S. M.; Wilde, M. M. D.; Thai, K.; Gravel, M. *J. Am. Chem. Soc.* **2014**, *136*, 7539–7542.

23) Moore, J. L; Silvestri, A. P.; Read de Alaniz, J.; DiRocco, D. A.; Rovis, T. *Org. Lett.* **2011**, *13*, 1742-1745.

24) Domingo, L. R.; Zaragozá, R. J.; Saéz, J. A.; Arnó, M. *Molecules* **2012**, *17*, 1335-1353.

25) See Appendix I.

26) Read de Alaniz, J.; Rovis, T. *J. Am. Chem. Soc.* **2005**, *127*, 6284-6289.

27) Our mathematical system considers only two variables for one equation, one for each of the two formed enantiomers. A system that includes multiple stereocenters is currently being worked on.

28) Chiral catalysts/ligands should be in equal grades of purity, otherwise error will be substantially propagated.

29) A simple plug-and-play Microsoft Excel script for an expedited solution for k_{rel} values is attached – see attached files.

30) Yu, R. T.; Rovis, T. *J. Am. Chem. Soc.* **2006**, *128*, 12370–12371.

31) Friedman, R. K.; Oberg, K. M.; Dalton, D. M.; Rovis, T. *Pure Appl. Chem.* **2010**, *82*, 1353-1364.

32) Yu, R. T.; Rovis, T. *J. Am. Chem. Soc.* **2006**, *128*, 2782–2783.

33) Dalton, D. M.; Oberg, K. M.; Yu R. T.; Lee, E. E.; Perreault, S.; Oinen, M. E.; Pease, M. L.; Malik, G.; Rovis, T. *J. Am. Chem. Soc.* **2009**, *131*, 15717–15728.

34) Bars, J. L.; Haussner, T.; Lang, J.; Pfaltz, A.; Blackmond, D. G. *Adv. Synth. Catal.* **2001**, *343*, 207-214.

35) Dalton, D. M.; Rappé, A. K.; Rovis, T. *Chem. Sci.* **2013**, *4*, 2062-2070.

36) Yu, R. T.; Lee, E. E.; Malik, G.; Rovis, T. *Angew. Chem. Int. Ed.* **2009**, *48*, 2379 –2382.

APPENDIX

General Methods

All reactions were carried out in oven-dried glassware with magnetic stirring. ACS grade MeOH, DCM, Et_2O, Toluene, MeCN and reagents were purchased from TCI, Strem, Alfa Aesar, and Sigma-Aldrich and were used without further purification. When necessary, organic solvents were routinely dried and/or distilled prior to use and stored over molecular sieves under argon. Column chromatography was performed on Silicycle® SilicaFlash® P60 (230-400 mesh) silica gel. Thin layer chromatography was performed on Silicycle® 250µm silica gel 60A plates. Visualization was accomplished with UV light (254 nm) or potassium permanganate. ^{1}H, ^{19}F, and ^{13}C-NMR spectra were collected at ambient temperature on a Bruker 400 MHz spectrometer. Chemical shifts are expressed as parts per million (δ, ppm) and are referenced to Acetone-D6 (206.26 ppm for ^{13}C-NMR; 2.05 ppm for ^{1}H-NMR). Deuterated solvents were purchased from Cambridge Isotope Laboratories and were used without further purification. Proton signal data uses the following abbreviations: s = singlet, d = doublet, t = triplet, q = quartet, quint. = quintet, sext. = sextet, oct. = octuplet, and m = multiplet. Mass spectra were obtained on a Waters XEVO G2-XS QToF mass spectrometer equipped with a UPC2 SFC inlet, on-board fluidics, an ESI probe, an APCI probe, and an ASAP (HRMS). $[Rh(ethylene)_2Cl]_2$ was purchased from Strem Chemicals. Unless otherwise indicated, all commercially available starting materials were purchased from Aldrich Chemicals and used without further purification.

Synthesis of Substrates

Ethyl (E)-4-(2-formylphenoxy)but-2-enoate (10)

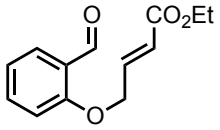

10

A slightly modified procedure was used for the synthesis of **10***:*[1] A 100 mL round-bottom flask was charged with salicaldehyde (654 μL; 750 mg; 6.142 mmol; 1.0 eq.), 60 mL acetone (0.1 M), then K_2CO_3 (1.273 g; 1.5 eq.). This mixture was stirred at room temperature for 10 minutes. Neat ethyl 4-bromocrotonate (930 μL; 6.756 mmol; 1.1 eq.) is subsequently added in one portion. The reaction is stirred for 16 hours, upon which the stir-bar is removed and the reaction is concentrated *in vacuo* to dryness. The crude material was quenched with 30 mL water and extracted (3x) with diethyl ether. The combined organic layers were washed with brine, and further dried with Na_2SO_4. The solvent was removed under pressure and the crude product was purified by flash chromatography on silica gel (10% EtOAc/Hex) to afford 1.178 g of product **10** (82%) as a pale-yellow solid. *Characterization data for this product matches previously reported in the literature*.[1]

Ethyl (E)-5-(2-formylphenyl)pent-2-enoate (12)

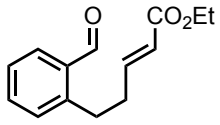

12

A slightly modified procedure was used for the synthesis of **12***:*[2] A flame-dried 250 mL 2-necked round-bottom flask was charged with 1,2-dihydronaphthalene (752 μL; 750 mg; 5.761 mmol; 1.0 eq.) and 95 mL DCM (0.06 M). The reaction mixture was cooled to -78 °C and was sparged with O_2 for 5 minutes. Ozone was then bubbled through the solution until a light-blue color persists (~10-15 minutes). O_2 is, again, bubbled through the solution until the reaction flask is colorless. Triphenylphosphine (2.267 g; 1.5 eq.) was then added in one portion and the reaction mixture was stirred and allowed to go to room temperature overnight. The reaction was then concentrated *in vacuo* to dryness [**CAUTION!! Unquenched ozonides present an explosion hazard – it is crucial to make sure that all ozonides have been completely reduced before concentration**]. A separate 100 mL solution of diethyl ether was cooled to -78 °C, poured into the dry crude mixture, sonicated for ~1 minute, and filtered over a celite plug (this procedure was repeated 3x). The combined ether solution was rotovapped, and purified via flash chromatography over silica gel (100% Hexanes) to afford 747 mg of 2-(3-oxopropyl)benzaldehyde (80%) as a clear oil, which was then immediately dissolved with 15 mL of a 3:1 toluene:acetonitrile solvent mixture (0.3 M) in a flame-dried 50 mL round-bottom flask under a N_2 atmosphere. The reaction mixture was cooled to -78 °C, upon which ethyl (triphenylphosphoranylidene)acetate (1.365 g; 3.917 mmol; 0.85 eq.) was added portion-wise over 10 minutes and stirred overnight to room temperature (16 hr). The solvent was removed under pressure and the crude product was purified by flash chromatography on silica gel (slow gradient from 100% Hex to 20% EtOAc/Hex; ~15 column volumes) to afford 449 mg of product **12** (42%) as a clear oil, which was stored at -10 °C under Argon for future use. *Characterization data for this product matches previously reported in the literature*.[2]

5-Isocyanatopent-1-ene (14)

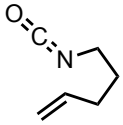

14

A slightly modified procedure was used for the synthesis of **14***:*[3] [**CAUTION!! Neat acyl azide presents potential explosion hazards – for safety, do not exceed 10 mmol reaction scales with this preparation. For a larger scale, an alternative procedure is best suited.**[4] A flame-dried 50 mL round-bottom flask filled with N_2 was charged with 5-hexenoic acid (500 mL; 480 mg; 4.210 mmol; 1.0 eq.), and 4.5 mL DCM (0.95 M). The reaction mixture was cooled to -10 °C, added triethylamine (622 μL; 452 mg; 4.463 mmol; 1.06 eq.) in one portion, and stirred for 5 minutes. Diphenyl phosphoryl azide (962 μL; 1.228 mg; 4.463 mmol; 1.06 eq.) was then added dropwise over a period of 10 minutes and the reaction mixture was stirred at around -10 - 0 °C for 4 hours. The cold solution was then concentrated at room temperature to remove DCM (Warning: do not exceed a vacuum of 160 mmHg – resulting acyl azide is volatile) and filtered over a silica plug with 25 mL of a 2% EtOAc/Hex solvent mixture. The solvent mixture was then removed *in vacuo* (not exceeding 160 mmHg) at room temperature. The resulting neat acyl azide was allowed to sit under N_2 in 4.5 mL $CDCl_3$ (0.95 M) overnight until fully converted to isocyanate **14**, which upon removal of $CDCl_3$ exists as a clear liquid (369 mg; 79%). *Characterization data for this product matches previously reported in the literature*.[3]

Synthesis of Chiral Complexes

(S)-5-(3-Methoxy-3-oxopropyl)-2-(perfluorophenyl)-5,6-dihydro-8H-[1,2,4]triazolo[3,4-c][1,4]oxazin-2-ium tetrafluoroborate (C-5)

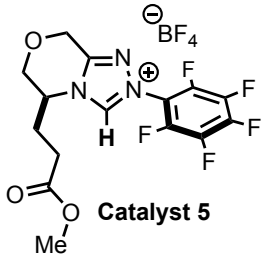

Catalyst 5

A slightly modified procedure for the synthesis of **C-1** *was used for the synthesis of* **C-5***:*[5] A flame-dried 100 mL round-bottom flask was charged with methyl (*S*)-3-(5-oxomorpholin-3-yl)propanoate (438 mg; 2.343 mmol; 1.0 eq.) and 10 mL of DCM (0.23 M). Trimethyloxonium tetrafluoroborate (353 mg; 2.389 mmol; 1.02 eq.) was added and the reaction mixture was stirred overnight (16 hours) at room temperature. Pentafluorophenylhydrazine (464 mg; 1.00 eq.) was then added in a single portion and stirred for approximately 5 hours. The solvent was removed *in vacuo* and the crude solid was triturated with diethyl ether several times. The flask containing the solid was outfitted with a reflux condenser and purged three times with N_2. 10 mL acetonitrile (0.23 M) and trimethyl orthoformate (2.563 mL; 23.430 mmol; 10.0 eq.) was then added and heated to 100 °C. The reaction progress was carefully monitored via UPLC. Once complete (~3 hours), the solvents were removed under pressure and dried *in vacuo*. The crude product was then refluxed in 10 mL of anhydrous toluene (0.23 M) overnight (16 hours), and purified via flash chromatography on silica gel (slow gradient from 100% DCM to 10% MeOH/DCM) to afford analytically pure **C-5** as an amorphous solid (327 mg; 30%). ^{1}H-NMR (400 MHz, Acetone-D6), δ 10.49 (1H, s), 5.27-5.11 (2H, dd, *J* = 2.1, 5.9 Hz), 4.98 (1H, m), 4.31-4.18 (2H, ddd, *J* = 0.5, 1.6, 3.9 Hz), 3.53 (3H, s), 2.61-2.53 (2H, m), 2.49-2.29 (2H, m); ^{13}C -NMR (400 MHz, Acetone-D6) δ 173.3, 152.7, 146.8, 146.0 (m), 143.1 (m), 140.3 (m), 137.8 (m), 66.8, 62.6, 57.6, 52.0, 31.2, 28.4; ^{19}F -NMR (400 MHz, Acetone-D6) δ -146.7 (2F, m), -150.2 (1F, tt, *J* = 0.5, 1.1, 2.8, 3.3 Hz), -151.9 ($^{10}BF_4$), -152.0 ($^{11}BF_4$), -162.1 (2F, m); HRMS (ESI+) calculated for $C_{15}H_{13}F_5N_3O_3$ 378.0877 – Found 378.0874.

(S)-2-(Perfluorophenyl)-5-propyl-5,6-dihydro-8H-[1,2,4]triazolo[3,4-c][1,4]oxazin-2-ium tetrafluoroborate (C-6)

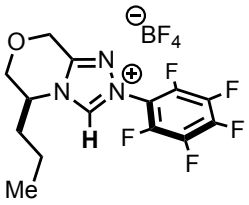

Catalyst 6

A slightly modified procedure for the synthesis of **C-1** *was used for the synthesis of* **C-6***:*[5] A flame-dried 100 mL round-bottom flask was charged with (S)-5-propylmorpholin-3-one (335 mg; 2.343 mmol; 1.0 eq.) and 10 mL of DCM (0.23 M). Trimethyloxonium tetrafluoroborate (353 mg; 2.389 mmol; 1.02 eq.) was added and the reaction mixture was stirred overnight (16 hours) at room temperature. Pentafluorophenylhydrazine (464 mg; 1.00 eq.) was then added in a single portion and stirred for approximately 5 hours. The solvent was removed *in vacuo* and the crude solid was triturated with diethyl ether several times. The flask containing the solid was outfitted with a reflux condenser and purged three times with N_2. 10 mL acetonitrile (0.23 M) and trimethyl orthoformate (2.563 mL; 23.430 mmol; 10.0 eq.) was then added and heated to 100 °C. The reaction progress was carefully monitored via UPLC. Once complete (~5 hours), the solvents were removed under pressure and dried *in vacuo*. The crude product was then refluxed in 10 mL of anhydrous toluene (0.23 M) overnight (24 hours), and purified via flash chromatography on silica gel (slow gradient from 100% DCM to 10% MeOH/DCM) to afford analytically pure **C-5** (503 mg; 51%) as an amorphous solid. ^{1}H-NMR (400 MHz, Acetone-D6), δ 10.55 (1H, s), 5.38-5.26 (2H, dd, *J* = 2.1, 3.8 Hz), 5.01 (1H, m), 4.46-4.26 (2H, ddd, *J* = 0.5, 1.6, 8.0 Hz), 2.32-2.10 (2H, m), 1.66-1.56 (2H, m) 1.04 (3H, t, *J* = 0.9 Hz); ^{13}C -NMR (400 MHz, Acetone-D6) δ 151.8, 145.7, 144.7 (m), 142.2 (m), 139.5 (m), 137.0 (m), 66.0, 61.7, 57.5, 33.9, 18.1, 13.05; ^{19}F -NMR (400 MHz, Acetone-D6) δ -146.7 (2F, m), -150.3 (1F, tt, *J* = 0.5, 1.1, 2.8, 3.3 Hz), -151.9 ($^{10}BF_4$), -152.0 ($^{11}BF_4$), -162.2 (2F, m); HRMS (ESI+) calculated for $C_{14}H_{13}F_5N_3O$ 334.0979 – Found 334.0976.

(S)-2-(Perfluorophenyl)-5-phenethyl-5,6-dihydro-8H-[1,2,4]triazolo[3,4-c][1,4]oxazin-2-ium tetrafluoroborate (C-7)

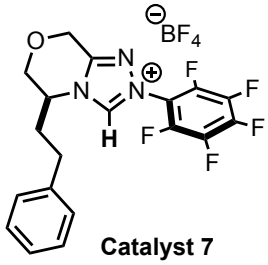

Catalyst 7

A slightly modified procedure for the synthesis of **C-1** *was used for the synthesis of* **C-6***:*[5] A flame-dried 100 mL round-bottom flask was charged with (*S*)-5-phenethylmorpholin-3-one (481 mg; 2.343 mmol; 1.0 eq.) and 10 mL of DCM (0.23 M). Trimethyloxonium tetrafluoroborate (353 mg; 2.389 mmol; 1.02 eq.) was added and the reaction mixture was stirred overnight (16 hours) at room temperature. Pentafluorophenylhydrazine (464 mg; 1.00 eq.) was then added in a single portion and stirred for approximately 5 hours. The solvent was removed *in vacuo* and the crude solid was triturated with diethyl ether several times. The flask containing the solid was outfitted with a reflux condenser and purged three times with N_2. 10 mL acetonitrile (0.23 M) and trimethyl orthoformate (2.563 mL; 23.430 mmol; 10.0 eq.) was then added and heated to 100 °C. The reaction progress was carefully monitored via UPLC. Once complete (~5 hours), the solvents were removed under pressure and dried *in vacuo*. The crude product was then refluxed in 10 mL of anhydrous toluene (0.23 M) overnight (16 hours), and purified via flash chromatography on silica gel (slow gradient from 100% DCM to 10% MeOH/DCM) to afford analytically pure **C-5** as an amorphous solid (430

mg; 38%). ^{1}H-NMR (400 MHz, Acetone-D6), δ 10.68 (1H, s), 7.32-7.28 (4H, m), 7.21 (1H, m), 5.39-5.25 (2H, dd, *J* = 2.1, 3.7 Hz), 5.08 (1H, m) 4.51-4.32 (2H, ddd, *J* = 0.5, 1.6, 5.0 Hz), 3.00-2.86 (2H, m) 2.69-2.40 (2H, m); ^{13}C -NMR (400 MHz, Acetone-D6) δ 152.9, 146.9, 145.5 (m), 143.1 (m), 141.5, 140.6 (m), 138.0 (m), 129.6, 129.3, 127.3, 67.0, 62.8, 58.5, 35.0, 31.9; ^{19}F -NMR (400 MHz, Acetone-D6) δ -146.7 (2F, m), -150.0 (1F, tt, *J* = 0.5, 1.1, 2.8, 3.3 Hz), -151.6 ($^{10}BF_4$), -151.7 ($^{11}BF_4$), -161.9 (2F, m); HRMS (ESI+) calculated for $C_{19}H_{15}F_5N_3O$ 396.1135 – Found 396.1134.

1-((3aR,8aR)-4,4,8,8-Tetrakis(3,5-bis(trifluoromethyl)phenyl)-2,2-dimethyltetrahydro-[1,3]dioxolo[4,5-e][1,3,2]dioxaphosphepin-6-yl)pyrrolidine (L-8)

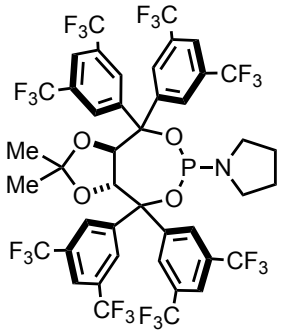

Ligand 8

A modified procedure was used for the synthesis of **L-8**:[6] A flame-dried 100 mL round-bottom flask filled with N_2 was charged with 1-bromo-3,5-bis(trifluoromethyl)benzene (1.410 mL; 8.178 mmol; 6.0 eq.) and 14 mL diethyl ether (0.6 M). The reaction was cooled to -78 °C and stirred for 5 minutes. *n*-BuLi (5.111 mL of 1.6 M solution in Hexanes; 6.0 eq.) was added dropwise over 5 minutes. Once the addition was completed, the reaction was stirred in 0 °C for 1 hour, and then lowered back down to -78 °C. A premixed solution of (−)-dimethyl 2,3-O-isopropylidene-L-tartrate (250 μL; 1.363 mmol; 1.0 eq.) in 13 mL of diethyl ether (0.1 M) was added dropwise over 15 minutes. The reaction was allowed to stir to ambient temperature over 2 hours. The mixture was then quenched with 15 mL of water, extracted several times with diethyl ether, and subsequently washed with brine and then dried with Na_2SO_4. The crude mixture was purified via flash column chromatography on silica gel (slow gradient from 100% Hexanes to 10% EtOAc/Hex) to afford ((4R,5R)-2,2-dimethyl-1,3-dioxolane-4,5-diyl)bis(bis(3,5-bis(trifluoromethyl)phenyl)methanol) as a white foamy solid (702 mg, 51% yield), which was then submitted to a flame-dried 100 mL round-bottom flask filled with N_2 and filled with 3 mL of anhydrous THF (0.25 M). The mixture was cooled to 0 °C and stirred for 5 minutes. Triethylamine (329 μL; 239 mg; 3.4 eq.) was added in one portion, followed by a 5-minute dropwise addition of PCl_3 (73 μL; 115 mg; 1.2 eq.). The solution is stirred to room temperature over 45 minutes, cooled down again to 0 °C, and added pyrrolidine (143 μL; 124 mg; 2.5 eq.) dropwise over 5 minutes. The reaction was stirred overnight and the solvent removed via rotary evaporation. The crude mixture was then purified via flash column chromatography on silica gel (slow gradient from 100% Hexanes to 10% EtOAc/Hex) to afford **L-8** as a white foamy solid (308 mg; 40% yield), which was then stored in a drybox filled with argon for future use. *Characterization data for this product matches previously reported in the literature*.[6]

General Procedures for Benchmarking Protocol

General Procedure for the NHC-Catalyzed Intramolecular Stetter Reaction

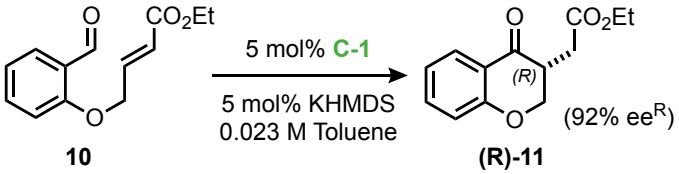

Stock solutions of **10** (1.0 M in toluene), **C-1** (0.1 M in toluene), and KHMDS (0.1 M in toluene) were freshly prepared inside a wet-glovebox under N_2 atmosphere. From these stock solutions, **C-1** (6.9 μL; 5 mol%) was dosed inside a scrupulously dried 1-dram vial, upon which 600 μL of degassed and anhydrous toluene (0.023 M) was added. KHMDS (6.9 μL from 0.1 M stock solution; 5 mol%) was added and the reaction was stirred for 5 minutes. Substrate **10** was then dosed (13.8 μL from 1.0 M stock solution; 1.0 eq.) and the reaction was stirred for 1 hour. The reaction mixture was then concentrated to dryness *in vacuo*. The crude reaction mixture was filtered over a celite plug with DCM and then subject to analysis by chiral-phase HPLC. The enantiomeric excess of product **11** was determined via separation, according to a slightly modified literature method,[7] using a Daicel Chirapak AD-H column with 90:10 Hex:IPA at 1.0 mL/min (major enantiomer for **C-1**: 9.1 min; minor enantiomer: 12.4 min).

General Procedure for the NHC-Catalyzed Intramolecular Stetter Reaction in MeCN

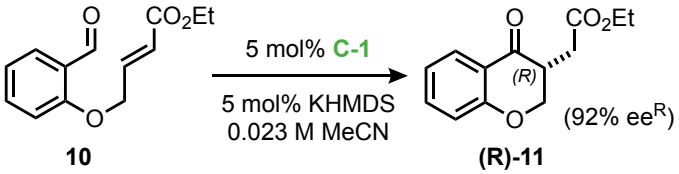

Stock solutions of **10** (1.0 M in MeCN), **C-1** (0.1 M in toluene), and KHMDS (0.1 M in toluene) were freshly prepared inside a wet-glovebox under N_2 atmosphere. From these stock solutions, **C-1** (6.9 μL; 5 mol%) was dosed inside a scrupulously dried 1-dram vial, upon which 150 μL of degassed and anhydrous toluene (0.09 M) was added. KHMDS (6.9 μL from 0.1 M stock solution; 5 mol%) was added and the reaction was stirred for 5 minutes. The reaction was then removed of all solvent and HMDS *in vacuo*. To the crude mixture was added 600 μL MeCN (0.023 M), followed by substrate **10** (13.8 μL from 1.0 M stock solution; 5 mol%) and the reaction was stirred for 1 hour. The reaction mixture was then concentrated to dryness *in vacuo*. The crude reaction mixture was filtered over a celite plug with DCM and then subject to analysis by chiral-phase HPLC.

General Procedure for the Stetter Reaction Competition Experiment

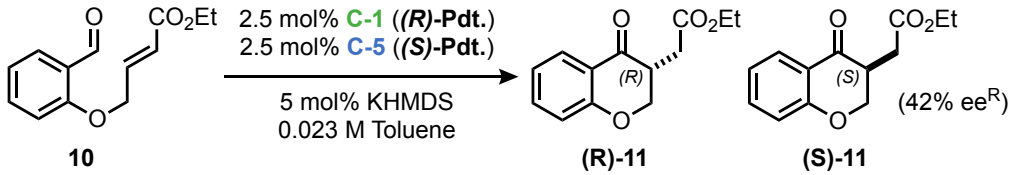

Stock solutions of **10** (1.0 M in toluene), **C-1** (0.1 M in toluene), **C-5** (0.1 M in toluene), and KHMDS (0.1 M in toluene) were freshly prepared inside a wet-glovebox under N_2 atmosphere. From these stock solutions, **C-1** (3.45 μL; 2.5 mol%) and **C-5** (3.45 μL; 2.5 mol%) were dosed inside a scrupulously dried 1-dram vial, upon which 600 μL of degassed and anhydrous toluene (0.023 M) was added. KHMDS (6.9 μL from 0.1 M stock solution; 5 mol%) was added and the reaction was stirred for 5 minutes. Substrate **10** was then dosed (13.8 μL from 0.1 M stock solution; 5 mol%) and the reaction was stirred for 1 hour. The reaction mixture was then concentrated to dryness *in vacuo*. The crude reaction mixture was filtered over a celite plug with DCM and then subject to analysis by chiral-phase HPLC. [**Note: Competition experiments in MeCN were run following the procedure described directly above**]

General Procedure for the Rh(I)-Catalyzed [2+2+2] Cycloaddition

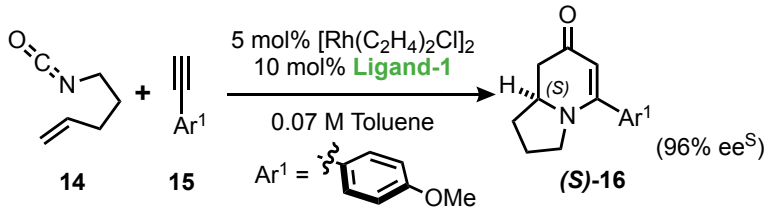

Stock solutions of **L-1** (0.01 M in CH_2Cl_2), and $[Rh(C_2H_4)_2Cl]_2$ (0.01 M in CH_2Cl_2) were freshly prepared inside a wet-glovebox under N_2 atmosphere. From these stock solutions, $[Rh(C_2H_4)_2Cl]_2$ (0.075 mL; 5 mol%) was dosed inside a scrupulously dried 1-dram vial, upon which 0.150 mL of degassed and anhydrous CH_2Cl_2 (0.005 M relative to catalyst) was added. **L-1** (0.150 mL; 10 mol%) was then added and the reaction was stirred for 30 minutes. The reaction was then removed of all solvent *in vacuo*. 0.300 mL of toluene (0.07 M) was subsequently added to the chiral Rh-complex, followed by Substrate **14** (15.0 μL from 1.0 M stock solution; 0.015 mmol; 1.0 eq.) and then Substrate **15** (3.89 μL; 0.030 mmol; 2.0 eq.). The reaction was taken out of the glovebox, lined with Teflon tape, and stirred overnight (16 hours) at 110 °C. The reaction mixture was then concentrated to dryness *in vacuo*. The crude reaction mixture was filtered over a celite plug with DCM and then subject to analysis by chiral-phase HPLC. The enantiomeric excess of product **11** was determined via separation, according to a slightly modified literature method,[8] using a Daicel Chirapak OD-H column with 80:20 Hex:IPA at 0.5 mL/min (major enantiomer for **L-1**: 34.2 min; minor enantiomer: 29.5 min).

General Procedure for the [2+2+2] Cycloaddition Competition Experiment

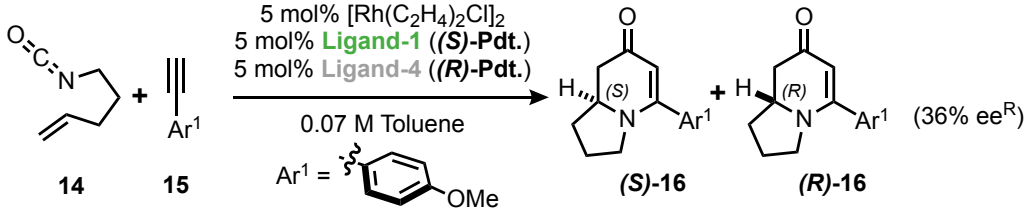

Stock solutions of **L-1** (0.01 M in CH_2Cl_2), **L-4** (0.01 M in CH_2Cl_2), and $[Rh(C_2H_4)_2Cl]_2$ (0.01 M in $CHCl_3$) were freshly prepared inside a wet-glovebox under N_2 atmosphere. From these stock solutions, $[Rh(C_2H_4)_2Cl]_2$ (0.075 mL; 5 mol%) was dosed inside a scrupulously dried 1-dram vial, upon which 0.150 mL of degassed and anhydrous $CHCl_3$ (0.005 M relative to catalyst) was added. **L-1** (0.075 mL from 0.01 M stock solution; 5 mol%), followed by **L-4** (0.075 mL from 0.01 M stock solution; 5 mol%), was then added and the reaction was stirred for 30 minutes. The reaction was then removed of all solvent *in vacuo*. 0.300 mL of toluene (0.07 M) was subsequently added to the chiral Rh-complex, followed by Substrate **14** (15.0 µL from 0.1 M stock solution; 0.015 mmol; 1.0 eq.) and then Substrate **15** (3.89 µL; 0.030 mmol; 2.0 eq.). The reaction was taken out of the glovebox, lined with Teflon tape, and stirred overnight (16 hours) at 110 °C. The reaction mixture was then concentrated to dryness *in vacuo*. The crude reaction mixture was filtered over a celite plug with DCM and then subject to analysis by chiral-phase HPLC.

Sample Calculations of k_{rel} from Experimental Data

C-1 vs C-5 for Intramolecular Stetter Product 11

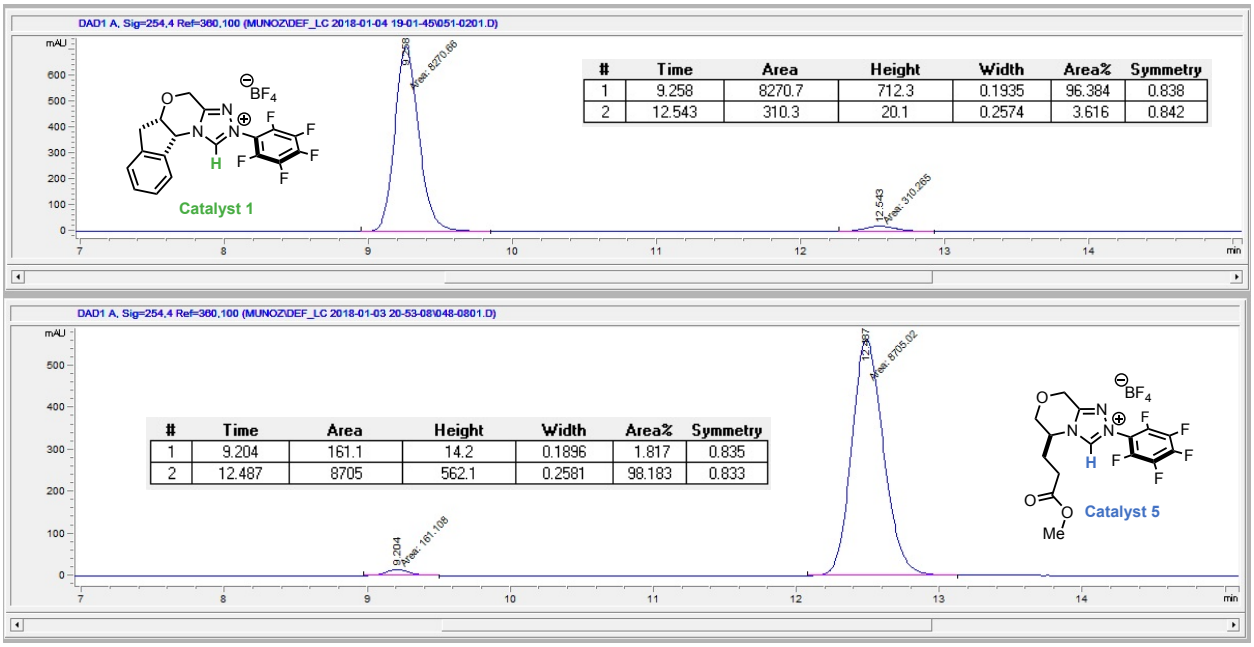

#	Time	Area	Height	Width	Area%	Symmetry
1	9.258	8270.7	712.3	0.1935	96.384	0.838
2	12.543	310.3	20.1	0.2574	3.616	0.842

#	Time	Area	Height	Width	Area%	Symmetry
1	9.204	161.1	14.2	0.1896	1.817	0.835
2	12.487	8705	562.1	0.2581	98.183	0.833

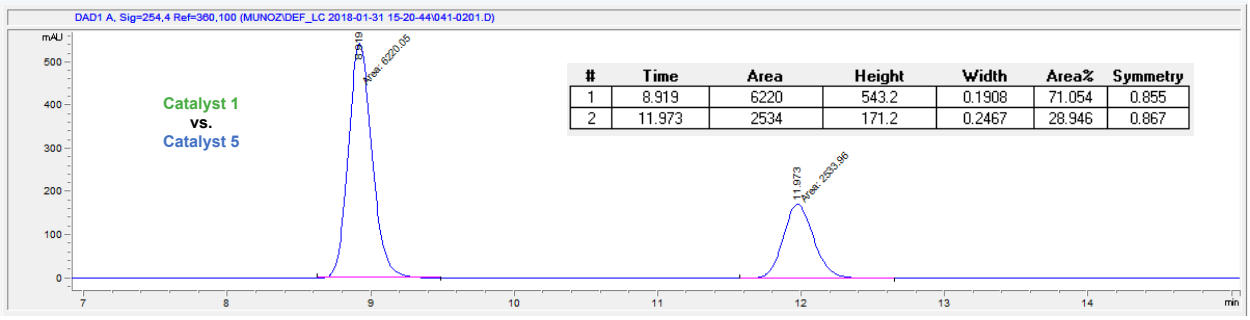

#	Time	Area	Height	Width	Area%	Symmetry
1	8.919	6220	543.2	0.1908	71.054	0.855
2	11.973	2534	171.2	0.2467	28.946	0.867

Step 1: The enantioselectivities for both catalysts employed in the reaction must be known prior to running the competition experiment. The reaction with **C-1** in toluene gives a peak area of 8270.7 mAU/min for **(*R*)-11** and 310.3 mAU/min for **(*S*)-11**, which gives an ee of 93% according to equation 1.

$$ee = \frac{([R] - [S])}{([R] + [S])} \qquad (1)$$

The same is done for benchmarking catalyst **C-1** in toluene, which gives a peak area of 8705 mAU/min for **(*S*)-11** and 161.1 mAU/min for **(*R*)-11**. Using equation 2, the ee for this catalyst is 96%.

$$ee = \frac{([S] - [R])}{([S] + [R])} \qquad (2)$$

Step 2: The competition experiment is performed according to the procedure listed above (*see General Procedure for the Stetter Reaction Competition Experiment*). The ee for all subsequent competition experiments is calculated according to equation 1, where the major enantiomer for the benchmarking catalyst/ligand is treated as the major component. [Note: This treatment is universal, as well as in those instances where a negative ee is given (*see L-1 vs L-4 for Rh(I)-Catalyzed [2+2+2]*)]. In this case, the ee for the competition between benchmarking catalyst **C-1** and **C-5**, which gives a peak area of 6220 mAU/min for **(*R*)-11** and 2534 mAU/min for **(*S*)-11**, is 42%. This procedure is repeated as desired for a series of catalysts that wish to be benchmarked for a model reaction.

Step 3: In order to solve for k_{rel}, we must first express the 3 ee's obtained above as ratios and substitute where appropriate in equation 3.

$$Comp^S = x^S + y^S$$
$$Comp^R = t^R + u^R \qquad (3)$$

Here, $Comp^S$ and $Comp^R$ refer to the ratio of (*S*)- to (*R*)-product, respectively, as measured by the competition experiment in the previous step. Variables x^S and t^R denote the amount of (*S*)- and (*R*)-product that is formed by benchmarking catalyst – variables y^S and u^R are the expressions for

the catalyst that is being benchmarked. For benchmarking **C-1**, 93% can be expressed as a ratio of 96.50^R : 3.50^S, which is then reduced to 27.57^R : 1^S. The same is done for **C-5**, which gives a ratio of 49.00^S : 1.00^R. For the competition experiment between benchmarking **C-1** and **C-5**, which gives 42% ee, the ratio is expressed as 71.00^R : 29.00^S and is not reduced further. Thus, $Comp^S$ = 0.29 and $Comp^R$ = 0.71. At this point we wish to express variable *t* in terms of *x*, and *u* in terms of *y*. Since *x* and *t* are both expressions of the same catalyst, we can say that $t = 27.57x$. If we do the same for **C-5** we obtain the expression $49.00u = y$. We multiply both sides of this expression by the reciprocal of 49 and obtain the relationship $u = 0.02041y$. Equation 3 is expressed for these variables and solved simply as follows:

$$0.29 = x + y$$
$$0.71 = 27.57x + 0.02041y$$

$$0.71 = 27.57(0.29 - y) + 0.02041y$$

$$y = 0.26444$$
$$x = 0.02556$$

At this point, we obtain our k_{rel} by substituting our *y* and *x* values into equation 4 as shown below, giving us a krel of 0.370 for the competition between **C-5** and **C-1**.

$$k_{rel} = \frac{\textbf{C-5}}{\textbf{C-1}} = \frac{u + y}{t + x} = \frac{0.02041y + y}{27.57x + x} = \mathbf{0.370} \qquad (4)$$

C-1 vs C-5 for Intramolecular Stetter Product 11 (*Using Microsoft Excel*)
This procedure may also be expedited in Microsoft Excel. The data points for the example shown above is highlighted in **Figure S1**.

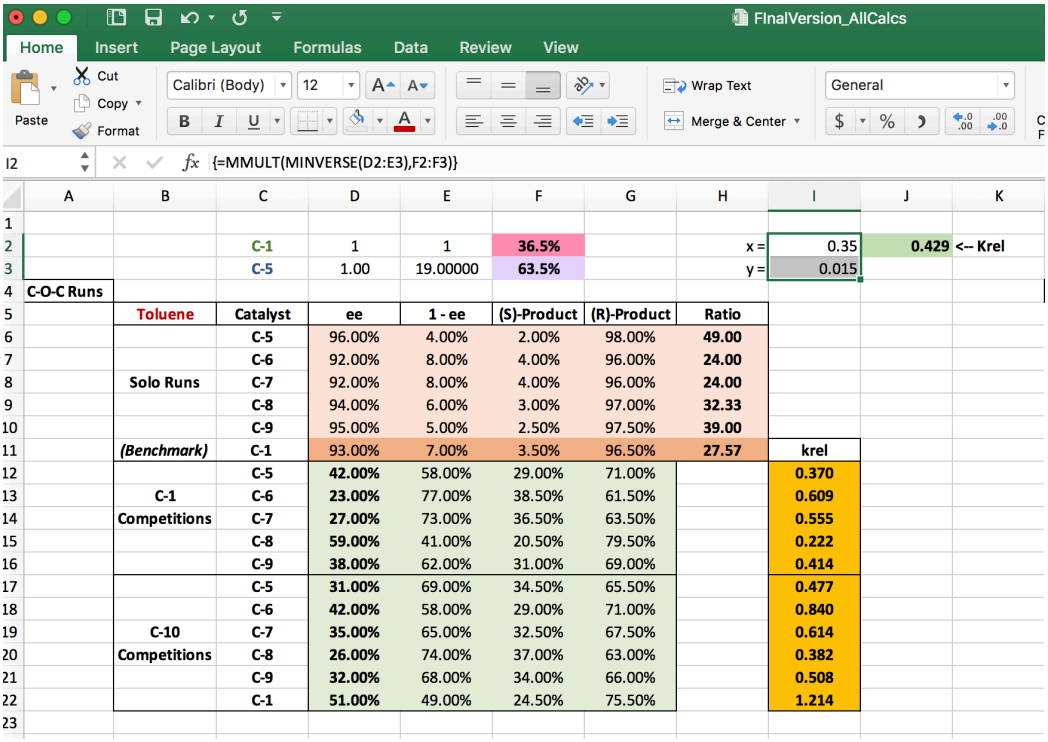

	A	B	C	D	E	F	G	H	I	J	K
1											
2			C-1	1	1	36.5%		x =	0.35	0.429	<-- Krel
3			C-5	1.00	19.00000	63.5%		y =	0.015		
4	C-O-C Runs										
5		Toluene	Catalyst	ee	1 - ee	(S)-Product	(R)-Product	Ratio			
6			C-5	96.00%	4.00%	2.00%	98.00%	49.00			
7			C-6	92.00%	8.00%	4.00%	96.00%	24.00			
8		Solo Runs	C-7	92.00%	8.00%	4.00%	96.00%	24.00			
9			C-8	94.00%	6.00%	3.00%	97.00%	32.33			
10			C-9	95.00%	5.00%	2.50%	97.50%	39.00			
11		*(Benchmark)*	C-1	93.00%	7.00%	3.50%	96.50%	27.57	krel		
12			C-5	42.00%	58.00%	29.00%	71.00%		0.370		
13		C-1	C-6	23.00%	77.00%	38.50%	61.50%		0.609		
14		Competitions	C-7	27.00%	73.00%	36.50%	63.50%		0.555		
15			C-8	59.00%	41.00%	20.50%	79.50%		0.222		
16			C-9	38.00%	62.00%	31.00%	69.00%		0.414		
17			C-5	31.00%	69.00%	34.50%	65.50%		0.477		
18			C-6	42.00%	58.00%	29.00%	71.00%		0.840		
19		C-10	C-7	35.00%	65.00%	32.50%	67.50%		0.614		
20		Competitions	C-8	26.00%	74.00%	37.00%	63.00%		0.382		
21			C-9	32.00%	68.00%	34.00%	66.00%		0.508		
22			C-1	51.00%	49.00%	24.50%	75.50%		1.214		
23											

Figure S1. General layout for expedited k_{rel} solutions.

As is shown in **Figure S1**, the ratios are obtained first by inputting the ee as a percentage. Then the E-cells are defined as 1 – ee. F-cells are defined as E-cell/2. G-cells are defined as 1 – F-cells. H-cells are defined as G-cells/F-Cells. A simplified form of the equation 3 is written into the Excel sheet where cells D2 and E2 are variables *x* and *y* and cells D3 and E3 are variables *t* and *u* expressed in terms of *x* and *y*. F2 and F3 are expressed as percentages (e.g. 0.29 and 0.79, respectively). In order to solve for *x* and *y*, highlight two cells as is shown for I2 and I3. In the formula bar, enter the Excel functions "=MMULT(MINVERSE(range1),range2)" where range1 defines the variables and range 2 defines the ee ratios from the competition. For the case above, this should be entered as "=MMULT(MINVERSE(D2:D3),F2:F3)" [**NOTE:** Since this is a formula for an array, the formula **MUST** be entered using CTRL+SHIFT+ENTER, otherwise you will see a "#NAME?" error]. The k_{rel} formula is, for the case above, entered as "=(E3*I3+I3)/(D3*I2+I2)". For cases when using an achiral catalyst as a benchmark (*see C-5 vs C-10 (Achiral) for Intramolecular Stetter Product 13 below*), cell D3 will equal 1 and cell E3 should equal variable *u* expressed as *y*, which should reflect the original value and not the reciprocal (**Figure S2**).

C-5 vs C-10 (Achiral) for Intramolecular Stetter Product 13

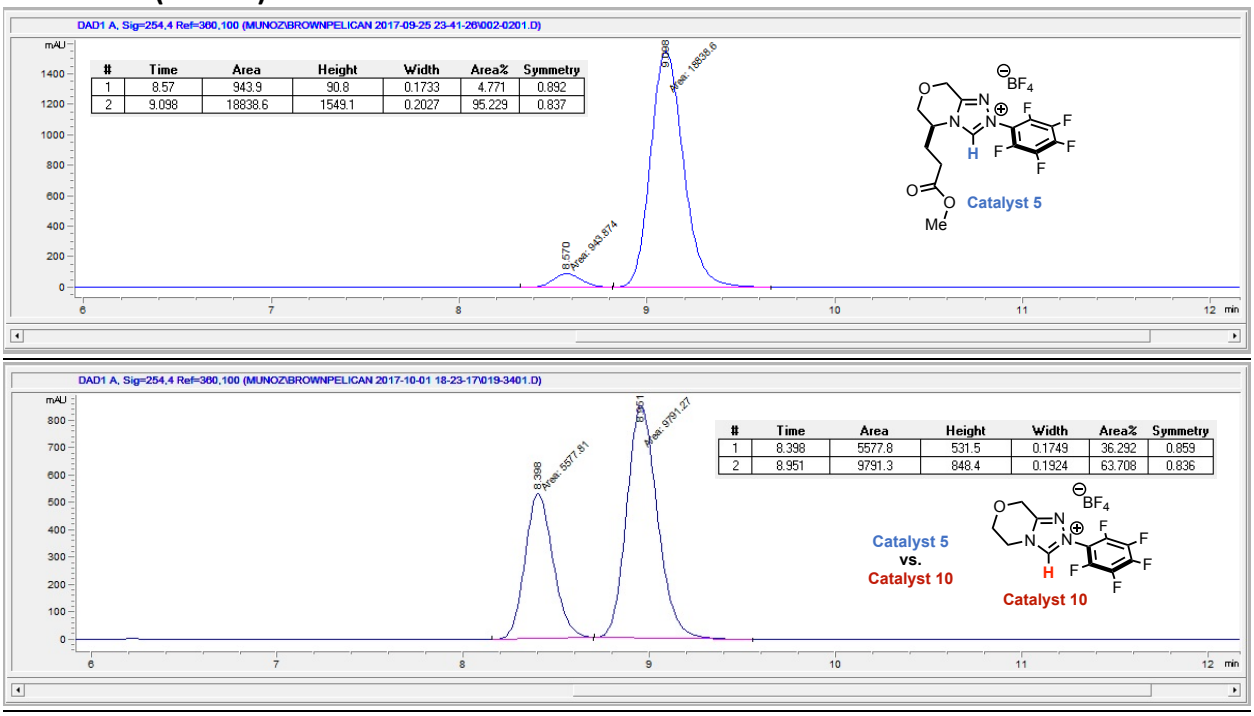

Step 1: The experiment for **C-5** in toluene gives a peak area of 18838.6 mAU/min for **(*R*)-13** and 943.9 mAU/min for **(*S*)-13**, which gives an ee of 90% according to equation 2. Achiral C-10 gives a racemic mixture.

$$ee = \frac{([R] - [S])}{([R] + [S])} \qquad (1)$$

Step 2: The competition experiment is performed according to the procedure listed above (*see General Procedure for the Stetter Reaction Competition Experiment*). In this case, the ee for the competition between benchmarking achiral catalyst **C-10** and **C-5**, which gives a peak area of 9791.3 mAU/min for **(*R*)-13** and 5577.8 mAU/min for **(*R*)-13**, is 27%. This procedure is repeated as desired for a series of catalysts that wish to be benchmarked for a model reaction.

Step 3: In order to solve for k_{rel}, we must first express the 2 ee's obtained above as ratios and substitute where appropriate in equation 3.

$$Comp^S = x^S + y^S$$
$$Comp^R = t^R + u^R \qquad (3)$$

For benchmarking **C-10**, 96% can be expressed as a ratio of $1^S : 1^R$. The same is done for **C-5**, which at 90% ee gives a ratio of $19.00^R : 1^S$. For the competition experiment between benchmarking **C-10** and **C-5**, which gives 27% ee, the ratio is expressed as $36.5^S : 63.5^R$ and is not reduced further. Thus, $Comp^R = 0.635$ and $Comp^S = 0.365$. At this point we wish to express variable *t* in terms of *x*, and *u* in terms of *y*. Since *x* and *t* are both expressions of the same catalyst, and **C-10** gives a

racemic product, we can say that $t = x$. If we do the same for **C-5** we obtain the expression $u = 19y$. Equation 3 is then expressed for these variables and solved simply as follows:

$$0.365 = x + y$$
$$0.635 = x + 19y$$

$$0.635 = 0.365 + 18y$$

$$y = 0.015$$
$$x = 0.350$$

At this point, we obtain our k_{rel} by substituting our y and x values into equation 4 as shown below, giving us a k_{rel} of 0.429 for the competition between **C-5** and **C-10**.

$$k_{rel} = \frac{\textbf{C-5}}{\textbf{C-10}} = \frac{u + y}{t + x} = \frac{19y + y}{x + x} = \mathbf{0.429} \qquad (4)$$

The Excel array formula above supports this calculation (**Figure S2** below).

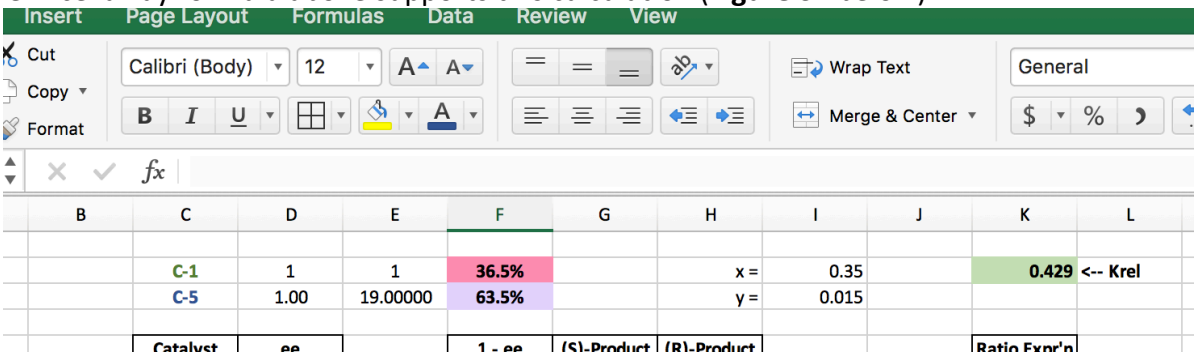

Figure S2. Expedited calculation for competition C-5 vs C-10.

L-1 vs L-4 for Rh(I)-Catalyzed [2+2+2] Product 16

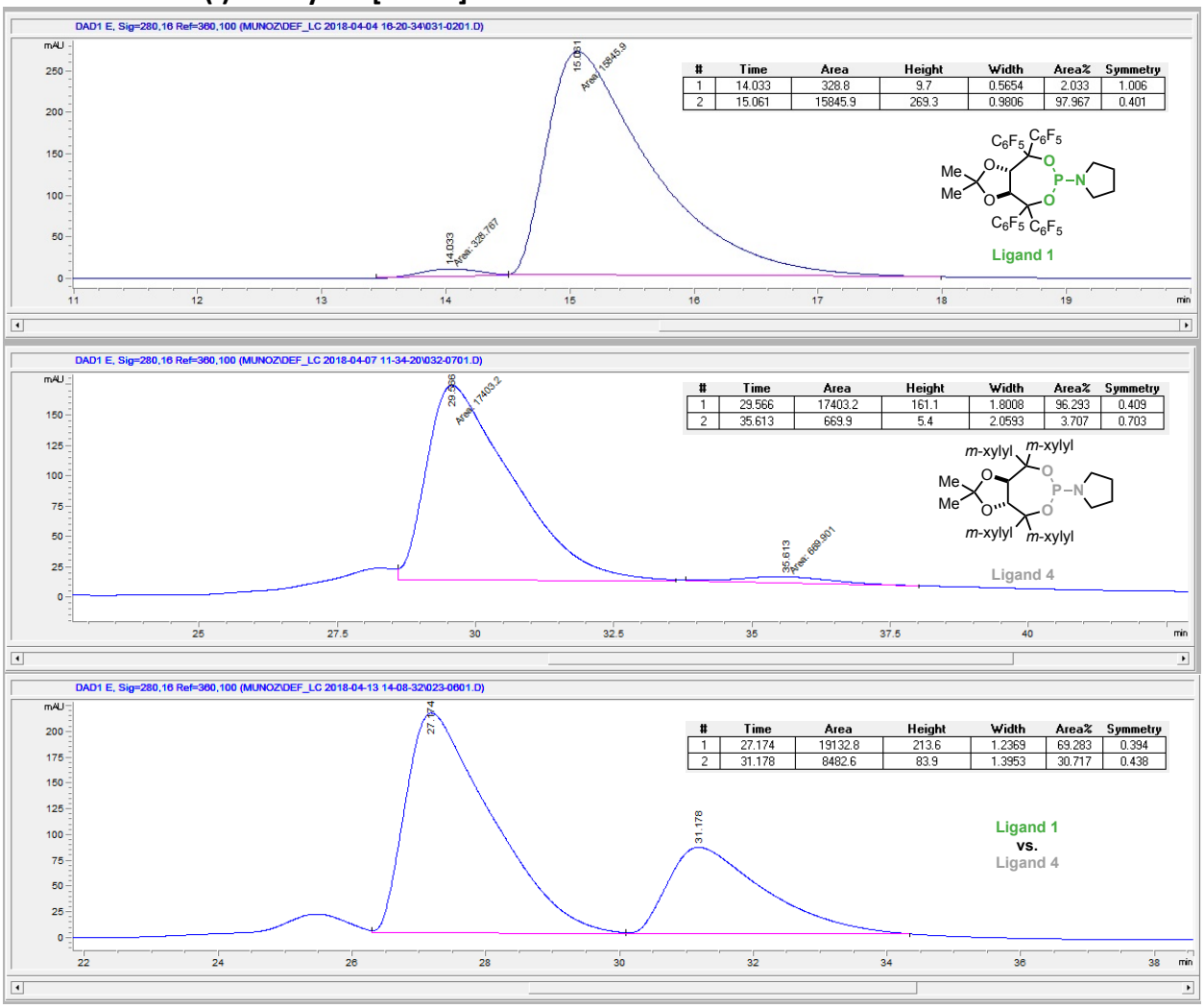

Step 1: The enantioselectivities for both catalysts employed in the reaction must be known prior to running the competition experiment. The reaction with **L-1** in toluene gives a peak area of 15845.9 mAU/min for **(*S*)-16** and 328.8 mAU/min for **(*R*)-16**, which gives an ee of 96% according to equation 2.

$$ee = \frac{([S] - [R])}{([S] + [R])} \qquad (2)$$

The same is done for benchmarking catalyst **L-4** in toluene, which gives a peak area of 17403.2 mAU/min for **(*R*)-16** and 669.9 mAU/min for **(*S*)-16**. Using equation 1, the ee for this catalyst is 93%.

$$ee = \frac{([R] - [S])}{([R] + [S])} \qquad (1)$$

Step 2: The competition experiment is performed according to the procedure listed above (*see General Procedure for the [2+2+2] Cycloaddition Competition Experiment*). The ee for all subsequent competition experiments is calculated according to equation 2, where the major enantiomer for the benchmarking catalyst/ligand is treated as the major component. In this case, the ee for the competition between benchmarking catalyst **L-1** and **L-3**, which gives a peak area of 8482.6 mAU/min for **(*S*)-16** and 19132.8 mAU/min for **(*R*)-16**, is -36%. This procedure is repeated as desired for a series of catalysts that wish to be benchmarked for a model reaction.

Step 3: In order to solve for k_{rel}, we must first express the 3 ee's obtained above as ratios and substitute where appropriate in equation 3.

$$Comp^R = x^R + y^R$$
$$Comp^S = t^S + u^S \qquad (3)$$

For benchmarking **L-1**, 96% can be expressed as a ratio of $98^S : 2^R$, which is then reduced to $49^S : 1^R$. The same is done for **L-2**, which gives a ratio of $27.57^R : 1^S$. For the competition experiment between benchmarking **C-1** and **C-5**, which gives -36% ee, the ratio is expressed as $32^S : 68^R$ and is not reduced further. Thus, $Comp^R = 0.68$ and $Comp^S = 0.32$. At this point we wish to express variable *t* in terms of *x*, and *u* in terms of *y*. Since *x* and *t* are both expressions of the same catalyst, we can say that $t = 49x$. If we do the same for **C-5** we obtain the expression $27.57u = y$. We multiply both sides of this expression by the reciprocal of 27.57 and obtain the relationship $u = 0.03627y$. Equation 3 is expressed for these variables and solved simply as follows:

$$0.68 = x + y$$
$$0.32 = 49x + 0.03627y$$

$$0.32 = 49(0.68 - y) + 0.03627y$$

$$y = 0.67397$$
$$x = 0.00603$$

At this point, we obtain our k_{rel} by substituting our *y* and *x* values into equation 4 as shown below, giving us a k_{rel} of 2.316 for the competition between **L-4** and **L-1**.

$$k_{rel} = \frac{\textbf{L-4}}{\textbf{L-1}} = \frac{u + y}{t + x} = \frac{0.03627y + y}{49x + x} = \mathbf{2.316} \qquad (4)$$

Computational Details

k_{rel} Values for Product 11

Toluene	Catalyst	ee	1 - ee	(S)-Product	(R)-Product	Ratio	
	C-5	96.00%	4.00%	2.00%	98.00%	**49.00**	
	C-6	92.00%	8.00%	4.00%	96.00%	**24.00**	
Solo Runs Product 11	C-7	92.00%	8.00%	4.00%	96.00%	**24.00**	
	C-8	94.00%	6.00%	3.00%	97.00%	**32.33**	
	C-9	95.00%	5.00%	2.50%	97.50%	**39.00**	
(Benchmark) →	C-1	93.00%	7.00%	3.50%	96.50%	**27.57**	krel
	C-5	**42.00%**	58.00%	29.00%	71.00%		**0.370**
C-1	C-6	**23.00%**	77.00%	38.50%	61.50%		**0.609**
Competitions	C-7	**27.00%**	73.00%	36.50%	63.50%		**0.555**
	C-8	**59.00%**	41.00%	20.50%	79.50%		**0.222**
	C-9	**38.00%**	62.00%	31.00%	69.00%		**0.414**
	C-5	**31.00%**	69.00%	34.50%	65.50%		**0.477**
	C-6	**42.00%**	58.00%	29.00%	71.00%		**0.840**
C-10	C-7	**35.00%**	65.00%	32.50%	67.50%		**0.614**
Competitions	C-8	**26.00%**	74.00%	37.00%	63.00%		**0.382**
	C-9	**32.00%**	68.00%	34.00%	66.00%		**0.508**
	C-1	**51.00%**	49.00%	24.50%	75.50%		**1.214**

Table S1. First trial k_{rel}-values for the competition experiments of Product **11** where **C-1** and **C-10** are benchmarking NHC catalysts in Toluene.

Toluene	Catalyst	ee	1 - ee	(S)-Product	(R)-Product	Ratio	
	C-5	96.00%	4.00%	2.00%	98.00%	**49.00**	
	C-6	93.00%	7.00%	3.50%	96.50%	**27.57**	
Solo Runs Product 11	C-7	93.00%	7.00%	3.50%	96.50%	**27.57**	
	C-8	94.00%	6.00%	3.00%	97.00%	**32.33**	
	C-9	95.00%	5.00%	2.50%	97.50%	**39.00**	
(Benchmark) →	C-1	93.00%	7.00%	3.50%	96.50%	**27.57**	krel
	C-5	**44.00%**	56.00%	28.00%	72.00%		**0.370**
C-1	C-6	**17.00%**	83.00%	41.50%	58.50%		**0.691**
Competitions	C-7	**29.00%**	71.00%	35.50%	64.50%		**0.525**
	C-8	**63.00%**	37.00%	18.50%	81.50%		**0.191**
	C-9	**35.00%**	65.00%	32.50%	67.50%		**0.446**
	C-5	**32.00%**	68.00%	34.00%	66.00%		**0.500**
	C-6	**44.00%**	56.00%	28.00%	72.00%		**0.898**
C-10	C-7	**36.00%**	64.00%	32.00%	68.00%		**0.632**
Competitions	C-8	**30.00%**	70.00%	35.00%	65.00%		**0.362**
	C-9	**30.00%**	70.00%	35.00%	65.00%		**0.462**
	C-1	**54.00%**	46.00%	23.00%	77.00%		**1.385**

Table S2. Second trial k_{rel}-values for the competition experiments of Product **11** where **C-1** and **C-10** are benchmarking NHC catalysts in Toluene.

Toluene	Catalyst	ee	1 - ee	(S)-Product	(R)-Product	Ratio	
	C-5	97.00%	3.00%	1.50%	98.50%	**65.67**	
	C-6	91.00%	9.00%	4.50%	95.50%	**21.22**	
Solo Runs Product 11	C-7	92.00%	8.00%	4.00%	96.00%	**24.00**	
	C-8	95.00%	5.00%	2.50%	97.50%	**39.00**	
	C-9	94.00%	6.00%	3.00%	97.00%	**32.33**	
(Benchmark) →	C-1	94.00%	6.00%	3.00%	97.00%	**32.33**	**krel**
	C-5	**39.00%**	61.00%	30.50%	69.50%		**0.404**
C-1	C-6	**26.00%**	74.00%	37.00%	63.00%		**0.581**
Competitions	C-7	**27.00%**	73.00%	36.50%	63.50%		**0.563**
	C-8	**54.00%**	46.00%	23.00%	77.00%		**0.268**
	C-9	**33.00%**	67.00%	33.50%	66.50%		**0.480**
	C-5	**28.00%**	72.00%	36.00%	64.00%		**0.406**
	C-6	**38.00%**	62.00%	31.00%	69.00%		**0.717**
C-10	C-7	**38.00%**	62.00%	31.00%	69.00%		**0.704**
Competitions	C-8	**24.00%**	76.00%	38.00%	62.00%		**0.338**
	C-9	**29.00%**	71.00%	35.50%	64.50%		**0.446**
	C-1	**53.00%**	47.00%	23.50%	76.50%		**1.293**

Table S3. Third trial k_{rel}-values for the competition experiments of Product **11** where **C-1** and **C-10** are benchmarking NHC catalysts in Toluene.

THF	Catalyst	ee	1 - ee	(S)-Product	(R)-Product	Ratio	
	C-5	85.00%	15.00%	7.50%	92.50%	**12.33**	
	C-6	82.00%	18.00%	9.00%	91.00%	**10.11**	
Solo Runs Product 11	C-7	83.00%	17.00%	8.50%	91.50%	**10.76**	
	C-8	90.00%	10.00%	5.00%	95.00%	**19.00**	
	C-9	83.00%	17.00%	8.50%	91.50%	**10.76**	
(Benchmark) →	C-1	88.00%	12.00%	6.00%	94.00%	**15.67**	**krel**
	C-5	**33.00%**	67.00%	33.50%	66.50%		**0.466**
C-1	C-6	**12.00%**	88.00%	44.00%	56.00%		**0.809**
Competitions	C-7	**34.00%**	66.00%	33.00%	67.00%		**0.462**
	C-8	**47.00%**	53.00%	26.50%	73.50%		**0.299**
	C-9	**50.00%**	50.00%	25.00%	75.00%		**0.286**
	C-5	**32.00%**	68.00%	34.00%	66.00%		**0.604**
	C-6	**40.00%**	60.00%	30.00%	70.00%		**0.952**
C-10	C-7	**30.00%**	70.00%	35.00%	65.00%		**0.566**
Competitions	C-8	**28.00%**	72.00%	36.00%	64.00%		**0.452**
	C-9	**24.00%**	76.00%	38.00%	62.00%		**0.407**
	C-1	**54.00%**	46.00%	23.00%	77.00%		**1.588**

Table S4. First trial k_{rel}-values for the competition experiments of Product **11** where **C-1** and **C-10** are benchmarking NHC catalysts in THF.

THF	Catalyst	ee	1 - ee	(S)-Product	(R)-Product	Ratio	
	C-5	86.00%	14.00%	7.00%	93.00%	**13.29**	
	C-6	83.00%	17.00%	8.50%	91.50%	**10.76**	
Solo Runs Product 11	C-7	83.00%	17.00%	8.50%	91.50%	**10.76**	
	C-8	88.00%	12.00%	6.00%	94.00%	**15.67**	
	C-9	82.00%	18.00%	9.00%	91.00%	**10.11**	
(Benchmark) →	C-1	90.00%	10.00%	5.00%	95.00%	**19.00**	**krel**
	C-5	**38.00%**	62.00%	31.00%	69.00%		**0.419**
C-1	C-6	**10.00%**	90.00%	45.00%	55.00%		**0.860**
Competitions	C-7	**36.00%**	64.00%	32.00%	68.00%		**0.454**
	C-8	**48.00%**	52.00%	26.00%	74.00%		**0.309**
	C-9	**48.00%**	52.00%	26.00%	74.00%		**0.323**
	C-5	**32.00%**	68.00%	34.00%	66.00%		**0.593**
	C-6	**40.00%**	60.00%	30.00%	70.00%		**0.930**
C-10	C-7	**26.00%**	74.00%	37.00%	63.00%		**0.456**
Competitions	C-8	**27.00%**	73.00%	36.50%	63.50%		**0.443**
	C-9	**22.00%**	78.00%	39.00%	61.00%		**0.367**
	C-1	**54.00%**	46.00%	23.00%	77.00%		**1.500**

Table S5. Second trial k_{rel}-values for the competition experiments of Product **11** where **C-1** and **C-10** are benchmarking NHC catalysts in THF.

MeCN	Catalyst	ee	1 - ee	(S)-Product	(R)-Product	Ratio	
	C-5	82.00%	18.00%	9.00%	91.00%	**10.11**	
	C-6	89.00%	11.00%	5.50%	94.50%	**17.18**	
Solo Runs Product 11	C-7	82.00%	18.00%	9.00%	91.00%	**10.11**	
	C-8	86.00%	14.00%	7.00%	93.00%	**13.29**	
	C-9	83.00%	17.00%	8.50%	91.50%	**10.76**	
(Benchmark) →	C-1	88.00%	12.00%	6.00%	94.00%	**15.67**	**krel**
	C-5	**23.00%**	77.00%	38.50%	61.50%		**0.619**
C-1	C-6	**25.00%**	75.00%	37.50%	62.50%		**0.553**
Competitions	C-7	**27.00%**	73.00%	36.50%	63.50%		**0.560**
	C-8	**18.00%**	82.00%	41.00%	59.00%		**0.673**
	C-9	**16.00%**	84.00%	42.00%	58.00%		**0.727**
	C-5	**33.00%**	67.00%	33.50%	66.50%		**0.673**
	C-6	**35.00%**	65.00%	32.50%	67.50%		**0.648**
C-10	C-7	**34.00%**	66.00%	33.00%	67.00%		**0.708**
Competitions	C-8	**45.00%**	55.00%	27.50%	72.50%		**1.097**
	C-9	**44.00%**	56.00%	28.00%	72.00%		**1.128**
	C-1	**55.00%**	45.00%	22.50%	77.50%		**1.600**

Table S6. Third trial k_{rel}-values for the competition experiments of Product **11** where **C-1** and **C-10** are benchmarking NHC catalysts in THF.

MeCN	Catalyst	ee	1 - ee	(S)-Product	(R)-Product	Ratio	
	C-5	87.00%	13.00%	6.50%	93.50%	**14.38**	
	C-6	84.00%	16.00%	8.00%	92.00%	**11.50**	
Solo Runs Product 11	C-7	86.00%	14.00%	7.00%	93.00%	**13.29**	
	C-8	91.00%	9.00%	4.50%	95.50%	**21.22**	
	C-9	87.00%	13.00%	6.50%	93.50%	**14.38**	
(Benchmark) →	C-1	92.00%	8.00%	4.00%	96.00%	**24.00**	**krel**
	C-5	**28.00%**	72.00%	36.00%	64.00%		**0.557**
C-1	C-6	**23.00%**	77.00%	38.50%	61.50%		**0.645**
Competitions	C-7	**29.00%**	71.00%	35.50%	64.50%		**0.548**
	C-8	**19.00%**	81.00%	40.50%	59.50%		**0.664**
	C-9	**19.00%**	81.00%	40.50%	59.50%		**0.689**
	C-5	**37.00%**	63.00%	31.50%	68.50%		**0.740**
	C-6	**36.00%**	64.00%	32.00%	68.00%		**0.750**
C-10	C-7	**36.00%**	64.00%	32.00%	68.00%		**0.720**
Competitions	C-8	**43.00%**	57.00%	28.50%	71.50%		**0.896**
	C-9	**42.00%**	58.00%	29.00%	71.00%		**0.933**
	C-1	**60.00%**	40.00%	20.00%	80.00%		**1.875**

Table S7. First trial k_{rel}-values for the competition experiments of Product **11** where **C-1** and **C-10** are benchmarking NHC catalysts in MeCN.

MeCN	Catalyst	ee	1 - ee	(S)-Product	(R)-Product	Ratio	
	C-5	85.00%	15.00%	7.50%	92.50%	**12.33**	
	C-6	86.00%	14.00%	7.00%	93.00%	**13.29**	
Solo Runs Product 11	C-7	88.00%	12.00%	6.00%	94.00%	**15.67**	
	C-8	87.00%	13.00%	6.50%	93.50%	**14.38**	
	C-9	88.00%	12.00%	6.00%	94.00%	**15.67**	
(Benchmark) →	C-1	91.00%	9.00%	4.50%	95.50%	**21.22**	**krel**
	C-5	**36.00%**	64.00%	32.00%	68.00%		**0.455**
C-1	C-6	**24.00%**	76.00%	38.00%	62.00%		**0.609**
Competitions	C-7	**32.00%**	68.00%	34.00%	66.00%		**0.492**
	C-8	**26.00%**	74.00%	37.00%	63.00%		**0.575**
	C-9	**21.00%**	79.00%	39.50%	60.50%		**0.642**
	C-5	**43.00%**	57.00%	28.50%	71.50%		**1.024**
	C-6	**38.00%**	62.00%	31.00%	69.00%		**0.792**
C-10	C-7	**43.00%**	57.00%	28.50%	71.50%		**0.956**
Competitions	C-8	**40.00%**	60.00%	30.00%	70.00%		**0.851**
	C-9	**39.00%**	61.00%	30.50%	69.50%		**0.796**
	C-1	**56.00%**	44.00%	22.00%	78.00%		**1.600**

Table S8. Second trial k_{rel}-values for the competition experiments of Product **11** where **C-1** and **C-10** are benchmarking NHC catalysts in MeCN.

MeCN	Catalyst	ee	1 - ee	(S)-Product	(R)-Product	Ratio	
	C-5	82.00%	18.00%	9.00%	91.00%	**10.11**	
	C-6	89.00%	11.00%	5.50%	94.50%	**17.18**	
Solo Runs Product 11	C-7	82.00%	18.00%	9.00%	91.00%	**10.11**	
	C-8	86.00%	14.00%	7.00%	93.00%	**13.29**	
	C-9	83.00%	17.00%	8.50%	91.50%	**10.76**	
***(Benchmark)* →**	C-1	88.00%	12.00%	6.00%	94.00%	**15.67**	**krel**
	C-5	**23.00%**	77.00%	38.50%	61.50%		**0.619**
C-1	C-6	**25.00%**	75.00%	37.50%	62.50%		**0.553**
Competitions	C-7	**27.00%**	73.00%	36.50%	63.50%		**0.560**
	C-8	**18.00%**	82.00%	41.00%	59.00%		**0.673**
	C-9	**16.00%**	84.00%	42.00%	58.00%		**0.727**
	C-5	**33.00%**	67.00%	33.50%	66.50%		**0.673**
	C-6	**32.00%**	68.00%	34.00%	66.00%		**0.561**
C-10	C-7	**30.00%**	70.00%	35.00%	65.00%		**0.577**
Competitions	C-8	**45.00%**	55.00%	27.50%	72.50%		**1.097**
	C-9	**44.00%**	56.00%	28.00%	72.00%		**1.128**
	C-1	**55.00%**	45.00%	22.50%	77.50%		**1.667**

Table S9. Third trial k_{rel}-values for the competition experiments of Product **11** where **C-1** and **C-10** are benchmarking NHC catalysts in MeCN.

PhCF3	Catalyst	ee	1 - ee	(S)-Product	(R)-Product	Ratio	
	C-5	89.00%	11.00%	5.50%	94.50%	**17.18**	
	C-6	86.00%	14.00%	7.00%	93.00%	**13.29**	
Solo Runs Product 11	C-7	89.00%	11.00%	5.50%	94.50%	**17.18**	
	C-8	89.00%	11.00%	5.50%	94.50%	**17.18**	
	C-9	87.00%	13.00%	6.50%	93.50%	**14.38**	
***(Benchmark)* →**	C-1	81.00%	19.00%	9.50%	90.50%	**9.53**	**krel**
	C-5	**37.00%**	63.00%	31.50%	68.50%		**0.349**
C-1	C-6	**24.00%**	76.00%	38.00%	62.00%		**0.518**
Competitions	C-7	**43.00%**	57.00%	28.50%	71.50%		**0.288**
	C-8	**61.00%**	39.00%	19.50%	80.50%		**0.133**
	C-9	**45.00%**	55.00%	27.50%	72.50%		**0.273**
	C-5	**44.00%**	56.00%	28.00%	72.00%		**0.978**
	C-6	**50.00%**	50.00%	25.00%	75.00%		**1.389**
C-10	C-7	**40.00%**	60.00%	30.00%	70.00%		**0.816**
Competitions	C-8	**32.00%**	68.00%	34.00%	66.00%		**0.561**
	C-9	**38.00%**	62.00%	31.00%	69.00%		**0.776**
	C-1	**66.00%**	34.00%	17.00%	83.00%		**4.398**

Table S10. First trial k_{rel}-values for the competition experiments of Product **11** where **C-1** and **C-10** are benchmarking NHC catalysts in $PhCF_3$.

PhCF3	Catalyst	ee	1 - ee	(S)-Product	(R)-Product	Ratio	
	C-5	89.00%	11.00%	5.50%	94.50%	**17.18**	
	C-6	87.00%	13.00%	6.50%	93.50%	**14.38**	
Solo Runs Product 11	C-7	90.00%	10.00%	5.00%	95.00%	**19.00**	
	C-8	90.00%	10.00%	5.00%	95.00%	**19.00**	
	C-9	88.00%	12.00%	6.00%	94.00%	**15.67**	
***(Benchmark)* →**	C-1	80.00%	20.00%	10.00%	90.00%	**9.00**	**krel**
	C-5	**39.00%**	61.00%	30.50%	69.50%		**0.320**
C-1	C-6	**25.00%**	75.00%	37.50%	62.50%		**0.491**
Competitions	C-7	**42.00%**	58.00%	29.00%	71.00%		**0.288**
	C-8	**65.00%**	35.00%	17.50%	82.50%		**0.097**
	C-9	**47.00%**	53.00%	26.50%	73.50%		**0.244**
	C-5	**42.00%**	58.00%	29.00%	71.00%		**0.894**
	C-6	**50.00%**	50.00%	25.00%	75.00%		**1.351**
C-10	C-7	**49.00%**	51.00%	25.50%	74.50%		**1.195**
Competitions	C-8	**34.00%**	66.00%	33.00%	67.00%		**0.607**
	C-9	**39.00%**	61.00%	30.50%	69.50%		**0.796**
	C-1	**63.00%**	37.00%	18.50%	81.50%		**3.706**

Table S11. Second trial k_{rel}-values for the competition experiments of Product **11** where **C-1** and **C-10** are benchmarking NHC catalysts in $PhCF_3$.

PhCF3	Catalyst	ee	1 - ee	(S)-Product	(R)-Product	Ratio	
	C-5	88.00%	12.00%	6.00%	94.00%	**15.67**	
	C-6	86.00%	14.00%	7.00%	93.00%	**13.29**	
Solo Runs Product 11	C-7	89.00%	11.00%	5.50%	94.50%	**17.18**	
	C-8	86.00%	14.00%	7.00%	93.00%	**13.29**	
	C-9	88.00%	12.00%	6.00%	94.00%	**15.67**	
***(Benchmark)* →**	C-1	81.00%	19.00%	9.50%	90.50%	**9.53**	**krel**
	C-5	**36.00%**	64.00%	32.00%	68.00%		**0.363**
C-1	C-6	**21.00%**	79.00%	39.50%	60.50%		**0.561**
Competitions	C-7	**39.00%**	61.00%	30.50%	69.50%		**0.328**
	C-8	**59.00%**	41.00%	20.50%	79.50%		**0.152**
	C-9	**45.00%**	55.00%	27.50%	72.50%		**0.271**
	C-5	**48.00%**	52.00%	26.00%	74.00%		**1.200**
	C-6	**48.00%**	52.00%	26.00%	74.00%		**1.263**
C-10	C-7	**39.00%**	61.00%	30.50%	69.50%		**0.780**
Competitions	C-8	**36.00%**	64.00%	32.00%	68.00%		**0.720**
	C-9	**32.00%**	68.00%	34.00%	66.00%		**0.571**
	C-1	**65.00%**	35.00%	17.50%	82.50%		**4.061**

Table S12. Third trial k_{rel}-values for the competition experiments of Product **11** where **C-1** and **C-10** are benchmarking NHC catalysts in $PhCF_3$.

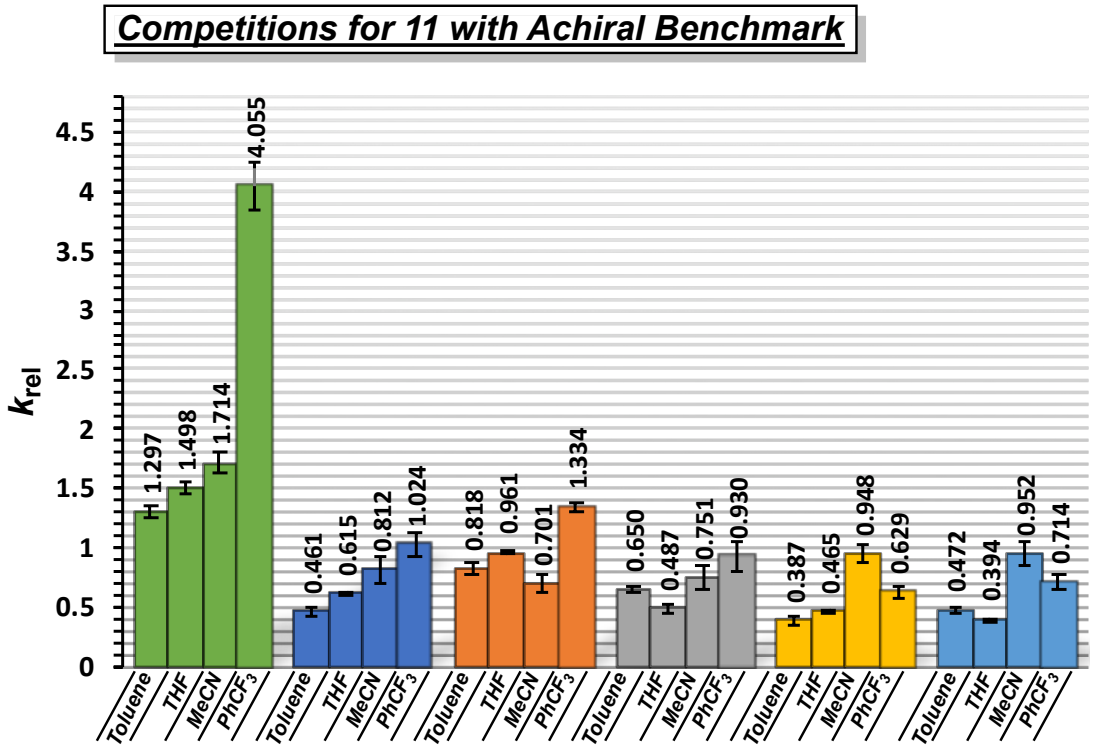

Figure S3. k_{rel}-values for the competition experiments of Product **11** where **C-10** is the benchmarking NHC catalyst in a variety of solvents.

k_{rel} Values for Product 13

Toluene	Catalyst	ee	1 - ee	(S)-Product	(R)-Product	Ratio	
	C-5	90.00%	10.00%	5.00%	95.00%	**19.00**	
	C-6	94.00%	6.00%	3.00%	97.00%	**32.33**	
Solo Runs Product 13	C-7	94.00%	6.00%	3.00%	97.00%	**32.33**	
	C-8	96.00%	4.00%	2.00%	98.00%	**49.00**	
	C-9	95.00%	5.00%	2.50%	97.50%	**39.00**	
(Benchmark) →	C-1	95.00%	5.00%	2.50%	97.50%	**39.00**	krel
	C-5	**-13.00%**	113.00%	56.50%	43.50%		**1.403**
C-1	C-6	**-32.00%**	132.00%	66.00%	34.00%		**2.048**
Competitions	C-7	**-10.00%**	110.00%	55.00%	45.00%		**1.333**
	C-8	**8.00%**	92.00%	46.00%	54.00%		**0.837**
	C-9	**22.00%**	78.00%	39.00%	61.00%		**0.624**
	C-5	**27.00%**	73.00%	36.50%	63.50%		**0.429**
	C-6	**29.00%**	71.00%	35.50%	64.50%		**0.446**
C-10	C-7	**25.00%**	75.00%	37.50%	62.50%		**0.362**
Competitions	C-8	**17.00%**	83.00%	41.50%	58.50%		**0.215**
	C-9	**13.00%**	87.00%	43.50%	56.50%		**0.159**
	C-1	**18.00%**	82.00%	41.00%	59.00%		**0.234**

Table S13. First trial k_{rel}-values for the competition experiments of Product **11** where **C-1** and **C-10** are benchmarking NHC catalysts in toluene.

Toluene	Catalyst	ee	1 - ee	(S)-Product	(R)-Product	Ratio	
	C-5	91.00%	9.00%	4.50%	95.50%	**21.22**	
	C-6	94.00%	6.00%	3.00%	97.00%	**32.33**	
Solo Runs	C-7	94.00%	6.00%	3.00%	97.00%	**32.33**	
Product 13	C-8	95.00%	5.00%	2.50%	97.50%	**39.00**	
	C-9	96.00%	4.00%	2.00%	98.00%	**49.00**	
(Benchmark) →	C-1	96.00%	4.00%	2.00%	98.00%	**49.00**	**krel**
	C-5	**-14.00%**	114.00%	57.00%	43.00%		**1.429**
C-1	C-6	**-30.00%**	130.00%	65.00%	35.00%		**1.969**
Competitions	C-7	**-14.00%**	114.00%	57.00%	43.00%		**1.375**
	C-8	**12.00%**	88.00%	44.00%	56.00%		**0.785**
	C-9	**30.00%**	70.00%	35.00%	65.00%		**0.524**
	C-5	**27.00%**	73.00%	36.50%	63.50%		**0.422**
	C-6	**31.00%**	69.00%	34.50%	65.50%		**0.492**
C-10	C-7	**27.00%**	73.00%	36.50%	63.50%		**0.403**
Competitions	C-8	**19.00%**	81.00%	40.50%	59.50%		**0.250**
	C-9	**14.00%**	86.00%	43.00%	57.00%		**0.173**
	C-1	**19.00%**	81.00%	40.50%	59.50%		**0.250**

Table S14. Second trial k_{rel}-values for the competition experiments of Product **11** where **C-1** and **C-10** are benchmarking NHC catalysts in toluene.

Toluene	Catalyst	ee	1 - ee	(S)-Product	(R)-Product	Ratio	
	C-5	90.00%	10.00%	5.00%	95.00%	**19.00**	
	C-6	92.00%	8.00%	4.00%	96.00%	**24.00**	
Solo Runs	C-7	93.00%	7.00%	3.50%	96.50%	**27.57**	
Product 13	C-8	96.00%	4.00%	2.00%	98.00%	**49.00**	
	C-9	95.00%	5.00%	2.50%	97.50%	**39.00**	
(Benchmark) →	C-1	93.00%	7.00%	3.50%	96.50%	**27.57**	**krel**
	C-5	**-10.00%**	110.00%	55.00%	45.00%		**1.287**
C-1	C-6	**-33.00%**	133.00%	66.50%	33.50%		**2.136**
Competitions	C-7	**-9.00%**	109.00%	54.50%	45.50%		**1.214**
	C-8	**10.00%**	90.00%	45.00%	55.00%		**0.783**
	C-9	**17.00%**	83.00%	41.50%	58.50%		**0.679**
	C-5	**22.00%**	78.00%	39.00%	61.00%		**0.385**
	C-6	**28.00%**	72.00%	36.00%	64.00%		**0.438**
C-10	C-7	**24.00%**	76.00%	38.00%	62.00%		**0.348**
Competitions	C-8	**14.00%**	86.00%	43.00%	57.00%		**0.215**
	C-9	**15.00%**	85.00%	42.50%	57.50%		**0.188**
	C-1	**16.00%**	84.00%	42.00%	58.00%		**0.208**

Table S15. Third trial k_{rel}-values for the competition experiments of Product **11** where **C-1** and **C-10** are benchmarking NHC catalysts in toluene.

THF	Catalyst	ee	1 - ee	(S)-Product	(R)-Product	Ratio	
	C-5	94.00%	6.00%	3.00%	97.00%	**32.33**	
	C-6	95.00%	5.00%	2.50%	97.50%	**39.00**	
Solo Runs	C-7	94.00%	6.00%	3.00%	97.00%	**32.33**	
Product 13	C-8	85.00%	15.00%	7.50%	92.50%	**12.33**	
	C-9	55.00%	45.00%	22.50%	77.50%	**3.44**	
(Benchmark) →	C-1	97.00%	3.00%	1.50%	98.50%	**65.67**	**krel**
	C-5	**30.00%**	70.00%	35.00%	65.00%		**0.540**
C-1	C-6	**2.00%**	98.00%	49.00%	51.00%		**0.979**
Competitions	C-7	**17.00%**	83.00%	41.50%	58.50%		**0.721**
	C-8	**52.00%**	48.00%	24.00%	76.00%		**0.328**
	C-9	**41.00%**	59.00%	29.50%	70.50%		**0.584**
	C-5	**35.00%**	65.00%	32.50%	67.50%		**0.593**
	C-6	**46.00%**	54.00%	27.00%	73.00%		**0.939**
C-10	C-7	**39.00%**	61.00%	30.50%	69.50%		**0.709**
Competitions	C-8	**28.00%**	72.00%	36.00%	64.00%		**0.491**
	C-9	**21.00%**	79.00%	39.50%	60.50%		**0.618**
	C-1	**61.00%**	39.00%	19.50%	80.50%		**1.694**

Table S16. First trial k_{rel}-values for the competition experiments of Product **11** where **C-1** and **C-10** are benchmarking NHC catalysts in THF.

THF	Catalyst	ee	1 - ee	(S)-Product	(R)-Product	Ratio	
	C-5	96.00%	4.00%	2.00%	98.00%	**49.00**	
	C-6	93.00%	7.00%	3.50%	96.50%	**27.57**	
Solo Runs	C-7	95.00%	5.00%	2.50%	97.50%	**39.00**	
Product 13	C-8	88.00%	12.00%	6.00%	94.00%	**15.67**	
	C-9	63.00%	37.00%	18.50%	81.50%	**4.41**	
(Benchmark) →	C-1	96.00%	4.00%	2.00%	98.00%	**49.00**	**krel**
	C-5	**34.00%**	66.00%	33.00%	67.00%		**0.477**
C-1	C-6	**7.00%**	93.00%	46.50%	53.50%		**0.890**
Competitions	C-7	**15.00%**	85.00%	42.50%	57.50%		**0.736**
	C-8	**48.00%**	52.00%	26.00%	74.00%		**0.353**
	C-9	**50.00%**	50.00%	25.00%	75.00%		**0.407**
	C-5	**37.00%**	63.00%	31.50%	68.50%		**0.627**
	C-6	**42.00%**	58.00%	29.00%	71.00%		**0.824**
C-10	C-7	**42.00%**	58.00%	29.00%	71.00%		**0.792**
Competitions	C-8	**30.00%**	70.00%	35.00%	65.00%		**0.517**
	C-9	**26.00%**	74.00%	37.00%	63.00%		**0.702**
	C-1	**56.00%**	44.00%	22.00%	78.00%		**1.400**

Table S17. Second trial k_{rel}-values for the competition experiments of Product **11** where **C-1** and **C-10** are benchmarking NHC catalysts in THF.

THF	Catalyst	ee	1 - ee	(S)-Product	(R)-Product	Ratio	
	C-5	95.00%	5.00%	2.50%	97.50%	**39.00**	
	C-6	95.00%	5.00%	2.50%	97.50%	**39.00**	
Solo Runs Product 13	C-7	94.00%	6.00%	3.00%	97.00%	**32.33**	
	C-8	82.00%	18.00%	9.00%	91.00%	**10.11**	
	C-9	51.00%	49.00%	24.50%	75.50%	**3.08**	
(Benchmark) →	C-1	96.00%	4.00%	2.00%	98.00%	**49.00**	**krel**
	C-5	**32.00%**	68.00%	34.00%	66.00%		**0.504**
C-1	C-6	**-3.00%**	103.00%	51.50%	48.50%		**1.076**
Competitions	C-7	**10.00%**	90.00%	45.00%	55.00%		**0.827**
	C-8	**51.00%**	49.00%	24.50%	75.50%		**0.338**
	C-9	**39.00%**	61.00%	30.50%	69.50%		**0.633**
	C-5	**35.00%**	65.00%	32.50%	67.50%		**0.583**
	C-6	**45.00%**	55.00%	27.50%	72.50%		**0.900**
C-10	C-7	**40.00%**	60.00%	30.00%	70.00%		**0.741**
Competitions	C-8	**28.00%**	72.00%	36.00%	64.00%		**0.519**
	C-9	**24.00%**	76.00%	38.00%	62.00%		**0.890**
	C-1	**63.00%**	37.00%	18.50%	81.50%		**1.909**

Table S18. Third trial k_{rel}-values for the competition experiments of Product **11** where **C-1** and **C-10** are benchmarking NHC catalysts in THF.

MeCN	Catalyst	ee	1 - ee	(S)-Product	(R)-Product	Ratio	
	C-5	92.00%	8.00%	4.00%	96.00%	24.00	
	C-6	89.00%	11.00%	5.50%	94.50%	17.18	
Solo Runs Product 13	C-7	90.00%	10.00%	5.00%	95.00%	19.00	
	C-8	93.00%	7.00%	3.50%	96.50%	27.57	
	C-9	90.00%	10.00%	5.00%	95.00%	19.00	
(Benchmark) →	C-1	93.00%	7.00%	3.50%	96.50%	27.57	**krel**
	C-5	2.00%	98.00%	49.00%	51.00%		0.968
C-1	C-6	7.00%	93.00%	46.50%	53.50%		0.896
Competitions	C-7	7.00%	93.00%	46.50%	53.50%		0.887
	C-8	22.00%	78.00%	39.00%	61.00%		**0.617**
	C-9	20.00%	80.00%	40.00%	60.00%		0.664
	C-5	20.00%	80.00%	40.00%	60.00%		0.278
	C-6	19.00%	81.00%	40.50%	59.50%		0.271
C-10	C-7	19.00%	81.00%	40.50%	59.50%		0.268
Competitions	C-8	15.00%	85.00%	42.50%	57.50%		0.192
	C-9	15.00%	85.00%	42.50%	57.50%		0.200
	C-1	21.00%	79.00%	39.50%	60.50%		0.292

Table S19. First trial k_{rel}-values for the competition experiments of Product **11** where **C-1** and **C-10** are benchmarking NHC catalysts in MeCN.

MeCN	Catalyst	ee	1 - ee	(S)-Product	(R)-Product	Ratio	
	C-5	87.00%	13.00%	6.50%	93.50%	**14.38**	
	C-6	85.00%	15.00%	7.50%	92.50%	**12.33**	
Solo Runs Product 13	C-7	91.00%	9.00%	4.50%	95.50%	**21.22**	
	C-8	91.00%	9.00%	4.50%	95.50%	**21.22**	
	C-9	85.00%	15.00%	7.50%	92.50%	**12.33**	
(Benchmark) →	C-1	91.00%	9.00%	4.50%	95.50%	**21.22**	**krel**
	C-5	**4.00%**	96.00%	48.00%	52.00%		**0.956**
C-1	C-6	**2.00%**	98.00%	49.00%	51.00%		**1.023**
Competitions	C-7	**10.00%**	90.00%	45.00%	55.00%		**0.802**
	C-8	**13.00%**	87.00%	43.50%	56.50%		**0.750**
	C-9	**12.00%**	88.00%	44.00%	56.00%		**0.814**
	C-5	**14.00%**	86.00%	43.00%	57.00%		**0.192**
	C-6	**9.00%**	91.00%	45.50%	54.50%		**0.118**
C-10	C-7	**27.00%**	73.00%	36.50%	63.50%		**0.422**
Competitions	C-8	**18.00%**	82.00%	41.00%	59.00%		**0.247**
	C-9	**7.00%**	93.00%	46.50%	53.50%		**0.090**
	C-1	**21.00%**	79.00%	39.50%	60.50%		**0.300**

Table S20. Second trial k_{rel}-values for the competition experiments of Product **11** where **C-1** and **C-10** are benchmarking NHC catalysts in MeCN.

MeCN	Catalyst	ee	1 - ee	(S)-Product	(R)-Product	Ratio	
	C-5	89.00%	11.00%	5.50%	94.50%	**17.18**	
	C-6	90.00%	10.00%	5.00%	95.00%	**19.00**	
Solo Runs Product 13	C-7	88.00%	12.00%	6.00%	94.00%	**15.67**	
	C-8	90.00%	10.00%	5.00%	95.00%	**19.00**	
	C-9	86.00%	14.00%	7.00%	93.00%	**13.29**	
(Benchmark) →	C-1	89.00%	11.00%	5.50%	94.50%	**17.18**	**krel**
	C-5	**-5.00%**	105.00%	52.50%	47.50%		**1.119**
C-1	C-6	**9.00%**	91.00%	45.50%	54.50%		**0.808**
Competitions	C-7	**-1.00%**	101.00%	50.50%	49.50%		**1.034**
	C-8	**23.00%**	77.00%	38.50%	61.50%		**0.584**
	C-9	**22.00%**	78.00%	39.00%	61.00%		**0.620**
	C-5	**22.00%**	78.00%	39.00%	61.00%		**0.328**
	C-6	**20.00%**	80.00%	40.00%	60.00%		**0.286**
C-10	C-7	**14.00%**	86.00%	43.00%	57.00%		**0.189**
Competitions	C-8	**25.00%**	75.00%	37.50%	62.50%		**0.385**
	C-9	**19.00%**	81.00%	40.50%	59.50%		**0.284**
	C-1	**26.00%**	74.00%	37.00%	63.00%		**0.413**

Table S21. Third trial k_{rel}-values for the competition experiments of Product **11** where **C-1** and **C-10** are benchmarking NHC catalysts in MeCN.

PhCF3	Catalyst	ee	1 - ee	(S)-Product	(R)-Product	Ratio	
	C-5	91.00%	9.00%	4.50%	95.50%	**21.22**	
	C-6	90.00%	10.00%	5.00%	95.00%	**19.00**	
Solo Runs	C-7	92.00%	8.00%	4.00%	96.00%	**24.00**	
Product 13	C-8	94.00%	6.00%	3.00%	97.00%	**32.33**	
	C-9	94.00%	6.00%	3.00%	97.00%	**32.33**	
(Benchmark) →	C-1	88.00%	12.00%	6.00%	94.00%	**15.67**	**krel**
	C-5	**-13.00%**	113.00%	56.50%	43.50%		**1.295**
C-1	C-6	**-41.00%**	141.00%	70.50%	29.50%		**2.633**
Competitions	C-7	**-45.00%**	145.00%	72.50%	27.50%		**2.83**
	C-8	**-4.00%**	104.00%	52.00%	48.00%		**1.022**
	C-9	**1.00%**	99.00%	49.50%	50.50%		**0.916**
	C-5	**30.00%**	70.00%	35.00%	65.00%		**0.492**
	C-6	**31.00%**	69.00%	34.50%	65.50%		**0.525**
C-10	C-7	**35.00%**	65.00%	32.50%	67.50%		**0.614**
Competitions	C-8	**26.00%**	74.00%	37.00%	63.00%		**0.382**
	C-9	**24.00%**	76.00%	38.00%	62.00%		**0.343**
	C-1	**24.00%**	76.00%	38.00%	62.00%		**0.375**

Table S22. First trial k_{rel}-values for the competition experiments of Product **11** where **C-1** and **C-10** are benchmarking NHC catalysts in $PhCF_3$.

PhCF3	Catalyst	ee	1 - ee	(S)-Product	(R)-Product	Ratio	
	C-5	92.00%	8.00%	4.00%	96.00%	**24.00**	
	C-6	91.00%	9.00%	4.50%	95.50%	**21.22**	
Solo Runs	C-7	92.00%	8.00%	4.00%	96.00%	**24.00**	
Product 13	C-8	96.00%	4.00%	2.00%	98.00%	**49.00**	
	C-9	96.00%	4.00%	2.00%	98.00%	**49.00**	
(Benchmark) →	C-1	90.00%	10.00%	5.00%	95.00%	**19.00**	**krel**
	C-5	**-16.00%**	116.00%	58.00%	42.00%		**1.395**
C-1	C-6	**-38.00%**	138.00%	69.00%	31.00%		**2.415**
Competitions	C-7	**-40.00%**	140.00%	70.00%	30.00%		**2.500**
	C-8	**-8.00%**	108.00%	54.00%	46.00%		**1.114**
	C-9	**4.00%**	96.00%	48.00%	52.00%		**0.860**
	C-5	**33.00%**	67.00%	33.50%	66.50%		**0.559**
	C-6	**28.00%**	72.00%	36.00%	64.00%		**0.444**
C-10	C-7	**37.00%**	63.00%	31.50%	68.50%		**0.673**
Competitions	C-8	**27.00%**	73.00%	36.50%	63.50%		**0.391**
	C-9	**28.00%**	72.00%	36.00%	64.00%		**0.412**
	C-1	**26.00%**	74.00%	37.00%	63.00%		**0.406**

Table S23. Second trial k_{rel}-values for the competition experiments of Product **11** where **C-1** and **C-10** are benchmarking NHC catalysts in $PhCF_3$.

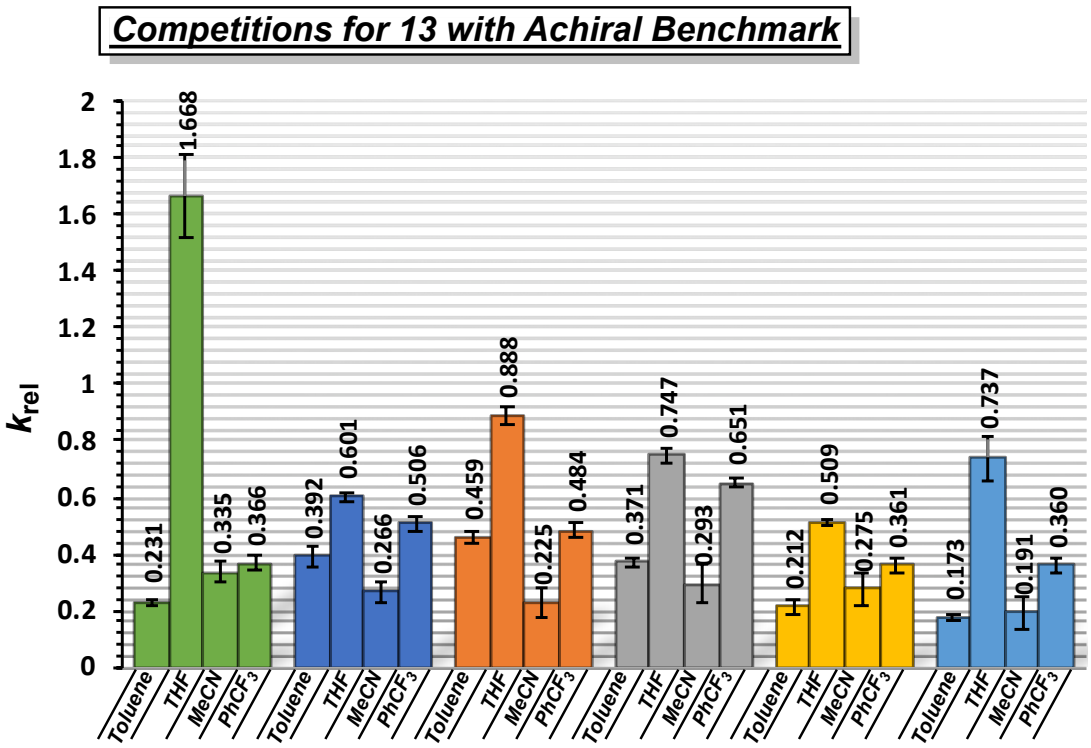

Figure S4. k_{rel}-values for the competition experiments of Product **13** where **C-10** is the benchmarking NHC catalyst in a variety of solvents.

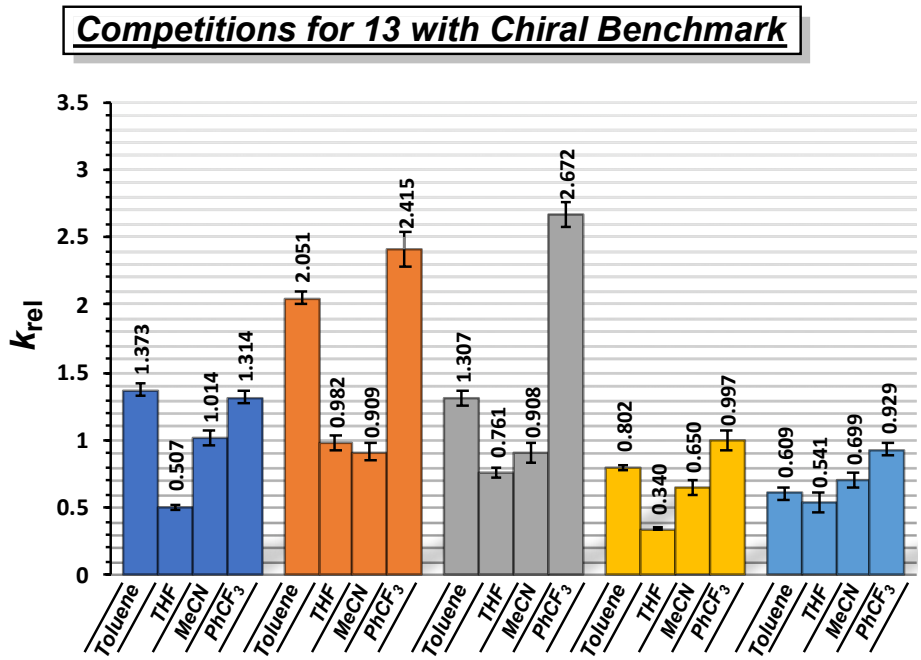

Table S5. k_{rel}-values for the competition experiments of Product **13** where **C-1** is the benchmarking NHC catalyst in a variety of solvents.

k_{rel} Values for Product 16

Toluene	Catalyst	ee	1 - ee	(S)-Product	(R)-Product	Ratio	
	L-2	77.00%	23.00%	11.50%	88.50%	**7.70**	
	L-3	87.00%	13.00%	6.50%	93.50%	**14.38**	
Solo Runs	L-4	93.00%	7.00%	3.50%	96.50%	**27.57**	
Product 16	L-5	7.00%	93.00%	46.50%	53.50%	**1.15**	
	L-6	-9.00%	109.00%	54.50%	45.50%	**0.83**	
	L-7	81.00%	19.00%	9.50%	90.50%	**9.53**	
	L-8	90.00%	10.00%	5.00%	95.00%	**19.00**	
(Benchmark) →	L-1	96.00%	4.00%	2.00%	98.00%	**49.00**	krel
	L-2	**83.00%**	17.00%	8.50%	91.50%		**0.081**
	L-3	**49.00%**	51.00%	25.50%	74.50%		**0.346**
L-1	L-4	**-36.00%**	136.00%	68.00%	32.00%		**2.316**
Competitions	L-5	**69.00%**	31.00%	15.50%	84.50%		**0.355**
	L-6	**80.00%**	20.00%	10.00%	90.00%		**0.226**
	L-7	**10.00%**	90.00%	45.00%	55.00%		**0.945**
	L-8	**-7.00%**	107.00%	53.50%	46.50%		**1.241**

Table S24. First trial k_{rel}-values for the competition experiments of Product **16** where **L-1** is the benchmarking ligand toluene.

Toluene	Catalyst	ee	1 - ee	(S)-Product	(R)-Product	Ratio	
	L-2	78.00%	22.00%	11.00%	89.00%	**8.09**	
	L-3	87.00%	13.00%	6.50%	93.50%	**14.38**	
Solo Runs	L-4	92.00%	8.00%	4.00%	96.00%	**24.00**	
Product 16	L-5	9.00%	91.00%	45.50%	54.50%	**1.20**	
	L-6	-12.00%	112.00%	56.00%	44.00%	**0.79**	
	L-7	83.00%	17.00%	8.50%	91.50%	**10.76**	
	L-8	92.00%	8.00%	4.00%	96.00%	**24.00**	
(Benchmark) →	L-1	95.00%	5.00%	2.50%	97.50%	**39.00**	krel
	L-2	**85.00%**	15.00%	7.50%	92.50%		**0.061**
	L-3	**52.00%**	48.00%	24.00%	76.00%		**0.309**
L-1	L-4	**-27.00%**	127.00%	63.50%	36.50%		**1.877**
Competitions	L-5	**73.00%**	27.00%	13.50%	86.50%		**0.268**
	L-6	**78.00%**	22.00%	11.00%	89.00%		**0.257**
	L-7	**-2.00%**	102.00%	51.00%	49.00%		**1.198**
	L-8	**-11.00%**	111.00%	55.50%	44.50%		**1.309**

Table S25. Second trial k_{rel}-values for the competition experiments of Product **16** where **L-1** is the benchmarking ligand toluene.

NMR Spectra

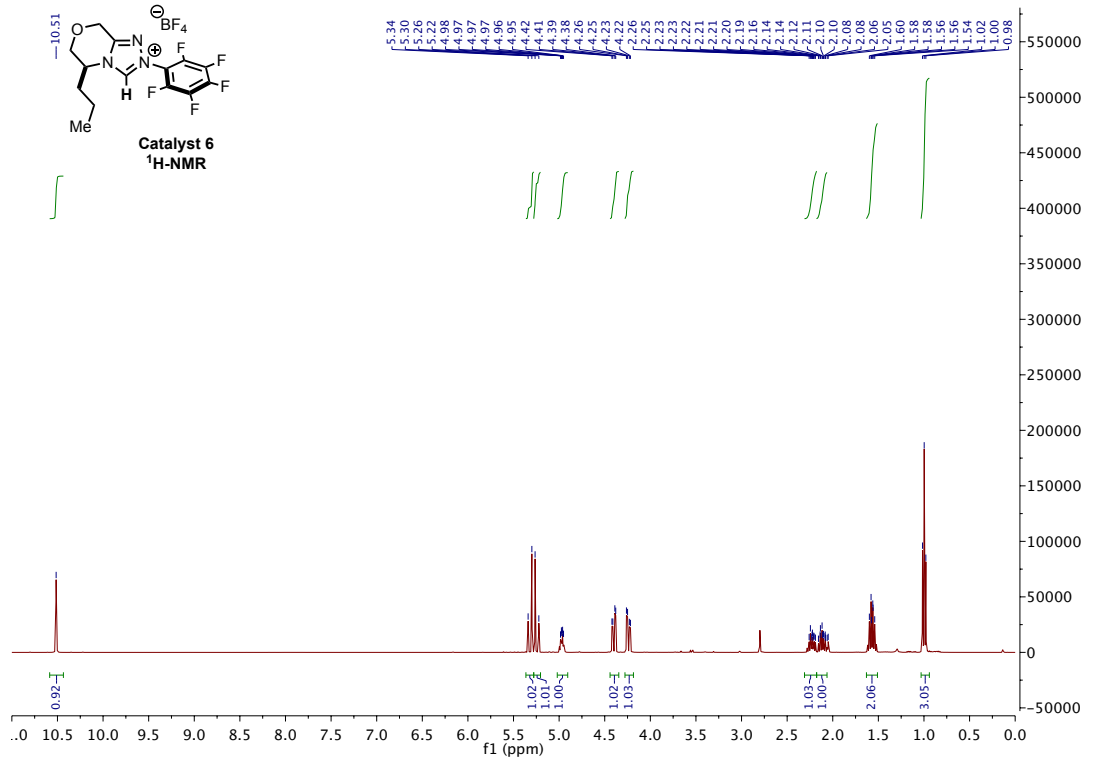

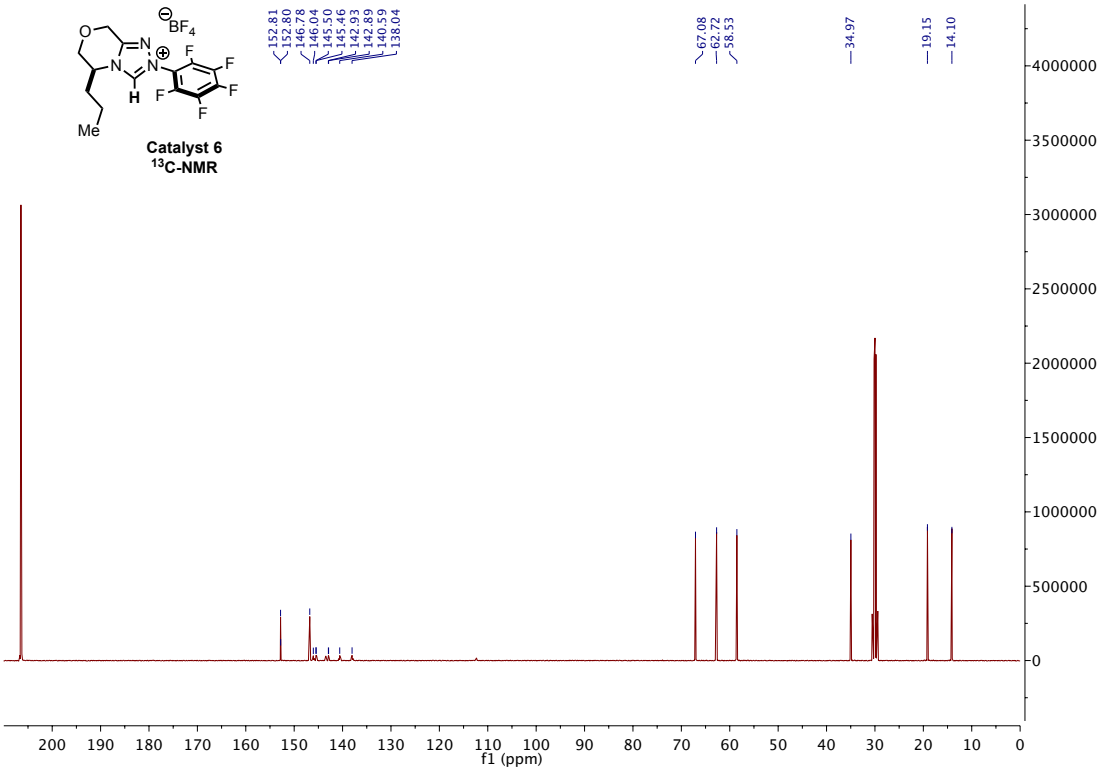

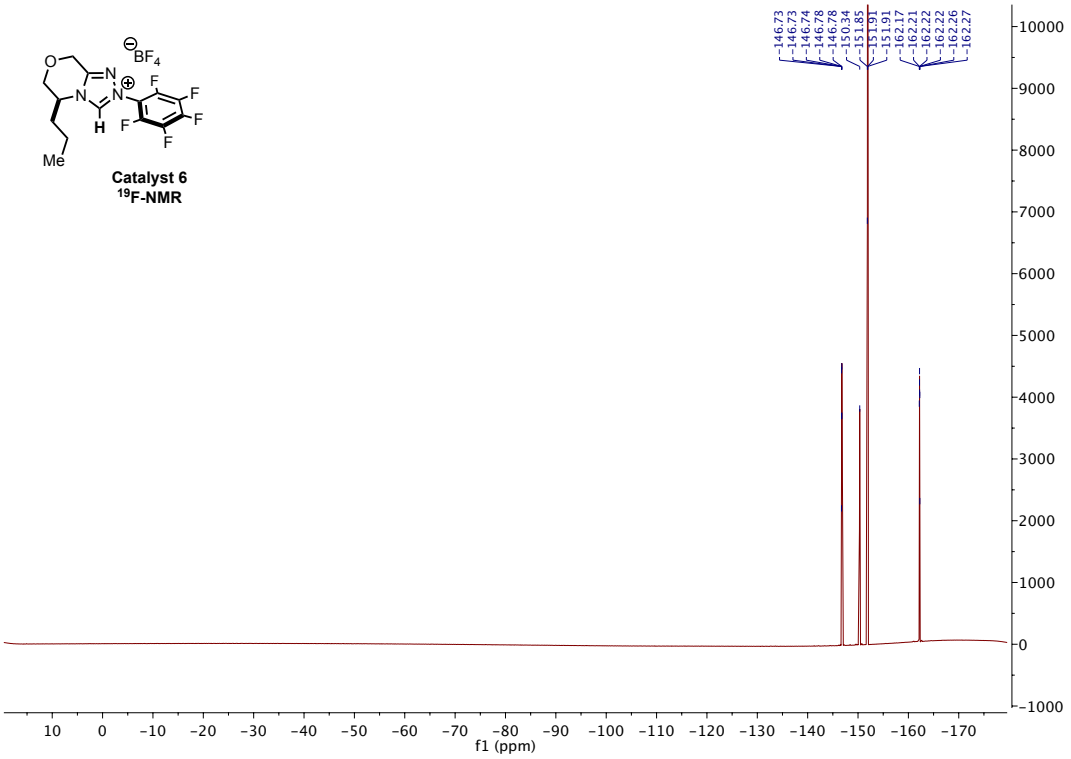
Catalyst 6
19F-NMR
f1 (ppm)

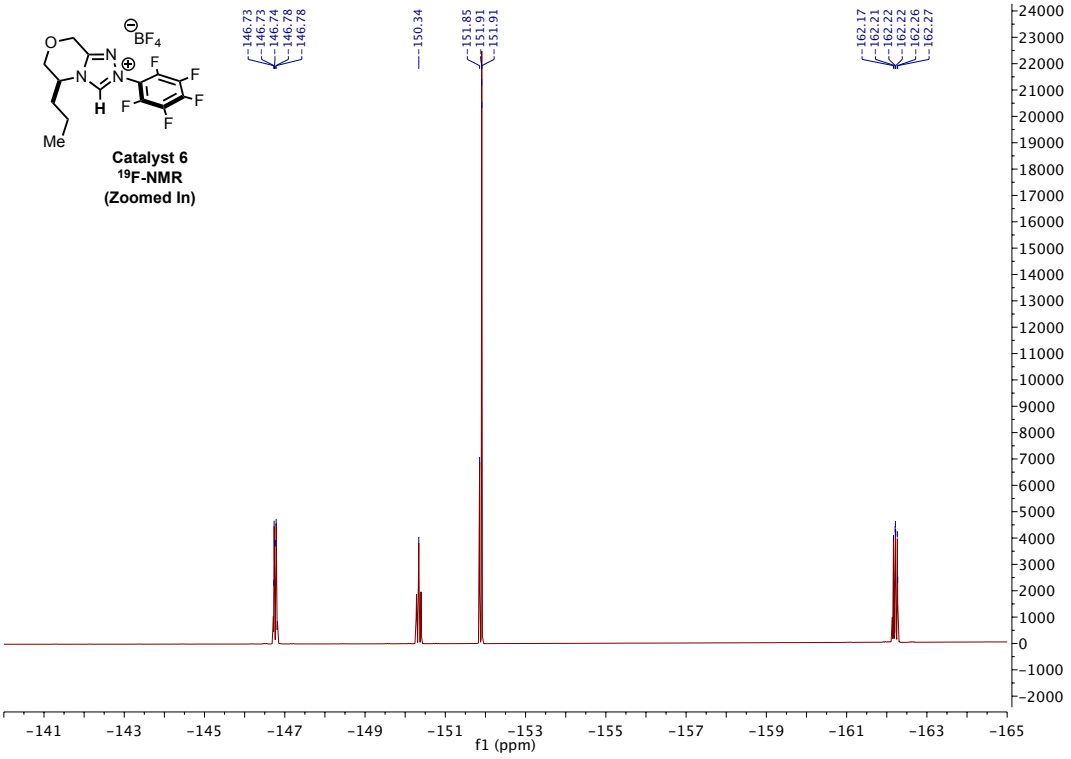
Catalyst 6
19F-NMR
(Zoomed In)
f1 (ppm)

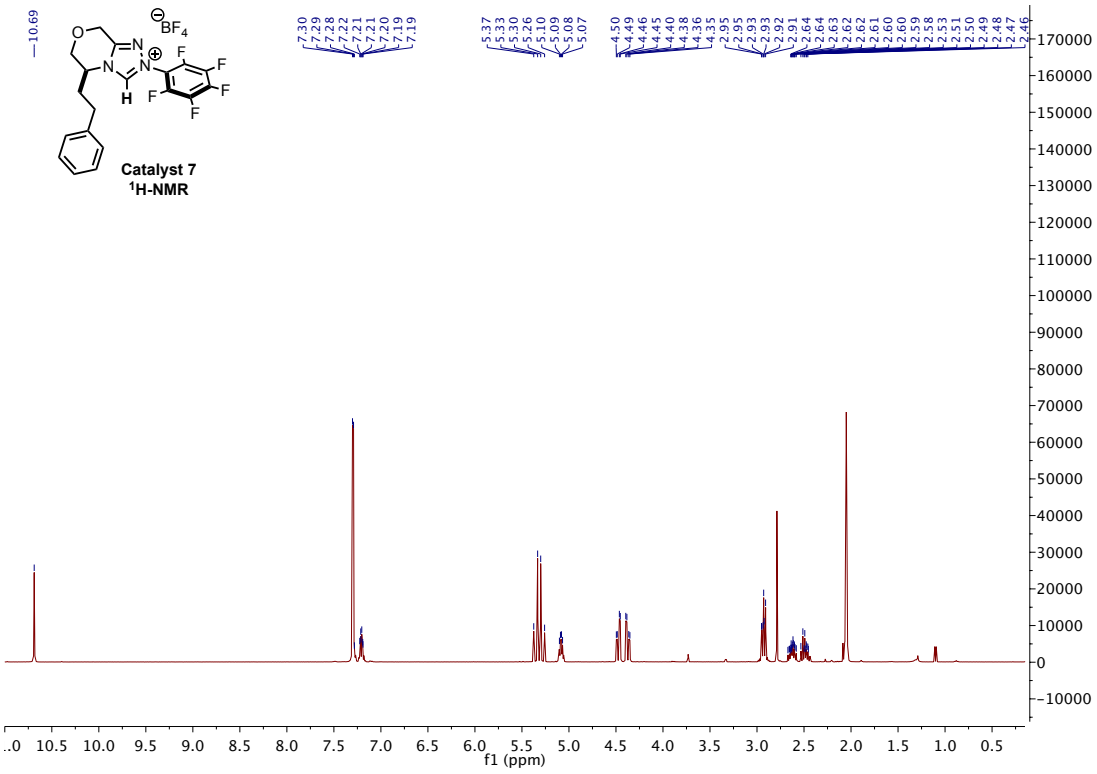
Catalyst 7
1H-NMR
f1 (ppm)

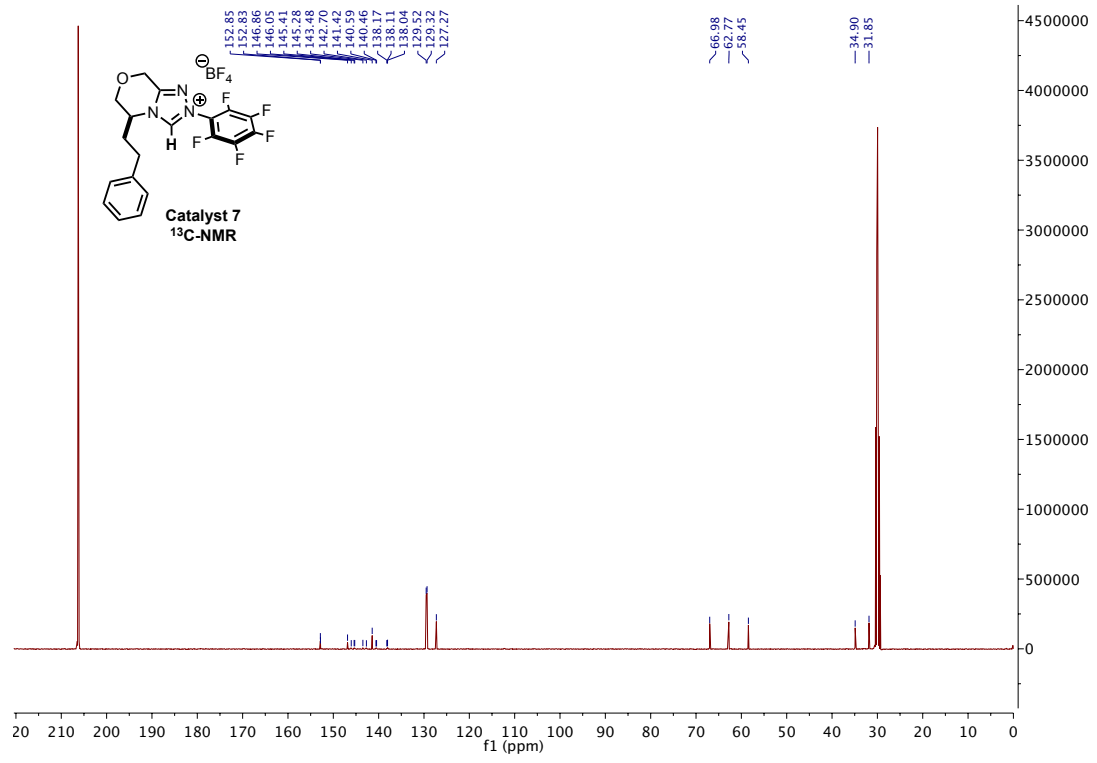
Catalyst 7
13C-NMR
f1 (ppm)

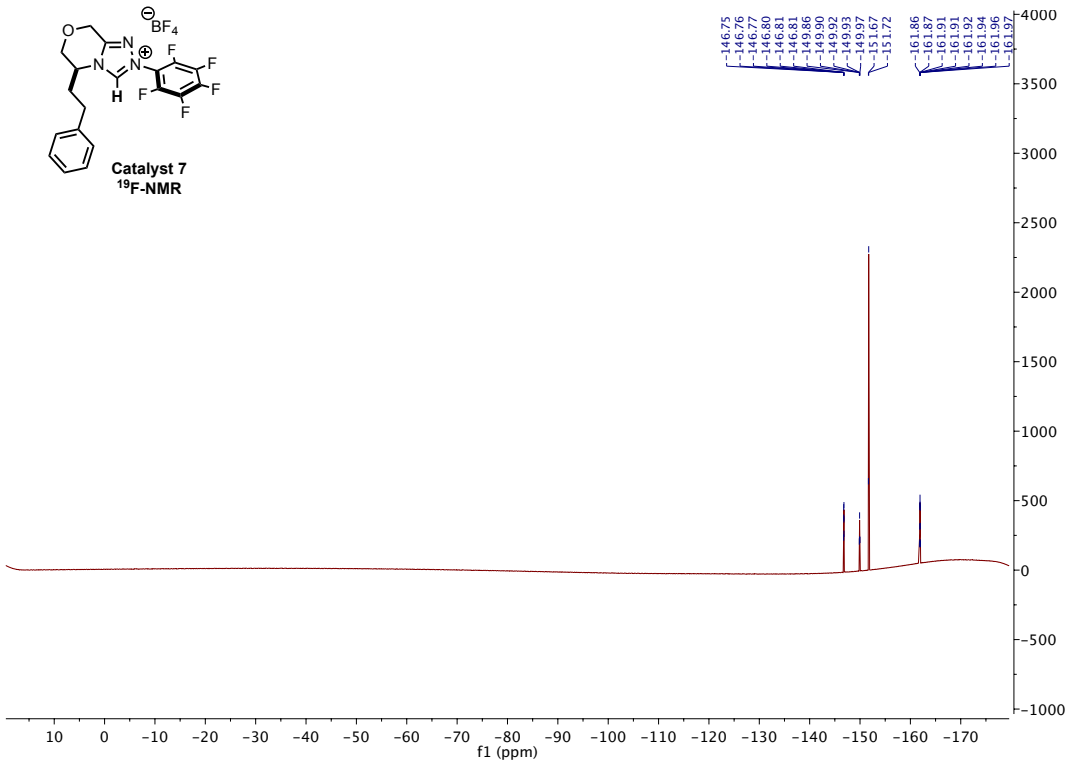
Catalyst 7
19F-NMR
f1 (ppm)

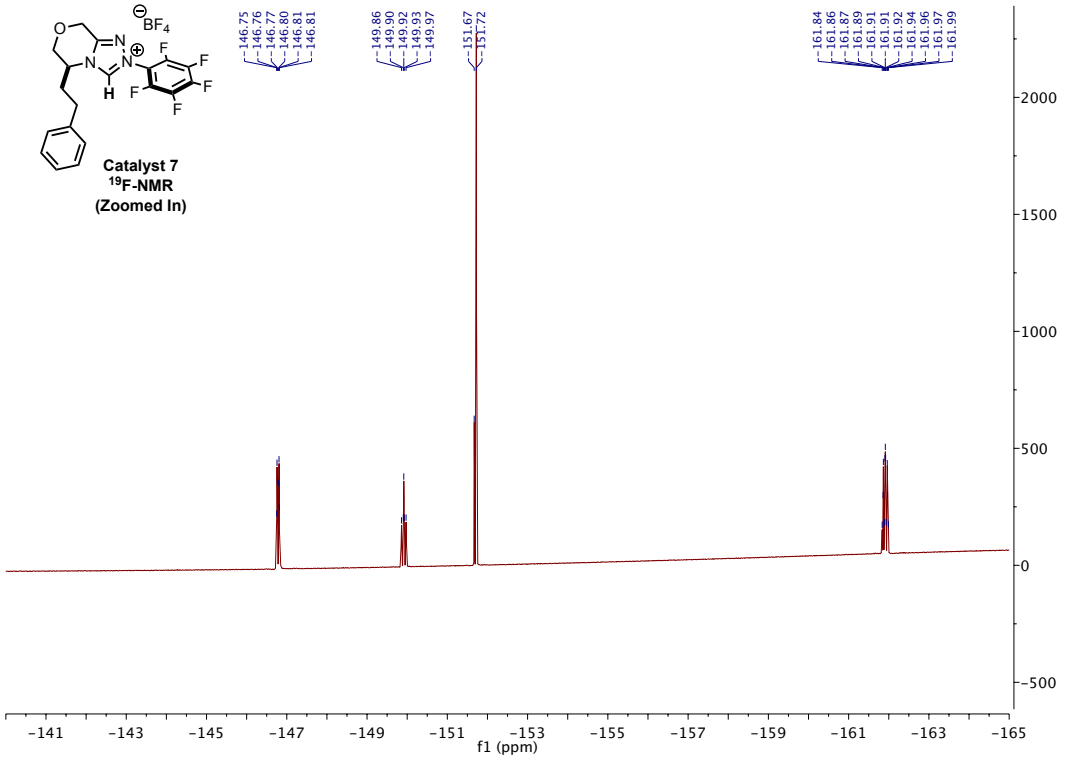
Catalyst 7
19F-NMR
(Zoomed In)
f1 (ppm)

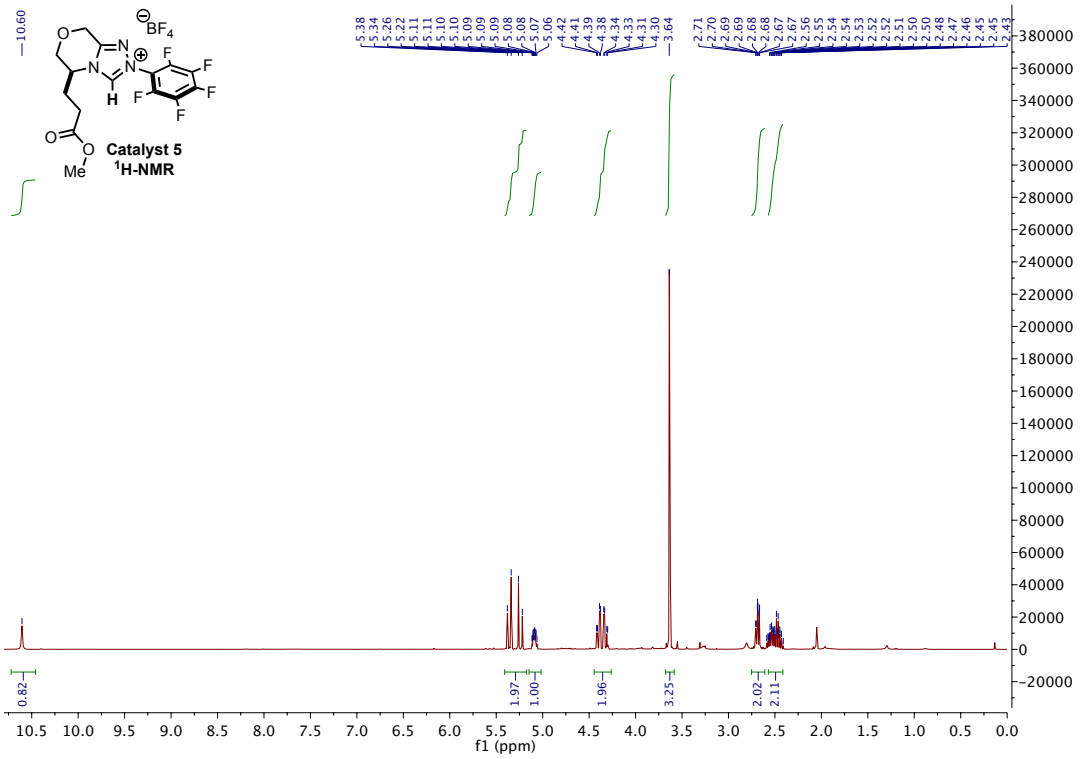
Catalyst 5
1H-NMR
f1 (ppm)

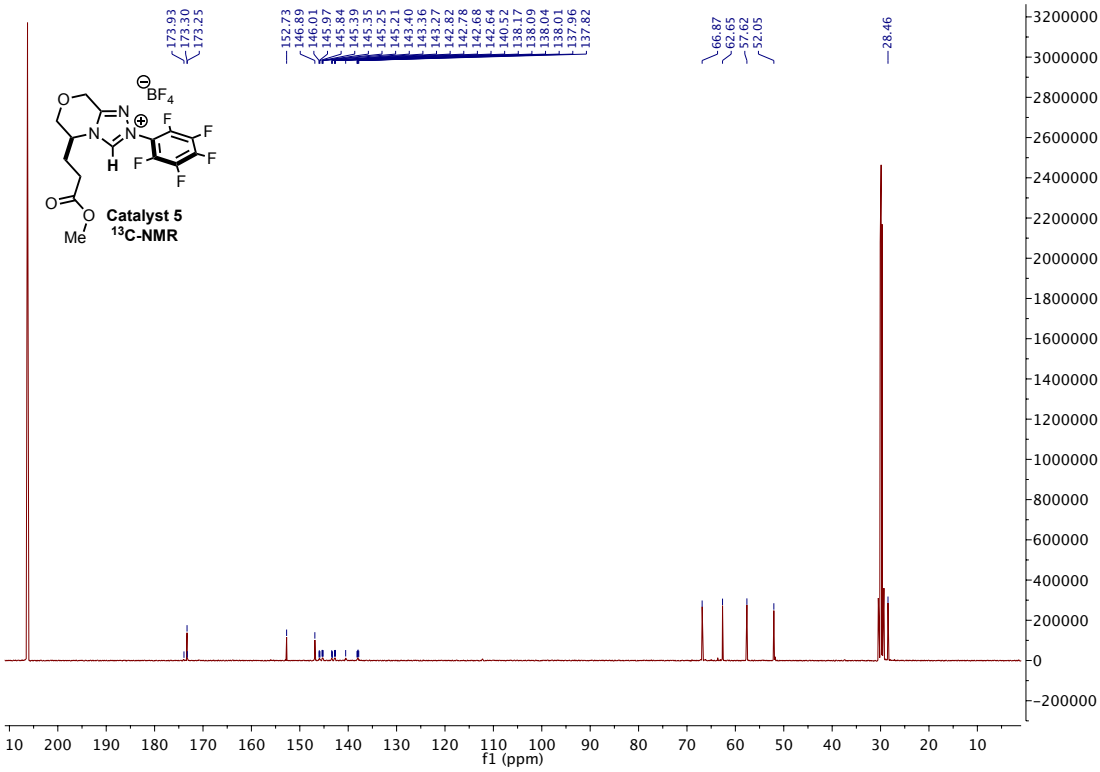
Catalyst 5
13C-NMR
f1 (ppm)

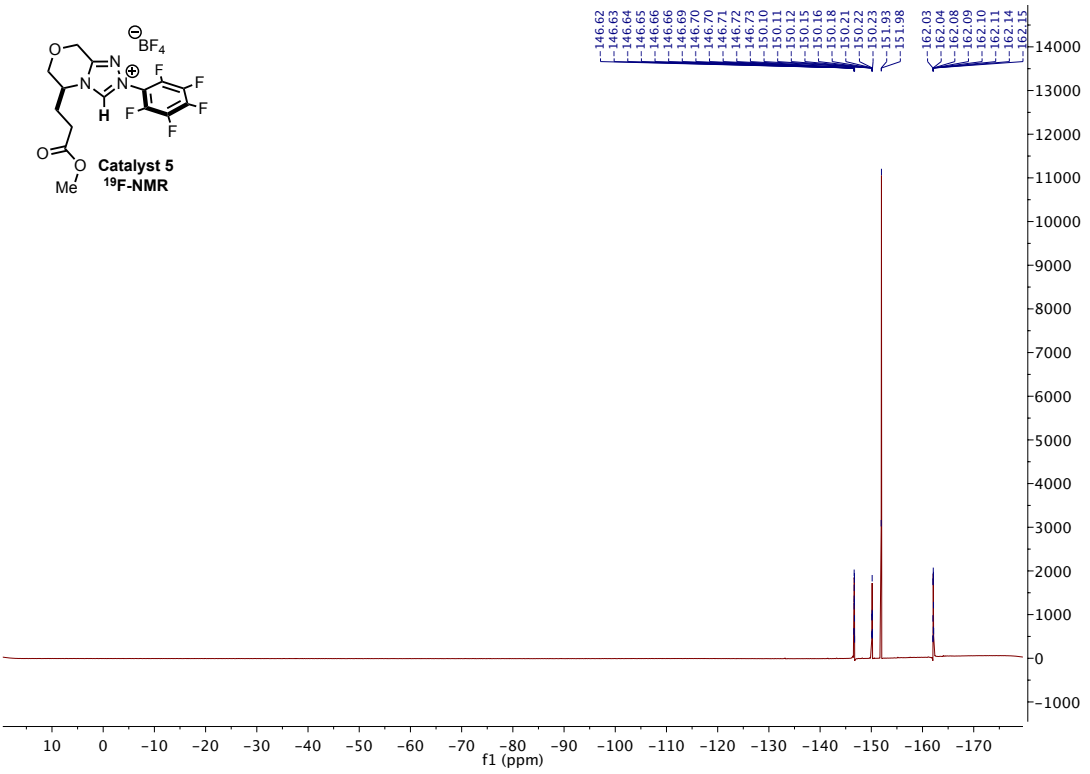
Catalyst 5
19F-NMR
f1 (ppm)

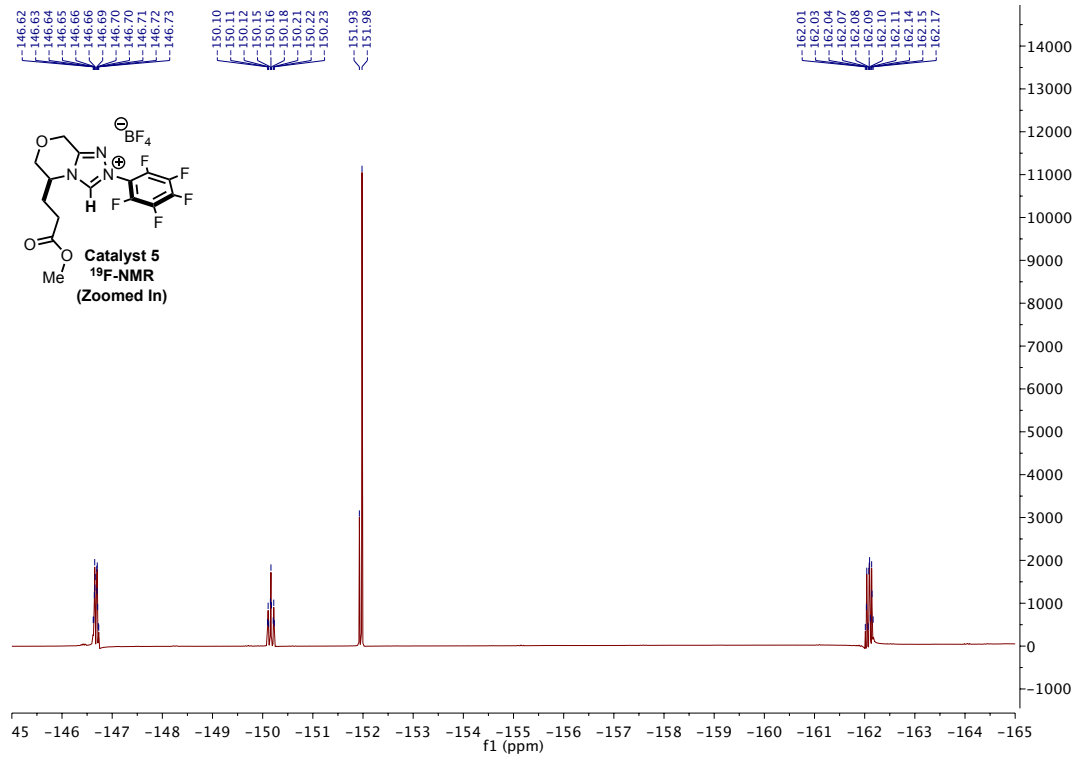
Catalyst 5
19F-NMR
(Zoomed In)
f1 (ppm)

References

1) Moore, J. L; Silvestri, A. P.; de Alaniz, J. R.; DiRocco, D. A.; Rovis, T. Org. Lett. 2011, 13, 1742-1745
2) Collett, C. J.; Masser, R. J.; Taylor, J. E.; Maguire, O. R.; O'Donoghue, A. C.; Smith, A. D. Angew. Chem. Int. Ed. 2015, 54, 6887 –6892
3) Yu, R. T.; Lee, E. E.; Malik, G.; Rovis, T. Angew. Chem. Int. Ed. 2009, 48, 2379 – 2382
4) Yu, R. T.; Rovis, T. J. Am. Chem. Soc. 2006, 128, 2782 – 2783
5) Kerr, M. S.; de Alaniz, J. R.; Rovis, T. J. Org. Chem., 2005, 70, 5725–5728
6) Dalton, D. M.; Rappé, A. K.; Rovis, T. Chem. Sci., 2013, 4, 2062 – 2070
7) de Alaniz, J. R.; Kerr, M. S.; Moore, J. L.; Rovis, T. J. Org. Chem., 2008, 73, 2033–2040
8) Yu, R. T.; Rovis, T. J. Am. Chem. Soc., 2006, 128, 12370–12371